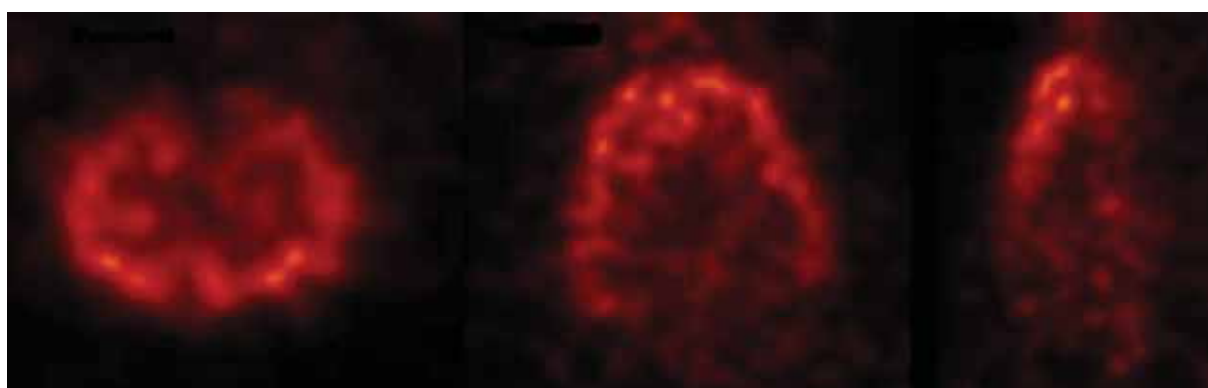UNIVERSITEIT
GENT

SYNTHESIS AND *IN VIVO* EVALUATION OF [^{123}I]-3-I-CO

A potential SPECT tracer for the serotonin 5-HT$_{2A}$ receptor

PROEFSCHRIFT

Voorgelegd tot het verkrijgen van de graad van

Doctor in de Farmaceutische Wetenschappen

aan de

Faculteit Farmaceutische Wetenschappen
Laboratorium voor Radiofarmacie
Universiteit Gent

Door:

Peter Blanckaert

Promotor: Prof. Dr. F. De Vos

2008

Front cover: Pinhole µSPECT imaging with [^{123}I]-R91150 (1 mCi, imaging 60 min after tracer injection) in Sprague-Dawley rats after administration of cyclosporin A (50 mg/kg, 30 min before tracer injection)

SYNTHESIS AND *IN VIVO* EVALUATION OF [^{123}I]-3-I-CO

A potential SPECT tracer for the serotonin 5-HT$_{2A}$ receptor

PROEFSCHRIFT

Voorgelegd tot het verkrijgen van de graad van

Doctor in de Farmaceutische Wetenschappen

aan de

Faculteit Farmaceutische Wetenschappen
Laboratorium voor Radiofarmacie
Universiteit Gent

Door:

Peter Blanckaert

Promotor: Prof. Dr. F. De Vos

2008

LEES – EN EXAMENCOMMISSIE

ACKNOWLEDGEMENTS

DANKWOORD

Dankwoorden zijn meestal de laatste dingen die worden neergeschreven in een thesis, en dat is in dit geval niet anders. Als ik stilsta bij de afgelopen zes jaar, kan ik enkel besluiten dat ik heel veel geleerd heb, over mezelf, over de anderen, en uiteraard ook over de serotonine-receptoren. De voorbije zes jaar waren op zijn minst gezegd interessant en leerrijk, maar ook een beetje frustrerend en vermoeiend. Ik richt dit dankwoord dan ook aan alle mensen die mij hebben gesteund tijdens het tot stand komen van dit doctoraatswerk, mensen die mij wisten te motiveren op moeilijke momenten, mensen die mij wisten te inspireren tijdens het onderzoek, en de mensen die samen met mij blij waren op succesvolle momenten.

LIST OF ABBREVIATIONS

Å   Angstrom, 1×10^{-10} meters

ABC   ATP-binding cassette

ATP   adenosine triphosphate

BBB   blood-brain barrier

BCRP   breast cancer resistance protein

BGO   bismuth germinate oxide

BI   binding index

BP   binding potential

CsA   cyclosporin A

CT   computed tomography

FDA   Food and Drug administration

FDG $[^{18}F]$-fluorodeoxyglucose

fMRI   functional magnetic resonance imaging

FOV   field-of-view

GSO   germanium oxyorthosilicate

HPLC   high performance liquid chromatography

ID   injected dose

iTLC   instant thin layer chromatography

i.v.   intravenously

.

K_d	dissociation constant
k_{off}	off rate constant
k_{on}	on rate constant
LRP	lung resistance protein
LSO	lutetium oxyorthosilicate
MDR	multidrug resistance
MRI	magnetic resonance imaging
MRP	multidrug resistance protein
NMR	nuclear magnetic resonance
PET	positron emission tomography
Pgp	P-glycoprotein
p.i.	post injection
SA	specific activity
SPECT	single photon emission computed tomography
$t_{1/2}$	half-life
TLC	thin layer chromatography

Serotonin is involved as a neurotransmitter in the pathophysiology of different psychiatric disorders such as depression, anxiety and anorexia nervosa. The serotonergic neurotransmission in the frontal cortex can be investigated by using the single photon emission computed tomography (SPECT) radiopharmaceutical ^{123}I-labelled 4-amino-N-[1-[3-(4-fluorophenoxy)propyl]-4-methyl-4-piperidinyl]-5-iodo-2-methoxybenzamide ([^{123}I]-5-I-R91150, figure 1, **2**) that binds selectively to the serotonin 5-HT$_{2A}$ receptor in the human brain.

P-glycoprotein (Pgp) is an ATP-dependent 170 kDa drug efflux pump, responsible a.o. for clearance of toxic compounds from the brain. It was shown previously by other authors that the tissue distribution of P-glycoprotein can be a major determinant for the pharmacokinetics of different Pgp substrates, especially in the blood-brain barrier. Modulation of P-glycoprotein activity with certain compounds (for example cyclosporin A and verapamil) might increase the pharmacological effects of Pgp substrates and is therefore potentially of clinical importance.

In this thesis, the influence of P-glycoprotein modulation on the pharmacokinetics and brain uptake of the 5-HT$_{2A}$ radioligand [^{123}I]-R91150 will be evaluated. We will investigate whether [^{123}I]-R91150 is a possible substrate for *in vivo* P-glycoprotein modulation by cyclosporin A in rodents. Also, the influence of Pgp modulation on the brain uptake and µSPECT imaging with [^{123}I]-R91150 will be studied in rodents.
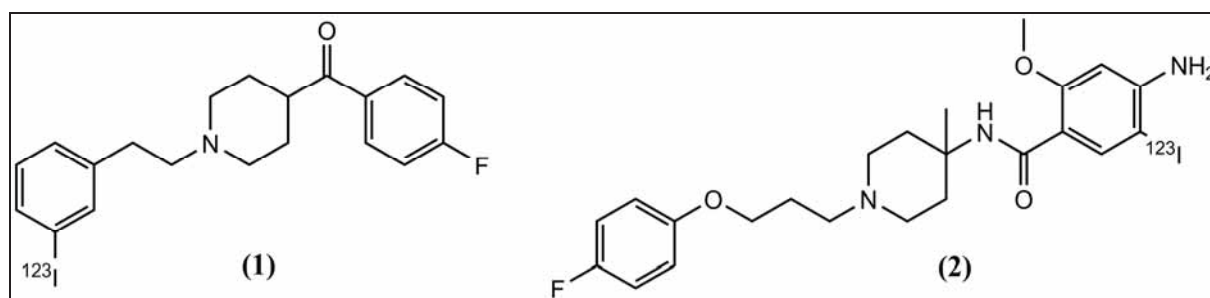
Figure 1: Structure of [^{123}I]-3-I-CO (**1**) and [^{123}I]-R91150 (**2**)

The second goal of this project was to synthesize a new selective ligand for the serotonin 5-HT$_{2A}$ receptor, label this molecule with ^{123}I and perform an *in vivo* evaluation to asses the potential of the radioligand for *in vivo* imaging of the serotonin 5-HT$_{2A}$ receptor with SPECT. [^{123}I]-3-I-CO ([^{123}I]-(4-fluorophenyl)[(3-iodophenetyl)piperidin-4-yl] methanone was selected as potential radioligand (figure 1, **1**). We will also investigate whether the brain uptake of [^{123}I]-3-I-CO is influenced by modulation of P-glycoprotein with cyclosporin A.

TABLE OF CONTENTS

Chapter 1

INTRODUCTION

༄༅༄༅

1. INTRODUCTION

1.1. Medical imaging

Medical imaging was initiated in the 19th century with the discovery of X-rays by Roentgen. Nowadays, different techniques and modalities are employed to visualize parts of the body or specific organs, for example the brain. In this chapter, X-ray/CT-imaging, MRI imaging and imaging with PET/SPECT will be discussed briefly. X-ray and CT-imaging provide images of the body and internal structures (= anatomical information), whereas PET and SPECT provide functional information. MRI provides both anatomical and functional information.

X-ray imaging was used in human medicine immediately after its discovery because of its enormous potential to visualize the human body. X-rays penetrate through most biological tissues and are 'recorded' on a film, providing a projection image of the human body. Penetration and absorption of X-rays depends on the density of the penetrated tissue.

Computed tomography imaging (CT-imaging) was developed to deal with the fact that normal X-ray imaging only provides a projection image, without three-dimensional information. In CT-imaging, the X-ray source turns around the patient, along with the X-ray detector. This way, X-ray CT-imaging produces thin slices of the whole body, approximately 1 mm thick. Modern CT-cameras are equipped with a ring of detectors. Acquisition time is limited to a few minutes for total body scans. The different projections are stitched together with software to yield a three-dimensional image of the human body.

1.1.1. Magnetic Resonance Imaging

Medical magnetic resonance imaging (MRI) is a technique for obtaining high-resolution images of various organs within the human body by mapping the distribution of hydrogen nuclei in the body. In MRI imaging, the patient is placed in a strong magnetic field generated by a superconducting magnet. The principles of NMR (nuclear magnetic resonance) are used in MRI. As atomic nuclei with an odd number of protons (for example ^{1}H) spin, they create micro-magnetic fields around themselves, causing a small magnetic moment. Atoms with an even proton number show no spin. When these atoms are placed in an external magnetic field, they will align themselves according to this field. By applying radio waves with a certain frequency, the nuclei disalign from the external magnetic field. When the radio wave application is halted, the nuclei will realign themselves with the magnetic field (= relaxation), while emitting a radio signal which can be detected externally. The relaxation time is also measured. The obtained data are then processed in a computer to yield three-dimensional images of organs and tissues.

There are different types of MRI imaging, amongst others diffusion MRI (measuring the diffusion pattern of water in biological tissues) and functional MRI (specific signals for certain molecules). Originally, nuclear magnetic imaging (NMR) techniques were used to elucidate the structure of chemical compounds

Disadvantages of MRI are inherent to the technique used: high costs, high magnetic fields and large space requirements for the equipment[1]. Characteristic is the loud noise of the MRI camera equipment.

1.1.2. Single Photon Emission Computed Tomography (SPECT)

1.1.2.1. SPECT

SPECT is the most used modality in nuclear medicine imaging. The first SPECT scanner was developed in 1957. Gamma-emitting radio-isotopes, coupled to a molecule with known pharmacological properties are used in SPECT imaging. The SPECT-tracer is injected, and the single photons emitted by the isotope are detected by a gamma-camera.

The camera consists of a collimator, a scintillation crystal and photomultiplier tubes, with associated electronics and computer equipment to perform the necessary manipulations and calculations (figure 1.1).
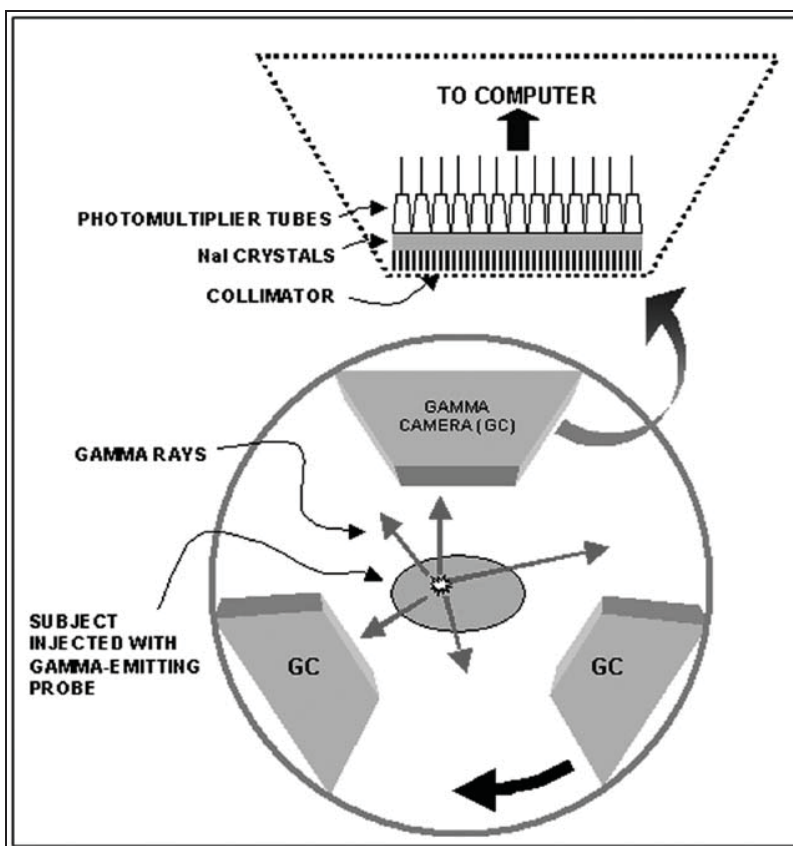
Figure 1.1: Operation principle of a SPECT-camera

The use of a collimator ensures that only photons reaching the detector in a ninety degree angle are detected. A scintillation crystal is used to convert the high-energy photons into light

photons. A sodium iodide crystal, doped with thallium is commonly used as the scintillator in SPECT imaging.

The photons are converted into an electrical signal (photo-electrical effect), which is amplified to a detectable level with photomultiplier tubes. The result is a radioactivity distribution image of the scanned object.

The most commonly used isotopes in SPECT imaging are ^{123}I (half-life: 13.2 h, E$_\gamma$: 159 keV and ^{99m}Tc (half-life: 6,07 h, E$_\gamma$: 143 keV). These isotopes are not commonly found in nature (or in many pharmaceutically active compounds), so incorporating them into biologically active molecules without changing the desired characteristics of the drug presents a difficult challenge.

Originally, only planar imaging with gamma cameras was possible. The obtained images are projection images, and the organ-of interest can be blocked by other organs lying in front of it. More recently, tomographic imaging techniques were developed – comparable to the principle of CT-scanning. This technique yields different 'slices' from the scanned object with a rotating gamma camera. Reconstruction takes place with a computer after the scan, and provides a three-dimensional image of the object (= SPECT, or Single Photon Emission Computed Tomography).

A major factor contributing to the relatively low resolution obtained with SPECT are the collimators. More recently, two-headed and triple-head rotating cameras have been developed, resulting in improved sensitivity and higher spatial resolution. Workable resolutions are 3-6 mm, a much lower resolution than those obtained with PET imaging.

Human SPECT cameras are not suited for imaging small animals with high resolution, for example the brain of a rat, or a whole mouse. High spatial resolution is required for small-animal imaging. The pinhole collimator is based on the camera obscura principle, where an image is magnified through a small hole (figure 1.2).
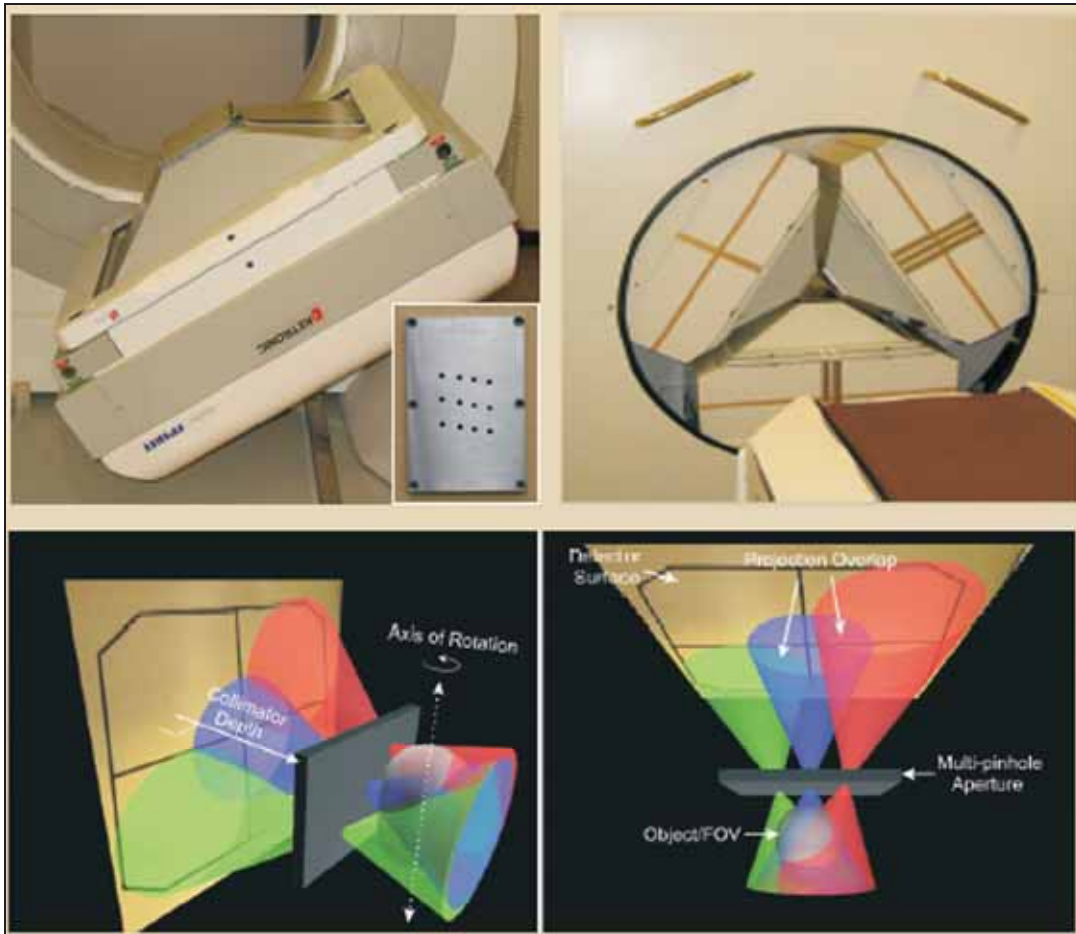
Figure 1.2: HiSPECT high resolution multi-pinhole SPECT imaging system[2]

By using pinhole apertures with a sufficiently small diameter, sub-millimetre spatial resolutions can be obtained[3].

By using multiple pinhole apertures and focussing them on different regions in the field-of-view (see figure 1.2), it is possible to increase the size of the field-of-view[4], and to image larger objects or animals.

During reconstruction of the scan, the different regions (one regions per pinhole-aperture) are 'stitched' together with software after recording the scan. Recently, clinically used SPECT cameras have been adapted to enable imaging of small animals, such as rats and mice. By using pinhole collimators, we were able to 'magnify' a small area, resulting in an image with higher resolution.

The system we used is called HiSPECT (Bioscan Inc, Germany)[5]. HiSPECT is a high resolution high sensitivity imaging module compatible with all commercial gamma cameras. The module consists of upgrading clinical gamma cameras with pyramidal collimators and task-based multi-pinhole apertures (figure 1.2). 9 Pinholes were used per camera head.

The camera used was a triple-headed clinical SPECT camera (Trionix Triad). Pinhole diameter was 1.0 mm for rat brain imaging. Resolution capabilities of this system were assessed with phantom images, and the smallest resolution attained was 0.8 mm.

1.1.3. Positron Emission Tomography (PET)

Positron emission tomography or PET is an important tool in nuclear medicine imaging and was developed in the early 1970's. Positron emission tomography employs radio-isotopes coupled to biologically active molecules with known pharmacological and physiological properties. The isotopes used in PET are positron-emitting isotopes. Decay of these isotopes results in the emission of positrons. When a positron at rest comes into contact with an electron, a process called annihilation takes place. Two anti-parallel photons with an energy of 511 keV each are emitted in opposite directions (figure 1.3).
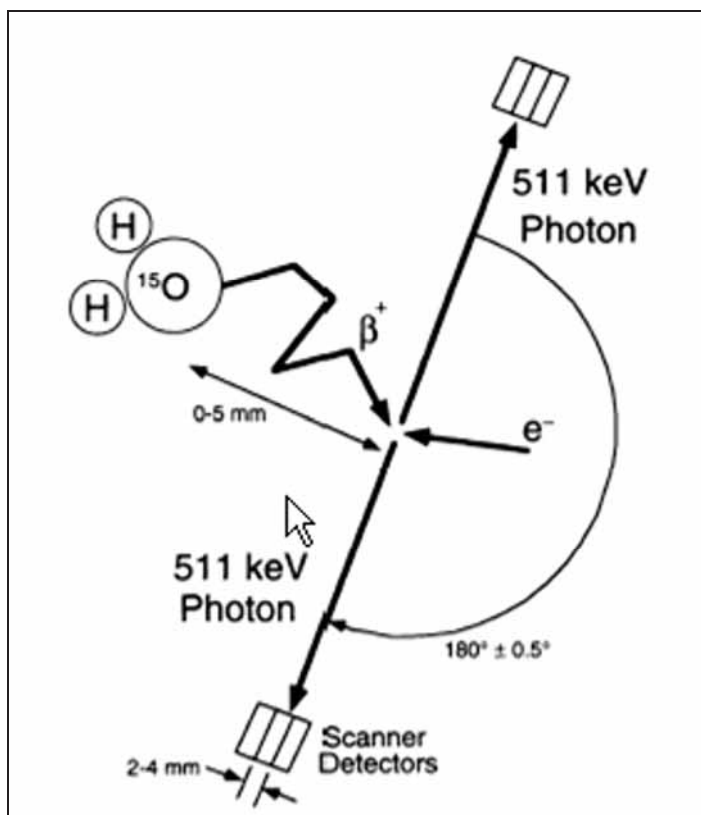
Figure 1.3: Principle of Positron Emission Tomography

A PET camera consists of a ring of detectors, coupled to photomultiplier tubes. Contrary to SPECT, no collimators are used, but imaging with PET is based on coincidence. As two anti-parallel photons are emitted in opposite directions after annihilation of a proton, they will be detected by two detectors at opposite sides of the PET-camera (figure 1.4). This coincidence detection of two photons defines a 'line' through the scanned object along which the annihilation event occurred.

Only these coincidence events are detected by the camera, eliminating the need for a collimator. As a result the sensitivity of a PET camera is much higher compared to the sensitivity of a collimated SPECT camera.
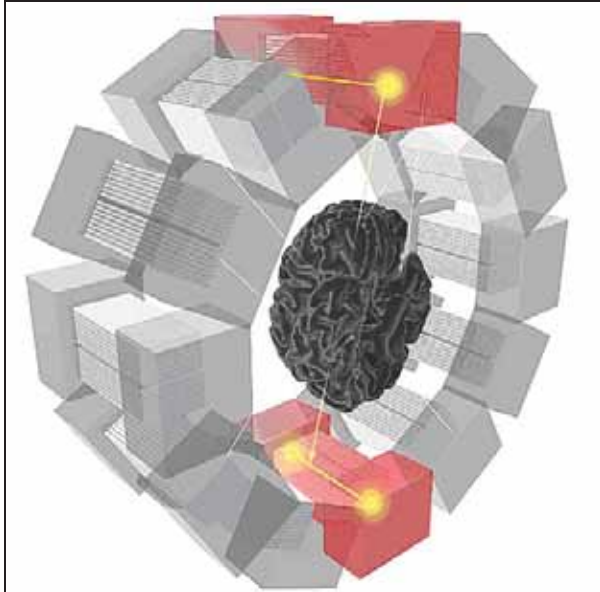
Figure 1.4: Structure of a positron emission tomography camera[6]

The isotopes most used for PET imaging include ^{18}F (half-life: 109.8 min), ^{13}N (half-life: 10 min), ^{15}O (half-life: 2.4 min) and ^{11}C (half-life: 20 min).

Contrary to SPECT, these isotopes are commonly found in almost all biologically active molecules (for example all neurotransmitters and glucose) and they can be incorporated into other molecules-of-interest without changing the molecule's pharmacological or physiological properties.

The scintillation crystals used in PET cameras were originally the same as those used in SPECT cameras (sodium iodide crystals doped with thallium). Other materials with better properties have become available for use in PET cameras, the most important being BGO (bismuth germinate oxide), GSO (germanium oxyorthosilicate) and LSO (lutetium oxyorthosilicate). The advantages of these new materials for detection in PET are higher density, faster decay times and higher light output.

The higher sensitivity and resolution (1.5 – 2 mm) of PET compared to SPECT is the most obvious advantage of positron emission tomography. Drawbacks include the costs of the instrumentation and the requirement of having a cyclotron installed on-site, due to the very short half-life of most positron-emitting isotopes.

1.2. Tracers/radiopharmaceuticals

The use of radiopharmaceuticals in diagnosis and treatment of different diseases is currently on the rise. In this thesis only the diagnostic use of radiopharmaceuticals will be discussed. Radiopharmaceuticals can also be used in the treatment of for example certain types of cancer. SPECT or PET imaging is performed a certain amount of time after injection (mostly intravenously) of the radiopharmaceutical, to allow the tracer to distribute in the body and (for brain tracers) reach the brain. When preparing a radiopharmaceutical, a radio-isotope is chemically bound to a molecule of interest. In most cases, this molecule has a specific target in the body, for example a certain receptor (sub)type. The goal of PET or SPECT imaging is to visualize this target *in vivo*.

All products administered to humans must meet certain minimum quality requirements. Since almost all (brain) tracers are injected intravenously, special measures have to be taken into account, as required for any substance-to-be-injected. Specific requirements for intravenous injection include sterility, pyrogenicity, isotonicity and pH requirements. Furthermore, radiopharmaceuticals have to comply with a set of demands, specific to radiopharmaceuticals. Of particular importance are chemical, radiochemical and radionuclidic purity. The tracer preparation needs to be chemically pure: no unlabelled impurities should be present; radiochemical purity is also important: the only labelled compound present in the preparation should be the desired radiopharmaceutical, no labelled impurities or unbound radioisotopes should be present. Finally, the tracer preparation needs to have a certain radionuclidic purity: only one radionuclide should be present in the preparation, and no contaminations with other radionuclides may occur.

Other demands have to be met before a molecule qualifies as a radiopharmaceutical.

The molecule must show high affinity towards its target (for example, the 5-HT$_{2A}$ receptor) and must be highly selective for the target (for example selectivity for the 5-HT$_{2A}$ receptor over the 5-HT$_{2C}$ receptor is important for a 5-HT$_{2A}$ brain tracer, a selectivity of at least 10 is desirable). Furthermore, the molecule should be able to reach its target; for a brain tracer, this means it needs to be able to cross the blood-brain barrier (BBB). As discussed earlier, for a molecule to pass the BBB, it needs certain characteristics, of which the logP is probably one of the most important. Too hydrophilic, and a molecule will not be able to pass through the BBB. Too lipophilic, and the molecule will show a high degree of aspecific binding in the brain, making good quality imaging impossible.

The partition coefficient (or logP) is the distribution coefficient between n-octanol and water. For radiotracers, it is calculated by dividing the tracer concentration present in the n-octanol layer with the tracer concentration present in the aqueous layer. For optimal penetration through the blood-brain barrier, a molecule needs to have a logP value between 1.5 and 2.7. Since metabolites can interact with the imaging process, it is important that the tracer has an adequate metabolisation profile. Aspecific binding to tissue should be as low as possible. Incorporation of a suitable radio-isotope should also be straightforward.

Lastly, specific activity is of critical importance. Specific activity of a radioligand can be defined as the ratio of the radioligand concentration to the total ligand concentration (radioligand + cold ligand with identical chemical structure). Specific activity is expressed as Ci/μmol or GBq/μmol. A preparation is carrier-free when only radioligand, and no cold ligand is present. As a general rule, specific activity needs to be as high as possible.

A lot of tracers currently exist for receptor brain imaging, spanning almost all receptor types and subtypes. Selective radioligands are available for the various neurotransmitter systems, enabling the visualization of receptor distribution in the normal brain and changes in receptor binding during various physiologic activities or resulting from pathologic conditions [7]. Studying these receptor systems with PET or SPECT will improve our understanding of complex brain functions and will provide more insight into the pathophysiology of neurologic and psychiatric diseases. PET and SPECT are techniques that provide methods of high sensitivity for measuring in vivo neurochemical and pharmacological effects at specific target-receptor proteins. Imaging of the 5-HT$_{2A}$ receptor *in vivo* can be used to asses receptor occupancy, guide dosing, examine cerebral and plasma pharmacokinetics and perhaps predict efficacy of a treatment with antipsychotic and mood-altering drugs that interact with targeted sites [8].

Brain tracers can be divided in two groups (PET tracers and SPECT tracers), depending on the isotope used for labelling. The most important clinically used SPECT tracers for brain receptor imaging are [123I]-β-CIT (dopamine transporter tracer), [123I]-R91150 (serotonin 5-HT$_{2A}$ receptor tracer), [123I]-ADAM (serotonin transporter tracer) and [123I]-iomazenil (benzodiazepine receptor tracer) (figure 1.5).
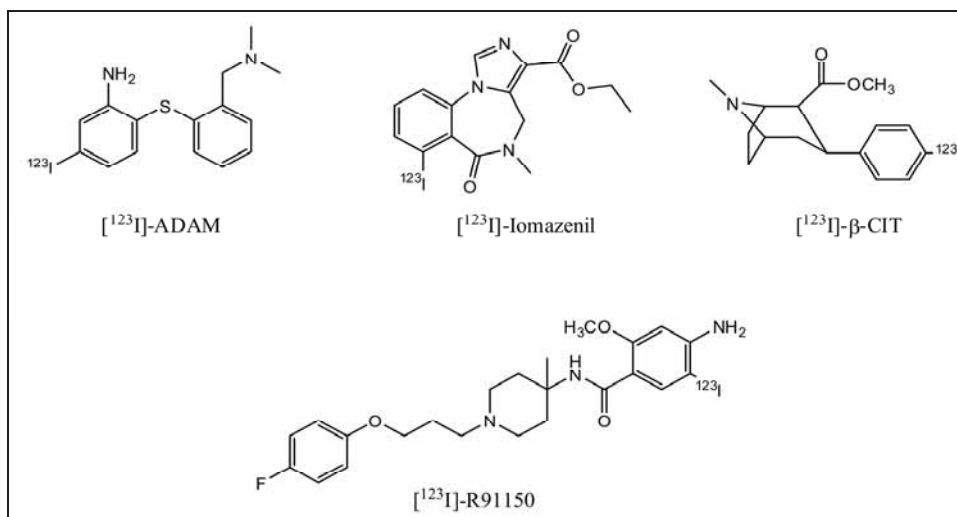
Figure 1.5: SPECT brain receptor tracers

The most important clinically used brain tracers for PET are $[^{11}C]$-Raclopride (selective dopamine D_2 tracer), $[^{11}C]$-WAY100635 (serotonin 5-HT$_{1A}$ receptor tracer), $[^{18}F]$-Altanserin (serotonin 5-HT$_{2A}$ receptor tracer), $[^{11}C]$-MDL100907 (serotonin 5-HT$_{2A}$ receptor tracer), $[^{11}C]$-PK11195 (peripheral benzodiazepine receptor tracer), $[^{11}C]$-Carfentanyl (opioid μ receptor tracer) and $[^{11}C]$-Flumazenil (tracer for GABA$_A$ and benzodiazepine receptors) (figure 1.6).
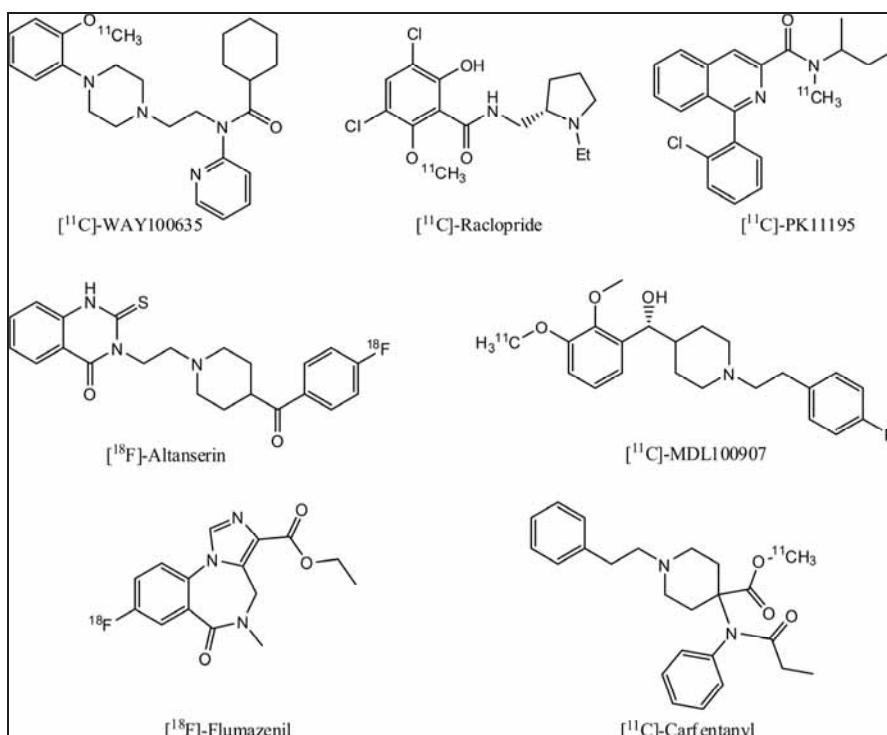
Figure 1.6: Brain receptor tracers for PET

1.3. Blood-brain barrier transport

The vertebrate brain and spinal cord, unlike other organs, are separated from the blood pool by the blood-brain barrier, which separates the circulating blood from interstitial fluid in the brain or spinal cord. The anatomic basis of the blood-brain barrier is situated at the brain microvascular endothelial wall, which has epithelial-like, high-resistance tight junctions. These tight junctions eliminate pores in the walls of brain capillaries, which are normally present in capillaries perfusing peripheral tissues[9].

The vertebrate brain capillary contains some special anatomic features[10] (figure 1.7):

     * high resistance, epithelial-like tight junctions

     * minimal endothelial pinocytosis

     * investment of more then 99 % of the brain surface of the endothelium by astrocyte foot processes.
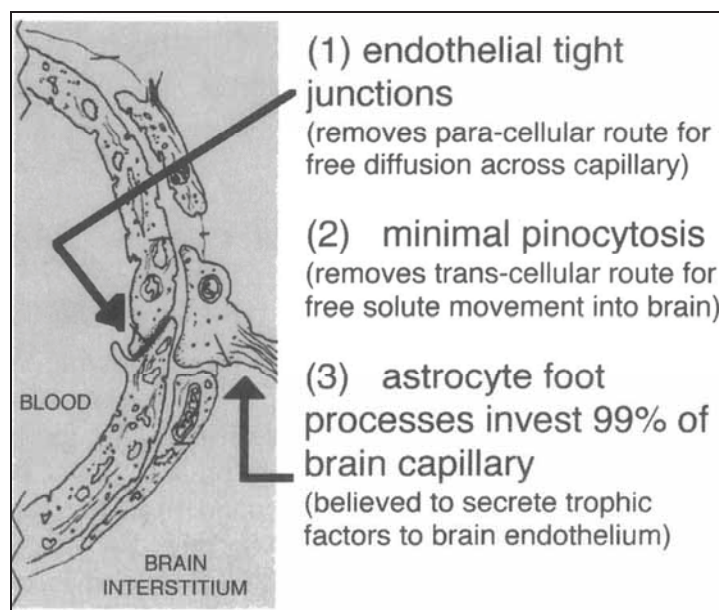
Figure 1.7: General scheme of anatomic specializations of the brain capillary endothelium[11].

The endothelium and not the astrocyte foot process comprises the permeability barrier. For example, the inability of horseradish peroxidase to cross the blood-brain barrier was demonstrated by light microscopic histochemistry[9].

For brain imaging studies, the radioligands have to be able to reach the brain. Most radioligands are injected intravenously, and are transported through the body to reach the brain by penetration of the blood-brain barrier (= influx). Compounds can penetrate the blood-brain barrier in different ways: an energy-dependent active transport process and transport based on passive diffusion. Compounds are cleared from the brain (= efflux) by different energy-dependent active transport processes. Some compounds can also be cleared from the brain by passive diffusion.

The different transport mechanisms through the blood-brain barrier are presented in figure 1.8.
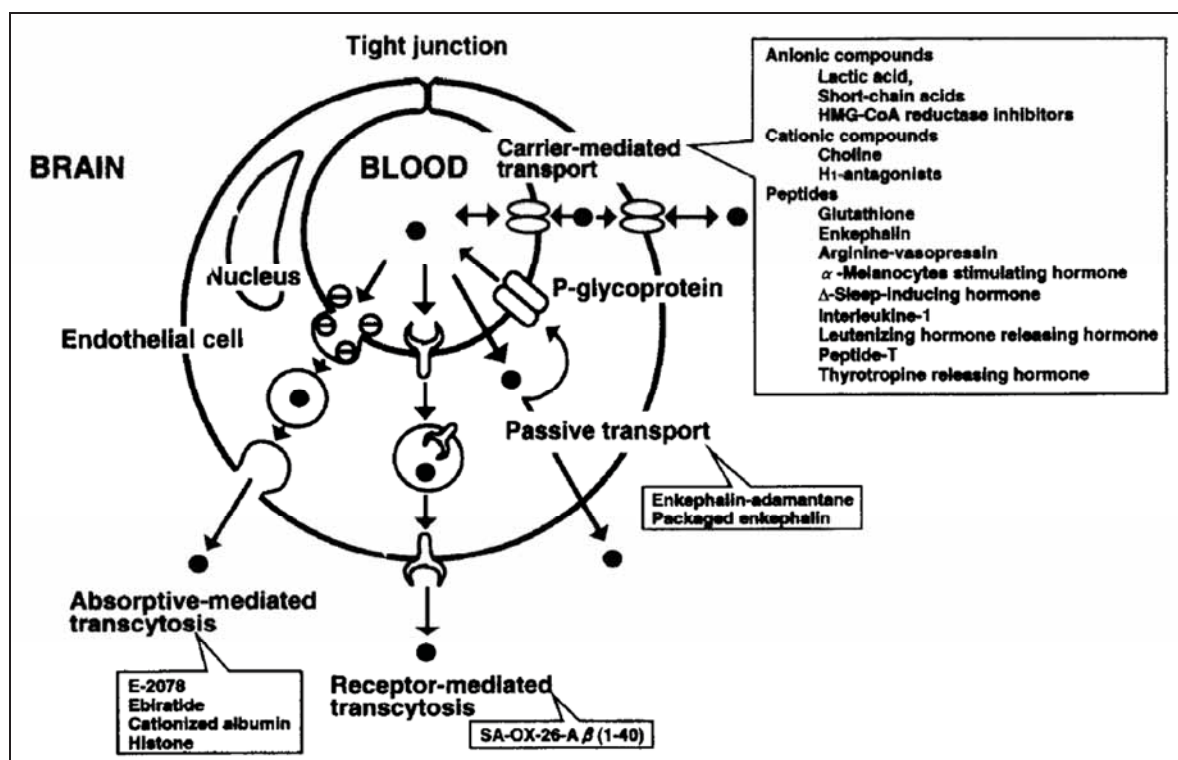
Figure 1.8: Blood-brain barrier transport mechanisms. Figure adapted from Tamai et al[12].

Several mechanisms exist for efflux of drugs out of the brain to the blood: P-glycoprotein, carrier-mediated transport and passive diffusion. The most important influx mechanisms are transcytosis (absorptive-mediated and receptor-mediated), passive transport and carrier-mediated transport.

1.3.1. Influx into the brain

1.3.1.1. Introduction

Two strategies exist to transport compounds into the brain. The first is a local invasive strategy where a compound is injected directly into the brain with a catheter. This method is rarely used. The second strategy is the non-invasive (systemic) strategy, where a compound is injected intravenously. It needs to penetrate the blood-brain barrier to be able to reach the brain.

* Local invasive strategies: Traditional invasive methods of brain drug delivery require access to the brain by a neurosurgeon (intracerebroventricular infusion, intracerebral implant). Disruption of the blood-brain barrier can also be used: the endothelial tight junctions may be transiently disrupted by infusion of 2M mannitol directly in the carotid artery[13], although there is evidence for chronic neuropathologic changes when the blood-brain barrier of normal brain is disrupted[14]. These effects may be related to the toxic effects of plasma albumin on astrocytes[15]. The use of multivesicular liposomes or intranasal pharmaceutical administration may hold promises for future drug delivery into the brain. Intranasal drug administration allows for direct entry of drugs into the olfactory lobe.

* Non-invasive (systemic) strategies: Traditional non-invasive drug delivery to the brain is based on transport through the blood-brain barrier. The delivery of drugs to the brain following systemic administration requires that the drug undergoes transport through the microvascular endothelial wall of the brain, which comprises the blood-brain barrier *in vivo*. Blood-brain barrier (BBB) transport occurs if the compound has access to endogenous transport pathways within the BBB. The systemic administration of drugs that have been formulated specially to enable the pharmaceutical to undergo transport through the brain capillary endothelium will allow for broad distribution of drugs into the entire brain parenchyma, as opposed to the local distribution in the brain that results from the use of localized invasive drug delivery. There are about 600 km of brain capillaries in human brain, and the surface area of the human brain capillary endothelium is about 12 m^2[16, 10]. This capillary endothelium is the major barrier preventing uptake of circulating drugs into the brain.

1.3.1.2.. Active influx mechanisms

There are several nutrient transport systems – intended to supply the brain with adequate nutrients - that mediate the influx of circulating nutrients from blood into brain interstitial fluid[17]. These transporters can also be portals of entry for drugs[12]. For a drug to be able to use these transporter systems, the drug must have a molecular structure mimicking the endogenous nutrient. For example, L-DOPA is an active CNS pharmaceutical, because this drug undergoes carrier-mediated transport across the blood-brain barrier on the neutral amino acid transport system in the brain capillary endothelium[18].

The GLUT1 isoform of the sodium-independent glucose transporter gene family is present within the BBB[19], and it has been suggested that glucuronidation of drugs may be a viable strategy for brain drug delivery[20]. Still it is more advantageous that the structure of the drug closely resembles that of an endogenous nutrient.

1.3.1.3. Passive diffusion

Two properties are of critical importance for a drug molecule to cross the blood-brain barrier: lipid solubility and molecular weight. Lipophilicity of a molecule is determined by its logP, or partition coefficient. $LogP_{pH7.4}$ values of 2 - 3 are ideal for adequate drug penetration into the brain[21]. A linear relationship exists between blood-brain barrier permeability and lipid solubility if the molecular weight of the molecule is under a certain threshold (figure 1.9).
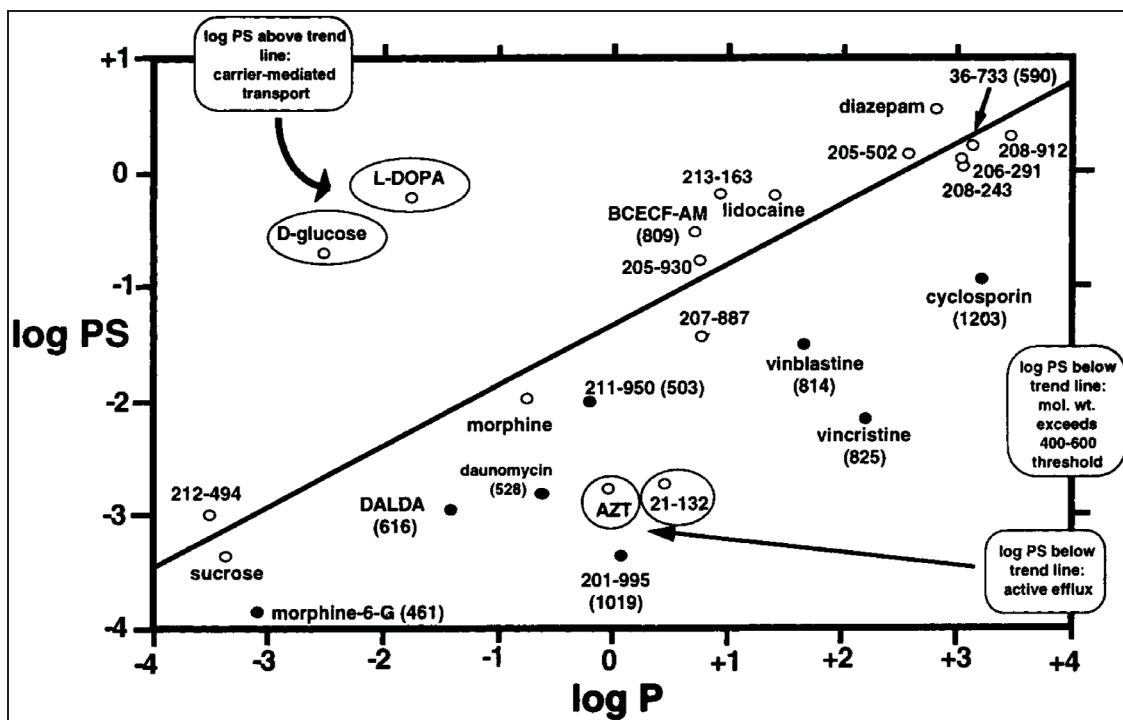
Figure 1.9: Blood-brain barrier permeability-surface area (PS) product plotted versus the 1-octanol/saline partition coefficient for different drugs.

This molecular weight threshold is about 400-600 Dalton[22]. Larger molecules (for example antibodies, large proteins) are not able to cross the blood-brain barrier.

1.3.2. Efflux out of the brain

Several drugs are actively transported out of the brain. For example, azidothymidine (AZT) actively effluxes from brain to blood across the blood-brain barrier[23, 24], and this accounts for the marked reduction in AZT penetration into brain parenchyma[25]. Other examples of blood-brain barrier efflux of small molecules include baclofen[26] and valproate[27]. Given the presence of active efflux systems for drugs at the blood-brain barrier, a new strategy for drug delivery to the brain, which emanates from an understanding of brain capillary transport biology, is based on the discovery of inhibitors of these active efflux systems. The coadministration of the inhibitor with the drug could allow for enhanced central nervous system (CNS) penetration of the pharmaceutical into the brain.

P-glycoprotein (Pgp) functions as an active efflux system at the brain capillary endothelium[28]. The concept that microvascular P-glycoprotein functions at the brain endothelium and acts as an active efflux system arose from observations that immunoactive P-glycoprotein is found in the microvasculature in either brain tissue sections or isolated brain capillaries[29, 30]. As shown in the bottom-right part of figure 1.9, some drugs (cyclosporin A, anthracyclines and the Vinca alkaloids vincristine and vinblastine) exhibit lower accumulation in the brain than would be expected from their lipophilic properties. Drug efflux by P-glycoprotein could account for this decreased accumulation. Tumor cells exposed to antitumor drugs such as the Vinca alkaloids or anthracyclines, sometimes acquire cross-resistance to other structurally unrelated compounds[31]. The function and structure of P-glycoprotein will further be discussed in detail.

1.3.3. P-glycoprotein

The ATP-binding cassette (ABC) transporters are a transmembrane family of proteins[32] that extrude various molecules across all cell membranes by using ATP hydrolysis energy. The transporters efflux compounds from the cytoplasm to the outside of the cell or into an intracellular compartment, such as the endoplasmatic reticulum, the mitochondria or the peroxisome[33]. In humans, 49 ABC genes, organized into seven subfamilies (A – G), have been reported, and many of these genes are involved in human genetic diseases and in multidrug resistance (MDR)[34]. The mechanism of MDR is mainly the cell overexpression of some ABC transporters localized in cell membrane such as P-glycoprotein (Pgp), breast cancer resistance protein (BCRP), multidrug resistance protein 1 – 7 (MRP1-7) and lung resistance protein (LRP)[35]. In recent years, many drugs have been evaluated as potential efflux pump inhibitors, such as the calcium channel blocker verapamil and the antisteroids such as tamoxifen.

This multidrug resistance is frequently characterized by overexpression of a 150 – 180 kDa transmembrane glycoprotein, P-glycoprotein, and a concomitant decrease of drug accumulation in the resistant cells compared with the drug-sensitive cell line[36, 37]. P-glycoprotein was thought to function as an ATP-dependent efflux pump that transports various drugs out of cells, thereby decreasing their accumulation within cells and consequently their efficacy[12]. P-glycoprotein has a very broad substrate specificity and the drugs involved in the multidrug resistance phenotype bind specifically to this glycoprotein[38, 39, 12]. Mammalian P-glycoproteins are encoded by a gene family containing two members in humans (MDR1 and MDR3) and three members in mice and Chinese hamsters (mdr1a, mdr1b and mdr2)[40, 40, 41]. In rats, mdr1b and mdr2 genes have been cloned[42, 43]. It has been shown that MDR1, mdr1a and mdr1b genes confer multidrug resistance, since they have drug transport activities, whereas the closely related MDR3 and mdr2 genes do not mediate such drug transport. From the viewpoint of multidrug resistance of cancer cells and influence on the pharmacokinetics of drugs (or brain tracers), P-glycoprotein encoded by MDR1, mdr1a and mdr1b genes is the most important.

Tissue	MDR1 (human)	mdr1a (mouse)	mdr1b (mouse)
Digestive tract			
Oesophagus	+	ND	ND
Stomach	+	−	+
Jejunum/Ileum	+ + +	+ + +	+
Colon	+ + +	+ + +	+
Liver	+ + +	+	+
Endocrine organs			
Thyroid	−	ND	ND
Adrenal	+ + + +	+ + + +	+ + + +
Ovary	+	+	+ +
Testis	+	+	−
Urogenital tract			
Kidney	+ + +	+	+ +
Bladder	+	ND	ND
Uterus	+	+	+
Uterus in pregnancy	+ +	+	+ + + +
Placenta	ND	−	+ + +
Prostate	+	ND	ND
Central nervous system	+ +	+	−
Other tissues			
Skeletal muscle	+	+	+
Heart muscle	ND	+	+
Lung	+	+ +	+
Spleen	+	+	+

The relative expression level is indicated by +, and very low or undetectable levels by −.
N.D. indicates that data are not available.
The data were mainly obtained by RNA analysis. From Schinkel et al. [109].

Table 1.1: Tissue distribution of human and mouse P-glycoprotein-mediated multidrug resistance-related genes.

P-glycoprotein is present in the plasma membrane of several normal tissues and tumor cells[29, 44]. These tissues include liver, kidney, intestine, adrenal gland, placenta, brain, testes and others. Since the expression in secretory organs such as liver and kidney is localized to the apical surface, P-glycoprotein could play a role in the excretion of drugs and metabolic products, and several studies have confirmed the importance of P-glycoprotein in the excretory functions of these tissues[45, 46].

More interesting is the expression in brain and testes, especially on the endothelial cells of capillary blood vessels of these tissues, since they are blood-tissue barrier sites which limit the entry of many toxic compounds. Accordingly, it is suggested that P-glycoprotein functions as a barrier, by excluding toxic compounds from cells. Table 1.1 summarizes the tissue distribution of P-glycoprotein encoded by human MDR1 and mouse mdr1a and mdr1b, evaluated by RNA analysis[47, 48]. Care is needed in interpreting results obtained in the mdr1a gene-knockout mice, because an increase or alteration of some other protein functionally related to the mdr1a gene product may compensate for loss of functions of the mdr1a gene product, leading to apparent absence of changes in drug pharmacokinetics in the knockout animals.

The transport function of P-glycoprotein at the blood-brain barrier was demonstrated using primary cultures of bovine brain capillary endothelial cells[49]. By immunohistochemical analysis, P-glycoprotein was found to be localized on the apical (blood-lumen) side membrane of a monolayer of primary cultured brain capillary endothelial cells. Such a localization at the luminal side was also demonstrated in bovine brain cortical slices. The expression of P-glycoprotein at the luminal side of the membrane was also demonstrated in mice[50]. Other animal species have also been shown to express P-glycoprotein. It was shown that a unidirectional P-glycoprotein-mediated flux occurs to the apical side of the membrane, out of the capillary endothelial cells.

The *in vivo* significance of P-glycoprotein can be examined by studying the effect of specific P-glycoprotein inhibitors on the brain disposition of P-glycoprotein substrates. Wang et al showed that [123I]-rhodamine accumulation in the brain increases with co-administration of a P-glycoprotein inhibitor, cyclosporin A, by using a brain microdialysis technique to quantify [123I]-rhodamine in the brain extracellular fluid[51].

Identification and classification of pharmaceuticals (or PET and SPECT tracers) as possible P-glycoprotein substrates or inhibitors is of crucial importance in the development of new CNS drugs or (brain) tracers. Several tracers for PET and SPECT have already been evaluated for P-glycoprotein modulation, amongst others [11C]-verapamil, [99mTc]-sestamibi, [131I]-MIBG and [11C]-WAY100635 (figure 1.10).

* [11C](R)-(-)-RWAY: Liow et al[52] investigated how P-glycoprotein and its blocking with cyclosporin A (CsA) affected rodent brain uptake of [11C](R)-(-)-RWAY, a radioligand for visualization of central serotonin 5-HT$_{1A}$ receptors. Pgp knockout mice had 2.8-fold greater brain uptake of [11C]-WAY than wild type ones. Similarly, cyclosporin A increased rat brain uptake 5-fold. CsA increased the plasma free fraction of the tracer in rats with a factor 2.7. Regional rat brain binding potential (BP) increased 27-70 % in the CsA-treated rats and the Pgp knockout mice. It was demonstrated that [11C](R)-(-)-RWAY is a Pgp substrate in rodents.

* [131I]-MIBG: It was clarified by Kiyono and others[53] whether [131I]-MIBG is a substrate for Pgp or not. Using a human cell line overexpressing P-glycoprotein, the researchers determined that [131I]-MIBG is not a substrate for P-glycoprotein.
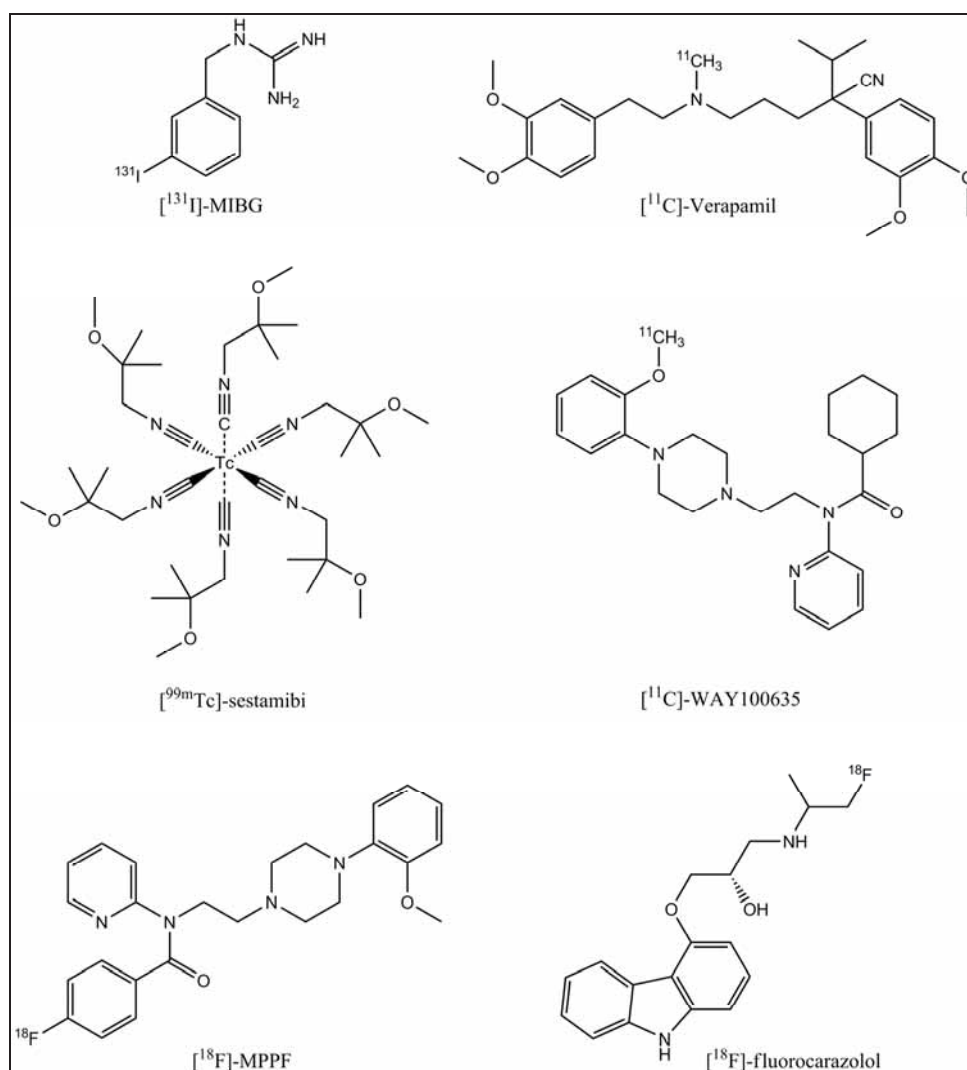
Figure 1.10: Tracers evaluated for potential P-glycoprotein modulation.

* [11C]-Verapamil: Lee et al investigated the P-glycoprotein function at the blood-brain barrier *in vivo* in non-human primates using [11C]-verapamil[54] and PET-scanning techniques. The inhibition of Pgp by PSC833 increased the brain uptake of [11C]-verapamil 4.61-fold. Treatment with PSC833 did not affect the blood [11C]-verapamil profile. It was concluded that [11C]-verapamil could be a powerful tool for evaluating Pgp function at the BBB in a non-invasive manner. Biodistribution studies by Hendrikse et al revealed 9.5-fold and 3.4-fold higher [11C]-verapamil concentration in the brain and testes of mdr1a(-/-) mice than in mdr1a(+/+) mice[55]. Cyclosporin A (50 mg/kg) increased [11C]-verapamil concentrations in brain and testes of mdr1a(+/+) mice with a factor 10.6 and 4.1 respectively. [11C]-Verapamil accumulation in the brain of mdr1a(+/+) mice was increased by cyclosporin A to levels comparable with those in mdr1a(-/-), indicating that reversal of Pgp mediated efflux can be monitored by PET. It was concluded that cyclosporin A could fully block the Pgp function in the blood-brain barrier, and that PET enables the *in vivo* measurement of Pgp function and reversal of its function non-invasively[55].

* [99mTc]-Sestamibi: [99mTc]-Sestamibi[56, 57] (figure 1.10) is widely used in nuclear medicine for assessment of myocardial perfusion[58]. It was demonstrated that [99mTc]-sestamibi is excreted from cells by P-glycoprotein[57].

* [18F]-MPPF: [18F]-MPPF, a 5-HT$_{1A}$ receptor ligand, showed a five- to ten-fold increase in brain uptake in rats after treatment of the animals with cyclosporin A[59].

* Brain uptake of the β-adrenergic receptor ligands [11C]-carazolol and [18F]-fluorocarazolol was increased in Pgp knockout mice and cyclosporin-treated rats. After cyclosporin A modulation, the uptake of [11C]-carazolol increased five- to six-fold. The regional distribution of the radioligands in the brain was not affected[59].

Quantitative PET studies in rodents on Pgp functionality demonstrated a dose-dependent increase of radioligands after administration of cyclosporin A. Brain uptake studies in rats were performed with [11C]-carvedilol using increasing concentrations of cyclosporin A (0, 5, 10, 15, 30 and 50 mg/kg animal weight) [59]. The results of this study are shown in figure 1.11.

We can conclude from figure 1.11 that maximal modulation of cyclosporin A on the brain radioactivity concentration of [11C]-carvedilol in rats was achieved at a cyclosporin A dosage of 50 mg/kg rat body weight.
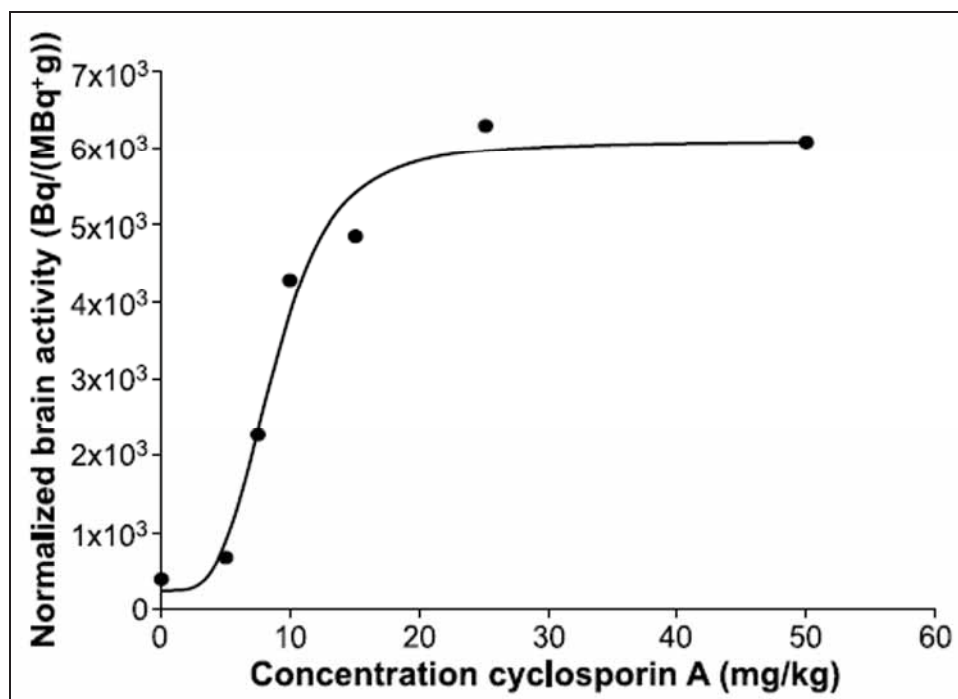
Figure 1.11: Influence of increasing concentrations of cyclosporin A on the accumulation of [11C]-carvedilol in rat brain. Data adapted from Elsinga et al[59].

The same dosage of 50 mg/kg cyclosporin A will be administered to the animals in our own cyclosporin A studies with [123I]-R91150 and [123I]-3-I-CO. Cyclosporin A will be administered through the penile vein in Sprague-Dawley rats, dissolved in a mixture of saline, ethanol and polyethoxylated castor oil for reasons of solubility, one hour before injection of the tracers.

The unusually low blood-brain barrier penetration of cyclosporin A has been explained in terms of the function of P-glycoprotein. Cyclosporin A is lipid-soluble, and it has a logP of 3.0. Since cyclosporin A inhibited the binding of the Vinca alkaloids to the P-glycoprotein expressed in multidrug-resistant tumor cells[60], it was thought that cyclosporin A is actively transported out of the brain. Great potential may lie in possibly enhancing the efficacy, or reduce the side effects, of drugs in the CNS by modulating the P-glycoprotein-mediated transport function, to increase or decrease the apparent blood-brain barrier permeability to the drugs, respectively[12].

A problem of human studies is the lack of potent Pgp modulators that can be administered to patients and healthy volunteers. In humans, cyclosporin A cannot be used as a modulator, since it acts as an immunosuppressive agent. Side effects that can occur are nephrotoxicity, pancreatitis, liver toxicity, tremors and GI-tract dysfunctions. In rodent studies, these undesired effects of cyclosporin A were not problematic since cyclosporin A was administered just before the study and the animals were sacrificed afterwards under isoflurane anaesthesia.

Data on application of other Pgp modulators in humans are available from studies in cancer patients only; their modulatory effect on Pgp in the brain barrier has not yet been reported. Ideally, Pgp modulators should lack pharmacokinetic interactions, e.g. via cytochrome P-450 3A4, and they should be non-toxic themselves.

Newly developed so-called 'third-generation' Pgp modulators such as OC 144-093, GF 120918, XR 9576 and VX 710 meet these requirements[61, 62, 63].

XR 9576 was successfully applied in studies of [^{18}F]-paclitaxel in nonhuman primates[64]. The increased accumulation of this radiotracer after XR 9576 was consistent with Pgp inhibition.

Ketoconazole, an antifungal agent, is also an inhibitor of Pgp function[65]. Ketoconazole has inhibitory potency for not only Pgp but for CYP3A4 also. The inhibitory potency of ketoconazole for Pgp was half that of cyclosporin A. Its main advantage is that it can be administered orally, and it is less toxic in humans than cyclosporin A. Possible effects of ketoconazole on neurotransmitter systems have to be taken into account when using this molecule for blocking Pgp activity.

1.4. References

1. Burton MW and Small SL. An introduction to functional magnetic resonance imaging. Neurologist 1999; 5:145-158.

2. schramm n, hoppin j, lackas c, engeland u, ebel g, van cauter s et al. HiSPECT: A multi-pinhole SPECT imaging module for small-animal research. Bioscan website 2007; Bioscan Inc, Washington DC, USA:

3. Beekman FJ, van der Have F, Vastenhouw B, van der Linden AJA, van Rijk PP, Burbach JPH et al. U-SPECT-I: A novel system for submillimeter-resolution tomography with radiolabeled molecules in mice. Journal of Nuclear Medicine 2005; 46:1194-1200.

4. vanhove C, defrise M, lahoutte T, Bossuyt A. Three-pinhole collimator to improve axial spatial resolution and sensitivity in pinhole SPECT. European Journal of Nuclear Medicine and Molecular Imaging 2008; 35:407-415.

5. schramm N, hoppin J, Lackas C., engeland U, ebel G, van cauter S et al. HiSPECT: A Multi-pinhole SPECT imaging module for small-animal research. Poster, 2006, research center julich, Bioscan Inc 2007;

6. Geneva University Hospital. taken from website (http://pinlab.hcuge.ch/Images/HPD_brainPET.jpg) - Division of Nuclear Medicine, Geneva University Hospital, Geneva, Switzerland.

7. Heiss WD and Herholz K. Brain receptor Imaging. Journal of Nuclear Medicine 2006; 47:302-312.

8. van Dyck CH, Tan PZ, Baldwin RM, Amici LA, Garg PK, Ng CK et al. PET quantification of 5-HT2A receptors in the human brain: A constant infusion paradigm with [F-18]altanserin. Journal of Nuclear Medicine 2000; 41:234-241.

9. Brightman M.W., Reese T.S., Feder N. Assessment with the electron-microscope of the permeability to peroxidase of cerebral endothelium and epithelium in mice and sharks. Capillary Permeability (Crone C and Lassen N A , eds), p 463 Munksgaard, Copenhagen, Danmark 1970; 2417-2424.

10. Pardridge WM. CNS drug design based on principles of blood-brain barrier transport. Journal of Neurochemistry 1998; 70:1781-1792.

11. Barnes NM and Sharp T. A review of central 5-HT receptors and their function. Neuropharmacology 1999; 38:1083-1152.

12. Tamai I and Tsuji A. Drug delivery through the blood-brain barrier. Advanced Drug Delivery Reviews 1996; 19:401-424.

13. Neuwelt EA and Rapoport SI. Modification of the Blood-Brain-Barrier in the Chemotherapy of Malignant Brain-Tumors. Federation Proceedings 1984; 43:214-219.

14. Salahuddin TS, Johansson BB, Kalimo H, Olsson Y. Structural-Changes in the Rat-Brain After Carotid Infusions of Hyperosmolar Solutions - An Electron-Microscopic Study. Acta Neuropathologica 1988; 77:5-13.

15. Nadal A, Fuentes E, Pastor J, Mcnaughton PA. Plasma-Albumin Is A Potent Trigger of Calcium Signals and Dna-Synthesis in Astrocytes. Proceedings of the National Academy of Sciences of the United States of America 1995; 92:1426-1430.

16. Pardridge WM, Golden PL, Kang YS, Bickel Y. Brain microvascular and astrocyte localization of P-glycoprotein. Journal of Neurochemistry 1997; 68:1278-1285.

17. Pardridge WM and Oldendorf WH. Transport of Metabolic Substrates Through Blood-Brain-Barrier. Journal of Neurochemistry 1977; 28:5-12.

18. Wade LA and Katzman R. Rat-Brain Regional Uptake and Decarboxylation of L-Dopa Following Carotid Injection. American Journal of Physiology 1975; 228:352-359.

19. Pardridge WM, Boado RJ, Farrell CR. Brain-Type Glucose Transporter (Glut-1) Is Selectively Localized to the Blood-Brain-Barrier - Studies with Quantitative Western Blotting and Insitu Hybridization. Journal of Biological Chemistry 1990; 265:18035-18040.

20. Polt R, Porreca F, Szabo LZ, Bilsky EJ, Davis P, Abbruscato TJ et al. Glycopeptide Enkephalin Analogs Produce Analgesia in Mice - Evidence for Penetration of the Blood-Brain-Barrier. Proceedings of the National Academy of Sciences of the United States of America 1994; 91:7114-7118.

21. Wilson AA, Jin L, Garcia A, DaSilva JN, Houle S. An admonition when measuring the lipophilicity of radiotracers using counting techniques. Applied Radiation and Isotopes 2001; 54:203-208.

22. Levin VA. Relationship of Octanol-Water Partition-Coefficient and Molecular-Weight to Rat-Brain Capillary-Permeability. J Med Chem 1980; 23:682-684.

23. Dykstra KH, Arya A, Arriola DM, Bungay PM, Morrison PF, Dedrick RL. Microdialysis Study of Zidovudine (Azt) Transport in Rat-Brain. Journal of Pharmacology and Experimental Therapeutics 1993; 267:1227-1236.

24. Takasawa K, Terasaki T, Suzuki H, Sugiyama Y. In vivo evidence for carrier-mediated efflux transport of 3'-azido-3'-deoxythymidine and 2',3'-dideoxyinosine across the blood-brain barrier via a probenecid-sensitive transport system. Journal of Pharmacology and Experimental Therapeutics 1997; 281:369-375.

25. Yarchoan R and Broder S. Development of Antiretroviral Therapy for the Acquired-Immunodeficiency-Syndrome and Related Disorders - A Progress Report. New England Journal of Medicine 1987; 316:557-564.

26. Deguchi Y, Inabe K, Tomiyasu K, Nozawa K, Yamada S, Kimura R. Study on brain interstitial fluid distribution and blood-brain barrier transport of baclofen in rats by microdialysis. Pharmaceutical Research 1995; 12:1838-1844.

27. Cornford EM, Diep CP, Pardridge WM. Blood-Brain Barrier Transport of Valproic Acid. Journal of Neurochemistry 1985; 44:1541-1550.

28. Begley DJ. The blood-brain barrier: Principles for targeting peptides and drugs to the central nervous system. Journal of Pharmacy and Pharmacology 1996; 48:136-146.

29. Cordon-Cardo C., O'Brien J.P., Casals D., Rittman-Grauer L., Biedler J.L., Melamed M.R. et al. Multidrug-resistance gene (P-glycoprotein) is expressed by endothelial cells at blood-brain barrier sites. Proceedings of the National Academy of Sciences of the United States of America 1989; 86:695-698.

30. Jette L, Tetu B, Beliveau R. High-Levels of P-Glycoprotein Detected in Isolated Brain Capillaries. Biochimica et Biophysica Acta 1993; 1150:147-154.

31. Biedler JL and Riehm H. Cellular Resistance to Actinomycin-D in Chinese Hamster Cells In-Vitro - Cross-Resistance, Radioautographic, and Cytogenetic Studies. Cancer Research 1970; 30:1174-&.

32. Klein I, Sarkadi B, Varadi A. An inventory of the human ABC proteins. Biochimica et Biophysica Acta-Biomembranes 1999; 1461:237-262.

33. Ayrton A and Morgan P. Role of transport proteins in drug absorption, distribution and excretion. Xenobiotica 2001; 31:469-497.

34. Dean M, Hamon Y, Chimini G. The human ATP-binding cassette (ABC) transporter superfamily. Journal of Lipid Research 2001; 42:1007-1017.

35. Leslie EM, Deeley RG, Cole SPC. Multidrug resistance proteins: role of P-glycoprotein, MRP1, MRP2, and BCRP (ABCG2) in tissue defense. Toxicology and Applied Pharmacology 2005; 204:216-237.

36. Juliano RL and Ling V. Surface Glycoprotein Modulating Drug Permeability in Chinese-Hamster Ovary Cell Mutants. Biochimica et Biophysica Acta 1976; 455:152-162.

37. Bradley G, Juranka PF, Ling V. Mechanism of Multidrug Resistance. Biochimica et Biophysica Acta 1988; 948:87-128.

38.   Safa AR, Glover CJ, Meyers MB, Biedler JL, Felsted RL. Vinblastine Photoaffinity-Labeling of A High-Molecular-Weight Surface-Membrane Glycoprotein Specific for Multidrug-Resistant Cells. Journal of Biological Chemistry 1986; 261:6137-6140.

39.   Safa AR. Photoaffinity-Labeling of the Multidrug-Resistance-Related P-Glycoprotein with Photoactive Analogs of Verapamil. Proceedings of the National Academy of Sciences of the United States of America 1988; 85:7187-7191.

40.   Endicott JA and Ling V. The Biochemistry of P-Glycoprotein-Mediated Multidrug Resistance. Annual Review of Biochemistry 1989; 58:137-171.

41.   gross P., Raymond M., Bell J., Housman D. Cloning and characterization of a second member of the mouse mdr gene family. Mol Cell Biol 1988; 8:2770-2778.

42.   Silverman JA, Raunio H, Gant TW, Thorgeirsson SS. Cloning and Characterization of A Member of the Rat Multidrug Resistance (Mdr) Gene Family. Gene 1991; 106:229-236.

43.   Brown PC, Thorgeirsson SS, Silverman JA. Cloning and Regulation of the Rat Mdr2 Gene. Nucleic Acids Research 1993; 21:3885-3891.

44.   Thiebaut F, Tsuruo T, Hamada H, Gottesman MM, Pastan I, Willingham MC. Cellular-Localization of the Multidrug-Resistance Gene-Product P-Glycoprotein in Normal Human-Tissues. Proceedings of the National Academy of Sciences of the United States of America 1987; 84:7735-7738.

45.   Watanabe T, Miyauchi S, Sawada Y, Iga T, Hanano M, Inaba M et al. Kinetic-Analysis of Hepatobiliary Transport of Vincristine in Perfused-Rat-Liver - Possible Roles of P-Glycoprotein in Biliary-Excretion of Vincristine. Journal of Hepatology 1992; 16:77-88.

46.   Tanigawara Y, Okamura N, Hirai M, Yasuhara M, Ueda K, Kioka N et al. Transport of Digoxin by Human P-Glycoprotein Expressed in A Porcine Kidney Epithelial-Cell Line (Llc-Pk1). Journal of Pharmacology and Experimental Therapeutics 1992; 263:840-845.

47. Schinkel AH, Mol CAAM, Wagenaar E, Vandeemter L, Smit JJM, Borst P. Multidrug-Resistance and the Role of P-Glycoprotein Knockout Mice. European Journal of Cancer 1995; 31A:1295-1298.

48. Schinkel AH. Pharmacological insights from P-glycoprotein knockout mice. International Journal of Clinical Pharmacology and Therapeutics 1998; 36:9-13.

49. Tsuji A, Terasaki T, Takabatake Y, Tenda Y, Tamai I, Yamashima T et al. P-Glycoprotein As the Drug Efflux Pump in Primary Cultured Bovine Brain Capillary Endothelial-Cells. Life Sciences 1992; 51:1427-1437.

50. Tatsuta T, Naito M, Ohhara T, Sugawara I, Tsuruo T. Functional Involvement of P-Glycoprotein in Blood-Brain-Barrier. Journal of Biological Chemistry 1992; 267:20383-20391.

51. Wang Q, Yang H, Miller DW, Elmquist WF. Effect of the P-Glycoprotein Inhibitor, Cyclosporine-A, on the Distribution of Rhodamine-123 to the Brain - An In-Vivo Microdialysis Study in Freely Moving Rats. Biochemical and Biophysical Research Communications 1995; 211:719-726.

52. Liow JS, Lu SY, McCarron JA, Hong JS, Musachio JL, Pike VW et al. Effect of a P-glycoprotein inhibitor, cyclosporin A, on the disposition in rodent brain and blood of the 5-HT1A receptor radioligand, [C-11](R)-(-)-RWAY. Synapse 2007; 61:96-105.

53. Kiyono Y, Yamashita T, Doi H, Kuge Y, Katsura T, Inui KI et al. Is MIBG a substrate of P-glycoprotein? European Journal of Nuclear Medicine and Molecular Imaging 2007; 34:448-452.

54. Lee YJ, Maeda J, Kusuhara H, Okauchi T, Inaji M, Nagai Y et al. In vivo evaluation of P-glycoprotein function at the blood-brain barrier in nonhuman primates using [C-11]verapamil. Journal of Pharmacology and Experimental Therapeutics 2006; 316:647-653.

55. Hendrikse NH, Schinkel AH, De Vries EGE, Fluks E, Van der Graaf WTA, Willemsen ATM et al. Complete in vivo reversal of P-glycoprotein pump function in the blood-brain barrier visualized with positron emission tomography. British Journal of Pharmacology 1998; 124:1413-1418.

56. Hendrikse NH, Franssen EJ, Van der Graaf WTA, Vaalburg W, De Vries EGE. Visualization of multidrug resistance in vivo. European Journal of Nuclear Medicine 1999; 26:283-293.

57. Joseph B, Bhargava KK, Malhi H, Schilsky ML, Jain D, Palestro CJ et al. Sestamibi is a substrate for MDR1 and MDR2 P-glycoprotein genes. European Journal of Nuclear Medicine and Molecular Imaging 2003; 30:1024-1031.

58. Jain D. Technetium-99m labeled myocardial perfusion imaging agents. Seminars in Nuclear Medicine 1999; 29:221-236.

59. Elsinga PH, Hendrikse NH, Bart J, van Waarde A, Vaalburg W. Positron emission tomography studies on binding of central nervous system drugs and P-glycoprotein function in the rodent brain. Molecular Imaging and Biology 2005; 7:37-44.

60. Tamai I and Safa AR. Competitive Interaction of Cyclosporins with the Vinca Alkaloid-Binding Site of P-Glycoprotein in Multidrug-Resistant Cells. Journal of Biological Chemistry 1990; 265:16509-16513.

61. Newman MJ, Rodarte JC, Benbatoul KD, Romano SJ, Zhang CZ, Krane S et al. Discovery and characterization of OC144-093, a novel inhibitor of P-glycoprotein-mediated multidrug resistance. Cancer Research 2000; 60:2964-2972.

62. Sparreboom A, Planting AST, Jewell RC, Paul EM, Wissel PS, de Bruijn P et al. Clinical pharmacokinetics of doxorubicin in combination with GF120918, a potent inhibitor of MDR1 P-glycoprotein. Annals of Oncology 1998; 9:144-144.

63. Mistry P, Stewart AJ, Dangerfield W, Okiji S, Liddle C, Bootle D et al. In vitro and in vivo reversal of P-glycoprotein-mediated multidrug resistance by a novel potent modulator, XR9576. Cancer Research 2001; 61:749-758.

64. Kurdziel KA, Kiesewetter DO, Carson RE, Eckelman WC, Herscovitch P. Biodistribution, radiation dose estimates, and in vivo Pgp modulation studies of F-18-paclitaxel in nonhuman primates. Journal of Nuclear Medicine 2003; 44:1330-1339.

65. Kageyama M, Namiki H, Fukushima H, Ito Y, Shibata N, Takada K. In vivo effects of cyclosporin A and ketoconazole on the pharmacokinetics of representative substrates for P-glycoprotein and cytochrome P450 (CYP) 3A in rats. Biological & Pharmaceutical Bulletin 2005; 28:316-322.

Chapter 2

SEROTONERGIC NEUROTRANSMISSION

♋♋♋

2. SEROTONERGIC NEUROTRANSMISSION

2.1. Serotonin

Serotonin was first isolated from blood in 1948, and was called serotonin because of its vasoconstrictive properties. The molecule was later identified as 5-hydroxytryptamine (5-HT). Serotonin is a well-known neurotransmitter, and its presence was demonstrated in central nervous system (CNS) and in the periphery of the body. In the CNS, serotonin plays a major role in regulating mood, appetite, sleep, anxiety, aggression and sexual functions. In the blood serotonin plays a role in the blood clotting process. Smooth muscle cells in the gastro-intestinal tract are also influenced by serotonin.

Dysfunctions in the serotonergic neurotransmission system are involved in several pathologies of the central nervous system. It has been demonstrated that serotonergic neurotransmission malfunctioning is implicated in pathologies such as anorexia nervosa, aggression, anxiety, schizophrenia and depression[1].

The biosynthesis of serotonin starts from L-tryptophane, an amino acid present in our daily diet (figure 2.1). L-Tryptophane is actively transported into the neurons in the brain, where it is hydroxylated to 5-hydroxytryptophane. The enzyme responsible for this conversion is tryptophane 5-hydroxylase. 5-Hydroxytryptophane is decarboxylated by an amino acid decarboxylase to yield serotonin, or 5-hydroxytryptamine (5-HT).
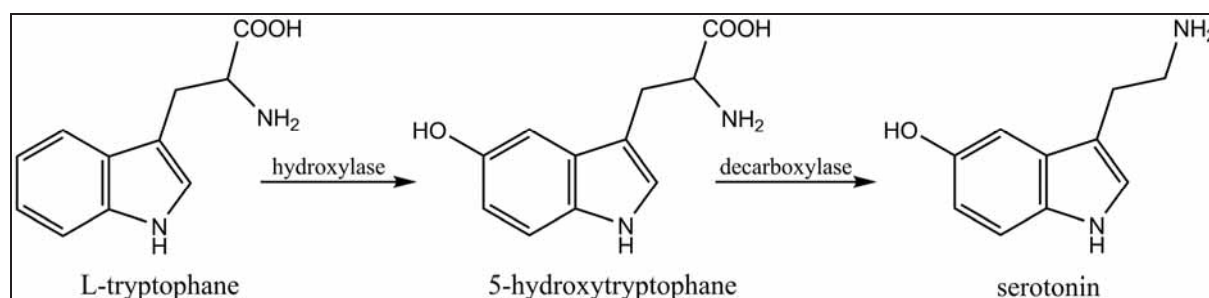
Figure 2.1: Biosynthesis of serotonin

Serotonin is stored in vesicles inside the neuron, which are transported into the synaps. After activation of the neuron, the vesicles fuse with the cell membrane and serotonin is released in the synaptic cleft.

Serotonin can be cleared from the synaptic cleft by re-uptake in the presynaptic neuron by a serotonin transporter, or it can be metabolised (figure 2.2) and removed from the body. The serotonin transporter recycles serotonin present in the synaptic cleft. It is actively pumped back into the presynaptic nerve terminal. Certain drugs (for example SSRI's) inhibit the function of the serotonin transporter, hereby increasing the amount of serotonin present in the synaptic cleft.

The most important pathways for metabolism of serotonin are shown in figure 2.2.
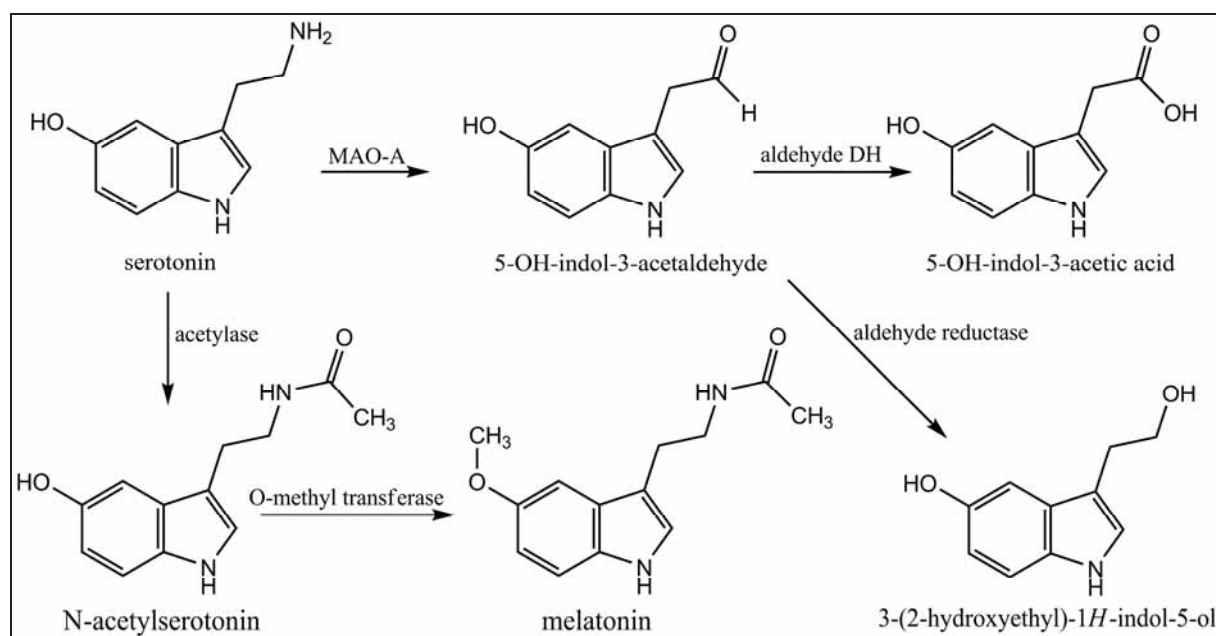
Figure 2.2: Main routes of serotonin metabolism.

The main enzyme responsible for the metabolism of serotonin is monoamineoxidase A (MAO A). Serotonin is transformed by MAO A to 5-hydroxyindol-3-acetaldehyde, which is further oxidised to 5-hydroxyindol-3-acetic acid by a aldehyde dehydrogenase enzyme. 5-Hydroxyindol-3-acetaldehyde can also be reduced to the corresponding alcohol, 3-(2-hydroxyethyl)-5-hydroxyindol, by a aldehyde reductase enzyme.

Serotonin can also be acetylated by an acetylase enzyme to N-acetylserotonin. N-Acetylserotonin can be methylated by an O-methyl transferase enzyme to yield melatonin, a hormone playing an important role in the regulation of the circadian rhythms of different biological functions.

2.2. The serotonergic system

The cell bodies of serotonergic neurons are located in the brain stem (figure 2.3).
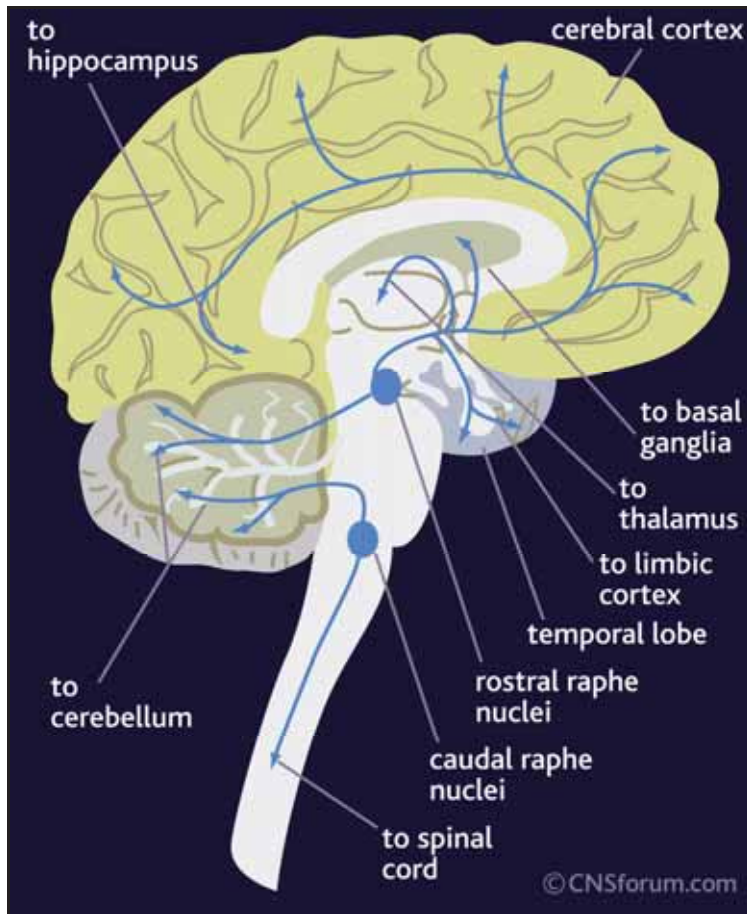
Figure 2.3: Serotonergic pathways in the brain[2]

There are two different serotonin pathways: the caudal and the rostral serotonergic pathway. The caudal pathway consists of serotonergic neurons with cell bodies located in the caudal raphe nuclei and caudal pons, and the axons projecting to the spinal cord. The cell bodies of serotonergic neurons in the rostral serotonergic pathway are located in the rostral raphe nuclei and have axons projecting to the limbic system (hippocampus, amygdala), basal ganglia (striatum and pallidum), hypothalamus, thalamus and cerebral cortex (figure 2.3). Serotonergic neurons in the hippocampus are known to be involved in the regulation of memory, serotonergic neurons in limbic areas such as the amygdala regulate mood.
The 5-HT neurons in the frontal cortex are responsible for cognition, memory and perception.

With the exception of the 5-HT$_3$ receptor, all serotonin receptors belong to the large family of G-protein coupled receptors (GPCR). These receptors are characterized by the presence of seven transmembrane helices, with the N-terminal located intracellular and the C-terminal located outside of the cell. The G-protein contains two functional units: the α-subunit and the βγ-subunit. The α-subunit has a large affinity for GDP, and shows GTP-ase activity. When the α-subunit is associated with GDP, the βγ-subunit is bound to the α-subunit. The GDP-αβγ-complex is the inactive form of the G-protein. The activation mechanism is shown in figure 2.4.
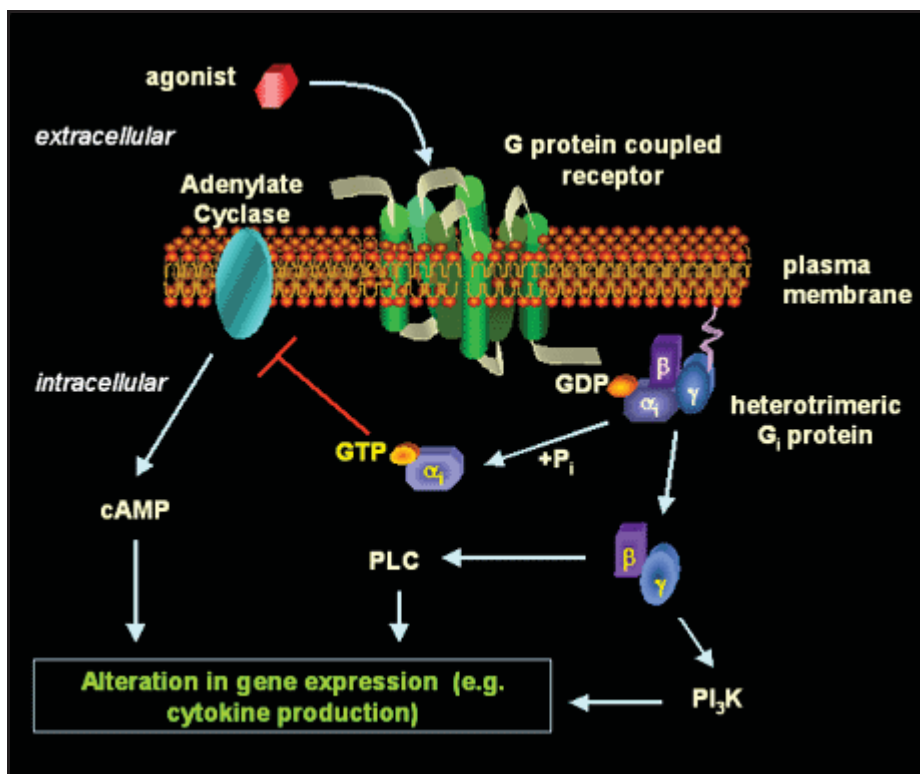
Figure 2.4: Mechanism of G-protein coupled receptor activation

Upon activation (by binding of serotonin or other 5-HT agonists to the receptor), the receptor conformation changes, resulting in the dissociation of the α-subunit from the receptor, GDP and the βγ-subunit, and association of the α-subunit with GTP. The activated α-subunit interacts with effector proteins (adenylate cyclase, phospholipase A and C) or ion channels. These effector proteins catalyse the production of second messenger molecules (cAMP, cGMP, DAG, IP$_3$), which in turn interact with ion channels or catalyse the production of mediating enzymes (protein kinase A and protein kinase C).

Phosphorylation of other enzymes by these protein kinases results in the biological effect of receptor activation. At the end of the cycle, the GTP-ase activity of the α-subunit is responsible for hydrolysis of the bound GTP to GDP. This hydrolysis results in dissociation of the α-GDP complex from the effector protein and re-association with the $\beta\gamma$-subunit.

G-protein coupled receptors generally have two 'states': a high affinity state and a low-affinity state. In the high affinity state, the receptor is coupled to the G-protein; in the low-affinity state, receptor and G-protein are not associated. Agonists only show affinity for the high-affinity state of a receptor, and can only bind to receptors coupled with the G-protein. Binding of the agonist results in dissociation of the receptor-G-protein complex, resulting in a drastically lowered affinity of the agonist for the receptor. This in turn causes dissociation of the agonist from the receptor. The affinity of antagonists for both receptor states is the same.

The 5-HT$_3$ receptor is not a GPCR, but rather a Na^+/K^+ ion channel, consisting of 5 individual units. Activation of the receptor leads to a rapid depolarisation of the neuron by an influx of Na^+ and Ca^{2+} and a K^+ efflux.

2.3. Serotonin receptors

Two types of serotonin receptors were discovered in 1957: the D- and the M-receptor type. The D-type receptor mediates the serotonin-induced contraction of smooth muscle cells. The M-type receptor mediates the serotonin-induced release of acetylcholine by the nerve terminals[3].

Receptor	Location	Agonist	Antagonist	Transduction	Sec. Messenger
5-HT$_{1A}$	Hippocampus Raphe nuclei	8-OH-DPAT	WAY100635	G$_{i/0}$	cAMP ↓
5-HT$_{1B}$	Striatum Hippocampus Olf. tubercle	CP931259589	SB224289	G$_{i/0}$	cAMP ↓
5-HT$_{1D}$	Raphe nuclei Subst. Nigra Globus pallidus	L694247	GR127935	G$_{i/0}$	cAMP ↓
5-ht$_{1E}$	Subst. nigra Globus pallidus	/	/	G$_{i/0}$	cAMP ↓
5-ht$_{1F}$	Hippocampus Fr. Cortex Raphe nuclei	/	/	G$_{i/0}$	cAMP ↓
5-HT$_{2A}$	Frontal cortex Olf. Tubercle Blood platelets	DOI	Ketanserin	G$_{q/II}$	IP$_3$/DAG ↑
5-HT$_{2B}$	Periphery	BW 723C86	SB204741	G$_{q/II}$	IP$_3$/DAG ↑
5-HT$_{2C}$	Choroid plexus Subst. Nigra Globus pallidus	Ro 60-0175	SB 242084	G$_{q/II}$	IP$_3$/DAG ↑
5-HT$_3$	Hippocampus Trig. Nucleus	m-CPBG	Granisetron		Na$^+$ ↑, K$^+$ ↓
5-HT$_4$	Olf. Tubercle Striatum Globus pallidus Subst. Nigra	Cisapride	GR113808	G$_s$	cAMP ↑
5-ht$_{5A}$	Hippocampus Hypothalamus	/	/	G$_s$?	
5-ht$_{5B}$	Hippocampus	/	/	unknown	
5-ht$_6$	Striatum Hippocampus Olf. Tubercle Frontal cortex	5-CT	/	G$_s$	cAMP ↑
5-HT$_7$	Hippocampus Thalamus	5-CT	SB258719	G$_s$	cAMP ↑

Table 2.1: Serotonin receptor classification and characteristic properties, adapted[4].

Many different (sub)types of serotonin receptors have been found in the human body. At present, the serotonin receptors are divided into seven classes, based on their structural, transductional and operational properties[1].

An overview of all serotonin receptors with their location, transduction and second messenger systems and an example of an agonist and antagonist at each receptor is given in table 2.1.

Receptor type and subtype, receptor structure, signal transduction, second messenger systems and localisation in the brain will be discussed in detail.

Many other neurotransmitter systems are present in the human body (a.o. noradrenalin, dopamine, GABA, acetylcholine, etc). Although their function is equally important, a discussion of these receptors falls outside the scope of this thesis. Other receptor types will not be discussed.

In 1986 the existence of three 5-HT receptor families, $5-HT_{1-3}$ (comprising five receptors/binding sites in total), was acknowledged, although more were suspected. At that time the function of individual 5-HT receptor subtypes in the brain was largely unclear. The application of molecular biological techniques has had a major impact on the 5-HT field, allowing the discovery of many additional 5-HT receptors[1]. Since 1986, the number of recognised mammalian 5-HT receptor subtypes in the CNS has more than doubled to 14, and these have been classified into seven receptor families ($5-HT_{1-7}$) on the basis of their structural, functional and to some extent pharmacological characteristics[5, 6].

The 5-HT receptor family are mostly seven putative transmembrane spanning, G-protein coupled metabotropic receptors, but one member of the family, the $5-HT_3$ receptor, is a ligand-gated ion channel. In the brain the function of many 5-HT receptors can now be equivocally associated with specific physiological response, ranging from modulation of neuronal activity and transmitter release to behavioural change.

Much effort has been directed towards understanding the function attributable to individual 5-HT receptors in the brain. This has been helped by the synthesis of a number of compounds that selectively interact with individual 5-HT receptor subtypes – although some 5-HT receptors still lack any selective ligands (e.g. $5-HT_{1E}$, $5-HT_{5A}$ and $5-HT_{5B}$ receptors).

In this chapter we will briefly discuss the serotonin receptor family, focussing particularly on the receptor of interest in this thesis, the serotonin $5-HT_{2A}$ receptor.

2.3.1. The 5-HT$_1$ receptors

The initial characterisation of the 5-HT$_1$ receptor family originated from radioligand binding studies which found high affinity binding sites for tritiated serotonin in rat cortex with low affinity for spiperone[7]. Subsequent studies identified further heterogeneity within the [^{3}H]-5-HT site, which initially accounted for the 5-HT$_{1A}$ and 5-HT$_{1B}$ receptors, and subsequently the 5-HT$_{1C}$ (now 5-HT$_{2C}$), 5-HT$_{1D}$ (now recognised as a combination of the species variant of the 5-HT$_{1B}$ receptor and the closely related 5-HT$_{1D}$ receptor), 5-HT$_{1E}$ and 5-HT$_{1F}$ receptors[1].

	1A	1B	1D	1E	1F	2A	2B	2C	3As	4	5A	5B	6	7
1A	100													
1B	43	100												
1D	43	63	100											
1E	40	48	48	100										
1F	42	49	49	57	100									
2A	31	31	29	34	32	100								
2B	35	27	27	30	29	45	100							
2C	32	28	30	32	33	51	42	100						
3As	≪10%[b]	≪10%[b]	≪10%[b]	≪10%[b]	≪10%[b]	≪10%[b]	≪10%[b]	≪10%[b]	100					
4	29	32	31	31	34	28	28	28	≪10%[b]	100				
5A	35	35	36	36	37	25	26	28	≪10%[b]	33	100			
5B	38	34	34	34	35	27	29	29	≪10%[b]	29	69	100		
6	34	31	32	32	32	28	27	27	≪10%[b]	27	30	32	100	
7	38	37	38	39	38	28	28	28	≪10%[b]	32	32	34	33	100

[a] The percentages were created using the algorithm of Needleman and Wunsch (1970) to find the alignment of two complete sequences that maximises the number of matches and minimises the number of gaps (GCG package, Genetics Computer Group, Inc.). Sequences as for Fig. 1.
[b] Due to the low percent amino acid identity, the program was unable to align the 5-HT$_{3As}$ receptor with the other 5-HT receptor sequences.

Table 2.2: Comparison of the percentage amino acid identity between the different human 5-HT receptor subtypes[1]

Old nomenclature		New nomenclature
Receptor	Species	
5-HT$_{1B}$	Rat	5-HT$_{1B}$[a]
5-HT$_{1D}$	Human, guinea pig	
5-HT$_{1Dβ}$	All species	
5-HT$_{1Dα}$	All species	5-HT$_{1D}$
5-HT$_2$	All species	5-HT$_{2A}$
5-HT D		
5-HT$_{2F}$	All species	5-HT$_{2B}$
5-HT$_{1C}$	All species	5-HT$_{2C}$

[a] Species equivalent, e.g. r5-HT$_{1B}$ for rodents and h5-HT$_{1B}$ for humans.

Table 2.3: Summary of recent important changes in 5-HT receptor nomenclature[1]

From table 2.2 it can be concluded that all receptors of the 5-HT$_1$ family have a high degree of amino acid sequence homology. All couple negatively to adenylate cyclase via G-proteins. Recent changes in 5-HT receptor nomenclature are indicated in table 2.3.

2.3.1.1. The 5-HT$_{1A}$ receptor

The first selective 5-HT$_{1A}$ receptor agonist that was discovered was 8-OH-DPAT. The synthesis of tritiated [^{3}H]-8-OH-DPAT and its application in *in vitro* assays provided the first pharmacological profile of the 5-HT$_{1A}$ binding site[8]. Buspirone and a series of structurally related 5-HT$_{1A}$ ligands had an anxiolytic and antidepressant effect when used in patients[9].

The 5-HT$_{1A}$ receptor was the first receptor to be fully sequenced and cloned, and it is perhaps the most extensively studied receptor, the main reason being the availability of the selective agonist 8-OH-DPAT that has allowed extensive biochemical, physiological and pharmacological receptor characterization. The distribution of the 5-HT$_{1A}$ receptor in brain has been mapped extensively by receptor autoradiography using a range of ligands including [^{3}H]-5-HT, [^{3}H]-8-OH-DPAT, [^{3}H]-ipsapirone and more recently [^{125}I]-p-MPPI and [^{3}H]-WAY100635. PET studies with [^{11}C]-WAY100635 have also been used to visualize 5-HT$_{1A}$ receptors in the living human brain[10].

The density of 5-HT$_{1A}$ binding sites is high in limbic brain areas, notably hippocampus, lateral septum, cortical areas (particularly cingulate and entorhinal cortex), and also the mesencephalic raphe nuclei (both dorsal and median raphe nuclei). In contrast, levels of 5-HT$_{1A}$ binding sites in the basal ganglia and cerebellum are barely detectable[1]. The distribution of mRNA encoding the 5-HT$_{1A}$ receptor is almost identical to that of the 5-HT$_{1A}$ binding site[11].

5-HT$_{1A}$ receptors are located both postsynaptic to 5-HT neurons (in forebrain regions), and also on the 5-HT neurons themselves at the level of the soma and dendrites in the mesencephalic and medullary raphe nuclei. At the cellular level, the presence of 5-HT$_{1A}$ receptors was demonstrated in cortical pyramidal neurons as well as pyramidal and granular neurons of the hippocampus[11]. In addition, the 5-HT$_{1A}$ receptor is expressed in serotonin-containing neurons in the raphe nuclei, cholinergic neurons in the septum and probably glutamergic neurons in cortex and hippocampus[12]. A recent detailed study of the ultrastructural location of the 5-HT$_{1A}$ receptor reports evidence that the receptor is present both at synaptic membranes and extrasynaptically[13].

Selective 5-HT$_{1A}$ receptor agonists include 8-OH-DPAT, dipropyl-5-CT and gepirone. Recently a number of 'silent' 5-HT$_{1A}$ receptor antagonists have been developed. These include WAY 100135, WAY 100635 and NAD-299.

The 5-HT$_{1A}$ receptor couples negatively via G-proteins (α_i) to adenylate cyclase in both rat and guinea pig hippocampal tissue and cell-lines stably expressing the cloned 5-HT$_{1A}$ receptor[14]. Electrophysiological experiments have established that 5-HT$_{1A}$ receptor activation causes neuronal hyperpolarisation, an effect mediated through the G-protein coupled opening of K$^+$ channels, and without the involvement of diffusible intracellular messengers such as cAMP[15]. The 5-HT$_{1A}$ receptor is reported to induce the secretion of a growth factor (protein S-100) from primary astrocyte cultures[16] and increase markers of growth in neuronal cultures[17].

Microdialysis studies have shown that 5-HT$_{1A}$ receptor agonists induce a fall in release of 5-HT in the forebrain of the rat *in vivo*, an effect which involves activation of the 5-HT$_{1A}$ autoreceptor. Many 5-HT$_{1A}$ receptor agonists cause a fall in 5-HT output, and these effects are blocked by selective 5-HT$_{1A}$ receptor antagonists[18].

8-OH-DPAT increases the release of acetylcholine in the cortex and hippocampus of guinea pigs and rats[19]. This effect is blocked by both selective (WAY100635) and non-selective (propanolol) 5-HT$_{1A}$ receptor antagonists[19] and appears to involve postsynaptic 5-HT$_{1A}$ receptors[20].

Level	Response	Mechanism
Cellular	Adenylate cyclase ($-$)	Post
Electrophysiological	Hyperpolarisation	Post
Behavioural	5-HT syndrome	Post
	Hypothermia	Pre/post
	Hyperphagia	Pre
	Anxiolysis	Pre/post
	Sexual behaviour ($+$)	Pre/post
	Discriminative stimulus	Pre/post
Neurochemical	5-HT release ($-$)	Pre
	Noradrenaline release ($+$)	Post
	Acetylcholine release ($+$)	Post
	Glutamate release ($-$)	?
Neuroendocrine	ACTH ($+$)	Post
	Prolactin ($+$)	Post

Table 2.4: Functional responses associated with activation of the central 5-HT$_{1A}$ receptor[1]

8-OH-DPAT increases the release of noradrenalin in many brain areas including the hypothalamus, hippocampus, frontal cortex and ventral tegmental area[21].

This effect is blocked by WAY100635. Other 5-HT$_{1A}$ ligands also increase noradrenalin, including buspirone and NAN-190[21].

In rats, administration of 8-OH-DPAT and other 5-HT$_{1A}$ receptor agonists causes a wide range of behavioural and physiological effects including hyperphagia, hypothermia, altered sexual behaviour and a tail flick response. A large amount of basic and clinical data attesting to the anxiolytic and antidepressant activity of 5-HT$_{1A}$ receptor agonists can be found in literature[22].

Further functional responses associated with activation of the central 5-HT$_{1A}$ receptor can be found in table 2.4 and will not be discussed further.

2.3.1.2. The 5-HT$_{1B}$ receptor

The 5-HT$_{1B}$ binding site was found in high levels in rodents (rats, mouse, hamster). The nomenclature for serotonin receptor classification was changed recently. This nomenclature change recognised that despite differing pharmacology, the human 5-HT$_{1D\beta}$ receptor is a species equivalent of the rodent 5-HT$_{1B}$ receptor. Therefore, the 5-HT$_{1D\beta}$ receptor was realigned to the 5-HT$_{1B}$ classification[23].

Autoradiographic studies using [^{3}H]-5-HT (in the presence of 8-OH-DPAT) demonstrate a high density of 5-HT$_{1B}$ sites in the rat basal ganglia (particularly the substantia nigra, globus pallidus, ventral pallidum and entopeduncular nucleus), but also many other regions[24].

The 5-HT$_{1B}$ receptors are located presynaptically and postsynaptically relative to the 5-HT neurons. Overall, the anatomical location of the 5-HT$_{1B}$ receptor provides strong evidence to support the idea that the 5-HT$_{1B}$ receptor has a role as both a 5-HT autoreceptor and 5-HT heteroreceptor, i.e. controlling neurotransmitter release.

A large number of ligands with high affinity for the 5-HT$_{1B}$ receptor is available, but most are not selective. The most difficult problem at present is discriminating between human 5-HT$_{1B}$ and 5-HT$_{1D}$ receptors.

The 5-HT$_{1B}$ receptor couples negatively to adenylate cyclase[25]. A number of compounds (for example ketanserin) demonstrate inverse agonist properties for the 5-HT$_{1B}$ receptor.

There is convincing evidence that the 5-HT$_{1B}$ receptor functions as a 5-HT autoreceptor: 5-HT$_{1B}$ agonists inhibit the release of serotonin from the 5-HT nerve terminals.

In some brain regions, the 5-HT$_{1B}$ receptor is transported to the nerve terminals and functions as a 5-HT heteroreceptor (i.e. a modulatory receptor located on non-5-HT terminals)[26]. Clear functional evidence of a heteroreceptor role for the 5-HT$_{1B}$ receptor comes from electrophysiological studies[27].

Level	Response	Mechanism
Cellular	Adenylate cyclase (−)	Post
Electrophysio-logical	Inhibition of evoked synaptic potentials	Pre (heteroceptor)
Behavioural	Locomotion/rotation (+)	Post
	Hypophagia	Pre
	Hypothermia (g. pig)	?
	Myoclonic jerks (g. pig)	?
Neurochemical	5-HT release (−)	Pre (autoreceptor)
	Acetylcholine release (−)	Pre (heteroceptor)

Table 2.5: Functional responses associated with activation of the brain 5-HT$_{1B}$ receptor[1]

There is evidence in mice that activation of the 5-HT$_{1B}$ receptor has a locomotor stimulant effect. The locomotor activating effects of for example the illicit drug MDMA may also be mediated via activation of the postsynaptic 5-HT$_{1B}$ receptor[28]. Other behavioural and physiological effects of activation of the central 5-HT$_{1B}$ receptor are shown in table 2.5 and include increased corticosterone and prolactin secretion, hypophagia and hypothermia. For example, 5-HT$_{1B}$ knock-out mice are more aggressive towards intruders then the wild-type mice.

2.3.1.3. The 5-HT$_{1D}$ receptor

The distribution of the 5-HT$_{1D}$ receptor has been difficult to determine because levels appear to be very low, and there is a lack of selective radioligands able to discriminate this receptor from the 5-HT$_{1B}$ receptor. Receptor autoradiographic studies in rats utilising [^{125}I]-GTI suggest that the 5-HT$_{1D}$ site is present in various regions but especially the basal ganglia (particularly the globus pallidus, substantia nigra and caudate putamen) and also the hippocampus and cortex[26]. A recent study in human brain revealed the presence of 5-HT$_{1D}$ receptors in the basal ganglia (globus pallidus and substantia nigra) as well as specific regions of the midbrain (periaqueductal grey) and spinal cord[29].

The human 5-HT$_{1D}$ and 5-HT$_{1B}$ receptors have drug binding profiles that are almost indistinguishable[14]: many of the ligands with high affinity for the 5-HT$_{1B}$ binding site also have high affinity for the 5-HT$_{1D}$ binding site. Ketanserin and ritanserin have some selectivity (15 – 30 fold) for the 5-HT$_{1D}$ receptor.

As of yet no second messenger response can be safely attributed to the 5-HT$_{1D}$ receptor expressed in native tissue.

The 5-HT$_{1D}$ receptor, like the 5-HT$_{1B}$ receptor, is located presynaptically on both 5-HT and non-5-HT neurons. There are several reports suggesting that the 5-HT$_{1D}$ receptor may have a 5-HT autoreceptor role in both the raphe nuclei and serotonergic nerve terminal regions. Some studies reported the 5-HT$_{1D}$ autoreceptor to actually be the 5-HT$_{1B}$ receptor instead. The presence of a 5-HT$_{1D}$ autoreceptor in brain remains a possibility although such a receptor may be restricted to some brain regions and/or be present amongst higher levels of 5-HT$_{1B}$ autoreceptors. There is limited functional data regarding a possible heteroreceptor role for the 5-HT$_{1D}$ receptor that certain anatomical data suggest. As yet no *in vivo* functional response can be safely ascribed to activation of the 5-HT$_{1D}$ receptor in the central nervous system. The most important problem is the lack of selective ligands that can discriminate between the 5-HT$_{1B}$ and the 5-HT$_{1D}$ receptor. Also, the very low levels of 5-HT$_{1D}$ receptors in human brain present a problem.

2.3.1.4. The 5-HT$_{1E}$ receptor

The human gene encoding for the 5-HT$_{1E}$ receptor was isolated in 1992[30]. Autoradiographic studies have revealed that in all species, high levels of 5-HT$_{1E}$ receptors were present in the cortex (particularly entorhinal cortex), caudate putamen and claustrum. Detectable levels were found in other areas, including hippocampus and amygdala.

Currently, there are no 5-HT$_{1E}$ receptor selective ligands available[1]. The 5-HT$_{1E}$ receptor is characterized by its high affinity for serotonin and lower affinity for 5-CT. A relative low affinity for sumatriptan sets it apart from the 5-HT$_{1F}$ binding site.

Little is known about the physiological role of the 5-HT$_{1E}$ receptor and its effects on neurons, although in expression systems the human 5-HT$_{1E}$ receptor has been shown to mediate a modest inhibition of adenylate cyclase[31].

<u>2.3.1.5. The 5-HT$_{1F}$ receptor</u>

The structural characteristics of the 5-HT$_{1F}$ receptor are similar to those of other members of the 5-HT$_1$ receptor family (e.g. intronless, seven transmembrane spanning regions), and the receptor has a high degree of homology with the 5-HT$_{1B}$, 5-HT$_{1D}$ and 5-HT$_{1E}$ receptors[32]. The distribution of 5-CT-insensitive [^{3}H]-sumatriptan binding sites demonstrates a very good correlation with the distribution of 5-HT$_{1F}$ mRNA in the guinea pig[26], with the highest levels of binding in cortical and hippocampal areas, claustrum and caudate nucleus. Although the receptor is located in parts of the basal ganglia, in contrast to 5-HT$_{1B}$ and 5-HT$_{1D}$ binding sites, 5-HT$_{1F}$ binding sites appear to be barely detectable in the substantia nigra[33], and generally the 5-HT$_{1F}$ receptor has a low abundance with a restricted distribution in the brain.

The high affinity for sumatriptan discriminates the 5-HT$_{1F}$ receptor from the 5-HT$_{1E}$ receptor. Recently, selective agonists for the 5-HT$_{1F}$ receptor have been synthesized[34].

The cloned human and mouse 5-HT$_{1F}$ receptors couple negatively to adenylate cyclase[32]. On the basis of its anatomical location, it is speculated that the 5-HT$_{1F}$ receptor plays a role in visual and cognitive function and as a serotonergic autoreceptor[33]. Initial studies with a novel 5-HT$_{1F}$ receptor agonist, LY334370, suggest that it does not evoke overt behavioural effects when administered to rats[35, 36].

2.3.2. The 5-HT$_2$ receptor family

The 5-HT$_2$ receptor family currently includes three receptor subtypes (5HT$_{2A}$, 5-HT$_{2B}$ and 5-HT$_{2C}$ receptors) which are similar in terms of molecular structure, pharmacology and signal transduction pathways. The amino acid sequences of the 5-HT$_2$ receptor family have a high degree of homology within the seven transmembrane domains but they are structurally distinct from other 5-HT receptors[37]. All genes in the 5-HT$_2$ receptor family have either two or three introns in the coding sequence[38], and all are coupled positively to phospholipase C and receptor activation results in mobilisation of intracellular calcium. Affinities of various ligands for the 5-HT$_2$ receptor family are shown in table 2.6.

	5-HT$_{2A}$	5-HT$_{2B}$	5-HT$_{2C}$
5-HT$_{2A}$ receptor			
Spiperone	8.8	5.5	5.9
MDL 100 907	9.4	n.d.	6.9
Ketanserin	8.9	5.4	7.0
5-HT$_{2B}$ receptor			
5-MeOT	7.4[a]	8.8[a]	6.2[a]
a-Methyl-5-HT	6.1[a]	8.4[a]	7.3[a]
SB 2044741	<5.3	7.8	<6.0
BW 723C86	<5.4[a]	7.9[a]	<6.9
5-HT$_{2C}$ receptor			
SB 242084	6.8	7.0	9.0
RS–102221	6.0	6.1	8.4
RO 60-0175	6.0	5.8	8.8
5-HT$_{2B/2C}$ receptors			
SB 200646A	5.2	7.5	6.9
mCPP	6.7	7.4[a]	7.8
SB 206553	5.8	8.9	7.9
Non-selective			
LY 53857	7.3	8.2	8.1
ICI 170809	9.1	n.d.	8.3
Ritanserin	8.8	8.3	8.9
Mianserin	8.1	7.3	8.0
DOI	7.3[a]	7.4[a]	7.8[a]

[a] pEC$_{50}$ value for agonist. 5-MeOT, 5-methoxytryptamine; n.d., not determined. Data were taken from Baxter et al. (1995) with additions from Bonhaus et al. (1997), Millan et al. (1997) and Kennett et al. (1996a,b, 1997a,b).

Table 2.6: Affinity (pK$_i$) of various ligands for the 5-HT$_2$ receptor family[1]

Some 5-HT$_2$ antagonists are currently undergoing clinical assessment as potential treatment for a range of central nervous system disorders including schizophrenia, anxiety, sleep and feeding disorders and migraine[37].

2.3.2.1. The 5-HT$_{2A}$ receptor

The central 5-HT$_{2A}$ receptor was initially detected in rat cortical membranes as a binding site with high affinity for [^{3}H]-spiperone[39, 7]. The human 5-HT$_{2A}$ receptor is located on chromosomes 13q14-q21 and has a relatively high amino acid sequence identity with the 5-HT$_{2C}$ receptor. The human 5-HT$_{2A}$ receptor is 87% homologous with its rat counterpart.

Receptor autoradiography studies using [^{3}H]-spiperone or [^{3}H]-ketanserin revealed high levels of 5-HT$_{2A}$ binding sites in many forebrain regions, but particularly cortical areas (neocortex, entorhinal and pyriform cortex, claustrum), caudate nucleus, nucleus accumbens, olfactory tubercle and hippocampus, in all species studied[24].

Various studies have investigated the cellular location of the 5-HT$_{2A}$ receptor in the brain. 5-HT$_{2A}$ mRNA has been found in neurons. In different brain locations, including the cortex, the 5-HT$_{2A}$ receptor is located on local (GABAergic) interneurons[40]. Recent data also indicate the presence of 5-HT$_{2A}$ receptors in cortical pyramidal (projection) neurons[40], which are known to be glutamergic. It is reported that 5-HT$_{2A}$ receptor-like immunoreactivity may be located in cholinergic neurons in the basal forebrain and specific nuclei in the brain stem[41].

A number of selective antagonists are available which greatly aid the delineation of the 5-HT$_2$ receptors in both *in vitro* and *in vivo* models (see table 2.6). MDL100907 is a newly developed, potent and selective antagonist of the 5-HT$_{2A}$ receptor which has lower affinity for the 5-HT$_{2C}$ receptors or other receptors[42].

All three 5-HT$_2$ receptor subtypes couple positively to phospholipase C and lead to an increased accumulation of inositol phosphate and intracellular Ca^{2+}[14]. Stimulation of the 5-HT$_{2A}$ receptor activates phospholipase C in brain tissue via G-protein coupling[43]. The hallucinogenic drugs DOI, DOB, DOM and LSD, have partial agonist properties at the 5-HT$_{2A}$ receptor. All 5-HT$_2$ receptors desensitize following prolonged exposure to serotonin and other agonists, although the sensitivity to agonists and mechanisms underlying desensitisation of each subtype (particularly 5-HT$_{2A}$ versus 5-HT$_{2C}$) may be different[44, 45].

Of current interest is evidence that stimulation of the 5-HT$_{2A}$ receptor causes activation of a biochemical cascade leading to altered expression of a number of genes including that of brain-derived neurotrophic factor (BDNF)[46]. These changes may be linked at least in part to the increase in expression of BDNF seen following repeated treatment with antidepressants[47, 48].

5-HT$_2$ receptor activation results in neuronal excitation in a variety of brain regions. Clear evidence for a 5-HT$_{2A}$ receptor mediated excitation in the cortex comes from intracellular recordings of interneurons in slices of rat pyriform cortex. 5-HT induced neuronal depolarisations have also been detected in slice preparations of the nucleus accumbens, neocortex, hippocampus, and all have the pharmacological characteristics of 5-HT$_{2A}$ receptor activation[1]. The excitatory responses to 5-HT$_{2A}$ receptor activation are associated with a reduction of potassium conductances[49]. Activation of the 5-HT$_{2A}$ receptor has an inhibitory effect on noradrenergic transmission. There is evidence from microdialysis studies in the awake rat that 5-HT$_{2A}$ receptor antagonists increase noradrenalin release[21]. The effects of 5-HT$_2$ receptor activation on noradrenergic neurons are likely to be indirect, possibly involving afferents to the locus coeruleus from the brain stem[49].

Level	Response	Mechanism
Cellular	Phosphatidyl inositide turnover (+)	Post
Electrophysio-logical	Neuronal depolarisation	Post
Behavioural	Head twitch (mouse)	Post
	Wet dog shake (rat)	Post
	Hyperthermia	Post
	Discriminative stimulus	Post
Neurochemical	Noradrenaline release (−)	Post
Neuroendocrine	Cortisol	Post
	ACTH	Post

Table 2.7: Functional responses associated with activation of the central 5-HT$_{2A}$ receptor[1]

Different behavioural effects of 5-HT$_{2A}$ receptor activation are shown in table 2.7. Head twitches (in mice) and wet dog shakes (rats) induced by drugs such as DOI are mediated by the 5-HT$_{2A}$ receptor (5-HT$_{2A}$ selective antagonists such as MDL100907 inhibit the head shake response while 5-HT$_{2B/2C}$ receptor selective antagonists do not[50]).

Activation of the 5-HT_{2A} receptor leads to a discriminative stimulus in rats. For example, animals trained to discriminate 5-HT_2 receptor agonists such as DOM, recognize its structural derivatives (DOI, DOB) but not 5-HT_1 receptor agonists.

An agonist action at 5-HT_2 receptors is likely to be involved in the mechanism of action of hallucinogenic drugs since there is a close correlation between the human hallucinogenic potency of 5-HT_2 receptor agonists and their affinity for the 5-HT_2 binding sites[51]. Currently, there is considerable interest in the role of the 5-HT_{2A} receptor in antipsychotic drug action.

Other responses to 5-HT_2 receptor agonists that may be mediated by the 5-HT_{2A} receptor include hyperthermia and neuroendocrine responses such as increased secretion of cortisol, ACTH, renin and prolactin[52] (see table 2.7).

2.3.2.2. The 5-HT_{2B} receptor

The human 5-HT_{2B} receptor (481 amino acids) is relatively homologous with the human 5-HT_{2A} and 5-HT_{2C} receptors. The distribution of the 5-HT_{2B} receptor in brain is very limited (relative to 5-HT_{2A} and 5-HT_{2C} receptors) but potentially of functional importance. Its distribution in rat brain is restricted to a few brain regions, particularly cerebellum, lateral septum, hypothalamus and amygdala.

As expected from the homologous sequences of the 5-HT_2 receptor family, the receptor binding properties of the human 5-HT_{2B} receptor compare well with those of the 5-HT_{2A} and 5-HT_{2C} receptors. For instance, the 5-HT_{2B} receptor has a low affinity for ritanserin but higher affinity for yohimbine than either the 5-HT_{2A} or 5-HT_{2C} receptor. The novel antagonist SB204741 is more than 20-60-fold more selective for the 5-HT_{2B} receptor versus the 5-HT_{2A}, 5-HT_{2C} and other receptors at which it has been tested[53, 37]. The affinity of a variety of ligands for the different 5-HT_2 receptor subtypes is shown in table 2.6.

Limited data are available regarding the functional effects of activation of the central 5-HT_{2B} receptor. It is thought that the native 5-HT_{2B} receptors in brain couple to phosphatidylinositol hydrolysis, a feature it has in common with the other two members of the 5-HT_2 receptor family. But this still needs to be proven for the 5-HT_{2B} receptor. Also, the 5-HT_{2B} receptor may play a role in anxiety[54].

2.3.2.3.The 5-HT$_{2C}$ receptor

The human 5-HT$_{2C}$ receptor is located on chromosome Xq24, and the 5-HT$_{2C}$ receptor gene has three introns. There is a high sequence homology with the mouse, rat and human 5-HT$_{2C}$ receptors (> 80% in the transmembrane regions)[1].

There is little evidence for expression of the 5-HT$_{2C}$ receptor outside of the central nervous system. In addition to the very high levels detected in the choroid plexus, 5-HT$_{2C}$ binding sites are widely distributed and present in areas of the cortex (olfactory nucleus, pyriform, cingulate and retrosplenial), limbic system (nucleus accumbens, hippocampus, amygdala) and the basal ganglia (caudate nucleus, substantia nigra). The 5-HT$_{2C}$ receptor is located postsynaptically.

Most 5-HT$_2$ ligands do not discriminate sufficiently between the different 5-HT$_2$ receptor subtypes. A number of atypical and typical antipsychotic agents (including clozapine and chlorpromazine) have a relative high affinity for 5-HT$_{2C}$ binding sites, as do some conventional and atypical antidepressants (e.g. tricyclics, trazodone)[55].

Activation of the 5-HT$_{2C}$ receptor increases phospholipase C activity in choroid plexus of various species[43] and stably transfected cells via a G-protein coupled mechanism[14]. 5-HT$_{2C}$ receptors, in common with 5-HT$_{2A}$ receptors, also down-regulate in response to chronic exposure to both agonists and antagonists, which could in part relate to apparent inverse agonist properties[56].

Several behavioural responses have been associated with activation of central 5-HT$_{2C}$ receptors. These include hypolocomotion, hypophagia, anxiety, penile erections and hyperthermia[57]. Behavioural and other physiological responses of activation of the 5-HT$_{2C}$ receptor are shown in table 2.8.

Level	Response	Mechanism
Cellular	Phosphatidyl inositide turnover (+)	Post
Electrophysio-logical	Neuronal depolarisation	Post
Behavioural	Hypolocomotion	Post
	Hypophagia	Post
	Anxiogenesis	Post
	Penile erection	Post
Neurochemical	Noradrenaline/Dopamine release (−)	Post

Table 2.8: Functional responses associated with activation of the central 5-HT$_{2C}$ receptor[1]

When administered alone, 5-HT$_{2C}$ receptor antagonists are anxiolytic in various animal models[58].

2.3.3. The 5-HT$_3$ receptor

Contrary to the other serotonin receptor subtypes, the 5-HT$_3$ receptor is a ligand-gated ion-channel[59] which is comprised of multiple subunits. The ion channel is cation selective (with near equal permeability to both Na$^+$ and K$^+$) and is prone to rapid desensitization.

Highest levels of 5-HT$_3$ receptor binding sites are found within the dorsal vagal complex in the brainstem[60]. This region comprises the nucleus tractus solitarius, area postrema and dorsal motor nucleus of the vagus nerve which are intimately involved in the vomiting reflex; antagonism of 5-HT$_3$ receptors in these nuclei is likely to contribute to the anti-emetic effect of 5-HT$_3$ antagonists. 5-HT$_3$ receptor expression in the forebrain is low. Highest levels are expressed in regions such as the hippocampus, amygdala and superficial layers of the cerebral cortex.

Different ligands interact selectively with the 5-HT$_3$ receptor (e.g. antagonists granisetron, ondansetron and tropisetron). In addition to the 5-HT binding site, the 5-HT$_3$ receptor possesses additional pharmacologically distinct sites which mediate allosteric modulation of the receptor complex. For instance, electrophysiological data demonstrate that both ethanol and the active metabolite of chloral hydrate, trichloroethanol, increase the potency with which agonists activate the 5-HT$_3$ receptor complex[61].

Originally, 5-HT$_3$ receptor antagonists generated much optimism in the search for novel psychotropic agents. 5-HT$_3$ receptor antagonists were forwarded as potential therapeutic agents for a number of CNS disorders including anxiety, cognitive dysfunction and psychosis[1]. However, most of the clinical reports do not substantiate the predicted efficacy from the preclinical investigations.

Behavioural, neurochemical and electrophysiological investigations indicate that the 5-HT$_3$ receptor modulates dopaminergic neuron activity in the brain. 5-HT$_3$ receptor antagonists prevent the behavioural hyperactivity following an increase in extracellular dopamine levels in the nucleus accumbens, induced by a variety of pharmacological manipulations[62].

Neurochemical studies also support a facilitatory role of the 5-HT$_3$ receptor with respect to central dopaminergic function. Thus, dopamine release is increased from slices of rat nucleus accumbens[63] and striatum[64] following 5-HT$_3$ receptor activation.

A summary of functional responses associated with activation of the central 5-HT$_3$ receptor is shown in table 2.9.

Level	Response	Mechanism
Cellular	Cation channel (+)	Post
Electrophysiologi-cal	Depolarisation	Post
	LTP (−)	Post
Behavioural	Anxiolysis (antagonist)	Post
	Cognition (+antagonist)	Post
	Locomotion (− antagonist)	Post
	Reward (− antagonist)	Post
Neurochemical	5-HT release (+)	Post (indirect?)
	Acetylcholine release (−)	Post indirect
	GABA release (+)	Post
	CCK release (+)	Post
	Dopamine release (+)	Post

Table 2.9: Functional responses associated with activation of the central 5-HT$_3$ receptor[1]

2.3.4. The 5-HT$_4$ receptor

The 5-HT$_4$ receptor gene has been mapped to the long arm of human chromosome 5 (5q31-q33)[65]. The gene appears to be highly fragmented, containing at least five introns.

A consistent finding across all species investigated so far is the presence of relatively high levels of the 5-HT$_4$ receptor in the nigrostriatal and mesolimbic systems of the brain[66]. A number of highly selective ligands for the 5-HT$_4$ receptor is available (e.g. GR113808, SB204070). The 5-HT$_4$ receptor couples positively to adenylate cyclase[67]. Phosphorylation of native 5-HT$_4$ receptors expressed by both neurons and smooth muscle would appear to be largely responsible for the desensitisation of the 5-HT$_4$ receptor[68].

There are numerous reports demonstrating the ability of the 5-HT$_4$ receptor to modulate the activity of various neurons in the central nervous system. The ability of the 5-HT$_4$ receptor to facilitate acetylcholine release in the gastro-intestinal tract is well documented[69]. There is increasing evidence that the 5-HT$_4$ receptor also modulates dopamine release in the brain[70]. An overview of the functional responses associated with activation of the central 5-HT$_4$ receptor is shown in table 2.10.

Level	Response	Mechanism
Cellular	Adenylate cyclase (+)	Post
Electrophysiolog-ical	Reduce after-hyperpolarisation	Post
Behavioural	Anxiolysis and anxiogenesis (antagonists)	Post
	Cognition (+)	Post
Neurochemical	5-HT release (+)	Post (indirect?)
	Acetylcholine release (+)	Post
	Dopamine release (+)	Post (indirect)

Table 2.10: Functional responses associated with the activation of the central 5-HT$_4$ receptor[1]

Several reports indicate that activation of central 5-HT$_4$ receptors facilitates cognitive performance[71]. For instance, the 5-HT$_4$ receptor agonist BIMU1 has been shown to enhance the performance of rats in different behavioural models investigating both short-term and long-term memory[72]. Given the well-known association of acetylcholine and memory[73], the proposed ability of the 5-HT$_4$ receptor to facilitate cholinergic function within relevant

regions of the brain (e.g. cerebral cortex, hippocampus) provides a plausible explanation for the facilitation of cognitive performance following 5-HT$_4$ receptor activation.

The 5-HT$_4$ receptor has also been implicated in anxiety. The ability of 5-HT$_4$ receptor agonists to increase (and 5-HT$_4$ receptor antagonists to decrease) serotonin release in the dorsal hippocampus provides a relevant neurochemical mechanism for 5-HT$_4$ receptor-mediated modulation of anxiety.

2.3.5. 5-HT$_5$ receptors

The genomic structure of 5-HT$_{5A}$ and 5-HT$_{5B}$ genes was deduced by screening a mouse genomic library with probes corresponding to the mouse 5-HT$_{5A}$ and 5-HT$_{5B}$ receptor cDNAs. Both genes contain an intron at an identical position corresponding to the middle of the third cytoplasmatic loop[74]. The 5-HT$_{5A}$ gene was located on mouse chromosome 5 (position 5B) and human chromosome 7 (position 7q36). The 5-HT$_{5B}$ gene is located on mouse chromosome 1 (position 1F) and human chromosome 2 (position 2q11-13).

Both the 5-HT$_{5A}$ and 5-HT$_{5B}$ receptors are members of the seven putative transmembrane domain-G-protein coupled superfamily.

* 5-HT$_{5A}$ receptor:
In situ hybridisation studies revealed the presence of 5-HT$_{5A}$ receptor mRNA in both mouse and rat brain. In mouse brain, 5-HT$_{5A}$ receptor transcripts are associated with neurons within the cerebral cortex, the dentate gyrus and the pyramidal cell layer within the hippocampus[75]. Use of PCR detected 5-HT$_{5A}$ mRNA in mouse and human forebrain and cerebellum. Little information has been published concerning the effects of knocking out the 5-HT$_{5A}$ receptor, although mice lacking the receptor display increased locomotor activity and exploratory behaviour relative to wild-type animals[76].

* 5-HT$_{5B}$ receptor:
In situ hybridisation studies demonstrated a low specific signal in the supraoptic nucleus of the hypothalamus and some other rat brain regions (hippocampus, olfactory bulb, entorhinal cortex and pyriform cortex)[77].

2.3.6. The 5-HT$_6$ receptor

The 5-HT$_6$ receptor has seven hydrophobic regions spanning the cell membrane, which places the receptor in the G-protein-coupled, seven putative transmembrane domain receptor superfamily[78]. The receptor is prone to agonist-induced desensitisation which appears to be due principally to receptor phosphorylation catalysed by a cAMP-dependent protein kinase[79]. Genomic mapping identified the human 5-HT$_6$ receptor gene in the p35-36 portion of human chromosome 1[1]. A number of reports have demonstrated the differential distribution of 5-HT$_6$ receptor mRNA. The transcripts appear to be largely confined to the central nervous system, although low levels have been detected in the stomach and adrenal glands[80]. Within the brain, high levels of 5-HT$_6$ receptor mRNA are consistently detected within the striatum (caudate nucleus) of the rat, guinea pig and humans[80]. Relatively high levels are also detected in the olfactory tubercles, nucleus accumbens and hippocampus[78]. The level of expression of the 5-HT$_6$ receptor in the brain is generally low, making detailed investigation of the central localisation of the receptor difficult. It was speculated that 5-HT$_6$ receptors are located postsynaptically on the dendrites of excitatory pyramidal and granule cell neurons in the hippocampus[81].

Several antipsychotic and antidepressant drugs show interaction with the 5-HT$_6$ receptor. Recently, different compounds have been identified as selective 5-HT$_6$ receptor antagonists (e.g. Ro 04-6790 and Ro 63-0563[82]).

Consistent with its structure (i.e. seven transmembrane domains) , the 5-HT$_6$ receptor couples positively to a metabotropic transduction system which enhances adenylate cyclase activity[14]. Administration of the 5-HT$_6$ receptor selective agent Ro 04-6790 resulted in a higher incidence of yawning and stretching in rats[82]. The increase in the numbers of yawns and stretches was dose-related. An interaction between the 5-HT$_6$ receptor and the central acetylcholine system was also demonstrated[82].

2.3.7. The 5-HT$_7$ receptor

The 5-HT$_7$ receptor gene is located on human chromosome 10 (10q21-q24[83]) and contains two introns. The amino acid sequence of the 5-HT$_7$ receptor displays the characteristic seven putative membrane spanning regions[84] of the G-protein coupled receptor superfamily.

The 5-HT$_7$ receptor exhibits a distinct distribution in the central nervous system. In rat and guinea pig brain, both the mRNA and receptor binding sites display a similar distribution indicating that the receptor is expressed close to the site of synthesis[85]. 5-HT$_7$ receptor expression is relatively high within regions of the thalamus, hypothalamus and hippocampus, with generally lower levels in areas such as the cerebral cortex and amygdala[85].

The ability of a range of clinically utilised psychoactive agents to interact with the 5-HT$_7$ receptor at relevant concentrations (typical and atypical antipsychotics and antidepressants including clozapine[85]), similar to the 5-HT$_6$ receptor, suggests that this receptor may be important as a target in psychiatric conditions, although genetic variation within the 5-HT$_7$ receptor gene does not appear to be associated with either schizophrenia or bipolar affective disorder[86].

Activation of the 5-HT$_7$ receptor stimulates adenylate cyclase[84]. Consistent with other members of the G-protein coupled receptor superfamily, amino acid residues within the third intracellular loop of the 5-HT$_7$ receptor are likely to be involved in the coupling to Gα_S[87].

A summary of functional responses associated with activation of the central 5-HT$_7$ receptor is shown in table 2.11.

Level	Response	Mechanism
Cellular	Adenylate cyclase (+)	Post
Electrophysiolog-ical	Phase shift advance suprachiasmatic nucleus	Post

Table 2.11: Functional responses associated with activation of the central 5-HT$_7$ receptor[1]

A number of reports implicate a role for the 5-HT$_7$ receptor in the regulation of circadian rhythms. 5-HT$_7$ antagonists might have the ability to prevent audiogenic seizures in mice[88]. Whilst highly speculative, these studies might indicate a role for 5-HT$_7$ receptor antagonists in the treatment of epilepsy.

2.3.8. Summary

A striking feature of the 5-HT receptor subtypes is that each has a highly distinct pattern of distribution in the central nervous system, such that individual brain regions contain their own complement of 5-HT receptor subtypes. All of the receptors are located postsynaptically where some are known to modulate ion flux and cause neuronal depolarisation (5-HT_{2A}, 5-HT_{2C}, 5-HT_3 and 5-HT_4 receptors) or hyperpolarisation (5-HT_{1A} receptor). Certain 5-HT receptor subtypes (5-HT_{1A}, 5-HT_{1B} and possibly 5-HT_{1D}) are located on the 5-HT neurons themselves where they serve as 5-HT autoreceptors at the somatodendritic or nerve terminal level. Some 5-HT receptors ($5\text{-HT}1_{B,D}$, $5\text{-HT}_{2A,C}$, 5-HT_3 and 5-HT_4 receptors) are also located on the nerve terminals of non-5-HT neurons where they appear to function as heteroreceptors, regulating neurotransmitter release.

Activation of specific serotonin receptor subtypes can be linked with the modulation of specific behaviours. The 5-HT_{1A}, 5-HT_{2A} and 5-HT_{2C} receptors currently stand out in terms of the wide range of behaviours and physiological responses that agonists for these receptors can evoke. Selective antagonists have established a key role for the 5-HT_{2C} receptor in feeding and anxiety (along with the 5-HT_3 and 5-HT_4 receptor[1]). The clinical utility of certain 5-HT receptor selective ligands has been established in various neuropsychiatric disorders including major depression and anxiety (buspirone) and migraine (sumatriptan). Several clinical trials are ongoing, investigating the therapeutic usefulness of selective serotonin receptor ligands, including 5-HT_{1A} (auto)receptor antagonists (depression), 5-HT_{2A} antagonists (schizophrenia) and 5-HT_{2C} antagonists (anxiety).

2.4. References

1. Barnes NM and Sharp T. A review of central 5-HT receptors and their function. Neuropharmacology 1999; 38:1083-1152.

2. Obtained from Central Nervous System website. (**http://www.CNSforum.com**). 2008;

3. Gaddum JH and Picarelli ZP. Two kinds of tryptamine receptor (Reprinted from Brit J Pharmacol, vol 12, pg 323, 1957). British Journal of Pharmacology 1997; 120:134-139.

4. Vandecapelle M. Synthesis and in vivo evaluation of 5-HT1A radioligands. Doctoral thesis, Laboratory for Radiopharmacy, Ghent University, Ghent, Belgium 2004;

5. Hoyer D, Clarke DE, Fozard JR, Hartig PR, Martin GR, Mylecharane EJ et al. International Union of Pharmacology Classification of Receptors for 5-Hydroxytryptamine (Serotonin). Pharmacological Reviews 1994; 46:157-203.

6. Hoyer D and Martin G. 5-HT receptor classification and nomenclature: Towards a harmonization with the human genome. Neuropharmacology 1997; 36:419-428.

7. Peroutka SJ and Snyder SH. Multiple Serotonin Receptors - Differential Binding of [5-Hydroxytryptamine-H-3, [Lysergic-H-3 Acid Diethylamide and [H-3]Spiroperidol. Molecular Pharmacology 1979; 16:687-699.

8. Gozlan H, Elmestikawy S, Pichat L, Glowinski J, Hamon M. Identification of Pre-Synaptic Serotonin Autoreceptors Using A New Ligand - H-3-Pat. Nature 1983; 305:140-142.

9. Robinson DS, Sitsen JMA, Gibertini M. A review of the efficacy and tolerability of immediate-release and extended-release formulations of gepirone. Clinical Therapeutics 2003; 25:1618-1633.

10. Pike VW, McCarron JA, Lammerstma AA, Hume SP, Poole K, Grasby PM et al. First Delineation of 5-Ht1A Receptor in Human Brain with Pet and [C-11]Way-100635. European Journal of Pharmacology 1995; 283:R1-R3.

11. Burnet PWJ, Eastwood SL, Lacey K, Harrison PJ. The Distribution of 5-Ht1A and 5-Ht2A Receptor Messenger-Rna in Human Brain. Brain Research 1995; 676:157-168.

12. Kia HK, Brisorgueil MJ, Daval G, Langlois X, Hamon M, Verge D. Serotonin(1A) receptors are expressed by a subpopulation of cholinergic neurons in the rat medial septum and diagonal band of Broca - A double immunocytochemical study. Neuroscience 1996; 74:143-154.

13. Kia HK, Brisorgueil MJ, Hamon M, Calas A, Verge D. Ultrastructural localization of 5-hydroxytryptamine(1A) receptors in the rat brain. Journal of Neuroscience Research 1996; 46:697-708.

14. Boess FG and Martin IL. Molecular-Biology of 5-Ht Receptors. Neuropharmacology 1994; 33:275-317.

15. Nicoll RA, Malenka RC, Kauer JA. Functional Comparison of Neurotransmitter Receptor Subtypes in Mammalian Central-Nervous-System. Physiological Reviews 1990; 70:513-565.

16. Azmitia EC, Gannon PJ, Kheck NM, WhitakerAzmitia PM. Cellular localization of the 5-HT1A receptor in primate brain neurons and glial cells. Neuropsychopharmacology 1996; 14:35-46.

17. Riad M, Emerit MB, Hamon M. Neurotrophic Effects of Ipsapirone and Other 5-Ht1A Receptor Agonists on Septal Cholinergic Neurons in Culture. Developmental Brain Research 1994; 82:245-258.

18. Sharp T, Umbers V, Hjorth S. The role of 5-HT1A autoreceptors and alpha(1)-adrenoceptors in the inhibition of 5-HT release .2. NAN-190 and SDZ 216-525. Neuropharmacology 1996; 35:735-741.

19. Wilkinson LO, Middlemiss DN, Hutson PH. 5-Ht1A Receptor Activation Increases Hippocampal Acetylcholine Efflux and Motor-Activity in the Guinea-Pig - Agonist Efficacy Influences Functional-Activity In-Vivo. Journal of Pharmacology and Experimental Therapeutics 1994; 270:656-664.

20. Consolo S, Arnaboldi S, Ramponi S, Nannini L, Ladinsky H, Baldi G. Endogenous serotonin facilitates in vivo acetylcholine release in rat frontal cortex through 5-HT1B receptors. Journal of Pharmacology and Experimental Therapeutics 1996; 277:823-830.

21. Done CJG and Sharp T. Biochemical-Evidence for the Regulation of Central Noradrenergic Activity by 5-Ht1A and 5-Ht2 Receptors - Microdialysis Studies in the Awake and Anesthetized Rat. Neuropharmacology 1994; 33:411-421.

22. Handley SL. 5-Hydroxytryptamine Pathways in Anxiety and Its Treatment. Pharmacology & Therapeutics 1995; 66:103-148.

23. Hartig PR, Hoyer D, Humphrey PPA, Martin GR. Alignment of receptor nomenclature with the human genome: Classification of 5-HT1B and 5-HT1D receptor subtypes. Trends in Pharmacological Sciences 1996; 17:103-105.

24. Pazos A, Probst A, Palacios JM. Serotonin Receptors in the Human-Brain .4. Autoradiographic Mapping of Serotonin-2 Receptors. Neuroscience 1987; 21:123-139.

25. Adham N, Romanienko P, Hartig P, Weinshank RL, Branchek T. The Rat 5-Hydroxytryptamine1B Receptor Is the Species Homolog of the Human 5-Hydroxytryptamine1D-Beta Receptor. Molecular Pharmacology 1992; 41:1-7.

26. Bruinvels AT, Landwehrmeyer B, Gustafson EL, Durkin MM, Mengod G, Branchek TA et al. Localization of 5-Ht1B, 5-Ht1D-Alpha, 5-Ht1e and 5-Ht1F, Receptor Messenger-Rna in Rodent and Primate Brain. Neuropharmacology 1994; 33:367-386.

27. Bobker DH and Williams JT. Serotonin Agonists Inhibit Synaptic Potentials in the Rat Locus Ceruleus Invitro Via 5-Hydroxytryptamine1A and 5-Hydroxytryptamine-1B Receptors. Journal of Pharmacology and Experimental Therapeutics 1989; 250:37-43.

28. Geyer MA. Serotonergic functions in arousal and motor activity. Behavioural Brain Research 1995; 73:31-35.

29. Castro ME, Pascual J, Romon T, DelArco C, DelOlmo E, Pazos A. Differential distribution of [H-3]sumatriptan binding sites (5-HT1B, 5-HT1D and 5-HT1F receptors) in human brain: Focus on brainstem and spinal cord. Neuropharmacology 1997; 36:535-542.

30. Zgombick JM, Schechter LE, Macchi M, Hartig PR, Branchek TA, Weinshank RL. Human Gene S31 Encodes the Pharmacologically Defined Serotonin 5-Hydroxytryptamine-1e Receptor. Molecular Pharmacology 1992; 42:180-185.

31. Mcallister G, Charlesworth A, Snodin C, Beer MS, Noble AJ, Middlemiss DN et al. Molecular-Cloning of A Serotonin Receptor from Human Brain (5Ht1E) - A 5Th 5Ht1-Like Subtype. Proceedings of the National Academy of Sciences of the United States of America 1992; 89:5517-5521.

32. Adham N, Kao HT, Schechter LE, Bard J, Olsen M, Urquhart D et al. Cloning of Another Human Serotonin Receptor (5-Ht1F) - A 5Th 5-Ht1 Receptor Subtype Coupled to the Inhibition of Adenylate-Cyclase. Proceedings of the National Academy of Sciences of the United States of America 1993; 90:408-412.

33. Waeber C and Moskowitz MA. [H-3] Sumatriptan Labels Both 5-Ht1D and 5Ht(1F) Receptor-Binding Sites in the Guinea-Pig Brain - An Autoradiographic Study. Naunyn-Schmiedebergs Archives of Pharmacology 1995; 352:263-275.

34. Phebus LA, Johnson KW, Zgombick JM, Gilbert PJ, VanBelle K, Mancuso V et al. Characterization of LY344864 as a pharmacological tool to study 5-HT1F receptors: Binding affinities, brain penetration and activity in the neurogenic dural inflammation model of migraine. Life Sciences 1997; 61:2117-2126.

35. Lucaites VL, Krushinski JH, Schaus JM, Audia JE, Nelson DL. [H-3]LY334370, a novel radioligand for the 5-HT1F receptor. II. Autoradiographic localization in rat, guinea pig, monkey and human brain. Naunyn-Schmiedebergs Archives of Pharmacology 2005; 371:178-184.

36. Wainscott DB, Krushinski JH, Audia JE, Schaus JM, Zgombick JM, Lucaites VL et al. [H-3]LY334370, a novel radioligand for the $5-HT_{1F}$ receptor. I. In vitro characterization of binding properties. Naunyn-Schmiedebergs Archives of Pharmacology 2005; 371:169-177.

37. Baxter G, Kennett G, Blaney F, Blackburn T. $5-Ht_2$ Receptor Subtypes - A Family Re-United. Trends in Pharmacological Sciences 1995; 16:105-110.

38. Yu L, Nguyen H, Le H, Bloem LJ, Kozak CA, Hoffman BJ et al. The Mouse $5-Ht_{1C}$ Receptor Contains 8 Hydrophobic Domains and Is X-Linked. Molecular Brain Research 1991; 11:143-149.

39. Leysen JE, Niemegeers CJE, Tollenaere JP, Laduron PM. Serotonergic Component of Neuroleptic Receptors. Nature 1978; 272:168-171.

40. Burnet PWJ, Eastwood SL, Lacey K, Harrison PJ. The Distribution of $5-Ht_{1A}$ and $5-Ht_{2A}$ Receptor Messenger-Rna in Human Brain. Brain Research 1995; 676:157-168.

41. Morilak DA, Garlow SJ, Ciaranello RD. Immunocytochemical Localization and Description of Neurons Expressing Serotonin(2) Receptors in the Rat-Brain. Neuroscience 1993; 54:701-717.

42. Kehne JH, Baron BM, Carr AA, Chaney SF, Elands J, Feldman DJ et al. Preclinical characterization of the potential of the putative atypical antipsychotic MDL 100,907 as a potent $5-HT_{2A}$ antagonist with a favorable CNS safety profile. Journal of Pharmacology and Experimental Therapeutics 1996; 277:968-981.

43. Sanders-Bush E. Serotonin $5-HT_2$ receptors: Molecular and genomic diversity. Acta Pharmacologica Sinica 2006; 27:1-1.

44. Briddon SJ, Leslie RA, Elliott JM. Desensitization of the Transfected Human 5-Ht$_{2C}$ Receptor Is Accompanied by A Decreased Affinity of the Receptor for [H-3] 5-Ht. British Journal of Pharmacology 1995; 116:218-218.

45. Briddon SJ, Leslie RA, Elliott JM. Agonist-Induced Desensitization of Human 5-Ht$_{2C}$ Receptors Expressed in A Human Neuroblastoma Cell-Line. British Journal of Pharmacology 1995; 114:372-372.

46. Vaidya VA, Marek GJ, Aghajanian GK, Duman RS. 5-HT$_{2A}$ receptor-mediated regulation of brain-derived neurotrophic factor mRNA in the hippocampus and the neocortex. Journal of Neuroscience 1997; 17:2785-2795.

47. Duman RS. Drug action through gene transcription: Antidepressants. Naunyn-Schmiedebergs Archives of Pharmacology 1997; 355:S7-S7.

48. Duman RS, Heninger GR, Nestler EJ. A molecular and cellular theory of depression. Archives of General Psychiatry 1997; 54:597-606.

49. Marek GJ and Aghajanian GK. Protein-Kinase-C Inhibitors Enhance the 5-Ht$_{2A}$ Receptor-Mediated Excitatory Effects of Serotonin on Interneurons in Rat Piriform Cortex. Synapse 1995; 21:123-130.

50. Schreiber R, Brocco M, Audinot V, Gobert A, Veiga S, Millan MJ. (1-(2,5-Dimethoxy-4 Iodophenyl)-2-Aminopropane)-Induced Head-Twitches in the Rat Are Mediated by 5-Hydroxytryptamine (5-Ht)(2A) Receptors - Modulation by Novel 5-Ht$_{2A/2C}$ Antagonists, D-1 Antagonists and 5-Ht$_{1A}$ Agonists. Journal of Pharmacology and Experimental Therapeutics 1995; 273:101-112.

51. Glennon RA. Discriminative Stimulus Properties of Hallucinogens and Related Designer Drugs. Psychopharmacology 1990; 101:S68-S68.

52. Van de Kar LD, Javed A, Zhang YH, Serres F, Raap DK, Gray TS. 5-HT$_{2A}$ receptors stimulate ACTH, corticosterone, oxytocin, renin, and prolactin release and activate hypothalamic CRF and oxytocin-expressing cells. Journal of Neuroscience 2001; 21:3572-3579.

53. Bonhaus DW, Bach C, Desouza A, Salazar FHR, Matsuoka BD, Zuppan P et al. The Pharmacology and Distribution of Human 5-Hydroxytryptamine(2B) (5-Ht2B) Receptor Gene-Products - Comparison with 5-Ht2A and 5-Ht2C Receptors. British Journal of Pharmacology 1995; 115:622-628.

54. Duxon MS, Kennett GA, Lightowler S, Blackburn TP, Fone KCF. Activation of 5-HT2B receptors in the medial amygdala causes anxiolysis in the social interaction test in the rat. Neuropharmacology 1997; 36:601-608.

55. Jenck F, Moreau JL, Mutel V, Martin JR, Haefely WE. Evidence for A Role of 5-Ht1C Receptors in the Antiserotonergic Properties of Some Antidepressant Drugs. European Journal of Pharmacology 1993; 231:223-229.

56. Labrecque J, Fargin A, Bouvier M, Chidiac P, Dennis M. Serotonergic Antagonists Differentially Inhibit Spontaneous Activity and Decrease Ligand-Binding Capacity of the Rat 5-Hydroxytryptamine Type 2C Receptor in Sf9 Cells. Molecular Pharmacology 1995; 48:150-159.

57. Koek W, Jackson A, Colpaert FC. Behavioral Pharmacology of Antagonists at 5-Ht2/5-Ht1C Receptors. Neuroscience and Biobehavioral Reviews 1992; 16:95-105.

58. Kennett GA, Wood MD, Bright F, Trail B, Riley G, Holland V et al. SB 242084, a selective and brain penetrant 5-HT2C receptor antagonist. Neuropharmacology 1997; 36:609-620.

59. Maricq AV, Peterson AS, Brake AJ, Myers RM, Julius D. Primary Structure and Functional Expression of the 5Ht3 Receptor, A Serotonin-Gated Ion Channel. Science 1991; 254:432-437.

60. Pratt GD, Bowery NG, Kilpatrick GJ, Leslie RA, Barnes NM, Naylor RJ et al. Consensus Meeting Agrees Distribution of 5-Ht3 Receptors in Mammalian Hindbrain. Trends in Pharmacological Sciences 1990; 11:135-137.

61. Parker RMC, Bentley KR, Barnes NM. Allosteric modulation of 5-HT3 receptors: Focus on alcohols and anaesthetic agents. Trends in Pharmacological Sciences 1996; 17:95-99.

62. Bentley KR and Barnes NM. Therapeutic Potential of Serotonin 5-Ht3 Antagonists in Neuropsychiatric Disorders. Cns Drugs 1995; 3:363-392.

63. De Deurwaerdere P, Stinus L, Spampinato U. Opposite change of in vivo dopamine release in the rat nucleus accumbens and striatum that follows electrical stimulation of dorsal raphe nucleus: Role of 5-HT3 receptors. Journal of Neuroscience 1998; 18:6528-6538.

64. Blandina P, Goldfarb J, Craddockroyal B, Green JP. Release of Endogenous Dopamine by Stimulation of 5-Hydroxytryptamine-3 Receptors in Rat Striatum. Journal of Pharmacology and Experimental Therapeutics 1989; 251:803-809.

65. Cichon S, Kesper K, Propping P, Nothen MM. Assignment of the human serotonin 4 receptor gene (HTR4) to the long arm of chromosome 5 (5q31-q33). Molecular Membrane Biology 1998; 15:75-78.

66. Mengod G, Vilaro MT, Raurich A, LopezGimenez JF, Cortes R, Palacios JM. 5-HT receptors in mammalian brain: Receptor autoradiography and in situ hybridization studies of new ligands and newly identified receptors. Histochemical Journal 1996; 28:747-758.

67. VandenWyngaert I, Gommeren W, Verhasselt P, Jurzak M, Leysen J, Luyten W et al. Cloning and expression of a human serotonin 5-HT4 receptor cDNA. Journal of Neurochemistry 1997; 69:1810-1819.

68. Ronde P, Ansanay H, Dumuis A, Miller R, Bockaert J. Homologous Desensitization of 5-Hydroxytryptamine(4) Receptors in Rat Esophagus - Functional and 2Nd Messenger Studies. Journal of Pharmacology and Experimental Therapeutics 1995; 272:977-983.

69. Eglen RM, Jasper JR, Chang DJ, Martin GR. The 5-HT7 receptor: Orphan found. Trends in Pharmacological Sciences 1997; 18:104-107.

70. Benloucif S, Keegan MJ, Galloway MP. Serotonin-Facilitated Dopamine Release Invivo - Pharmacological Characterization. Journal of Pharmacology and Experimental Therapeutics 1993; 265:373-377.

71. Fontana DJ, Daniels SE, Wong EHF, Clark RD, Eglen RM. The effects of novel, selective 5-hydroxytryptamine (5-HT)(4) receptor ligands in rat spatial navigation. Neuropharmacology 1997; 36:689-696.

72. MarchettiGauthier E, Roman FS, Dumuis A, Bockaert J, SoumireuMourat B. BIMU1 increases associative memory in rats by activating 5-HT4 receptors. Neuropharmacology 1997; 36:697-706.

73. Bartus RT, Dean RL, Beer B, Lippa AS. The Cholinergic Hypothesis of Geriatric Memory Dysfunction. Science 1982; 217:408-417.

74. Matthes H, Boschert U, Amlaiky N, Grailhe R, Plassat JL, Muscatelli F et al. Mouse 5-Hydroxytryptamine5A and 5-Hydroxytryptamine5B Receptors Define A New Family of Serotonin Receptors - Cloning, Functional Expression, and Chromosomal Localization. Molecular Pharmacology 1993; 43:313-319.

75. Plassat JL, Boschert U, Amlaiky N, Hen R. The Mouse 5Ht5-Receptor Reveals A Remarkable Heterogeneity Within the 5Ht1D Receptor Family. Embo Journal 1992; 11:4779-4786.

76. Dulawa SC, Hen R, ScearceLevie K, Geyer MA. Serotonin(1B) receptor modulation of startle reactivity, habituation, and prepulse inhibition in wild-type and serotonin(1B) knockout mice. Psychopharmacology 1997; 132:125-134.

77. Erlander MG, Lovenberg TW, Baron BM, Delecea L, Danielson PE, Racke M et al. 2 Members of A Distinct Subfamily of 5-Hydroxytryptamine Receptors Differentially Expressed in Rat-Brain. Proceedings of the National Academy of Sciences of the United States of America 1993; 90:3452-3456.

78. Kohen R, Metcalf MA, Khan N, Druck T, Huebner K, Lachowicz JE et al. Cloning, characterization, and chromosomal localization of a human 5-HT6 serotonin receptor. Journal of Neurochemistry 1996; 66:47-56.

79. Sleight AJ, Boess FG, Bourson A, Sibley DR, Monsma FJ. 5-HT6 and 5-HT7 receptors: Molecular biology, functional correlates and possible therapeutic indications. Drug News & Perspectives 1997; 10:214-224.

80. Ruat M, Traiffort E, Arrang JM, Tardivellacombe J, Diaz J, Leurs R et al. A Novel Rat Serotonin (5-Ht6) Receptor - Molecular-Cloning, Localization and Stimulation of Camp Accumulation. Biochemical and Biophysical Research Communications 1993; 193:268-276.

81. Gerard C, Martres MP, Lefevre K, Miquel MC, Verge D, Lanfumey L et al. Immuno-localization of serotonin 5-HT6 receptor-like material in the rat central nervous system. Brain Research 1997; 746:207-219.

82. Sleight AJ, Boess FG, Bos M, Levet-Trafit B, Bourson A. The 5-hydroxytryptamine(6) receptor: localisation and function. Expert Opinion on Therapeutic Patents 1998; 8:1217-1224.

83. Gelernter J, Rao PA, Pauls DL, Hamblin MW, Sibley DR, Kidd KK. Assignment of the 5Ht7 Receptor Gene (Htr7) to Chromosome 10Q and Exclusion of Genetic-Linkage with Tourette Syndrome. Genomics 1995; 26:207-209.

84. Ruat M, Traiffort E, Leurs R, Tardivellacombe J, Diaz J, Arrang JM et al. Molecular-Cloning, Characterization, and Localization of A High-Affinity Serotonin Receptor (5-Ht(7)) Activating Camp Formation. Proceedings of the National Academy of Sciences of the United States of America 1993; 90:8547-8551.

85. Stowe RL and Barnes NM. Pharmacological characterisation and cellular distribution of 5-HT7 receptors in rat brain. Naunyn-Schmiedebergs Archives of Pharmacology 1998; 358:R108-R108.

86. Erdmann J, Nothen MM, ShimronAbarbanell D, Rietschel M, Albus M, Borrmann M et al. The human serotonin 7 (5-HT7) receptor gene: Genomic organization and systematic mutation screening in schizophrenia and bipolar affective disorder. Molecular Psychiatry 1996; 1:392-397.

87. Obosi LA, Hen R, Beadle DJ, Bermudez I, King LA. Mutational analysis of the mouse 5-HT7 receptor: importance of the third intracellular loop for receptor-G-protein interaction. Febs Letters 1997; 412:321-324.

88. Bourson A, Kapps V, Zwingelstein C, Rudler A, Boess FG, Sleight AJ. Correlation between 5-HT7 receptor affinity and protection against sound-induced seizures in DBA/2J mice. Naunyn-Schmiedebergs Archives of Pharmacology 1997; 356:820-826.

Chapter 3

INFLUENCE OF CYCLOSPORIN A ADMINISTRATION ON THE BRAIN UPTAKE OF [^{123}I]-R91150 IN RODENTS

ᏜᏜᏜ

3. *INFLUENCE OF CYCLOSPORIN A ADMINISTRATION ON THE BRAIN UPTAKE OF [^{123}I]-R91150 IN RODENTS*

While initially evaluating the potential of [^{123}I]-R91150 to visualize the 5-HT$_{2A}$ receptor *in vivo* with pinhole μSPECT, image quality was rather poor. In our search to increase the brain uptake of [^{123}I]-R91150 in rodents to enable good quality pinhole μSPECT images, we discovered that the pre-administration of cyclosporin A had a dramatic effect on the levels of [^{123}I]-R91150 radioactivity in rodent brain. Brain radioactivity concentrations increased 5 - 6 fold. This led us to further characterize the influence of cyclosporin A on the brain uptake of [^{123}I]-R91150.

Regional brain biodistribution studies and ketanserin displacement studies with and without cyclosporin A pre-treatment will be performed in rodents. The effect of increasing dosages of cyclosporin A on the brain uptake of [^{123}I]-R91150 will be studied in NMRI mice. The influence of cyclosporin A administration on pinhole μSPECT imaging will also be discussed. To exclude the effect of potential increased tracer metabolism under the influence of cyclosporin A, metabolite assays with [^{123}I]-R91150 will also be performed.

The obtained results will be used as a 'standard' to compare with the results from the biodistribution studies with a potential, in-house developed 5-HT$_{2A}$ tracer, [^{123}I]-3-I-CO (chapter 4).

3.1 Introduction

The first proposed SPECT tracer for the serotonin 5-HT$_{2A}$ receptor was 2-radioiodoketanserin, developed at the end of the 1980's[1]. This compound was used clinically for SPECT imaging of 5-HT$_{2A}$ receptors in depressed patients. The iodinated compound showed properties almost comparable to those of ketanserin (poor selectivity for 5-HT$_2$ versus H$_1$ and α_1-receptors) and high binding to serum proteins resulting in rather poor brain to blood ratios[2].

Later on R91150 was discovered and developed by the Janssen Research Foundation (Beerse, Belgium). R91150 or N-[(3-p-fluorophenyl-1-propyl)-4-methyl-4-piperidinyl]-4-amino-2-methoxybenzamide (structure shown in figure 3.1) is the precursor molecule for the radiosynthesis of the 5' iodo-derivative, named R93274. For reasons of simplicity and corresponding to the literature, we will further refer to the precursor as R91150 and to the [^{123}I]-5'-iodo-derivative as [^{123}I]-R91150. In view of a potential increased brain uptake due to an increase in lipophilicity, researchers at the Janssen Research Foundation also developed a derivative, mono-methylated on the 4-amino-function of the benzamide chain. N-methylation did not significantly increase the specific brain uptake, so it was decided to use the 5'-radioiodinated derivative [^{123}I]-R91150 in further research.
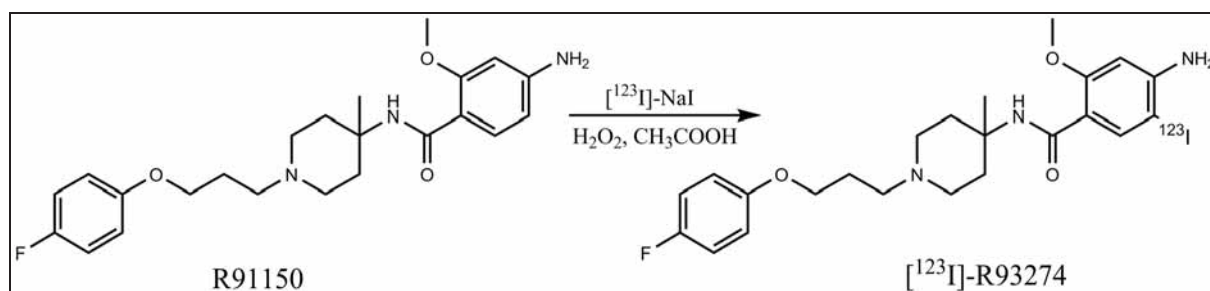
Figure 3.1: Chemical structure of R91150 and [^{123}I]-R91150

R93274 (5-I-R91150 or N-[(3-p-fluorophenyl-1-propyl)-4-methyl-4-piperidinyl]-4-amino-5-iodo-2-methoxybenzamide) is a selective iodinated 5-HT$_{2A}$ antagonist with high affinity (K$_d$ = 0.11 $\pm$ 0.1 nM) and selectivity for 5-HT$_{2A}$ receptors.

The selectivity of $[^{123}I]$-R91150 for 5-HT$_{2A}$ receptors with regard to other neurotransmitter systems such as other 5-HT receptors (including 5-HT$_{1A}$, 5-HT$_{1B}$, 5-HT$_{1D}$, 5-HT$_{2C}$, 5-HT$_3$), dopamine receptors, α_1 and α_2 adrenergic receptors and histamine receptors is at least a factor of 50[2, 3, 4]. IC$_{50}$ values for the different neurotransmitter systems are indicated in table 3.1.

	5-HT$_{2A}$[1]	5-HT$_{2C}$[2]	5-HT$_{1A}$	dopamine D$_2$	α_1-adrenergic
IC$_{50}$ (nM)	0,79	21	316	45	30

[1] IC$_{50}$ for inhibition of $[^3H]$-ketanserin binding to rat frontal cortex membranes, K$_i$ = 0.38 nM

[2] IC$_{50}$ for inhibition of $[^3H]$-mesulergine binding to pig choroid plexus, K$_i$ = 14.5 nM

Table 3.1: Selectivity of $[^{123}I]$-R91150 for different neurotransmitter systems

In vitro binding studies with $[^{123}I]$-R91150 to membrane preparations of rat frontal cortex revealed saturable binding (K$_d$ = 0.11 $\pm$ 0.01 nM, B$_{max}$ = 38.0 $\pm$ 0.7 fmoles/mg) and displacement of radioactivity by ketanserin and ritanserin. In vivo uptake of $[^{123}I]$-R91150 has been studied in rodents[2, 4]. In the *in vivo* studies, radioactivity concentrated in the cortical regions, with frontal to cerebellar ratios of 10 at 3h post injection. Frontal cortex to blood ratios of 6 were obtained. Radioactivity concentration values were dramatically reduced by either pre-treatment with the 5-HT$_{2A}$-selective antagonist ritanserin or displacement by ketanserin[2].

Brain radioactivity uptake of $[^{123}I]$-R91150 was also characterized in baboons[3]. The radioligand crossed the blood-brain barrier and concentrated in 5-HT$_{2A}$ receptor rich regions where it displayed specific, selective and reversible binding. However, brain uptake and target to background ratios were lower in baboons than in rodents, and $[^{123}I]$-R91150 was metabolized much more rapidly in baboons than in rats (at 3 h post injection, the parent compound radioactivity represented 95% of the plasma radioactivity in the rat, as opposed to 25% in baboons). The brain uptake of $[^{123}I]$-R91150 seems to be species-dependent[3].

Also, high radioactivity uptake was observed at the level of the eyes and orbital perioccular region (3.4 $\pm$ 0.4 % ID/g). Because of the proximity of the eye-area to the frontal cortex, frontal region-of-interest (ROI) radioactivity measurements could be contaminated by radioactivity originating from the eyes. In future experiments we will have to take this effect into account. The injection of ketanserin reduced the uptake in 5-HT$_{2A}$ receptor-rich regions to the levels observed in cerebellum. The cerebellar radioactivity was not affected by ketanserin administration, which confirmed the nonspecific nature of the uptake, as expected from the reported absence of 5-HT$_{2A}$ receptors in the cerebellum[5].

[^{123}I]-R91150 was evaluated in normal healthy dogs[6, 7, 8, 9]; influence of age and gender on the binding index of [^{123}I]-R91150 in canine brain was demonstrated. The tracer was also used in impulsive-aggressive dogs[10, 11, 12], and the effect of administering citalopram on the biodistribution of [^{123}I]-R91150 in impulsive-aggressive dogs was also investigated[13].

A number of clinical studies have already been performed with [^{123}I]-R91150 in healthy human volunteers[14, 15, 16, 17]. Maximal brain uptake was approximately 2% of total body counts at 180 min post injection[15] of [^{123}I]-R91150. Radioligand binding in the frontal cortex increased steadily over time, reaching a peak at approximately 100-120 min post injection. Frontal cortex-cerebellum activity ratios reached values of 1.4, and remained stable from approximately 100 min post injection onwards.

Age and gender had a significant effect on the 5-HT$_{2A}$ binding index in healthy human subjects[14, 18]. [^{123}I]-R91150 was also used to help elucidate the mechanism of action of MDMA[19].

Several clinical studies have also been performed in psychiatric patients. Psychiatric indications were a.o. anorexia nervosa[20], deliberate self-harm[21], schizophrenia[22], bulimia nervosa[23] and depression[24, 25]. [^{123}I]-R91150 was also used to monitor the effect of different antidepressant drugs on 5-HT$_{2A}$ binding index in human brain[26].

To demonstrate specificity of binding to the 5-HT$_{2A}$ receptor, specific 5-HT$_{2A}$ antagonists are used, such as ketanserin and ritanserin. We will use ketanserin tartrate and ritanserin for the *in vivo* displacement and blocking studies in this thesis (figure 3.2).
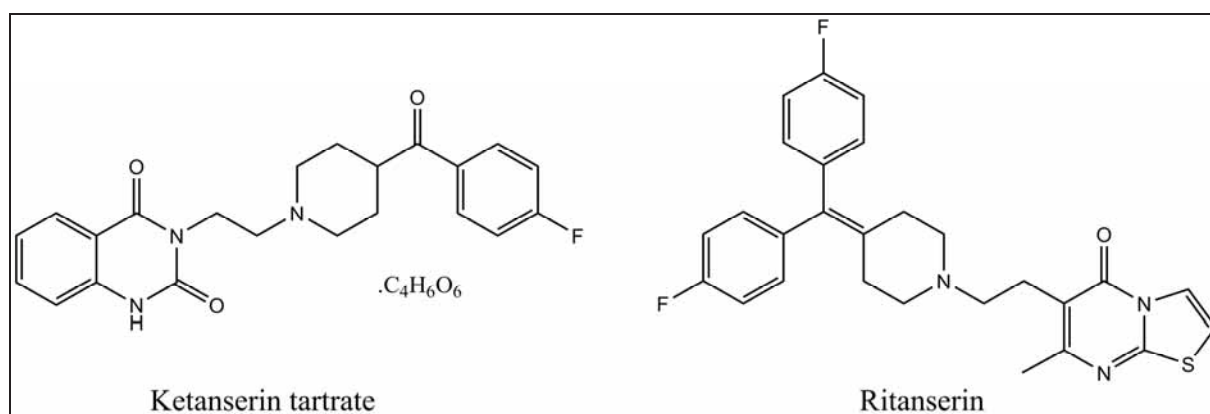
Figure 3.2: Structure of ketanserin and ritanserin

Ketanserin[27] (used as the tartrate salt, Tocris Cookson Inc, UK, figure 3.2 and table 3.2) is a selective 5-HT_{2A} serotonin receptor antagonist. It is also used to discriminate between 5-HT_{1D} and 5-HT_{1B} receptor subtypes. The correct amount of product was weighed and dissolved in warm 0.9% NaCl after sonication to a concentration of 5 mg/ml. A dosage of 1 mg per kg of bodyweight was used for *in vivo* displacement studies.

Ritanserin[28, 29] (Tocris Cookson Inc, UK, figure 3.2 and table 3.2) is a potent and long-acting 5-HT_{2A} receptor antagonist with *in vivo* anxiolytic properties. It was dissolved in 10% ethanol after sonication, and the dosage used was 2.5 mg per kg of bodyweight.

Receptor binding profiles of ketanserin and ritanserin for the different neurotransmitter systems were determined[30] at Janssen Research Foundation and are indicated in table 3.2.

	5-HT_{2A}	histamine-H_1	dopamine-D_2	α_1-adrenergic	α_2-adrenergic	5-HT_1
Ketanserin	1,7 ± 0,5	16 ± 5	620 ± 50	31 ± 2	> 1000	> 1000
Ritanserin	0,9 ± 0,1	35 ± 5	70 ± 30	97 ± 13	150 ± 25	> 1000

IC_{50} values are expressed as mean ± standard error in nanomolar (nM). Data adapted from Leysen et al[30].

Table 3.2: Receptor binding profiles of ketanserin and ritanserin

It is well established that the pharmacological properties of some serotonin receptors diverge widely across animal species[31]. For example, significant differences were observed when comparing the regional brain biodistribution of [^{123}I]-R91150 in different species.

In vivo studies in rats with [^{123}I]-R91150 showed preferential retention of radioactivity in the frontal cortex. Frontal cortex-to-cerebellum ratios increased from about 3 at 30 min post injection to a steady value of about 10 from 1h to 3h after radioligand injection. Displacement experiments with ketanserin demonstrated a reduction in frontal cortex radioactivity of about 40%[2]. Nevertheless, activity in frontal cortex after ketanserin displacement was still three times higher than the radioactivity levels observed in cerebellum. On the other hand, a blocking experiment with ritanserin demonstrated a decrease of frontal cortex activity to the level of radioactivity observed in cerebellum.

Brain uptake of [^{123}I]-R91150 was also characterized in baboons[3]. Highest brain uptake was observed in cortical areas, lowest uptake was observed in cerebellum and striatum. Injection of pharmacological doses of a 5-HT_{2A} antagonist (ketanserin) resulted in reduction of cortical and striatal radioactivity concentrations to the levels observed in cerebellum. However, brain uptake and target-to-background ratios were lower in baboons than in rats[4]: ratios of cortical tissues to cerebellum were about 1.5 at 150 min after injection of [^{123}I]-R91150.

The density of 5-HT$_{2A}$ receptors is about three times higher in the rat cortex compared to primate cortex[27]. For [^{123}I]-R91150, a higher nonspecific binding in baboon brain also contributed to the lower cortical to cerebellar ratio observed in baboons (1.5) compared to rats (10)[3].

We will investigate whether modulation of the drug efflux pumps in the blood-brain barrier will have an effect on the pharmacokinetic behaviour of [^{123}I]-R91150 in rodents. It has already been demonstrated by several authors[32, 33, 34, 35, 36] that tracer brain uptake is increased when P-glycoprotein efflux pumps are modulated by previous injections of cyclosporin A. It has been demonstrated that cyclosporin A is a potent modulator of P-glycoprotein[36, 37], and a dose-dependent inhibition of P-glycoprotein function by cyclosporin A has also been observed[32].

3.2. Radiosynthesis and purification of [^{123}I]-R91150

3.2.1. Introduction

[^{123}I]-R91150 was synthesized according to a modification of the original method [4]. Radio-iodination was performed by electrophilic substitution on the precursor R91150 (4-amino-N-[1-[3-(4-fluorophenoxy)-propyl]-4-methyl-4-piperidinyl]-2-methoxybenzamide). The 5-position of the methoxybenzamide group was iodinated. The precursor, R91150, was kindly donated by the Janssen Research Foundation (J&J, Beerse, Belgium). Samples of the precursor and the cold standard N-[(3-p-fluorophenyl-1-propyl)-4-methyl-4-piperidinyl]-4-amino-5-iodo-2-methoxy-benzamide were obtained from Janssen Pharmaceutica (Beerse, Belgium).

The reaction mechanism of the radiosynthesis is shown in figure 3.3.
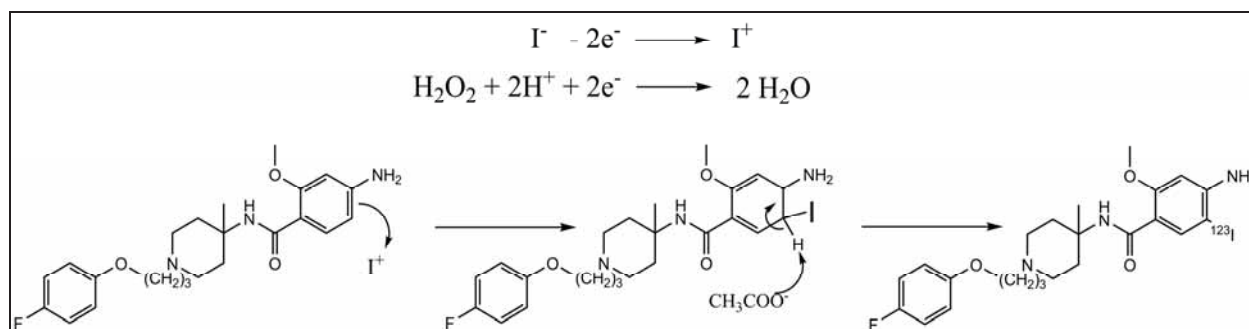
Figure 3.3: [^{123}I]-R91150 radiosynthesis: iodination reaction mechanism

The reaction mechanism of the radiosynthesis is an electrophilic substitution reaction.

The electrophilic species is the iodonium ion, I$^+$. The iodonium ion I$^+$ is formed *in situ* from the oxidation of radioiodide, I$^-$, under influence of 30 % hydrogen peroxide present in the reaction environment. The solvent used is glacial acetic acid, which provides the acidic environment necessary for the radiosynthesis reaction. At the end of the reaction, the excess H$_2$O$_2$ is neutralised by reduction with sodium sulphite. The used quenching solution is strongly basic (sodium sulphite in 3M NaOH solution) to neutralise the acid radiosynthesis mixture (containing glacial acetic acid). This is necessary prior to purification to avoid damage to the HPLC columns.

3.2.2. Radiosynthesis and purification of [^{123}I]-R91150

3.2.2.1. Radiosynthesis of [^{123}I]-R91150

0.5-1 mg of precursor was dissolved in 350 µL glacial acetic acid in a V-vial, and no carrier added [^{123}I]-solution (NaI in 0.05M NaOH, Amersham) was added. Cold sodium iodide was added as carrier (0.1 nmol cold NaI per 37 MBq of ^{123}I) to adjust the specific activity of the final tracer solution to 10 Ci/µmol. At 0, 10, 20 and 25 min, 35 µL of a H$_2$O$_2$-solution (30%, Sigma-Aldrich Belgium) was added to the vial. At 30 min the reaction was quenched by addition of 1 ml of sodium sulphite solution (126 mg/ml in 3M NaOH-solution). The radiosynthesis mixture was transferred to the HPLC system for purification.

3.2.2.2. Purification of [^{123}I]-R91150

Since the synthesis of [^{123}I]-R91150 was performed on a routine basis with high activities, a special purification-setup was constructed, allowing for a nearly hands-off semi-automatic purification of the radiotracer. This also provided a simple radioprotection solution during synthesis of the radiotracer.

The setup for purification of [^{123}I]-R91150 with HPLC (high performance liquid chromatography) is pictured in figure 3.4.

The routine synthesis setup is constructed with 3 valves: one 6-way HPLC valve (left on figure 3.4, Hamilton), one small 3-way rotary valve (Hamilton), and finally one HPLC injection valve (most right in figure 3.4, Valco HPLC injection valve). The valves are connected with HPLC tubing as indicated in figure 3.4. The system further consists of two peristaltic pumps (PP1 and PP2 on figure 3.4, Gilson Mini-Pulse 3, flow rate of respectively 5 ml/min and 1 ml/min), a HPLC pump (Waters 515 HPLC pump at a flow of 0.8 ml/min), a pre-column (in-house made using LichroPrep RP-8 25-40 µm silica gel, Merck), and a HPLC column (Lichrospher RP select B, 250 x 4 mm, 5 µm particle diameter). For detection, a single-channel UV-detector (Pye Unicam LC3 UV-detector at 254 nM) and radioactivity detector (Ludlum model 2200 scaler rate meter with NaI scintillation probe) were used, coupled to a data-recorder (Ankersmit A41 2-channel data recorder).
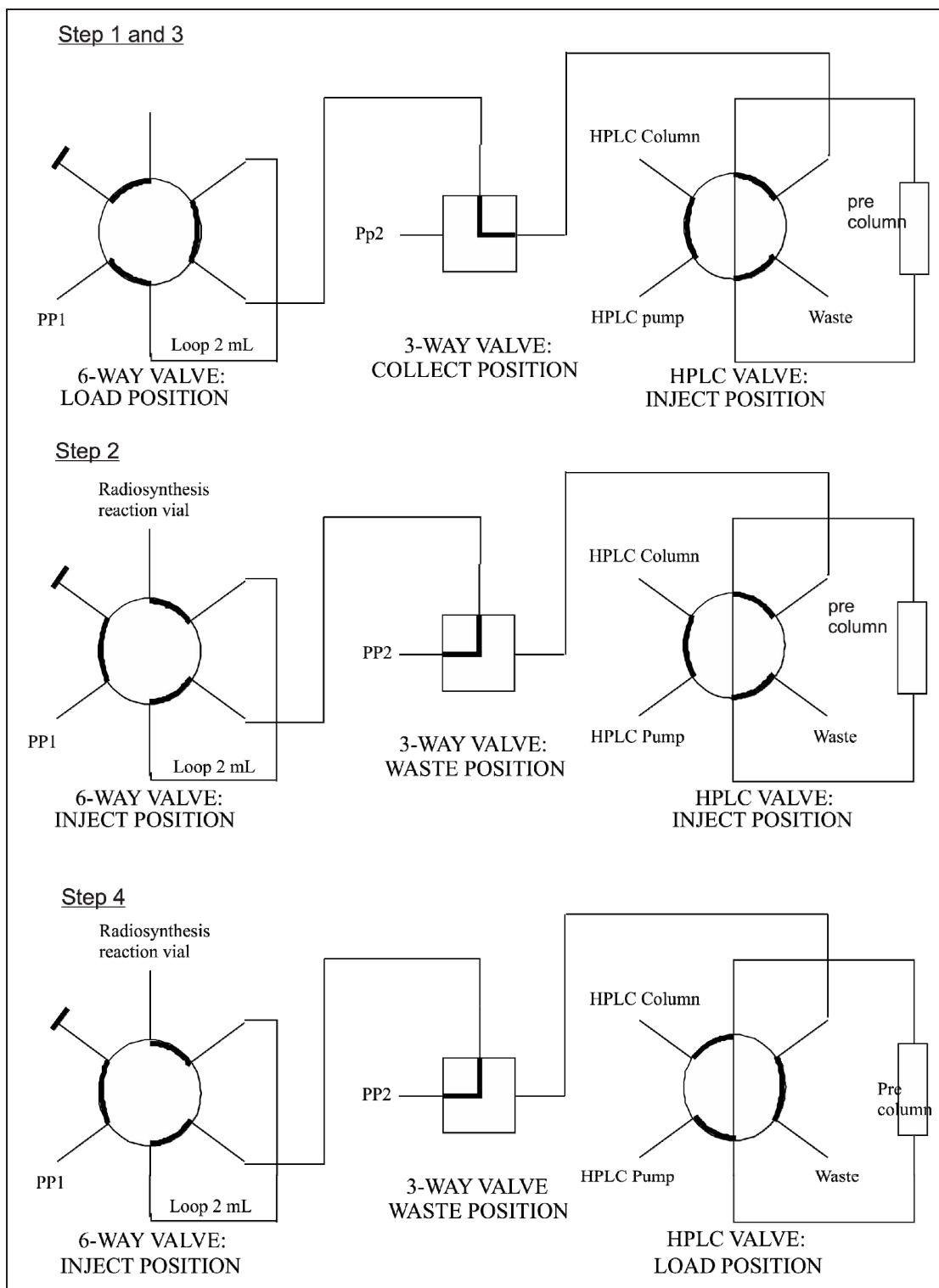
Figure 3.4: [^{123}I]-R91150 routine synthesis set-up

Another 3-way valve is connected to the outlet of the HPLC tubing, one outlet going to the waste bottle and the other outlet connected to a sterile collection vial via a syringe filter (0.22 μm, FP 13/0.2 RC-S, Schleicher&Schuell, Germany).

The purification process consists of 4 steps, which are indicated with their respective valve positions in figure 3.4:

* Step 1: This step is a rinsing step. Sterile, pyrogen- and dust-free water is used to rinse the 2 ml loop and pre-column. Flow rate: 5 ml/min. Time: 5 min.

* Step 2: Valves are positioned as depicted in figure 3.4. The synthesis vial containing the synthesis mixture is placed in a shielded vial, and connected to the first 6-way valve. Using peristaltic pump 2, the synthesis mixture is transferred to the 2-ml loop. Flow rate: 1 ml/min. Time: 2 min.

* Step 3: After changing valve positions, diluted sodium hydroxide solution (1 mM) and peristaltic pump 1 are used to transfer the reaction mixture (in the loop) to the pre-column. Radioactivity concentration on the pre-column is monitored, and the flow is stopped when the radioactivity concentration reaches a maximum. Flow rate: 5 ml/min. Time: 1 min.

* Step 4: In the final step the HPLC valve is switched, transferring the radioactivity contained on the precolumn to the HPLC column, and the HPLC run is started. A sterile sodium acetate buffer/ethanol solution (2.28 g NaOAc.3H_2O in 60 ml H_2O + 40 ml EtOH, adjusted to pH5) is used as eluent. Time: ± 25 min.

The fraction corresponding to [^{123}I]-R91150 (T_R = 22 min) was collected during 4 minutes (collection volume: 3.2 mL) (figure 3.5). Sterile water for injection is added (8-9 mL) to the collection vial to yield a sterile solution of [^{123}I]-R91150 (containing 10 % ethanol), ready for use. An aliquot of the tracer solution is withdrawn with a syringe for quality control purposes.

A typical UV- and radio-chromatogram for a routine [^{123}I]-R91150 synthesis run is shown in figure 3.5.
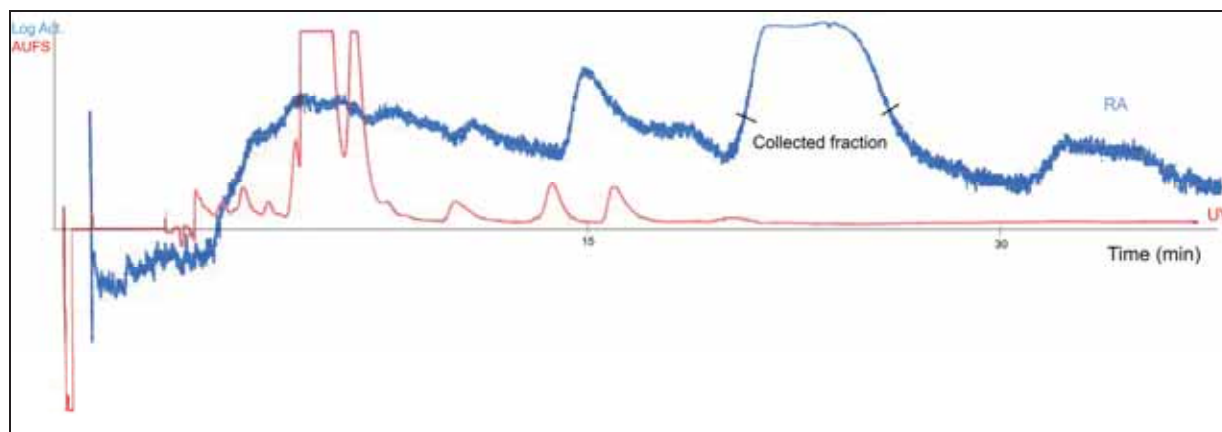
Figure 3.5: [^{123}I]-R91150 synthesis chromatogram. The red graph represents the UV-chromatogram (AUFS-values, detection at 254 nm), the blue graph is the radiochromatogram (Log Activity).

As can be seen in figure 3.5, the tracer elutes at about 22 minutes and is collected during 4 minutes. The large UV-peak, situated around 8 minutes, is the remainder of the precursor eluting from the HPLC column. The total synthesis, from the start of the radiosynthesis reaction to the collection of the purified tracer in the vial, could be completed in one hour. Exposure to radiation is kept to a minimum by using the synthesis unit.

With the setup described above, large amounts of [^{123}I]-R91150 (5 – 50 mCi of starting activity, resulting in 4 – 40 mCi of purified [^{123}I]-R91150 per synthesis run) could be routinely produced. The average yield of the radiosynthesis reaction was 75-80 %.

3.2.3. Quality control

3.2.3.1. Materials and methods

Quality control of the tracer was performed after synthesis by injecting an aliquot (50 µL) of the tracer solution onto an analytical HPLC column (Waters Lichrospher RP-8, 125 x 4 mm, 5 µm) using methanol/acetonitrile/water/acetic acid/triethylamine (190:260:550:1.5:2) as the eluent. A Waters Breeze HPLC system was used for quality control, consisting of a binary gradient system pump (flow rate: 1 ml/min), a Waters 2487 UV-detector (wavelength: 254 nm, AUFS: 0.001) and a Ludlum 2200 scaler rate meter equipped with a NaI scintillation probe.

3.2.3.2. Results

A typical quality control chromatogram can be found in figure 3.6.

In figure 3.6, the upper graph represents the UV-chromatogram, the lower graph represents the radiochromatogram. It is evident from the figure that only one peak was present in the radiochromatogram; by comparing its retention time with the retention time of an authentic cold standard of iodinated R91150, we were able to identify the product as genuine [^{123}I]-R91150. Only the injection peak was visible in the UV-chromatogram, no other peaks were present. The amount of product present in the tracer preparation was below the detection limit of the UV-detector (sensitivity 0.001 AUFS).
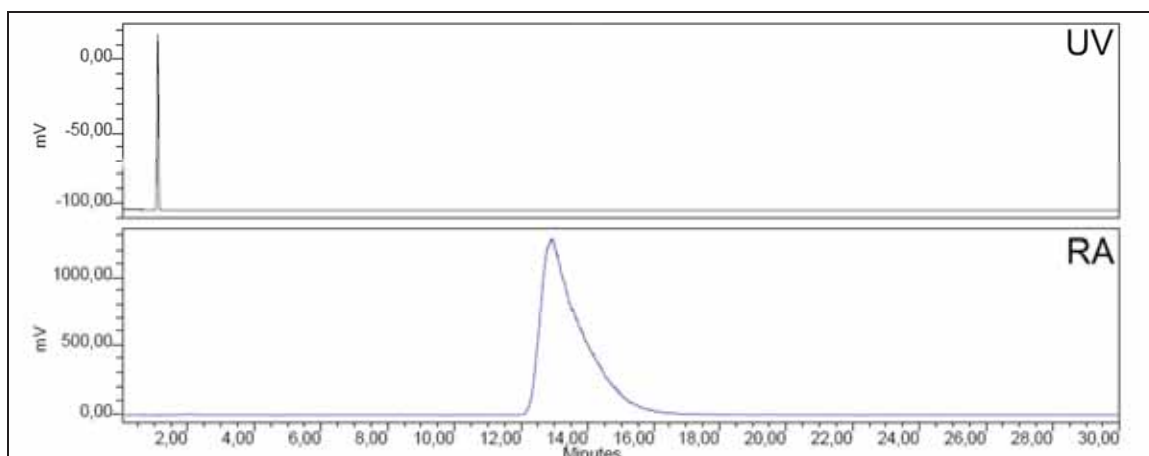
Figure 3.6: Analysis chromatogram of [^{123}I]-R91150 quality control

This is in accordance to the expected high specific activity of the tracer preparation (10 Ci/μmol).

Synthesis of [^{123}I]-R91150 and the subsequent quality control were performed on a weekly basis for several years. Starting activities of 5 to 50 mCi of [^{123}I]-NaI were used. Quality control of [^{123}I]-R91150 with the setup described above was fast (20 minutes) and accurate. Radiochemical purity was always higher then 95 %, and no UV-signal was ever present in the prepared tracer solution. Stability of the tracer was tested by injecting aliquots of the tracer preparation on the quality control HPLC system. The tracer was stable for at least 36 hours after synthesis (radiochemical purity > 95 %).

3.3. *In vivo* evaluation of [^{123}I]-R91150 in rodents

3.3.1. Influence of cyclosporin A on the biodistribution of [^{123}I]-R91150 in NMRI mice

<u>3.3.1.1. Materials and methods</u>

Male NMRI mice (weight 20 - 25 g) were obtained from Bioservices Inc. The animals were allowed to acclimatise for at least two days after arrival in the laboratory, with free access to water and food, under a light/dark cycle. Belgian law regulations on test animal well-being were followed to accommodate the housing for the animals. All experiments were pre-approved by the Ghent University Animal Ethics Committee under permit number ECP 06/18.

Male NMRI mice (n = 3 per time point) were injected in the tail vein with [^{123}I]-R91150 (10 - 15 μCi dissolved in ethanol/water for injection 10/90 v/v). At appropriate time points after the injection of [^{123}I]-R91150 (10 min, 30 min, 1 hour and 2 hours) the animals were sacrificed by decapitation under isoflurane anaesthesia. Blood was collected. The brain and other organs of interest (heart, lungs, stomach, liver, kidney, spleen, intestines, bladder and fat tissue) were rapidly removed. Blood and organs were weighed and counted for radioactivity in an automated gamma counter (Cobra, Packard Canberra). Aliquots of the injected tracer solution (n = 3) were weighed and counted for radioactivity to determine the injected radioactivity dose received by the animals. Results were corrected for decay and tissue radioactivity concentrations were expressed as a percentage of the injected dose per gram of tissue (% ID/g tissue, mean ± standard deviation values, n = 3).

A second group of animals was treated with cyclosporin A 1 hour before injection of [^{123}I]-R91150. Cyclosporin A (50 mg/ml[38], obtained from Sandoz, Basel, Switzerland) was formulated in cremophore EL (polyethoxylated castor oil, 650 mg/ml) containing 10% ethanol. The resulting solution was diluted ten times with water for injection before administration to the animals. The cyclosporin A dosage used was 50 mg per kg of bodyweight. The same biodistribution protocol as described above was followed.

To demonstrate the influence of cyclosporin A dosage on the brain uptake of [123I]-R91150, a third group of NMRI mice was injected in the tail vein with different dosages of cyclosporin A (0, 10, 20, 35 and 50 mg/kg bodyweight, n = 3 per concentration of cyclosporin A). Half an hour after the injection of the cyclosporin A solution, [123I]-R91150 (10 – 15 µCi dissolved in ethanol/water-for-injection 10/90 v/v) was injected in the tail vein. One hour after tracer injection, the animals were sacrificed by decapitation under isoflurane anaesthesia. The same biodistribution protocol as described above was applied, with the exception that only brain and blood samples were collected.

Results of the different groups were compared using non-parametric analysis (Mann-Whitney test, p-values < 0.05 were considered as statistically significant).

3.3.1.2. Results and discussion

The results of the biodistribution study with [123I]-R91150 in NMRI mice are shown in table 3.3 for the normal group, and table 3.4 for the cyclosporin A pre-treated group. Radioactivity concentrations for [123I]-R91150 in brain and blood are also shown in figure 3.7 for both the normal and the cyclosporin A pre-treated group.

	Time (min)			
	10	30	60	120
Blood	0,65 ± 0,05	0,57 ± 0,07	0,28 ± 0,05	0,22 ± 0,07
Brain	0,95 ± 0,02	0,87 ± 0,2	0,73 ± 0,01	0,44 ± 0,05
Heart	2,42 ± 0,4	1,28 ± 0,25	0,49 ± 0,09	0,22 ± 0,002
Lungs	23,0 ± 3,2	11,3 ± 3,2	3,54 ± 0,2	1,30 ± 0,03
Stomach	2,3 ± 0,4	5,89 ± 0,44	3,0 ± 1,2	3,84 ± 1,01
Spleen	4,12 ± 0,5	2,64 ± 0,32	0,99 ± 0,2	0,47 ± 0,008
Liver	8,2 ± 1,6	18,8 ± 5,7	5,7 ± 0,1	4,66 ± 0,97
Kidney	11,2 ± 0,5	9,07 ± 1,66	3,76 ± 0,45	2,78 ± 1,4
Small Int.	2,65 ± 0,6	7,42 ± 2,0	10,8 ± 2,1	8,06 ± 1,5
Large Int.	0,94 ± 0,2	0,85 ± 0,3	1,1 ± 0,12	6,13 ± 2,1
Bladder	1,89 ± 0,2	2,01 ± 0,6	4,42 ± 2,4	0,78 ± 0,41
Fat Tissue	1,67 ± 0,8	1,28 ± 0,6	4,6 ± 0,9	0,37 ± 0,1

Table 3.3: Results of [123I]-R91150 biodistribution in NMRI mice. Results are expressed as % ID/g tissue. Mean ± standard deviation values are shown (n = 3).

	Time (min)			
	10	**30**	**60**	**120**
Blood	0,76 ± 0,36	0,92 ± 0,40	0,77 ± 0,3	0,78 ± 0,4
Brain	3,65 ± 1,1	5,24 ± 0,9	5,2 ± 0,7	3,12 ± 1,1
Heart	0,90 ± 0,65	2,75 ± 0,5	1,6 ± 0,5	0,99 ± 0,18
Lungs	2,69 ± 1,3	9,18 ± 0,8	8,31 ± 0,6	1,70 ± 0,13
Stomach	3,04 ± 0,35	2,3 ± 0,15	3,74 ± 0,3	2,44 ± 0,6
Spleen	1,54 ± 0,7	4,02 ± 0,5	3,14 ± 0,2	2,56 ± 1,01
Liver	4,05 ± 0,78	6,97 ± 3,13	11,7 ± 6,1	3,89 ± 0,28
Kidney	5,49 ± 2,6	10,34 ± 5,1	8,32 ± 3,2	4,9 ± 1,77
Small Int.	4,78 ± 2,1	3,17 ± 0,49	9,92 ± 4,01	3,82 ± 1,49
Large Int.	0,32 ± 0,30	1,33 ± 0,5	0,92 ± 0,28	1,46 ± 0,64
Bladder	2,9 ± 0,49	7,9 ± 3,0	6,21 ± 2,69	4,87 ± 1,14
Fat Tissue	6,45 ± 1,2	2,75 ± 1,5	1,04 ± 0,07	0,61 ± 0,06

Table 3.4: Biodistribution with [123I]-R91150 in NMRI mice after treatment with cyclosporin A (50 mg/kg). Results are expressed as % ID/g tissue (mean ± standard deviation, n = 3).

For the control group, the brain uptake of [123I]-R91150 reached a maximum at 10 min after injection (0.95 ± 0.02 % ID/g tissue) and slowly decreased over time (0.44 ± 0.05 % ID/g tissue at 2 hours after injection). Brain radioactivity concentration was always higher than the blood radioactivity concentration (on average, the radioactivity concentration in blood was half of the concentration in brain). Blood radioactivity also decreased slowly over time (from 0.65 ± 0.05 % ID/g tissue to 0.22 ± 0.07 % ID/g tissue).

For the cyclosporin A pre-treated group, brain uptake was initially high (3.65 ± 1.1 % ID/g tissue at 10 min after injection) and remained high over time (3.12 ± 1.1 % ID/g tissue at 2 hours after injection). A maximum brain uptake of 5.24 ± 0.9 % ID/g tissue was reached 30 min after injection. Radioactivity uptake in blood was lower (between 0.76 % ID/g tissue and 0.92 % ID/g tissue) and remained constant over the examined time frame. Brain-to-blood ratios varied between 4.00 and 6.75.

The biodistribution data for blood and brain in the control group and the cyclosporin A pre-treated group were compared. The results of the comparison are depicted in figure 3.7.
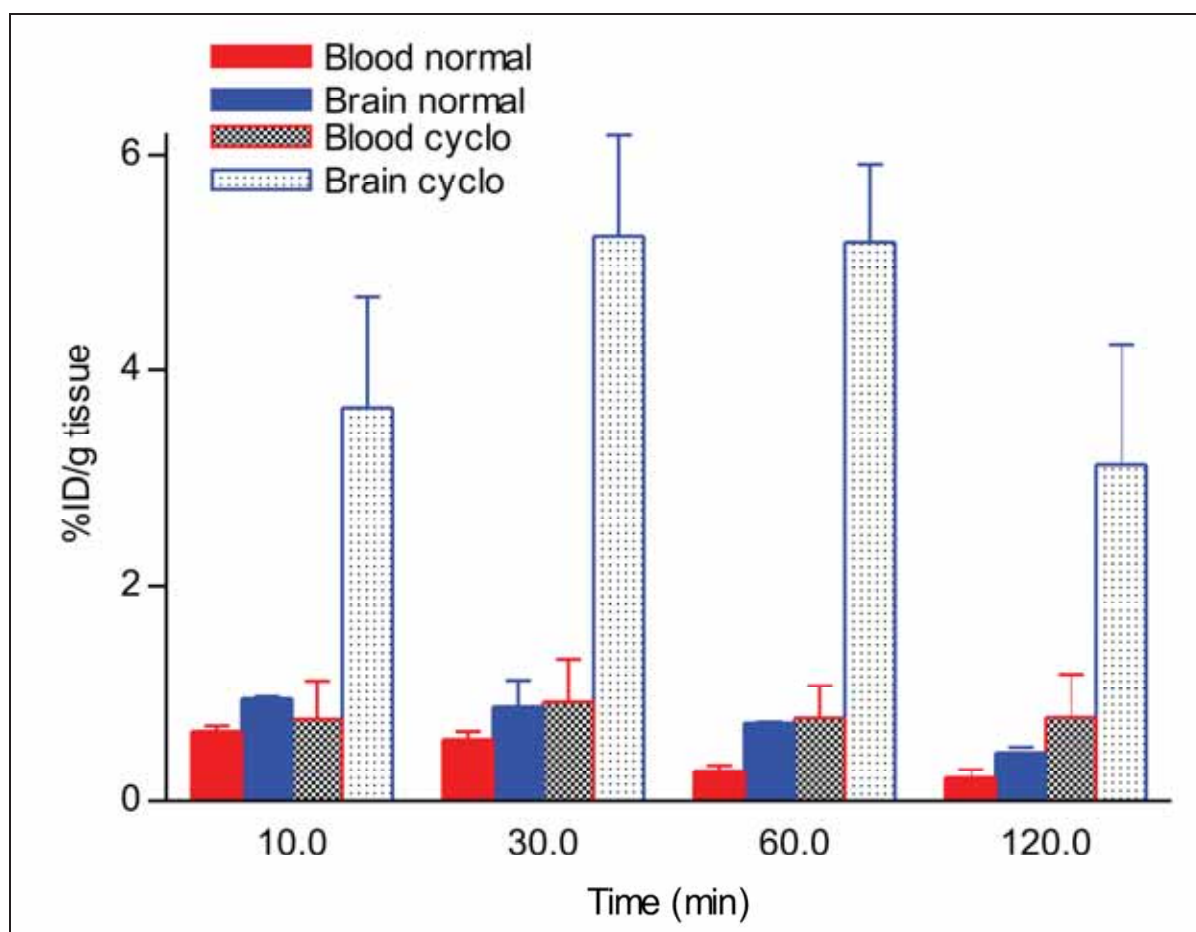
Figure 3.7: [^{123}I]-R91150 biodistribution data for blood and brain of NMRI mice. Results of the normal and the cyclosporin-treated group are shown. Results are expressed as % ID/g tissue (mean ± standard deviation values, n = 3 per time point).

The increase in brain radioactivity is clearly visualized: at 10 min post injection the uptake in brain was 3.8 times higher for the cyclosporin A pre-treated group compared to the control group. This difference became even higher at later time points (up to 7.1 times higher at 2 hours post injection). Consequently, the brain-to-blood ratios were much higher for the cyclosporin A pre-treated group compared to the non-treated control group. Although the blood radioactivity concentrations were higher after cyclosporin A pre-treatment (ratios between the cyclosporin A pre-treated group and the control group varied between 1.1 and 3.5), the uptake of radioactivity in the brain is much more increased (ratios between the cyclosporin A pre-treated group and the control group varied between 3.8 and 7.1), indicating that the difference in blood radioactivity concentration between the control group and the

cyclosporin A pre-treated group (and thus tracer influx to the brain) is not fully responsible for the increased cerebral radioactivity concentration.

The time difference between the cyclosporin A injection and the tracer injection was kept constant at 30 min. This influence has already been studied by other authors who demonstrated that the influence of cyclosporin A on the drug efflux of [^{11}C]-verapamil was constant at 15 min post injection of cyclosporin A [39].

These data are in good accordance with the function of P-glycoprotein as a drug efflux pump, and the blocking of its function by administration of cyclosporin A.

To further evaluate the possibility of [^{123}I]-R91150 as a substrate for the P-glycoprotein efflux pump, the sensitivity of [^{123}I]-R91150 brain uptake for cyclosporin A dosage was investigated in a dose-response study in NMRI mice. The results are shown in figure 3.8.
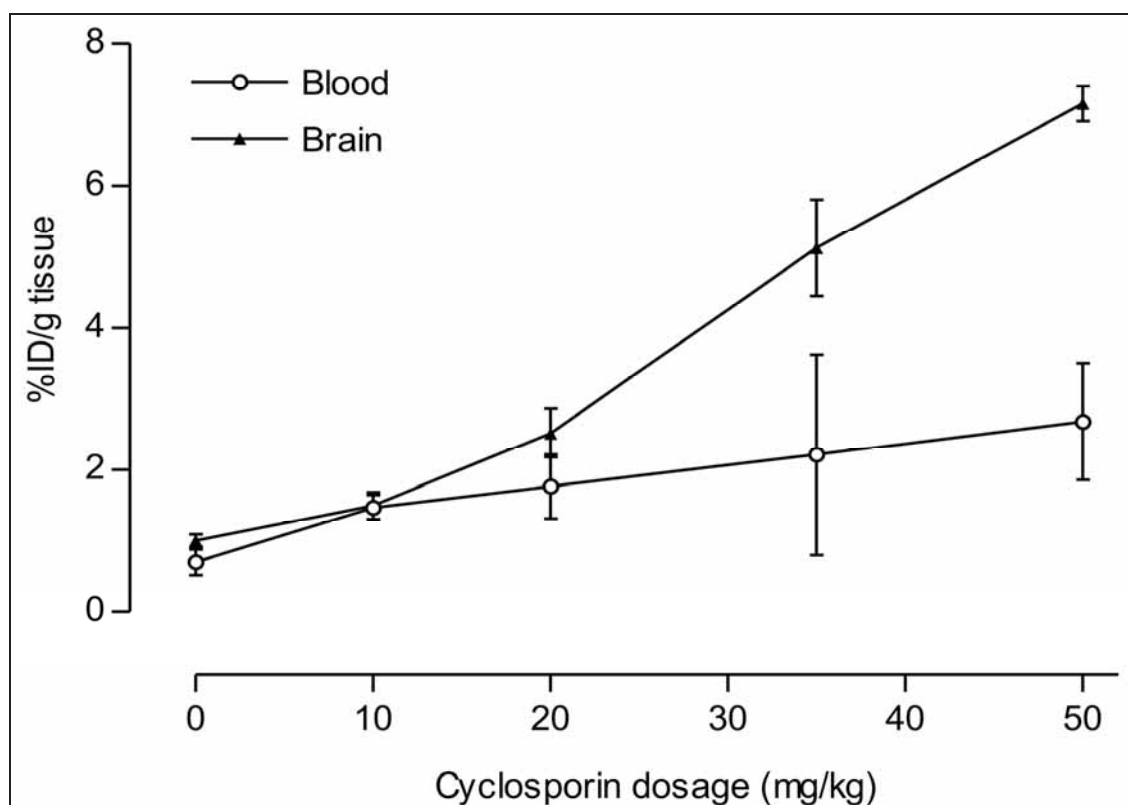
Figure 3.8: Influence of cyclosporin A dosage on the brain uptake of [^{123}I]-R91150 in NMRI mice. Results are expressed as % ID/g tissue (mean ± standard deviation values, n = 3 per dosage group).

Administration of cyclosporin A had a dose-dependent effect on the brain uptake of $[^{123}I]$-R91150 in mice. The highest influence was observed for the highest dosage of cyclosporin A (50 mg/kg). Lower dosages of cyclosporin A resulted in lower cerebral uptake. At all dosages uptake was significantly higher compared to the control group.

Unfortunately, we could not demonstrate a sigmoid relationship between the cyclosporin A dosage and the uptake of radioactivity in the brain, as some other authors did for $[^{11}C]$-GR218231 and $[^{11}C]$-verapamil [35, 38]. Due to the toxic effect of cyclosporin A, dosages higher than 50 mg/kg could not be administered to mice.

A small but continuous increase (not statistically different) in blood radioactivity concentration was observed, correlated to the cyclosporin A dosage examined. This could be explained by a possible influence of cyclosporin A on the plasma kinetics of $[^{123}I]$-R91150. A similar influence has been observed for etoposide [39]. It's also interesting to note that Liow et al. [40] demonstrated that under influence of cyclosporin A, the free non-protein-bound fraction in plasma of $[^{11}C]$-(R)-(-)-WAY, a radioligand for the 5-HT$_{1A}$ receptor, was increased 2.7-fold. The authors conclude that the increased brain uptake of $[^{11}C]$-(R)-(-)-WAY induced by cyclosporin A may be partly caused by displacement of the radioligand from the plasma proteins. The effect of cyclosporin A on the free fraction of $[^{123}I]$-R91150 and subsequent uptake in the brain has not been investigated.

Despite the fact that saturation could not be demonstrated by a sigmoid curve, and that cyclosporin A might have some effect on tracer plasma kinetics, the correlation between the cyclosporin A dosage and the dramatic increase in brain radioactivity concentration at all time points indicates that the P-glycoprotein efflux transporter is probably involved in the pharmacokinetics of $[^{123}I]$-R91150 in the brain.

Radioactivity concentrations for $[^{123}I]$-R91150 in lungs and heart were initially high, but decreased rapidly. These curves are probably a reflection of the blood pool radioactivity concentration. This might be the reason why some of the concentrations in heart and lungs are higher in the cyclosporin A pre-treated group compared to the control animals (especially at later time points).

The high tracer uptake in liver could be explained by biotransformation in the liver, followed by renal or biliary excretion of $[^{123}I]$-iodide or $[^{123}I]$-R91150.

Uptake in spleen is decreased in the cyclosporin A pre-treated group at 10 min post injection, but is elevated at all other time points, compared to the control group. Splenic P-glycoprotein pumps are supposed to be involved in the protection of the spleen. P-glycoprotein in the spleen extrudes the toxic unconjugated bilirubin, formed during haemolysis. Blockade of the efflux pump by cyclosporin A could give an explanation for the increased radioactivity levels in the spleen for the cyclosporin A pre-treated group.

From these experiments we can conclude that [^{123}I]-R91150 is a substrate for the P-glycoprotein efflux transporter. When the efflux pumps are inhibited by cyclosporin A, brain uptake is severely and dose-dependently increased (up to 7.1 times compared to the control group at a dosage of 50 mg/kg cyclosporin A). Studies in larger rodents (rats) are necessary to determine the effect of P-glycoprotein blocking on the regional brain distribution of [^{123}I]-R91150.

3.3.2. Influence of cyclosporin A on the regional brain biodistribution with [^{123}I]-R91150 in Sprague-Dawley rats

3.3.2.1. Materials and methods

Male Sprague-Dawley rats (weight 200 - 250 g) were obtained from Bioservices Inc. The animals were allowed to acclimatise for at least two days after arrival in the laboratory, with free access to water and food, under a light/dark cycle. Belgian law regulations on test animal well-being were followed to accommodate the housing for the animals. All experiments were pre-approved by the Ghent University Animal Ethics Committee under permit number ECP 06/18.

The animals (n = 3 per time point) were anesthetized with isoflurane and injected in the penile vein with [^{123}I]-R91150 (100-150 µCi dissolved in 10% ethanol in water for injection). At appropriate time points after injection of [^{123}I]-R91150 (10 min, 30 min, 1 hour, 2 hours and 4 hours) the animals were sacrificed by decapitation under isoflurane anaesthesia. Blood was collected by heart puncture. The brain was rapidly removed and dissected into the different brain regions: the cortex (which was further dissected into the frontal cortex, parietal cortex, occipital cortex and temporal cortex), cerebellum and the subcortical region. Brain and blood samples were weighed and counted for radioactivity with an automated gamma counter (Cobra, Packard Canberra). Aliquots of the injected tracer solution (n = 3) were weighed and counted for radioactivity to determine the injected radioactivity dose received by the animals. Results were corrected for decay and tissue radioactivity concentrations were expressed as a percentage of the injected dose per gram of tissue (% ID/g tissue, mean ± standard deviation values, n = 3).

The same biodistribution protocol was applied to a group of animals receiving cyclosporin A (50 mg/kg, preparation protocol: 3.3.1.1) one hour before injection of [^{123}I]-R91150. Results after cyclosporin A treatment were compared to the values obtained without pre-treatment.

To exclude possible interference of cremophore EL (used for solubilisation of cyclosporin A), three animals were injected with only the vehicle (cremophore EL, saline and 10% ethanol) 1h before [^{123}I]-R91150 injection.

3.3.2.2. Results

Results for the regional brain biodistribution study with $[^{123}I]$-R91150 in Sprague-Dawley rats are shown in table 3.5 for the normal group and table 3.6 for the cyclosporin-treated group.

	Time (min)				
	10	**30**	**60**	**120**	**240**
Blood	0,07 ± 0,007	0,052 ± 0,02	0,033 ± 0,002	0,024 ± 0,008	0,027 ± 0,003
Subcortical	0,17 ± 0,01	0,13 ± 0,002	0,070 ± 0,005	0,036 ± 0,006	0,034 ± 0,008
Temporal	0,20 ± 0,02	0,19 ± 0,02	0,13 ± 0,01	0,071 ± 0,01	0,080 ± 0,03
Frontal	0,28 ± 0,05	0,38 ± 0,001	0,24 ± 0,01	0,19 ± 0,02	0,18 ± 0,01
Parietal	0,20 ± 0,01	0,22 ± 0,001	0,23 ± 0,05	0,13 ± 0,01	0,10 ± 0,006
Occipital	0,19 ± 0,02	0,22 ± 0,08	0,16 ± 0,03	0,13 ± 0,05	0,05 ± 0,01
Cerebellum	0,12 ± 0,003	0,06 ± 0,002	0,04 ± 0,002	0,017 ± 0,002	0,01 ± 0,001

Table 3.5: Results of brain biodistribution study with $[^{123}I]$-R91150 in Sprague-Dawley rats (control group). Results are expressed as % ID/g tissue (mean ± standard deviation, n = 3).

	Time (min)				
	10	**30**	**60**	**120**	**240**
Blood	0,11 ± 0,04	0,08 ± 0,01	0,06 ± 0,004	0,05 ± 0,02	0,02 ± 0,01
Subcortical	0,71 ± 0,17	0,83 ± 0,09	0,65 ± 0,03	0,35 ± 0,09	0,10 ± 0,01
Temporal	1,36 ± 0,36	1,14 ± 0,21	0,78 ± 0,07	0,64 ± 0,05	0,29 ± 0,2
Frontal	1,49 ± 0,1	1,84 ± 0,1	1,58 ± 0,09	0,58 ± 0,14	0,57 ± 0,01
Parietal	1,11 ± 0,4	1,23 ± 0,22	1,35 ± 0,12	1,21 ± 0,27	1,13 ± 0,14
Occipital	1,08 ± 0,3	1,05 ± 0,26	1,07 ± 0,11	0,86 ± 0,17	0,34 ± 0,13
Cerebellum	0,43 ± 0,15	0,51 ± 0,02	0,45 ± 0,01	0,24 ± 0,01	0,09 ± 0,01

Table 3.6: Results of brain biodistribution study with $[^{123}I]$-R91150 in Sprague-Dawley rats after treatment with cyclosporin A (50 mg/kg). Results are expressed as % ID/g tissue (mean ± standard deviation, n = 3).

The results of the regional brain biodistribution study with $[^{123}I]$-R91150 in Sprague-Dawley rats are shown in figure 3.9 for both the normal and the cyclosporin A group. Radioactivity concentration values are indicated for blood, frontal cortex and cerebellum.
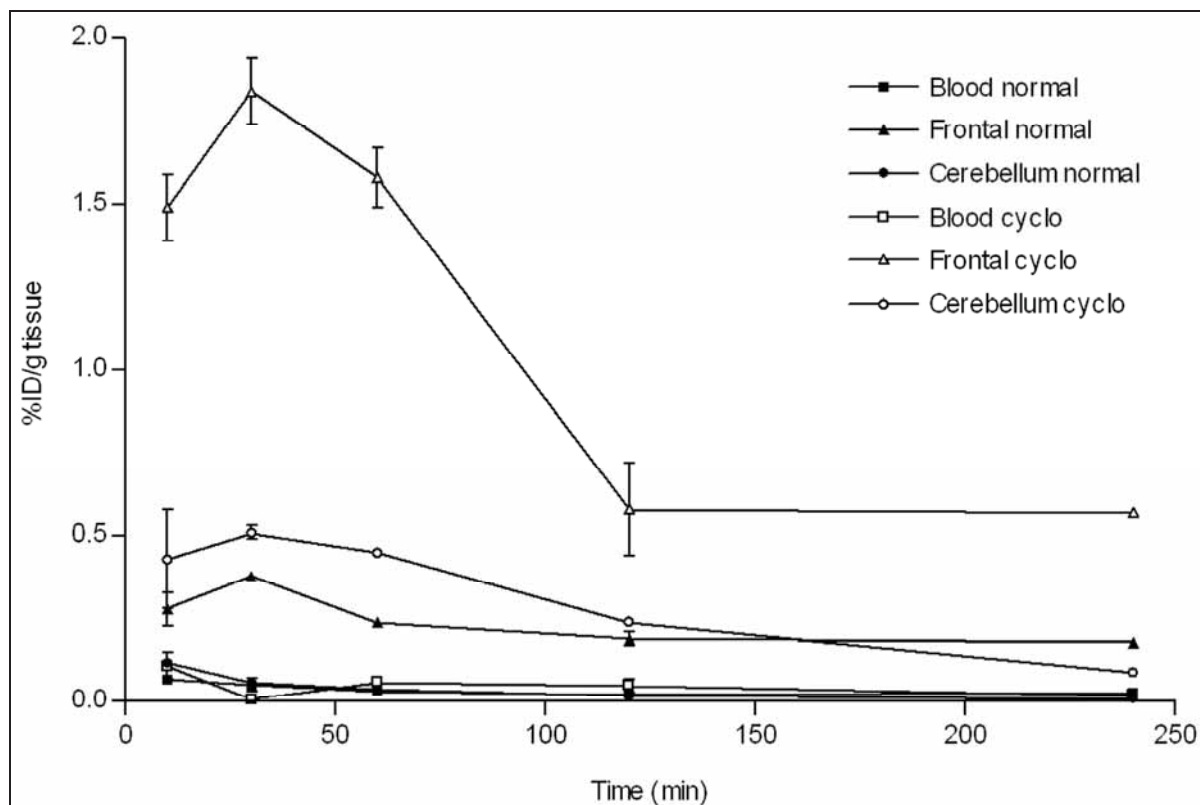
Figure 3.9: Results of the regional brain biodistribution study with [123I]-R91150 in male Sprague-Dawley rats, with and without cyclosporin A pre-treatment (50 mg/kg). Results are expressed as % ID/g tissue (mean ± standard deviation, n = 3 per time point).

It is clear from figure 3.9 that no significant difference in blood radioactivity concentration values could be observed between the normal and the cyclosporin group. For the cyclosporin-treated group, radioactivity concentration values in brain were substantially higher than those found in the control group. For example, at 1 hour after injection, radioactivity concentration in frontal cortex increased from 0.24 ± 0.0092 % ID/g tissue to 1.58 ± 0.097 % ID/g tissue after treatment with cyclosporin A. In the reference tissue, the cerebellum, radioactivity concentration increased from 0.038 ± 0.0023 % ID/g tissue at 1 hour after injection of [123I]-R91150 to 0.45 ± 0.017 % ID/g tissue after treatment of the animals with cyclosporin A.

For the control group, the highest [123I]-R91150 radioactivity concentration in brain was observed in the frontal cortex ($0,38 \pm 0,001$ % ID/g tissue at 30 min post injection, decreasing to 0.18 ± 0.01 % ID/g tissue at 4 hours post injection of [123I]-R91150). Radioactivity concentration in blood was substantially lower than in the brain: frontal cortex-to-blood radioactivity concentration ratios of about 7 were obtained throughout the study for the control group.

Radioactivity concentration levels in cerebellum approached the values found in blood, and starting from 1 hour after tracer injection, cerebellar radioactivity concentrations were lower than the blood radioactivity concentration values.

Minimal frontal cortex-to-cerebellum radioactivity concentration ratios of about 7 were observed starting 30 min after tracer injection, and the ratio reached a value of 18 at 4 hours after injection of [^{123}I]-R91150 for the control group.

For the cyclosporin A pre-treated group, highest [^{123}I]-R91150 radioactivity concentration in brain was observed in the frontal cortex (1.84 ± 0.1 % ID/g tissue at 30 min after tracer injection). Frontal cortex-to-blood radioactivity concentration ratios averaged 20 throughout the study. Cerebellum-to-blood radioactivity concentration ratios were substantially lower: an average ratio of about 4 was obtained throughout the study.

Frontal cortex-to-cerebellum radioactivity concentration ratios averaged around 4 in the cyclosporin A pre-treated group, which is substantially lower than the ratio of 7 obtained in the control group. No significant difference in blood radioactivity concentration could be observed between both groups.

On average, there was a five to six-fold increase in [^{123}I]-R91150 concentration in brain after cyclosporin A treatment. The other brain regions (temporal, parietal and occipital cortex) showed a similar increase in [^{123}I]-R91150 radioactivity concentration after treatment of the animals with cyclosporin A.

To exclude possible effects of cremophore EL, a blank test was performed. No modulating effects of cremophore EL on [^{123}I]-R91150 accumulation in the brain of Sprague-Dawley rats were measured (data not shown). These results are in accordance to the data obtained by other authors[41].

3.3.2.3. Discussion

The increase in [123I]-R91150 concentration in the brain of male Sprague-Dawley rats is as expected after cyclosporin A treatment considering the conclusion from the mouse cyclosporin A study that [123I]-R91150 is a substrate for P-glycoprotein *in vivo* in rodents. Theoretically, an increased brain uptake could be the result of a higher blood radioactivity concentration, resulting in an increased supply of tracer to the brain. Because no significant difference in blood radioactivity concentration was observed between the normal and the cyclosporin group, this situation could be ruled out, especially since a dose-response relation was observed between the amount of cyclosporin A administered and the corresponding tracer concentration in the brain.

The regional brain radioactivity concentration values for the normal group are in accordance with the original regional brain biodistribution study results obtained by Terriere et al[2], and can be compared with the results obtained with other 5-HT$_{2A}$ tracers, for example [11C]-MDL100907[42] and [18F]-altanserin[43, 44]. Both MDL and altanserin concentrated preferentially in (frontal) cortical tissues, and showed a (relative) absence of binding in cerebellum, confirming the usability of the cerebellum as a reference region in 5-HT$_{2A}$ brain studies when performing kinetic modelling studies according to the reference tissue model. However, [18F]-altanserin also showed considerable aspecific binding, for example to cerebellar tissues.

The results obtained in our studies with [123I]-R91150 and cyclosporin A can be compared with the results obtained by other authors with other (brain) tracers; generally, administration of cyclosporin A resulted in a large increase in brain radioactivity uptake. Regional tracer distribution in the brain was not affected by Pgp modulation. For example, the effect of cyclosporin A on the brain uptake of the 5-HT$_{1A}$ tracer [11C]-WAY100635 was investigated by Liow et al[40]. Cyclosporin A increased brain uptake of [11C]-WAY100635 in rats by a factor of five, which is in good accordance to our results obtained with [123I]-R91150 in rats. Similarly, [18F]-MPPF (also a 5-HT$_{1A}$ tracer) uptake in rat brain increased five- to tenfold after treatment of the animals with cyclosporin A[45].

Brain uptake of the β-adrenergic receptor ligands [11C]-carazolol and [18F]-fluorocarazolol was also increased in Pgp knockout mice and cyclosporin-treated rats[45]. Administration of cyclosporin A increased the levels of [11C]-verapamil about ten-fold in rat brain[46].

A significant difference was observed in the frontal cortex-to-cerebellum ratio between the control and the cyclosporin A treated group: average ratios of about 4 were obtained for the control group, and average ratios of about 7 were obtained for the cyclosporin A treated group. A possible explanation could be that the distribution of P-glycoprotein efflux pumps is not homogenous throughout the brain, resulting in regional effects. Also, aspecific binding in cerebellum could be higher than the aspecific binding in other brain regions, for example the cortex, resulting in a lower frontal cortex-to-cerebellum ratio in the cyclosporin A group.

3.3.3. Influence of cyclosporin A on the displacement of [^{123}I]-R91150 in the brain of Sprague-Dawley rats

3.3.3.1. Materials and methods

Ketanserin and ritanserin were used for the displacement studies in rodents. Ketanserin tartrate (1 mg/kg, dissolved in water/ethanol 95/5, Tocris, UK) was used for displacement studies. Male Sprague-Dawley rats (weight 200 – 250 g, n = 3 per group) were treated with cyclosporin A (50 mg/kg) 1 hour before the injection of [^{123}I]-R91150. Ketanserin was injected into the penile vein 30 min after injection of [^{123}I]-R91150. Ritanserin (obtained from Tocris Cookson, UK) was dissolved in a 5% ethanol solution at a concentration of 5 mg/ml. A dosage of 2.5 mg/kg bodyweight (0.5 ml injected solution) was administered to the animals 30 minutes after injection of [^{123}I]-R91150. The amount of radioactivity injected was approximately 100 – 200 µCi of [^{123}I]-R91150. The animals were sacrificed by decapitation under isoflurane anaesthesia one hour after tracer injection. Blood was collected and the brain was rapidly removed. The brain was dissected into different regions: cortex (frontal, temporal, parietal and occipital cortex), cerebellum and subcortical region. Blood and brain parts were weighed and counted for radioactivity with an automated gamma counter (Cobra, Packard Canberra). The results were corrected for decay and tissue radioactivity concentrations were expressed as a percentage of the injected dose per gram of tissue (% ID/g).

The biodistribution protocol described above was also applied to a group of animals that did not receive a pre-treatment with cyclosporin A. Results obtained from the cyclosporin-treated group were compared with the results obtained from the control group, and the results obtained after ketanserin and ritanserin were also compared.

For statistical analysis, the non-parametric Mann-Whitney test was used. P-values < 0.05 were considered statistically significant. All values are given as mean ± standard deviation, n = 3 animals per time point.

The influence of the displacement with ketanserin on the biodistribution with $[^{123}I]$-R91150 in Sprague-Dawley rats is shown in table 3.7 and figure 3.10 for the control group and the cyclosporin-treated group.

	Treatment group			
	Normal	Ketanserin	Cyclo	Cyclo-ket
Blood	0,033 ± 0,002	0,038 ± 0,002	0,06 ± 0,004	0,06 ± 0,003
Subcortical	0,070 ± 0,005	0,07 ± 0,006	0,65 ± 0,03	0,59 ± 0,06
Temporal	0,13 ± 0,01	0,10 ± 0,002	0,78 ± 0,07	0,68 ± 0,01
Frontal	0,24 ± 0,01	0,18 ± 0,005	1,58 ± 0,09	1,14 ± 0,17
Parietal	0,23 ± 0,05	0,15 ± 0,005	1,35 ± 0,12	0,90 ± 0,12
Occipital	0,16 ± 0,03	0,13 ± 0,02	1,07 ± 0,11	0,85 ± 0,03
Cerebellum	0,04 ± 0,002	0,04 ± 0,0004	0,45 ± 0,01	0,45 ± 0,04

Table 3.7: Results of the ketanserin displacement study with $[^{123}I]$-R91150 in male Sprague-Dawley rats. Results are expressed as % ID/g tissue (mean ± standard deviation, n = 3).
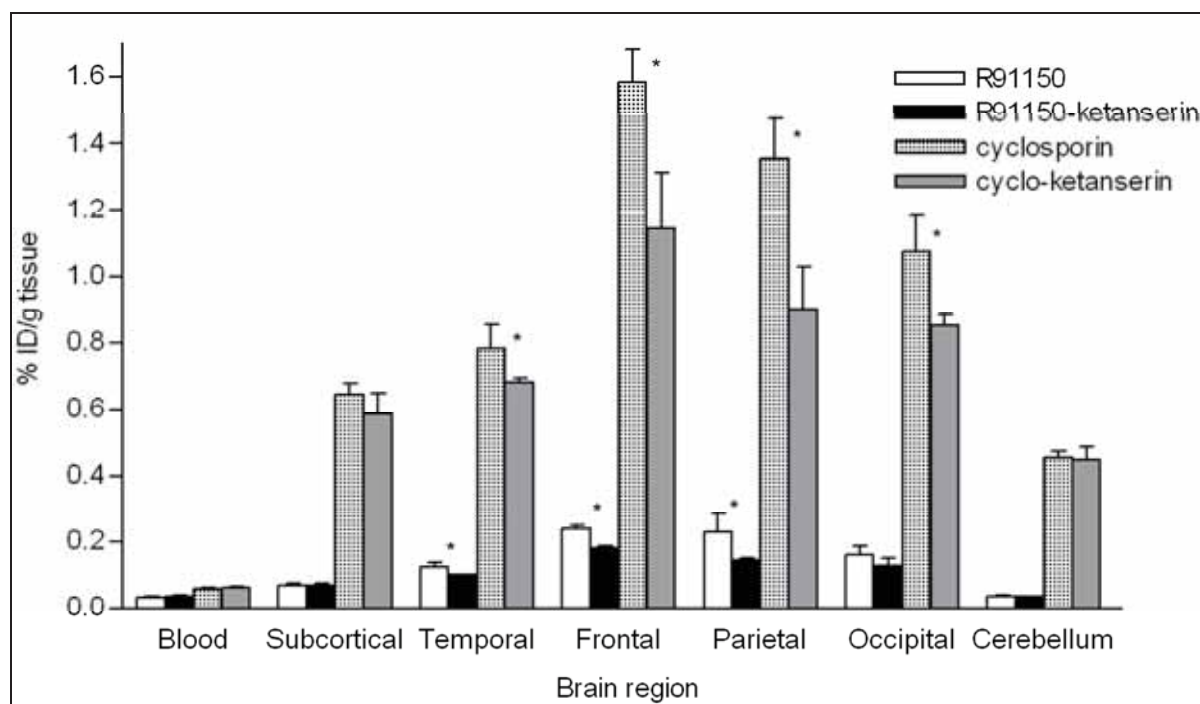

Figure 3.10: Influence of ketanserin displacement on the biodistribution of $[^{123}I]$-R91150 in Sprague-Dawley rats (results at 1 h). Results are expressed as % ID/g tissue (mean ± standard deviation, n = 3 per group). Significant differences between groups are indicated with * (p-value < 0.05).

Uptake of $[^{123}I]$-R91150 decreased with about 30% in frontal cortex after ketanserin displacement for the control group. No significant differences in $[^{123}I]$-R91150 radioactivity concentration were observed in blood, subcortical regions and the cerebellum (figure 3.10). For example, radioactivity concentration values for frontal cortex decreased from 0.24 ± 0.0092 % ID/g tissue for the normal group to 0.18 ± 0.005 % ID/g tissue for the ketanserin displacement group (a decrease in radioactivity concentration of 25 %).

For the cyclosporin pre-treated group, the same reduction in frontal cortex radioactivity concentration (about 30%) was observed after displacement of the radioligand with ketanserin. Radioactivity concentration in cerebellum did not change significantly after displacement with ketanserin. Other cortical areas showed the same behaviour, both for the control as for the cyclosporin-treated group (figure 3.10). Frontal cortex radioactivity concentration values for the cyclosporin-treated group were 1.58 ± 0.097 % ID/g tissue and 1.14 ± 0.15 % ID/g tissue respectively (which amounts to the same reduction in radioactivity concentration as the untreated group, a 25 % decrease after displacement with ketanserin).

As mentioned earlier, in cerebellum there was no significant difference between the normal and the ketanserin group, in both the control (0.038 ± 0.002 % ID/g tissue and 0.0379 ± 0.004 % ID/g tissue respectively) and the cyclosporin A pre-treated animals (0.456 ± 0.017 % ID/g tissue and 0.450 ± 0.038 % ID/g tissue respectively). Radioactivity concentration in blood did not change significantly after ketanserin displacement.

To exclude possible ketanserin-specific effects and as control, a displacement experiment with another known 5-HT$_{2A}$ antagonist, ritanserin, was performed. The results of this experiment can be found in figure 3.11 and table 3.8.
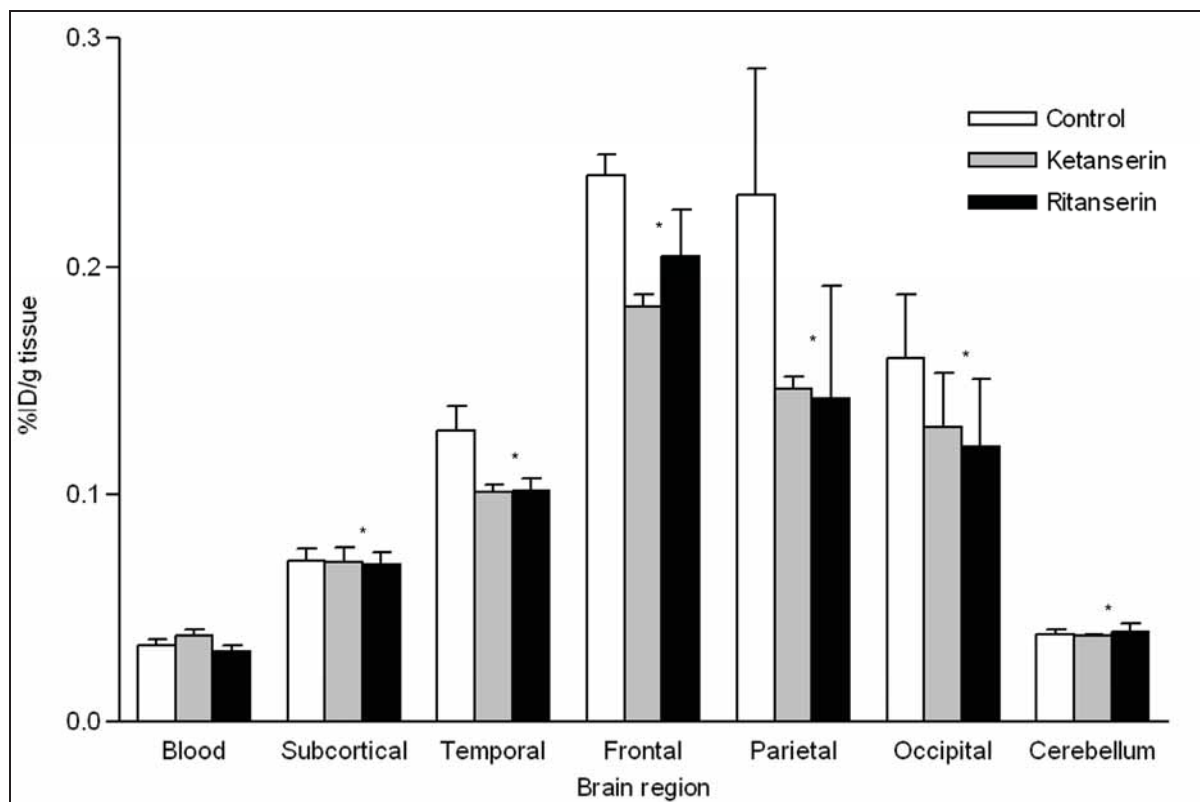
Figure 3.11: Results of the [^{123}I]-R91150 biodistribution study after ketanserin and ritanserin displacement, 1 hour after injection of [^{123}I]-R91150. Results are expressed as % ID/g tissue (mean ± standard deviation, n = 3 per time point, * indicates a p-value > 0.05).

	Treatment group			
	Normal	**Ritanserin**	**Cyclosporin**	**Cyclo-Rit**
Blood	0,033 ± 0,002	0,03 ± 0,002	0,06 ± 0,004	0,045 ± 0,006
Subcortical	0,070 ± 0,005	0,069 ± 0,005	0,65 ± 0,03	0,64 ± 0,09
Temporal	0,13 ± 0,01	0,10 ± 0,005	0,78 ± 0,07	0,75 ± 0,06
Frontal	0,24 ± 0,01	0,20 ± 0,02	1,58 ± 0,09	1,14 ± 0,13
Parietal	0,23 ± 0,05	0,14 ± 0,05	1,35 ± 0,12	1,07 ± 0,18
Occipital	0,16 ± 0,03	0,12 ± 0,03	1,07 ± 0,11	0,93 ± 0,08
Cerebellum	0,04 ± 0,002	0,04 ± 0,004	0,45 ± 0,01	0,45 ± 0,06

Table 3.8: Results of the ritanserin displacement study with [^{123}I]-R91150 in male Sprague-Dawley rats. Results are expressed as % ID/g tissue (mean ± standard deviation, n = 3).

No significant differences were observed between the results obtained after ketanserin displacement and the results obtained after displacement of [^{123}I]-R91150 with ritanserin, indicating that the used dosages of the displacing compound were adequate for fully displacing [^{123}I]-R91150 from the 5-HT$_{2A}$ receptor.

Higher dosages of ketanserin were tested (up to 5 mg/kg, data not shown), but no further displacement of [123I]-R91150 was observed between this higher dosage and the 'standard' dosage (1 mg/kg ketanserin) obtained from literature[16, 17, 7].

3.3.3.3. Discussion

The results obtained in the ketanserin displacement studies are in accordance with the known localization of 5-HT$_{2A}$ receptors in the brain[47]. The cerebellum is used as a reference region in 5-HT$_{2A}$ imaging studies because it contains very low levels of 5-HT$_{2A}$ receptors. Binding of the radioligand in cerebellum is generally regarded as aspecific binding of the tracer to proteins and lipids in the brain.

However, our research demonstrated that a significant amount of [123I]-R91150 radioactivity remained present in frontal cortex after displacement with ketanserin or ritanserin. About 30% of the activity bound to frontal cortex could be displaced by 5-HT$_{2A}$ antagonists, and radioactivity levels in frontal cortex after displacement were about 3-4 times higher than the levels observed in cerebellum. The same observation was seen for the other cortical brain regions. The same reduction in cortical radioactivity concentration (about 30%) was obtained for the control group as for the cyclosporin A pre-treated group.

Our results can be compared to the original results obtained in Wistar rats at the Janssen Research Foundation[2]: displacement of [123I]-R91150 by ketanserin (0.63 mg/kg) resulted in a reduction of activity in frontal cortex with about 35%, whereas cerebellar activity did not change significantly. Radioactivity levels in frontal cortex did not decrease to the levels observed in cerebellum after ketanserin displacement; on the other hand, after blocking of tracer binding by ritanserin (2.5 mg/kg), radioactivity concentration in frontal cortex decreased to the level observed in cerebellum. This result could not be repeated in our ritanserin displacement study; a considerable amount of aspecific binding remained in cerebellum.

Other known 5-HT$_{2A}$ tracers, for example [11C]-MDL100907 and [18F]-altanserin showed acceptable aspecific binding in frontal cortex, but both tracers also showed higher aspecific binding in cerebellum. In all brain areas, the nonspecific binding of [18F]-altanserin was significantly higher than that for [11C]-MDL100907[43]. This finding can not be well-explained by the estimated lipophilicity for the two radioligands, as their log P values are similar.

[123]I-R91150 shows even more aspecific binding in cerebellum, although the lipophilicity of ^{123}I-R91150 is comparable to those of [11C]-MDL100907 and [18F]-altanserin.

It is known that the degree of nonspecific binding cannot be predicted from the lipophilicity (log P) of a tracer alone[48]. Nevertheless, a PET study in Cynomolgus monkeys with [11C]-MDL100907 demonstrated that a considerable amount of radioactivity remained in frontal cortex after displacement or blocking with ketanserin[49], although it is generally accepted that, of all known 5-HT$_{2A}$ tracers, [11C]-MDL100907 demonstrates the least amount of aspecific binding to brain tissues[47, 50].

3.3.4. Influence of cyclosporin A on pinhole μSPECT imaging with [^{123}I]-R91150 in Sprague-Dawley rats

3.3.4.1. Materials and methods

μSPECT image acquisition was performed on a U-SPECT-II (Milabs, Utrecht, the Netherlands) equipped with a dedicated 75 pinhole high-resolution rat collimator.

Male Sprague-Dawley rats (250 – 266 g) were anesthetized with isoflurane and injected with cyclosporin A (50 mg/kg) in the tail vein. 30 minutes later [^{123}I]-R91150 (800 μCi) was injected into the tail vein. Another 40 minutes later a U-SPECT-II scan was performed using the rat collimator (75 pinholes of 1.0 mm) for a continuous 60 minutes (12 frames of 5 minutes) with list mode output enabled.

As a reference animals were also scanned in a similar protocol but without administration of cyclosporin A. A 20 % photo peak was selected around 159 keV while background correction was performed using two additional 10 % windows around 133 and 188 keV.

The time frames from 45 to 75 min post-injection were selected and the data were reconstructed on 0.75 mm voxels by 3 iterations of 16 OSEM subsets. The images were 3D postfiltered by a 15 pixel Gaussian kernel with a width of 1.5 mm.

Two regions-of-interest (ROI's) were drawn around the frontal cortex and the cerebellum using Amide (OpenSource) with 3D Freehand on the coronal slices. The mean value and standard deviation over all voxels in the respective ROI's were calculated for post-analysis. All experiments were conducted following the principles of laboratory animal care and the Belgian law on the protection of animals. Our research protocol was approved by the Ghent University Hospital ethical committee (ECP 06-18).

3.3.4.2. Results and discussion

A pinhole µSPECT scan with [^{123}I]-R91150 after animal treatment with cyclosporin A is shown in figure 3.12. Highest uptake of [^{123}I]-R91150 was found in cortical tissues, lowest concentration of radioactivity was observed in cerebellum.
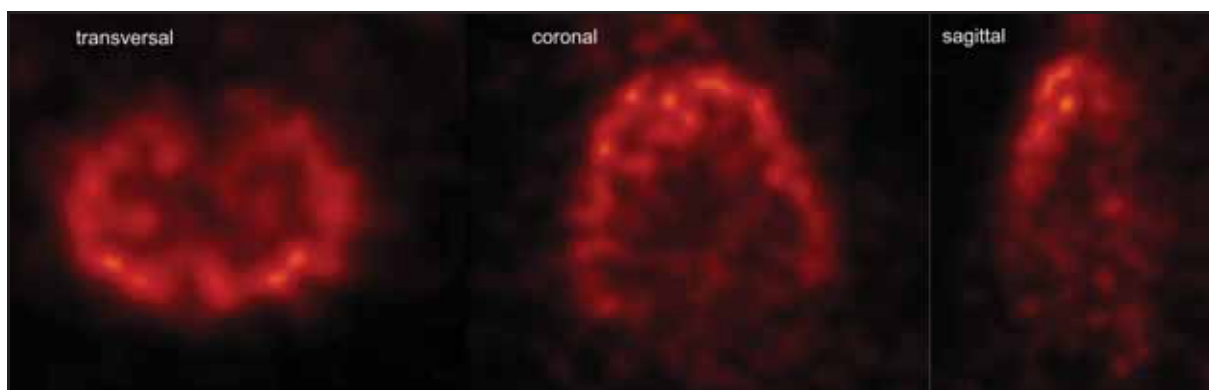
Figure 3.12: Brain pinhole µSPECT imaging with [^{123}I]-R91150 (800 µCi) in Sprague-Dawley rats. The animals were treated with cyclosporin A (50 mg/kg) 30 minutes before tracer injection (time frame scanned: 45 to 75 minutes after tracer injection).

Regions-of-interest (ROI) were drawn around cerebellum and frontal region of the cortical tissues. Tracer uptake in the cerebellum was used as a reference for non-specific binding.
For semi-quantification, the binding index (BI) was estimated as (mean counts in frontal cortex)/(mean counts in cerebellum).

Results of the pinhole µSPECT imaging study for both the control and the cyclosporin A treated group are shown in figure 3.13. Regions-of-interest were drawn around cortical tissue and cerebellum.
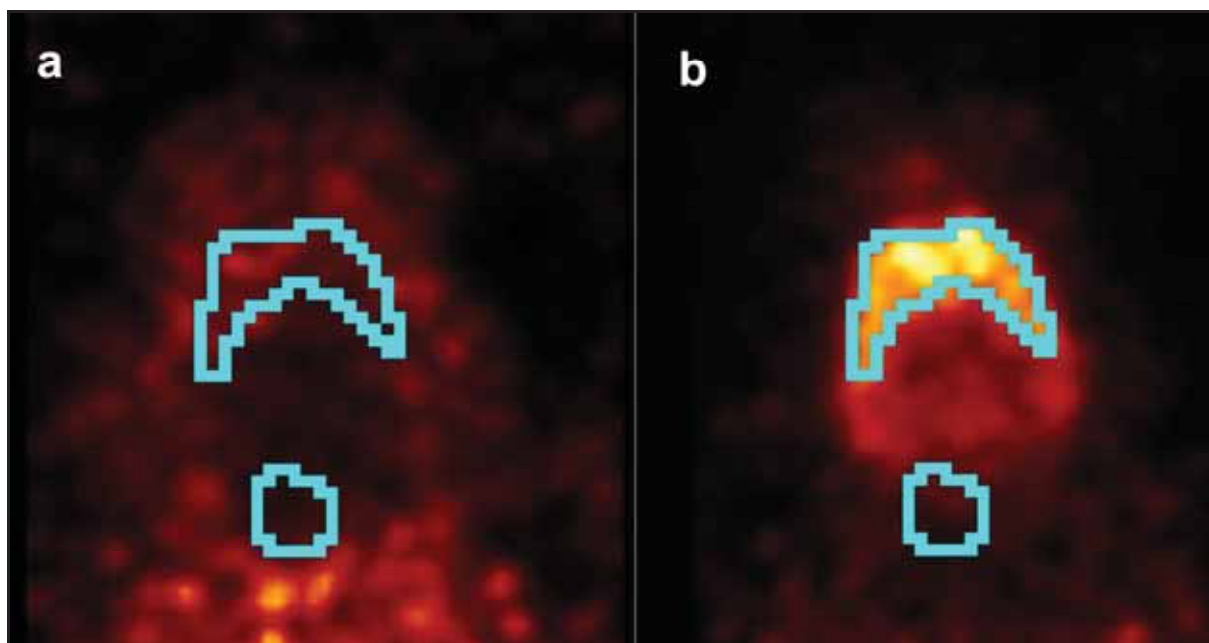
Figure 3.13: Pinhole µSPECT imaging with [^{123}I]-R91150 in Sprague-Dawley rats. Part a: control group; part b: result after cyclosporin A treatment. Regions-of-interest were drawn around the frontal cortical tissues and around the cerebellum.

A large difference in imaging quality was observed between the control and the cyclosporin A treated group. In the control group, hardly any brain radioactivity was observed (figure 3.13 part a): cortical tissues were not visible on the images, and the low count rate made data-analysis problematic. On the other hand, after treatment of the animals with cyclosporin A, the quality of the µSPECT images with [^{123}I]-R91150 improved markedly (figure 3.13 part b): cortical tissues could be clearly visualized, in contrast to the results obtained in the control group.

A cortex-to-cerebellum ratio of about 3.2 was obtained for the cyclosporin A group, a value which is in accordance to the values obtained after dissection in the rat regional brain biodistribution studies with [^{123}I]-R91150.

These results confirm that [^{123}I]-R91150 is a substrate for the P-glycoprotein efflux transporter *in vivo* in rodents; pre-treatment of the animals with cyclosporin A resulted in a markedly increased tracer concentration in the brain.

3.3.5. Influence of cyclosporin A administration on the metabolism of [^{123}I]-R91150 in Sprague-Dawley rats

3.3.5.1. Materials and methods

For determination of possible lipophilic metabolites of [^{123}I]-R91150, male Sprague-Dawley rats (200 - 250 g, n = 3) were injected with approximately 20 MBq of [^{123}I]-R91150. One hour after tracer injection the animals were sacrificed by decapitation, blood was collected in heparinised tubes and the brain was quickly removed by dissection. Blood was centrifuged for 3 min at 3000g and plasma was separated from the pellet. Plasma (500 µl) was mixed with acetonitrile (1 ml). The mixture was vortexed on ice for 10 sec and centrifuged for 3 min at 3000g. Brain tissue was homogenized in acetonitrile (2 ml) for 30 sec and the mixture was centrifuged for 3 min at 3000g. The acetonitrile fraction was filtered through a 0.22 µm syringe filter to remove insoluble impurities, and injected onto the HPLC system for metabolite analysis. The HPLC system consisted of a semi-preparative HPLC pump (Shimadzu LC-8A pump, flow rate of 5 ml/min), a semi-preparative HPLC column (Alltech Econosphere RP-C$_{18}$ 10 mm ID x 250 mm, 10 µm) and radioactivity detector (Ludlum Model 2200 scaler rate meter equipped with a Ludlum 402 NaI scintillation crystal). A 40/60 mixture of ethanol and buffer (0.02 M phosphate buffer pH 7.4) was used as the eluent. An aliquot of authentic [^{123}I]-R91150 solution was also injected on the HPLC system to determine the retention time of unmetabolised [^{123}I]-R91150. Blood and brain samples were analyzed. Radioactivity extraction efficiency was calculated.

The same procedure was applied to blood and brain samples of mice pre-treated with cyclosporin A (50 mg/kg) one hour before injection of the radioligand [^{123}I]-R91150. Results for both groups were compared.

3.3.5.2. Results

Efficiency of the [123I]-R91150 radioactivity extraction process was always higher then 90%. Metabolites of [123I]-R91150 in blood and brain samples of Sprague-Dawley rats were determined. The metabolite assay results for the brain samples can be seen in figure 3.14.
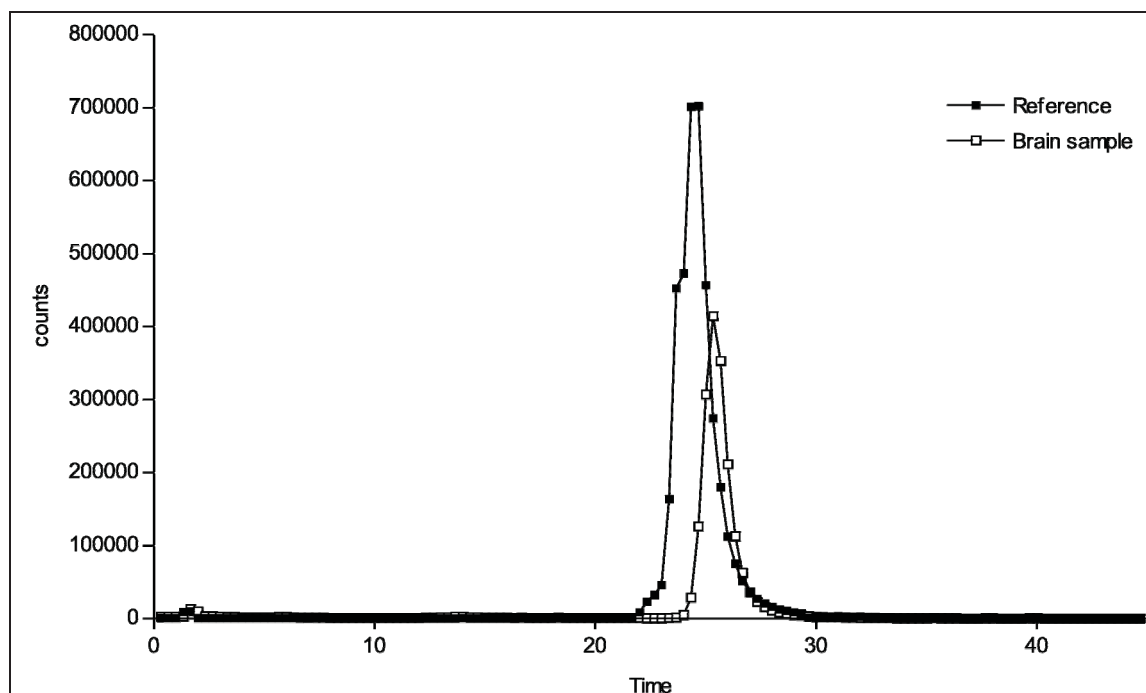
Figure 3.14: [123I]-R91150 HPLC metabolite assay: reference standard and brain sample

As can be seen in figure 3.14, only one radiolabelled product was present in the brain samples of the normal group. This product was identified as unmetabolised [123I]-R91150 by comparison of the retention time with the retention time of an authentic [123I]-R91150 reference standard. No lipophilic metabolites could be detected in blood or brain of the normal group. Besides unmetabolised [123I]-R91150, a small amount of free radioiodide was present in the blood samples, probably due to *in vivo* dehalogenation of the tracer. These results are in good accordance with the data obtained from human and dog metabolite studies[16, 17, 7, 9].

Metabolites in blood and brain of Sprague-Dawley rats pre-treated with cyclosporin A (50 mg/kg, one hour before tracer injection) were determined to exclude possible interference of cyclosporin A with the *in vivo* metabolism of [^{123}I]-R91150. No lipophilic metabolites could be detected in blood or brain after cyclosporin A treatment. The only radiolabelled product found in brain samples was unmetabolised [^{123}I]-R91150. A small amount of free radioiodine was present in the blood samples, probably due to *in vivo* deiodination of the tracer.

3.4. Discussion

The human mdr1 gene (that encodes P-glycoprotein) has several single nucleotide polymorphisms that can change the pharmacokinetics of drugs that are substrates for this transporter [36]. This could possibly lead to successful scans in one patient, and failed scans in another, and is very important in patients treated with high doses of Pgp modulators such as cyclosporin A. Therefore it is necessary in the development of new tracers to determine if their brain efflux is modulated by P-glycoprotein. It is also of interest to know whether the biodistribution of tracers presently used in clinic is influenced by P-glycoprotein. In this regard, several clinically used tracers have already been examined as substrates for P-glycoprotein [33, 34, 51, 36, 52, 53].

The [^{123}I]-R91150 NMRI mouse biodistribution studies, Sprague-Dawley rat regional brain biodistribution studies and the rat μSPECT imaging study all revealed a 4 to 6-fold increase in brain [^{123}I]-R91150 radioactivity concentration after blocking of P-glycoprotein with cyclosporin A. Radioactivity concentration in blood did not increase significantly after treatment of the rats with cyclosporin A. Theoretically, an increased brain uptake can be the result of an increased tracer influx in the brain, or a decreased tracer efflux out of the brain. Since we blocked the function of Pgp as a drug efflux protein, the increase in [^{123}I]-R91150 brain uptake should be the result of decreased tracer efflux out of the brain. This is in accordance with the localization and function of P-glycoprotein as efflux-protein at the blood-brain barrier [36]. The results are also in accordance to the dose-response curve obtained in mice by administering different dosages of cyclosporin A and evaluating the influence on brain tracer concentration. Moreover, the rat biodistribution studies demonstrated no increased supply of tracer to the brain (blood radioactivity concentration did not increase significantly after treatment of the animals with cyclosporin A).

The increased [^{123}I]-R91150 uptake in Sprague-Dawley rat brain after cyclosporin A treatment could not be fully displaced by ketanserin or ritanserin (figure 3.11), indicating that at least part of the increase in [^{123}I]-R91150 radioactivity concentration is due to increased aspecific binding of the tracer in the brain. This can also be seen in the increased radioactivity uptake after cyclosporin A treatment in the reference area, the cerebellum. Residual binding in brain cortical tissues of animals receiving [^{123}I]-R91150 and ketanserin or ritanserin was also considerable.

Our results are in accordance with other, previously published studies investigating the effect of cyclosporin A administration on the brain uptake of different radiotracers [36]. Similarly to the results of Liow et al, brain uptake of [123I]-R91150 increased 4 to 6-fold.

The fact that [123I]-R91150 radioactivity concentration in cortex remains high after ketanserin displacement can be caused by different factors: the amount of ketanserin administered could have been too low, resulting in only partial displacement of [123I]-R91150 from the $5-HT_{2A}$ receptor. Another cause could be that the time period between radioligand injection and ketanserin displacement was too short. Different dosages of ketanserin (up to a dosage of 5 mg/kg - or five times the standard dosage) were tested; higher dosages did not result in higher displacement of [123I]-R91150 in cortex. The time period between tracer injection and injection of the displacing compound was based on data obtained from literature, and is used by almost all researchers investigating brain neurotransmitter receptors.

The remaining activity in cortex after displacement can also be the result of aspecific binding to brain tissue. In this case, the question remains why the amount of aspecific binding in cortex is higher than the amount of aspecific binding observed in cerebellum.

It could also be possible that the high remaining radioactivity in cortex after displacement is the result of a certain affinity of [123I]-R91150 for other receptor (sub)types. This should be investigated further.

Future work will reveal possible changes in [123I]-R91150 free plasma fraction under the influence of cyclosporin A, to exclude the effect of possible displacement of the tracer from plasma proteins, also resulting in an increased tracer influx to the brain and increased brain uptake.

Cyclosporin A administration resulted in a vastly improved quality of the pinhole μSPECT images with [123I]-R91150 in rodents. When visually inspecting the effect of cyclosporin A administration on the μSPECT images, the increase in radioactivity concentration is very clearly visible, as shown in figure 3.13. The brain was hardly visible when only the tracer [123I]-R91150 was administered (figure 3.13 part a), in contrast with for example human trials where the tracer does show good brain uptake [16, 17]. After pre-treatment with cyclosporin A, the frontal cortex became clearly visible (figure 3.13 part b).

The consequences of these results are not clear yet. Perhaps there could be some future in using P-glycoprotein blocking agents to improve the brain uptake of tracers that otherwise show a limited penetration in the brain, and to improve PET or SPECT imaging quality.

3.5. Conclusion

The influence of cyclosporin A pre-treatment on the biodistribution with [^{123}I]-R91150 was evaluated in NMRI mice and Sprague-Dawley rats. The effect of cyclosporin A administration on the quality of the pinhole µSPECT images in Sprague-Dawley rats with [^{123}I]-R91150 was evaluated as well. From the obtained results it can be concluded that [^{123}I]-R91150 is a substrate for P-glycoprotein in NMRI mice and Sprague-Dawley rats.

In NMRI mice, a dose-dependent influence of cyclosporin A on the brain uptake of [^{123}I]-R91150 was observed, indicating that the increased tracer brain concentration is the result of a decreased tracer efflux out of the brain after blocking of the P-glycoprotein efflux transporter by cyclosporin A. Pre-treatment of Sprague-Dawley rats with cyclosporin A resulted in an increased brain uptake of [^{123}I]-R91150 and a drastically improved quality of the obtained µSPECT images. Therefore, we suggest further exploration of the use of cyclosporin A (or other less toxic P-glycoprotein blocking agents) to improve the otherwise limited brain uptake of some radioligands for brain imaging.

3.6. References

1. Mertens J, Gysemans M, Hermanne A, Terriere D. Radiosynthesis of 2-Radiobromo-Ketanserin, A Potential Invivo 5Ht2 Receptor Tracer with Pet. European Journal of Nuclear Medicine 1992; 19:626-626.

2. Terriere D, Janssen PMP, Gommeren W, Gysemans M, Mertens JJR, Leysen JE. Evaluation of Radioiodo-4-Amino-N-[1-[3-(4-Fluorophenoxy)-Propyl]-4-Methyl-4-Piperidinyl]-5-Iodo-2-Methoxybenzamide As A Potential 5Ht2 Receptor Tracer for Spe(C)T. Nuclear Medicine and Biology 1995; 22:1005-1010.

3. Abidargham A, ZeaPonce Y, Terrier D, AlTikriti M, Baldwin RM, Hoffer P et al. Preclinical evaluation of [I-123]R93274 as a SPECT radiotracer for imaging 5-HT2A receptors. European Journal of Pharmacology 1997; 321:285-293.

4. Mertens J, Terriere D, Sipido V, Gommeren W, Janssen PMF, Leysen JE. Radiosynthesis of A New Radioiodinated Ligand for Serotonin-5Ht(2)-Receptors, A Promising Tracer for Gamma-Emission Tomography. Journal of Labelled Compounds & Radiopharmaceuticals 1994; 34:795-806.

5. Schotte A, Maloteaux JM, Laduron PM. Characterization and Regional Distribution of Serotonin S-2 Receptors in Human-Brain. Brain Research 1983; 276:231-235.

6. Peremans K, Audenaert K, Blanckaert P, Jacobs F, Coopman F, Verschooten F et al. Effects of aging on brain perfusion and serotonin-2A receptor binding in the normal canine brain measured with single photon emission tomography. Progress in Neuro-Psychopharmacology & Biological Psychiatry 2002; 26:1393-1404.

7. Peremans K, Audenaert K, Jacobs F, Dumont F, De Vos F, Van de Wiele C et al. Biodistribution and displacement studies of the selective 5-HT2A receptor antagonist I-123-5-I-R91150 in the normal dog. Nuclear Medicine Communications 2002; 23:1019-1027.

8. Peremans K, Audenaert K, Coopman F, Jacobs F, Dumont F, Slegers G et al. Regional binding index of the radiolabeled selective 5-ht2a antagonist I-123-5-1-r91150 in the normal canine brain imaged with single photon emission computed tomography. Veterinary Radiology & Ultrasound 2003; 44:344-351.

9. Peremans KY, Peremans K, Audenaert K, De Bondt P, Van de Wiele C, Dumont F et al. In vivo evaluation of serotonin-2a receptors in normal canine brain: A SPECT study with a selective 5-HT2a receptor ligand labelled with 123I. European Journal of Nuclear Medicine 2001; 28:1191-1191.

10. Peremans K, Audenaert K, Coopman F, Hoybergs Y, Slegers G, Van Bree H et al. Functional brain imaging of serotonin-2A receptors in impulsive dogs: A pilot study. Vlaams Diergeneeskundig Tijdschrift 2002; 71:340-347.

11. Peremans K, Audenaert K, Coopman F, Hoybergs Y, Slegers G, Van Bree H et al. Functional brain imaging of serotonin-2A receptors in impulsive dogs: A pilot study. Vlaams Diergeneeskundig Tijdschrift 2002; 71:340-347.

12. Peremans K, Audenaert K, Coopman F, Blanckaert P, Jacobs F, Otte A et al. Estimates of regional cerebral blood flow and 5-HT2A receptor density in impulsive, aggressive dogs with Tc-99m-ECD and I-123-5-I-R91150. European Journal of Nuclear Medicine and Molecular Imaging 2003; 30:1538-1546.

13. Peremans K, Audenaert K, Hoybergs Y, Otte A, Goethals I, Gielen I et al. The effect of citalopram hydrobromide on 5-HT2A receptors in the impulsive-aggressive dog, as measured with I-123-5-I-R91150 SPECT. European Journal of Nuclear Medicine and Molecular Imaging 2005; 32:708-716.

14. Baeken C, D'haenen H, Flamen P, Mertens J, Terriere D, Chavatte K et al. I-123-5-I-R91150, a new single-photon emission tomography ligand for 5-HT2A receptors: influence of age and gender in healthy subjects. European Journal of Nuclear Medicine 1998; 25:1617-1622.

15. Busatto GF, Pilowsky LS, Costa DC, Mertens J, Terriere D, Ell PJ et al. Initial evaluation of I-123-5-I-R91150, a selective 5-HT2A ligand for single-photon emission tomography, in healthy human subjects. European Journal of Nuclear Medicine 1997; 24:119-124.

16. Catafau AM, Danus M, Bullich S, Llop J, Perich J, Cunningham VJ et al. Characterization of the SPECT 5-HT2A receptor ligand I-123-R91150 in healthy volunteers: Part 1 - Pseudoequilibrium interval and quantification methods. Journal of Nuclear Medicine 2006; 47:919-928.

17. Catafau AM, Danus M, Bullich S, Nucci G, Llop J, Abanades S et al. Characterization of the SPECT 5-HT2A receptor ligand I-123-R91150 in healthy volunteers: Part 2 - Ketanserin displacement. Journal of Nuclear Medicine 2006; 47:929-937.

18. Versijpt J, Van Laere KJ, Dumont F, Decoo D, Vandecapelle M, Santens P et al. Imaging of the 5-HT2A system: age-, gender-, and Alzheimer's disease-related findings. Neurobiology of Aging 2003; 24:553-561.

19. Reneman L and Booij J. Former "Ecstasy" use is associated with an upregulation of 5-HT receptors in the occipital cortex as visualised with [I-123]R91150 SPECT. Journal of Nuclear Medicine 1999; 40:275P-275P.

20. Audenaert K, Van Laere K, Dumont F, Vervaet M, Goethals I, Slegers G et al. Decreased 5-HT2a receptor binding in patients with anorexia nervosa. Journal of Nuclear Medicine 2003; 44:163-169.

21. Audenaert K, Van Laere K, Dumont F, Slegers G, Mertens J, Van Heeringen C et al. Decreased frontal serotonin 5-HT2a receptor binding index in deliberate self-harm patients. European Journal of Nuclear Medicine 2001; 28:175-182.

22. Dean B, Hayes W, Hill C, Copolov D. Decreased Serotonin(2A) receptors in Brodmann's area 9 from schizophrenic subjects - A pathological or pharmacological phenomenon? Molecular and Chemical Neuropathology 1998; 34:133-145.

23. Goethals I, Vervaet M, Audenaert K, Van de Wiele C, Ham H, Vandecapelle M et al. Comparison of cortical 5-HT2A receptor binding in bulimia nervosa patients and healthy volunteers. American Journal of Psychiatry 2004; 161:1916-1918.

24. Schins A, Van Kroonenburgh M, Van Laere K, D'haenen H, Lousberg R, Crijns H et al. Increased cerebral serotonin-2A receptor binding in depressed patients with myocardial infarction. Psychiatry Research-Neuroimaging 2005; 139:155-163.

25. Van Heeringen C, Audenaert K, Van Laere K, Dumont F, Slegers G, Mertens J et al. Prefrontal 5-HT2a receptor binding index, hopelessness and personality characteristics in attempted suicide. Journal of Affective Disorders 2003; 74:149-158.

26. Travis MJ, Busatto GF, Pilowsky LS, Mulligan R, Acton PD, Gacinovic S et al. 5-HT2A receptor blockade in patients with schizophrenia treated with risperidone or clozapine - A SPET study using the novel 5-HT2A ligand I-123-5-I-R-91150. British Journal of Psychiatry 1998; 173:236-241.

27. Leysen JE, Awouters F, Kennis L, Laduron PM, Vandenberk J, Janssen PAJ. Receptor-Binding Profile of R-41-468, A Novel Antagonist at 5-Ht2 Receptors. Life Sciences 1981; 28:1015-1022.

28. Janssen PAJ. Pharmacology of Potent and Selective S2-Serotonergic Antagonists. Journal of Cardiovascular Pharmacology 1985; 7:S2-S11.

29. Leysen JE, Gommeren W, VanGompel P, Wynants J, Janssen PFM, Laduron PM. Receptor-Binding Properties Invitro and Invivo of Ritanserin - A Very Potent and Long-Acting Serotonin-S-2 Antagonist. Molecular Pharmacology 1985; 27:600-611.

30. Leysen JE, Gommeren W, VanGompel P, Wynants J, Janssen PFM, Laduron PM. Receptor-Binding Properties Invitro and Invivo of Ritanserin - A Very Potent and Long-Acting Serotonin-S-2 Antagonist. Molecular Pharmacology 1985; 27:600-611.

31. Aloyo VJ and Harvey JA. Antagonist binding at 5-HT2A and 5-HT2C receptors in the rabbit: High correlation with the profile for the human receptors. European Journal of Pharmacology 2000; 406:163-169.

32. Hendrikse NH, Schinkel AH, De Vries EGE, Fluks E, Van der Graaf WTA, Willemsen ATM et al. Complete in vivo reversal of P-glycoprotein pump function in the blood-brain barrier visualized with positron emission tomography. British Journal of Pharmacology 1998; 124:1413-1418.

33. Ishiwata K, Kawamura K, Yanai K, Hendrikse NH. In vivo evaluation of P-glycoprotein modulation of 8 PET radioligands used clinically. Journal of Nuclear Medicine 2007; 48:81-87.

34. Joseph B, Bhargava KK, Malhi H, Schilsky ML, Jain D, Palestro CJ et al. Sestamibi is a substrate for MDR1 and MDR2 P-glycoprotein genes. European Journal of Nuclear Medicine and Molecular Imaging 2003; 30:1024-1031.

35. Lee YJ, Maeda J, Kusuhara H, Okauchi T, Inaji M, Nagai Y et al. In vivo evaluation of P-glycoprotein function at the blood-brain barrier in nonhuman primates using [C-11]verapamil. Journal of Pharmacology and Experimental Therapeutics 2006; 316:647-653.

36. Liow JS, Lu SY, McCarron JA, Hong JS, Musachio JL, Pike VW et al. Effect of a P-glycoprotein inhibitor, cyclosporin A, on the disposition in rodent brain and blood of the 5-HT1A receptor radioligand, [C-11](R)-(-)-RWAY. Synapse 2007; 61:96-105.

37. Syvanen S, Blomquist G, Sprycha M, Hoglund AU, Roman M, Eriksson O et al. Duration and degree of cyclosporin induced P-glycoprotein inhibition in the rat blood-brain barrier can be studied with PET. Neuroimage 2006; 32:1134-1141.

38. de Vries EFJ, Kortekaas R, van Waarde A, Dijkstra D, Elsinga PH, Vaalburg W. Synthesis and evaluation of dopamine D-3 receptor antagonist C-11-GR218231 as PET tracer for P-glycoprotein. Journal of Nuclear Medicine 2005; 46:1384-1392.

39. Carcel-Trullols J, Torres-Molina F, Araico A, Saadeddin A, Peris JE. Effect of cyclosporine A on the tissue distribution and pharmacokinetics of etoposide. Cancer Chemotherapy and Pharmacology 2004; 54:153-160.

40. Liow JS, Lu SY, McCarron JA, Hong JS, Musachio JL, Pike VW et al. Effect of a P-glycoprotein inhibitor, cyclosporin A, on the disposition in rodent brain and blood of the 5-HT1A receptor radioligand, [C-11](R)-(-)-RWAY. Synapse 2007; 61:96-105.

41. Hendrikse NH, Schinkel AH, De Vries EGE, Fluks E, Van der Graaf WTA, Willemsen ATM et al. Complete in vivo reversal of P-glycoprotein pump function in the blood-brain barrier visualized with positron emission tomography. British Journal of Pharmacology 1998; 124:1413-1418.

42. Halldin C, Lundkvist C, Ginovart N, Nyberg S, Hall H, Swahn CG et al. [C-11]MDL 100907, a radioligand for selective imaging of 5-HT2A receptors with PET. Journal of Nuclear Medicine 1996; 37:424-424.

43. Kristiansen H, Elfving B, Plenge P, Pinborg LH, Gillings N, Knudsen GM. Binding characteristics of the 5-HT2A receptor antagonists altanserin and MDL 100907. Synapse 2005; 58:249-257.

44. Tan PZ, Baldwin RM, van Dyck CH, Al-Tikriti M, Roth B, Khan N et al. Characterization of radioactive metabolites of 5-HT2A receptor PET ligand [F-18]altanserin in human and rodent. Nuclear Medicine and Biology 1999; 26:601-608.

45. Elsinga PH, Hendrikse NH, Bart J, van Waarde A, Vaalburg W. Positron emission tomography studies on binding of central nervous system drugs and P-glycoprotein function in the rodent brain. Molecular Imaging and Biology 2005; 7:37-44.

46. Hendrikse NH, Schinkel AH, De Vries EGE, Fluks E, Van der Graaf WTA, Willemsen ATM et al. Complete in vivo reversal of P-glycoprotein pump function in the blood-brain barrier visualized with positron emission tomography. British Journal of Pharmacology 1998; 124:1413-1418.

47. Lopez-Gimenez JF, Vilaro MT, Palacios JM, Mengod G. [H-3]MDL 100,907 labels 5-HT2A serotonin receptors selectively in primate brain. Neuropharmacology 1998; 37:1147-1158.

48. Laruelle M, Slifstein M, Huang Y. Relationships between radiotracer properties and image quality in molecular imaging of the brain with positron emission tomography. Molecular Imaging and Biology 2003; 5:363-375.

49. Lundkvist C, Halldin C, Ginovart N, Nyberg S, Swahn CG, Carr AA et al. [C-11]MDL 100907, a radioligand for selective imaging of 5-HT2A receptors with positron emission tomography. Life Sciences 1996; 58:L187-L192.

50. LopezGimenez JF, Mengod G, Palacios JM, Vilaro MT. Selective visualization of rat brain 5-HT2A receptors by autoradiography with [H-3]MDL 100,907. Naunyn-Schmiedebergs Archives of Pharmacology 1997; 356:446-454.

51. Kiyono Y, Yamashita T, Doi H, Kuge Y, Katsura T, Inui KI et al. Is MIBG a substrate of P-glycoprotein? European Journal of Nuclear Medicine and Molecular Imaging 2007; 34:448-452.

52. Takano A, Kusuhara H, Suhara T, Ieiri I, Morimoto T, Lee YJ et al. Evaluation of in vivo P-glycoprotein function at the blood-brain barrier among MDR1 gene polymorphisms by using C-11-verapamil. Journal of Nuclear Medicine 2006; 47:1427-1433.

53. vanAsperen J, Schinkel AH, Beijnen JH, Nooijen WJ, Borst P, Vantellingen O. Altered pharmacokinetics of vinblastine in Mdr1a P-glycoprotein-deficient mice. Journal of the National Cancer Institute 1996; 88:994-999.

Chapter 4

SYNTHESIS OF [^{123}I]-3-I-CO

❦❦❦

4. SYNTHESIS OF [¹²³I]-(4-FLUOROPHENYL) [1-(3-IODOPHENETHYL)PIPERIDIN-4-YL] METHANONE

4.1. Selection of the molecule

4.1.1. Introduction

The aim of this research is the precursor synthesis and radiosynthesis of [¹²³I]-(4-fluorophenyl)[1-(3-iodophenethyl)piperidin-4-yl]methanone ([¹²³I]-3-I-CO, figure 4.1). The potential of this tracer to visualize the serotonin 5-HT$_{2A}$ receptor *in vivo* with pinhole μSPECT will be evaluated. The molecule was selected based on an article by Xing Fu and co-workers, published in 2002 in the Journal of Medicinal Chemistry [1].

3-I-CO is a 4-fluorobenzoyl-piperidine derivative structurally related to ketanserin and setoperone. (4-Fluorophenyl)[1-(3-iodophenethyl)piperidin-4-yl]methanone shows excellent affinity for the human serotonin 5-HT$_{2A}$ receptor (K_i = 0.51 nM). The assay was performed with the membranes of cells transfected with human 5-HT$_{2A}$ genes, using tritiated ketanserin (1.2 nM) as ligand and altanserin (10 μM) for the blank test.
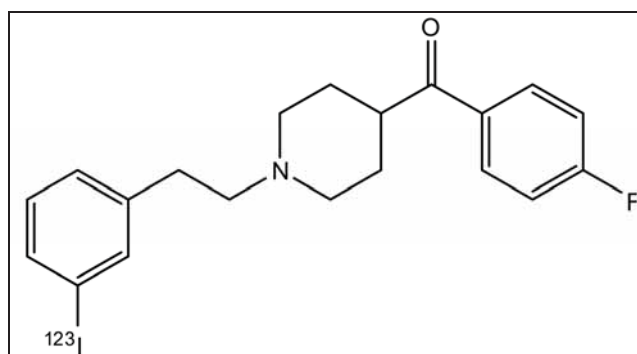
Figure 4.1: [¹²³I]-(4-fluorophenyl)[1-(3-iodophenethyl)piperidin-4-yl]methanone ([¹²³I]-3-I-CO)

4.1.2. The 5-HT$_{2A}$ receptor: modelling

A good starting point for the homology building of G-protein coupled receptor models is the crystal structure of bovine rhodopsin, although the low-sequence homology (~ 20 %) between 5-HT$_2$ receptors and rhodopsin makes the application of standard homology modelling methods difficult. The structure of the 5-HT$_{2A}$ receptor model[2] with ketanserin docked in the binding site is shown in figure 4.2. The transmembrane helices are clearly visible in figure 4.2.
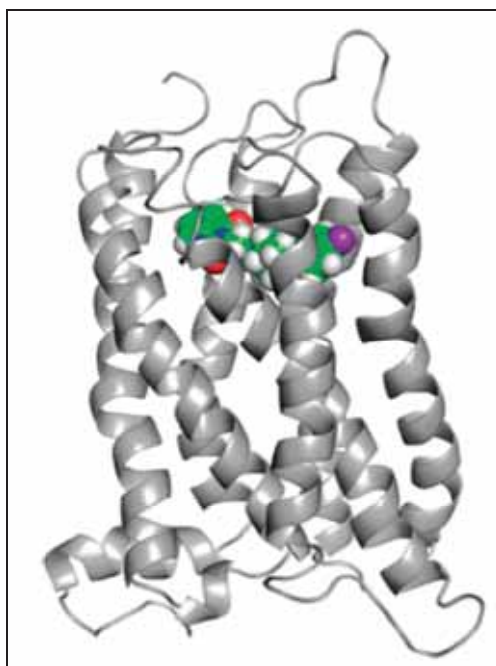
Figure 4.2: Structure of the 5-HT$_{2A}$ receptor model. The figure shows a molecule of ketanserin docked in the binding site. Adapted from Dezi et al[2].

The reasons for choosing ketanserin (figure 4.3) as ligand are two-fold: first, ketanserin is a well-known ligand for the 5-HT$_{2A}$ receptor and second, ketanserin exhibits a large chemical similarity with other 5-HT$_{2A}$ ligands (for example [^{123}I]-3-I-CO).
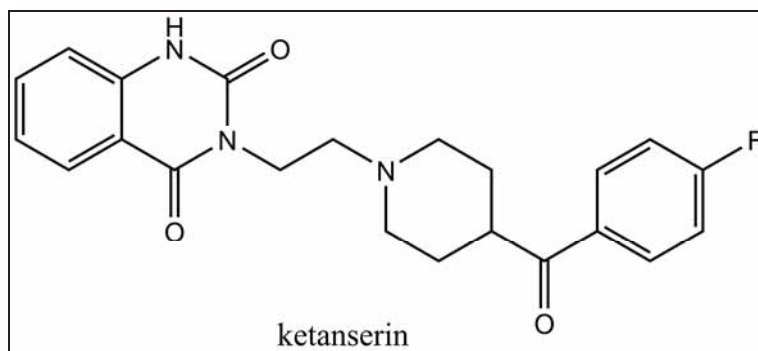
Figure 4.3: Chemical structure of ketanserin.

Several amino acid residues in the binding site are important for interaction with 5-HT$_{2A}$ ligands. In figure 4.4, ketanserin is docked in the active binding pocket of the 5-HT$_{2A}$ receptor, and the amino acid residues responsible for interaction with 5-HT$_{2A}$ ligands are shown. The most important amino acid residues, responsible for binding of ketanserin to the receptor, are also indicated in figure 4.4.

The binding site is located approximately parallel to the transmembrane helices. The ligand makes polar contacts mainly with residues in helices 3 and 7, as well as with some residues of the extracellular loop 2. Hydrophobic contacts are observed with residues of helices 5 and 6. The amino acids making the most relevant interactions with ketanserin are Asp3.32, Ser3.36, Trp3.28, Phe6.51, Tyr7.43 and Ser161. Their mechanism of action will be discussed briefly.
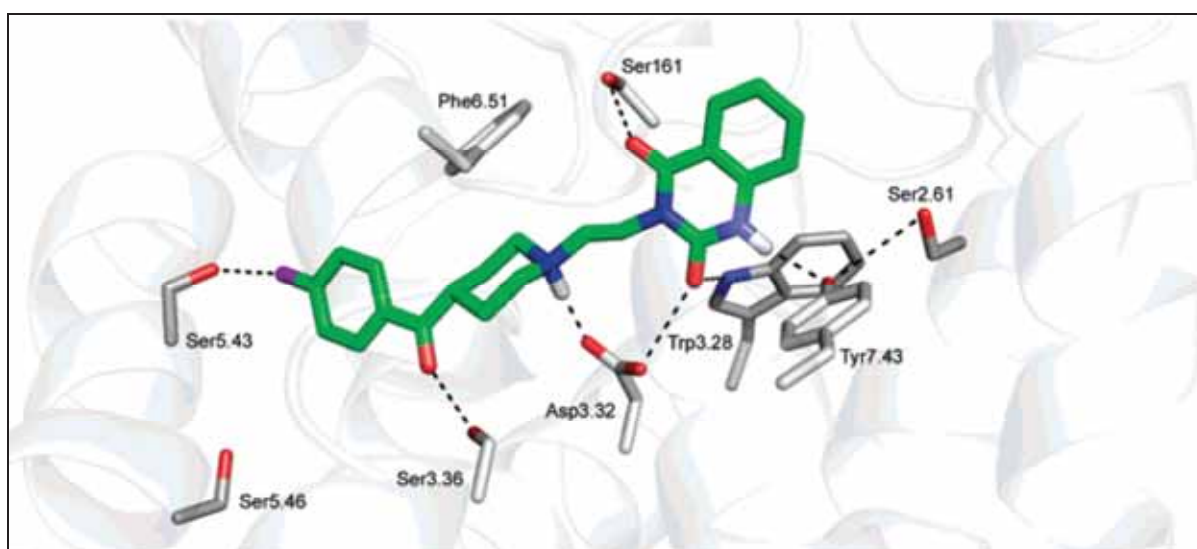
Figure 4.4: Binding site of the 5-HT$_{2A}$ receptor complexed with a molecule of ketanserin. Only residues involved in relevant interactions are depicted. Taken from Dezi et al[2].

It is evident from figure 4.4 that the side chain of Asp3.32 and the charged nitrogen of ketanserin interact, making a charge-reinforced hydrogen bond.

The phenyl ring of the Phe6.51 side chain adopts a conformation parallel to the ketanserin piperidine ring, where the aliphatic carbons directly linked to the charged ketanserin nitrogen (holding a positive partial charge) can make favorable interactions with the phenyl ring of the Phe6.51 side chain. The result is a kind of electrostatic "sandwich", in which ketanserin makes favorable interactions with Asp3.32 on one side and with Phe6.51 on the opposite side. The other oxygen atom of the Asp3.32 side chain is at hydrogen-bonding distance of one of the carbonyl oxygen atoms of the ketanserin benzouracil moiety, which seems to be also involved in an additional hydrogen bond with the indolic nitrogen of Trp3.28.

The benzouracil moiety seems to participate in two additional polar interactions: one between the remaining carbonyl oxygen and the hydroxyl of Ser161, the other between one nitrogen and the Tyr7.43 phenolic hydroxyl group. This last interaction seems to stabilize the position of Tyr7.43 in an orientation in which it can establish an additional hydrogen bond with Ser2.61. With respect to the p-fluorobenzoyl moiety, the carbonyl oxygen makes a hydrogen bond with the side chain of Ser3.36.

The percentage of hydrogen bonding between the amino acid residues and ketanserin is shown in table 4.1.

residue	% hydrogen bond
Asp3.32	100
Ser3.36	21
Ser161	27
Trp3.28	76
Tyr7.43	18

Table 4.1: Hydrogen bonding between ketanserin and the respective amino acid residues. Adapted from Dezi et al[2].

Deeper inside the binding pocket, the p-fluorobenzoyl is immersed in a hydrophobic pocket involving residues Val5.39 and Leu163. The size of this hydrophobic pocket is delimited by Phe6.52, a residue that is part of the so-called hydrophobic toggle switch, a set of three residues (Phe6.51, Phe6.52 and Trp6.48), which are known to participate in a coordinated conformational change, potentially important for the activation process[3, 4, 5, 6].

Apart from this role, the conformational changes of these three residues are very important for determining the size of the hydrophobic pocket, which in turn conditions the orientation of the p-fluorobenzoyl moiety.

The fluorine substituent of the aromatic ring is located close to the Ser5.43 and Ser5.46, which are residues that have been postulated to be relevant for the binding of serotonin[7, 8]. Table 4.2 shows the effect of selectively 'disabling' one or more amino acid residues in the active binding site via mutagenesis experiments, hereby emphasizing the importance of the function of the different amino acid residues in the binding process.

mutation	K_i variation > (fold)	interactions observed in complex
Trp6.48Ala	100	part of the aromatic cluster, delimiting binding site
Asp3.32Asn	75	charge-reinforced hydrogen bond with charged piperidine nitrogen atom
Phe6.52Tyr	73	near the p-flurobenzyl moiety
Tyr7.43Ala	20	hydrogen bonded to the benzouracil moiety
Phe6.51Ala	12	Van der Waals contact with piperidine ring
Asp2.50Asn	10	
Trp1.34Ala	10	

Table 4.2: Residues involved in the binding of ketanserin to the 5-HT$_{2A}$ receptor. Data obtained from mutagenesis experiments[2].

Most of the 5-HT$_{2A}$ antagonists share relevant structural features with ketanserin, like the presence of a piperidine ring, the linear shape with aromatic rings at both ends, and hydrogen-bond acceptor and donor groups at an intermediate position.

This similarity justifies the use of the above-described ketanserin-conditioned binding pocket to carry out docking simulations with other possible 5-HT$_{2A}$ antagonists. For example, the structure of [^{123}I]-3-I-CO and ketanserin are very similar, so we can assume that [^{123}I]-3-I-CO uses the same interactions as ketanserin with the amino acid residues in the active binding site of the 5-HT$_{2A}$ receptor.

4.1.3. Properties of [^{123}I]-3-I-CO

Knowledge of the localization and the functional roles of the large number of serotonin receptors, including the 5-HT$_{2A}$ receptor, remains incomplete. A powerful method for contributing to such knowledge is the use of clinical anatomical and functional radionuclide brain imaging with PET (positron emission tomography) and SPECT (single photon emission computed tomography). These techniques provide methods of high sensitivity for measuring *in vivo* neurochemical and pharmacological effects at specific target-receptor proteins. Development of improved radiotracers for PET (labeled with ^{18}F and ^{11}C) and SPECT (^{123}I) with high specific uptake and selectivity for 5-HT$_{2A}$ receptors would therefore be very useful. Among the reported ligands for the 5-HT$_{2A}$ receptor[9] , the two structurally related compounds altanserin and MDL-100907 have relative high affinity and selectivity for the 5-HT$_{2A}$ receptor compared to other serotonin receptors[10, 11] (chemical structures are shown in figure 4.5).
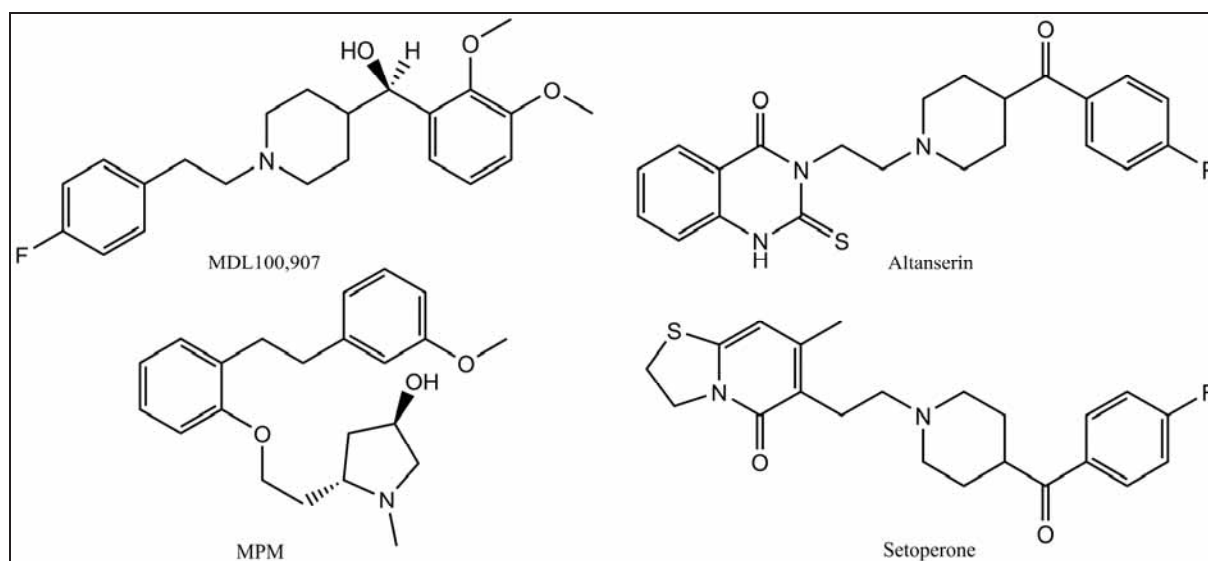

Figure 4.5: 5-HT$_{2A}$ selective ligands

[^{18}F]-Altanserin (K_i(5-HT$_{2A}$): 0.30 nM, 20-fold 2A/2C selectivity) and [^{11}C]-MDL-100907 (K_i(5-HT$_{2A}$): 0.36 nM, 300-fold selectivity 2A/2C) have been developed for *in vivo* imaging[12, 13]. However, neither is fully satisfactory, owing to limitations of potency, selectivity or biological half-life.

Notably, the selectivity of altanserin for 5-HT$_{2A}$ over 5-HT$_{2C}$ is about 20-fold. Quantitative *in vivo* imaging of 5-HT$_{2A}$ receptors with [^{18}F]-altanserin has been problematic because of lipophilic radiometabolites that cross the blood-brain barrier, and slow kinetics[14, 15, 16].

Although MDL-100907 has a high affinity and selectivity for the 5-HT$_{2A}$ receptor, its radiolabelling with short-lived ^{11}C (half-life of 20 min) limits its suitability to short-term studies, particularly because this tracer demonstrates slow *in vivo* kinetics[17].

Prabhakaran et al also developed a [^{11}C]-labeled ligand ([^{11}C]-AC90179) for PET imaging of the 5-HT$_{2A}$ receptors, but due to lack of tracer binding and specific binding, this ligand could not be used for *in vivo* imaging[18].

[^{18}F]-Setoperone was also used to image the 5-HT$_{2A}$ receptors in humans with PET[19]. Also ritanserin was labelled with [^{18}F] and used as a 5-HT$_{2A}$ receptor tracer[20].

Recently, [^{11}C]-MPM was developed by Kumar et al[21] as a potential PET ligand for the 5-HT$_{2A}$ receptor. Partial specific binding to cerebellum and high aspecific binding limit the clinical usefulness of this radioligand.

[^{123}I]-R91150 (see chapter 3) is currently used in evaluating patient condition with several psychiatric conditions[22, 23]. Limitations observed with this tracer were high aspecific binding *in vitro* and *in vivo*, which makes binding assays rather problematic.

A more ideal radioligand for clinical *in vivo* imaging of 5-HT$_{2A}$ receptors would have high 5-HT$_{2A}$ potency (K_i < 1 nM) and selectivity (> 50-fold) toward other, particularly 5-HT receptors, and be radiolabeled with ^{18}F (half-life of 110 min) or ^{123}I (half-life of 13.2 h)[1]. Novel compounds were developed by Fu et al[1] based on common structural features of altanserin and MDL-100907 to provide a new series of 4'-substituted phenyl-4-piperidinylmethanol and benzoyl-4-piperidine derivatives, of which the evaluated tracer [^{123}I]-3-I-CO is a member.

Potency and selectivity at the 5-HT$_{2A}$ receptor depended significantly on the length of the alkyl link of the piperidine ring to a phenyl moiety. Generally, compounds with an ethylene bridge (n = 2 carbon atoms) to the second phenyl moiety have higher 5-HT$_{2A}$ potency than those with a methylene bridge (n = 1 carbon atom). Some of the ethylene-bridge compounds show high 5-HT$_{2A}$ potency but only limited selectivity, limiting their candidacy for brain-imaging radioligand development[1].

The nature of the linking moiety to a second phenyl ring (carbonyl or methanol) or the para-substituent on that ring (F or NO_2) all yielded some compounds with relatively high 5-HT_{2A} affinity. Also, in general, for the other phenyl ring, para-substituted iodinated derivatives were found to be less potent at the 5-HT_{2A} receptors than the corresponding ortho- and meta-substituted positional isomers.

Reduction of the carbonyl-function leads to the formation of a racemic alcohol by virtue of the asymmetric center introduced in the structure by $NaBH_4$ reduction. One enantiomer may be more potent, as suggested by the previous report that (R)-(+)MDL-100907 had 30-times greater selectivity to 5-HT_{2A} over 5-HT_{2C} receptors than the (S)-(-)-enantiomer[24].

As mentioned earlier, one of the most important criteria for a good 5-HT_{2A} receptor tracer is the selectivity over another serotonin receptor subtype, the 5-HT_{2C} receptor. For example, altanserin has a $5\text{-HT}_{2A}/5\text{-HT}_{2C}$ selectivity ratio of 20[1]. The selectivity ratio of $[^{123}I]$-3-I-CO for the 5-HT_{2C} receptor compared to the 5-HT_{2A} receptor is a factor of 33 ($K_{i\ (5\text{-HT2C})} = 16.6$ nM). It was determined on PO-1C cells transfected with human 5-HT_{2C} genes, using tritiated mesulergine (1.0 nM) as the ligand and clozapine (10 µM) for the blank assay. Selectivity for the 5-HT_{2A} receptor compared to the human 5-HT_6 receptor is a factor of 100 ($K_{i\ (5\text{-HT6})} = 48.9$ nM). Selectivity for the 5-HT_{2A} receptor compared to the human 5-HT_7 receptor is a factor of 17 ($K_{i\ (5\text{-HT7})} = 8.76$ nM). For the serotonin 5-HT_6 and 5-HT_7 assays, tritiated LSD (1.0 nM, lysergic acid diethylamide) was used for the binding test and clozapine (10 µM) for the blanks.

Selectivity of (4-fluorophenyl)[1-(3-iodophenethyl)piperidin-4-yl]methanone over other neurotransmitter receptors was also evaluated. Especially selectivity over dopamine D_2 receptors is important For the dopamine class of receptors, affinity for the dopamine D_2 receptor was tested on rat caudate-putamen brain tissue using tritiated nemonapride (0.075 nM) as ligand and haloperidol (10 µm) for the blank test. Selectivity of 3-I-CO for the 5-HT_{2A} receptor compared to the dopamine D_2 receptor was a factor 100 ($K_i\ (D_2) = 51.8$ nM) (Table 4.3).

Receptor type	Membrane source	[³H]-ligand (nM)	Blank (µm)
5-HT$_2$r	rat forebrain	ketanserin (1,2)	cinanserin (1,0)
5-HT$_{2A}$h	GF-62 cells	ketanserin (1,2)	altanserin (1,0)
5-HT$_{2C}$h	PO-1C cells	mesulergine (1,0)	clozapine (10)
5-HT$_6$h	HD-6 cells	LSD (1,0)	clozapine (10)
5-HT$_7$h	HD-7 cells	LSD (1,0)	clozapine (10)
D$_2$	rat caudate	nemonapride (0,075)	haloperidol (10)
α$_1$	rat brain	prazosin (0,20)	phentolamine (2)
α$_2$	rat brain	prazosin (1,0)	phentolamine (10)

Table 4.3: 3-I-CO radioaffinity assay conditions for different neurotransmitter receptors (adapted from Fu et al [1], J. Med. Chem. 2002, 45, 2319-2324).

Affinity for the adrenergic receptor types was tested on rat whole brain tissue samples using tritiated prazosin (0.2 – 1 nM) for the binding assay and phentolamine (2 – 10 µM) for the blank assay (Table 4.3). Selectivity for the serotonin 5-HT$_{2A}$ receptor compared to the adrenergic α$_1$ receptor was only a factor 10 (K_i (α$_1$) = 4.92 nM). Selectivity over the adrenergic α$_2$ receptor was a factor 500 (K_i (α$_2$) = 244 nM). All K_i values tested for 3-I-CO are shown in table 4.4.

Receptor Affinity (K_i, nM)						
5-HT$_{2A}$	5-HT$_{2C}$	5-HT$_6$	5-HT$_7$	D$_2$	α$_1$	α$_2$
0.51	16.6	48.9	8.76	51.8	4.92	244

Table 4.4: Receptor affinities of 3-I-CO for different neurotransmitter receptor systems.

4.1.4. Objectives

In this chapter we will present the synthesis of the precursor for radiolabelling and the radiosynthesis of [^{123}I]-3-I-CO, along with its purification and quality control. The *in vitro* properties of [^{123}I]-3-I-CO (specific activity, partition coefficient) will also be determined.

The potential tracer will be evaluated *in vivo*, starting with NMRI mouse biodistribution studies to assess the potential of [^{123}I]-3-I-CO to penetrate the blood-brain barrier.

Regional brain biodistribution studies will be performed in larger animals (Sprague-Dawley rats) to evaluate if [^{123}I]-3-I-CO does indeed bind to brain regions containing large amounts of 5-HT$_{2A}$ receptors.

Specificity of tracer binding in rat brain will be determined by a displacement study with a known 5-HT$_{2A}$ antagonist, ketanserin. Metabolite assays will be performed on the brain and blood of all species studies, to guarantee that the measured activity in brain tissue is due to unchanged [^{123}I]-3-I-CO, and not to possible metabolites of the tracer.

Since the goal of this research is to evaluate whether [^{123}I]-3-I-CO could possibly be used as a 5-HT$_{2A}$ receptor tracer *in vivo*, a pinhole μSPECT imaging study will be performed with [^{123}I]-3-I-CO in Sprague-Dawley rats.

It was recently discovered that the brain uptake of many clinically used SPECT and PET tracers could be improved by blocking the effect of P-glycoprotein (Pgp), an efflux pump at the blood-brain barrier [25, 26, 27, 28, 29, 30, 31]. Therefore, the effect of blocking Pgp function (for example by administration of cyclosporin A) on the brain uptake and biodistribution of [^{123}I]-3-I-CO will also be evaluated. Possible increased tracer metabolism under the influence of cyclosporin A administration will be excluded. The influence of cyclosporin A administration on the pinhole μSPECT imaging studies in Sprague-Dawley rats will also be evaluated.

4.2. Precursor synthesis

[^{123}I]-(4-fluorophenyl)[1-(3-iodophenethyl)piperidin-4-yl]methanone   ([^{123}I]-3-ICO)   was synthesized starting from the corresponding tributylstannyl-derivative (4-fluorophenyl)[1-(3-tributylstannylphenethyl)piperidin-4-yl]methanone (**6**). The tributylstannyl-precursor was synthesized in four steps starting from 3-bromophenylacetic acid (**1**), which was commercially available (figure 4.6).
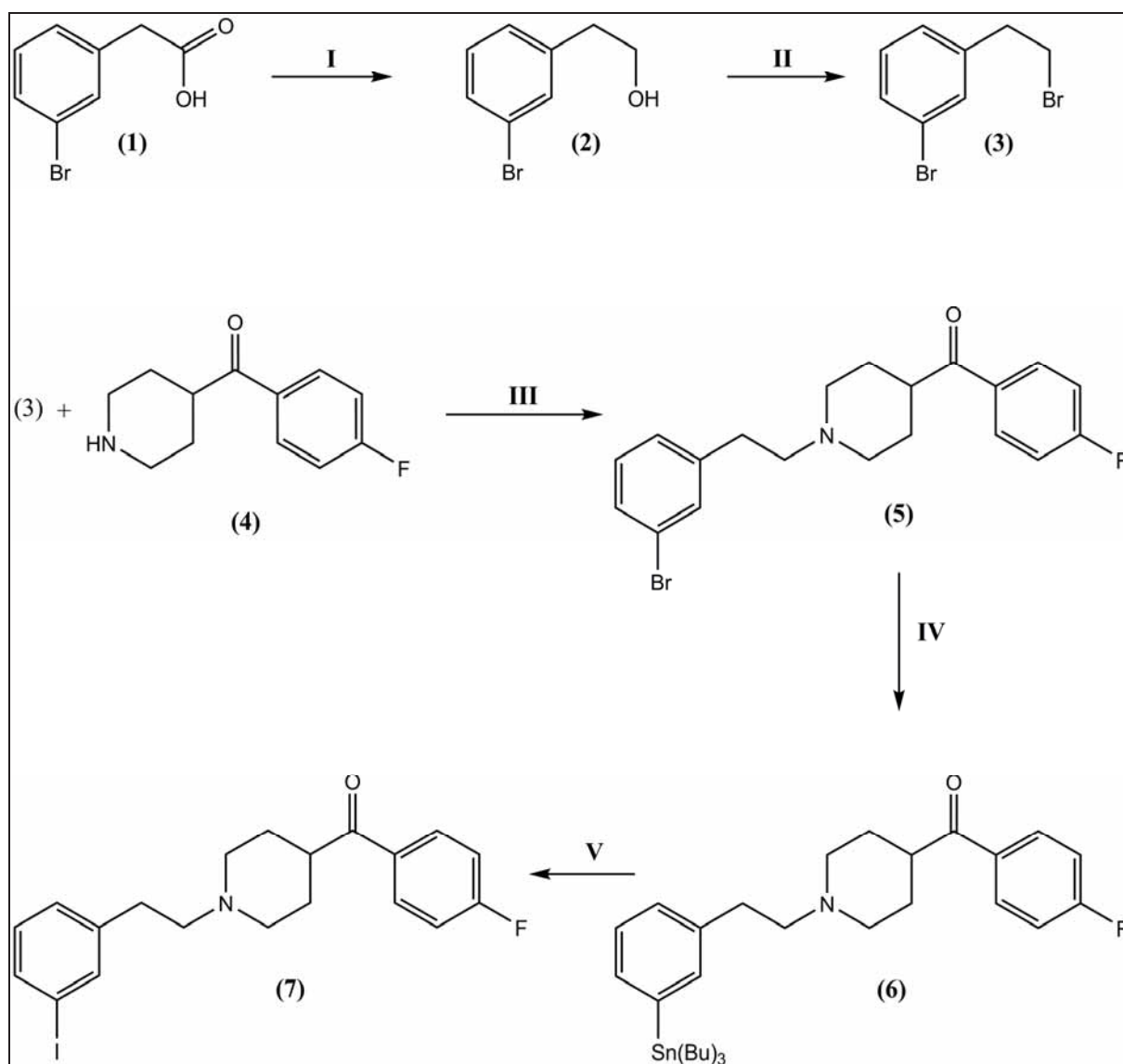

Figure 4.6: Synthesis of (4-fluorophenyl)(1-(3-(tributylstannyl)phenethyl)piperidin-4-yl)methanone (**6**)

3-Bromophenylacetic acid (**1**) was reduced to the alcohol 2-(3-bromophenyl)ethanol (**2**) with borohydride-tetrahydrofuran (figure 4.6). The alcohol function was replaced by bromine with phosphorus tribromide, resulting in 1-bromo-3-(2-bromoethyl)benzene (**3**). This brominated compound (**3**) was then coupled with 4-(4-fluorobenzoyl)piperidine (**4**) in a nucleophilic substitution reaction, yielding (4-fluorophenyl)(1-(3-bromophenethyl)piperidin-4-yl)methanone (**5**). Finally, the bromine-atom of (**5**) was replaced by a tributylstannyl-group by reaction with hexabutylditin, and (4-fluorophenyl)(1-(3-(tributylstannyl)phenethyl)piperidin-4-yl)methanone (**6**) was obtained. This tributylstannylprecursor (**6**) was used for the radiosynthesis of $[^{123}I]$-(4-fluorophenyl)[1-(3-iodophenethyl)piperidin-4-yl]methanone. It was also used to synthesize the cold iodinated compound (**7**), used as a reference during quality control of the tracer.

Compound (**4**), 4-(4-fluorobenzoyl)piperidine, was synthesized in a 4-step reaction sequence, starting from piperidine-4-carboxylic acid (**4a**) (figure 4.7).

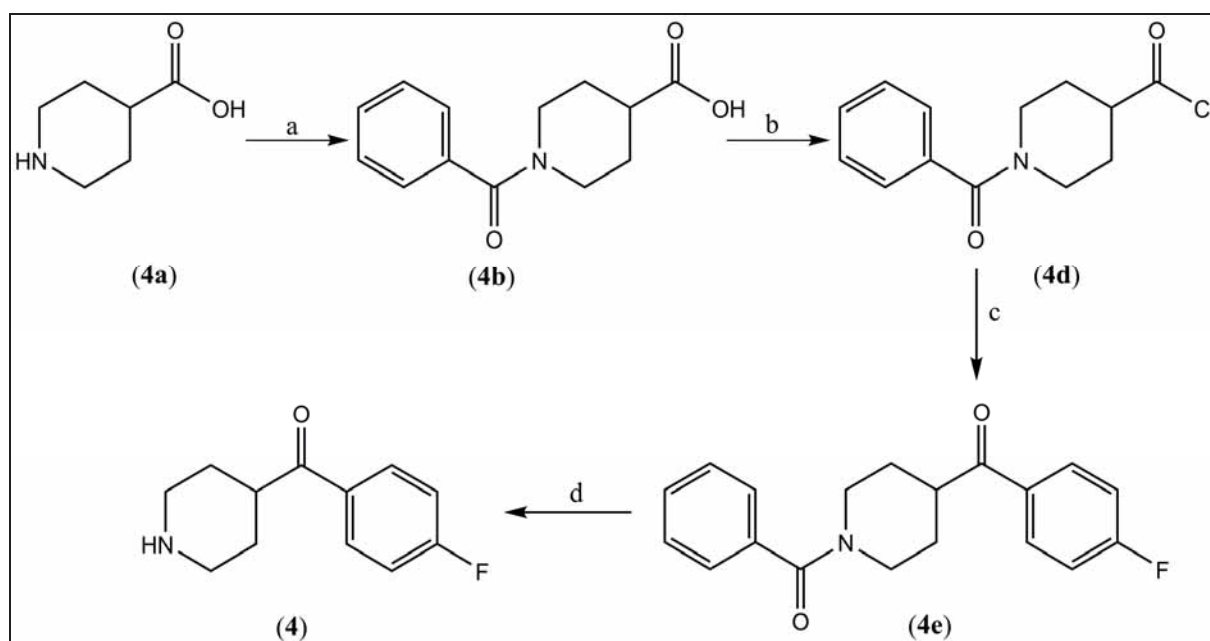Figure 4.7: Synthesis pathway of 4-(4-fluorobenzoyl)piperidine (**4**). a) K_2CO_3, H_2O, 0 °C, then benzoyl chloride, 0 °C → room temperature; b) $SOCl_2$, CH_2Cl_2, 40 °C; c) $AlCl_3$, fluorobenzene, CH_2Cl_2, 40 °C; d) HCl, H_2O, 100 °C.

Piperidine-4-carboxylic acid (**4a**) was protected by N-acylation with benzoyl chloride to yield the corresponding benzamide 1-benzoylpiperidine-4-carboxylic acid (**4b**). This benzamide was treated with thionylchloride to obtain the chlorinated compound (**4d**), which was immediately used in an aluminium chloride catalyzed Friedel-Crafts reaction with fluorobenzene to obtain the compound (1-benzoylpiperidin-4-yl)(4-flurophenyl)methanone (**4e**). The N-benzoyl protecting group of (**4e**) was removed under acidic conditions to afford compound (**4**), 4-(4-fluorobenzoyl)piperidine.

All chemicals and reagents were purchased from Sigma-Aldrich (St-Louis, MO, USA) or Acros Organics (Geel, Belgium) and were used without further purification unless specified otherwise. HPLC and flash chromatography solvents were purchased from Chemlab NV (Belgium). Organic reactions were monitored by normal phase thin layer chromatography (TLC) with UV detection at 254 nm where possible (TLC, Polygram Sil G/UV$_{254}$, 200 μm, Machery-Nagel, Germany). Purification of non-radioactive products was achieved with flash column chromatography on silica gel (240-400 mesh, 60 Å, Sigma-Aldrich, Belgium) using a glass column (36 mm x 460 mm, Büchi) and a Waters LC-8A preparative HPLC pump at a flow rate of 60 ml/min. Solvent systems are indicated in the text. For mixed solvent systems, ratios are given with respect to volumes.

^{1}H-NMR spectra were recorded on a Varian 300 MHz FT-NMR spectrometer (Laboratory for Medicinal Chemistry, Ghent University, Belgium). Chemical shifts were recorded in ppm (δ) relative to an internal tetramethylsilane (TMS) standard in either acetone-d$_6$, dimethyl-sulfoxide-d$_6$ or chloroform-d$_3$. Mass spectrometry was performed on a Waters Micromass ZMD mass-spectrometer with an electrospray-ionization (ESI) probe. Samples were recorded in the positive (MH$^+$) mode. Samples were dissolved in methanol at a concentration of 0.050 mg/ml. No carrier added (n.c.a.) [^{123}I]-NaI (formulated in 0.05 M NaOH) was purchased from GE Healthcare Biosciences (Diegem, Belgium).

4.2.1. Synthesis of 2-(3-bromophenyl)ethanol (2)

2-(3-Bromophenyl)ethanol (**2**) was synthesized from 3-bromophenylacetic acid (**1**) using a reduction with borohydride-tetrahydrofuran complex (borane, $BH_3.THF$). The hydride addition reaction mechanism is shown in figure 4.8.
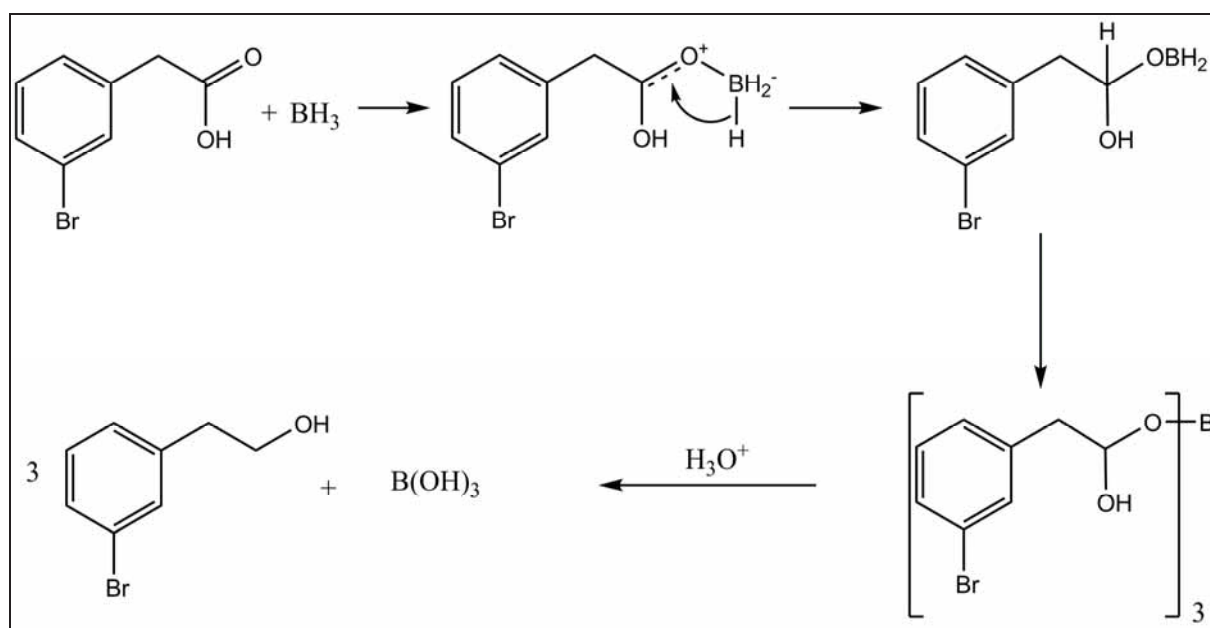
Figure 4.8: Mechanism of 3-bromophenylacetic acid reduction with BH_3

3-Bromophenylacetic acid (**1**) (5g, 23 mmol) was added dropwise to a cooled solution of borohydride-tetrahydrofuran complex ($BH_3.THF$, 35 mmol) under nitrogen atmosphere. The mixture was slowly warmed to room temperature and stirred for 2h. The reaction was quenched by addition of a 50/50 mixture of water and acetic acid (50 ml). THF was removed by evaporation under reduced pressure. Saturated $NaHCO_3$ solution (100 ml) was added, and the mixture was extracted with dichloromethane (3 x 100 ml). The organic phases were combined, washed once with saturated NaCl solution (100 ml) and dried over anhydrous sodium sulphate. After filtration, the solvent was removed by evaporation under reduced pressure. A light yellow oil was obtained (3.7g, 80%) which was used without further purification.

^{1}H-NMR (d_3-CH_3Cl, δ): 7.40-7.25 (m, 2H, 2-ArH and 4-ArH), 7.15-7.05 (m, 2H, 5-ArH and 6-ArH), 4.78 (t, 1H, -OH), 3.86 (m, 2H, R-CH_2-OH), 2.74 (t, 2H, Ar-CH_2-R).
ESI-MS: 183 (MH^+ minus H_2O).

4.2.2. Synthesis of 1-bromo-3-(2-bromoethyl)benzene (3)

1-Bromo-3-(2-bromoethyl)benzene (**3**) was synthesized by reacting 2-(3-bromophenyl)ethanol (**2**) with phosphorus tribromide. The reaction mechanism is shown in figure 4.9. First an ester is formed with PBr_3. After protonation, this ester becomes a good leaving group for nucleophilic substitution with the bromide anion. Finally, 3 moles of brominated compound (**3**) and 1 mole of H_3PO_3 are formed for every mole of PBr_3 used (figure 4.9).
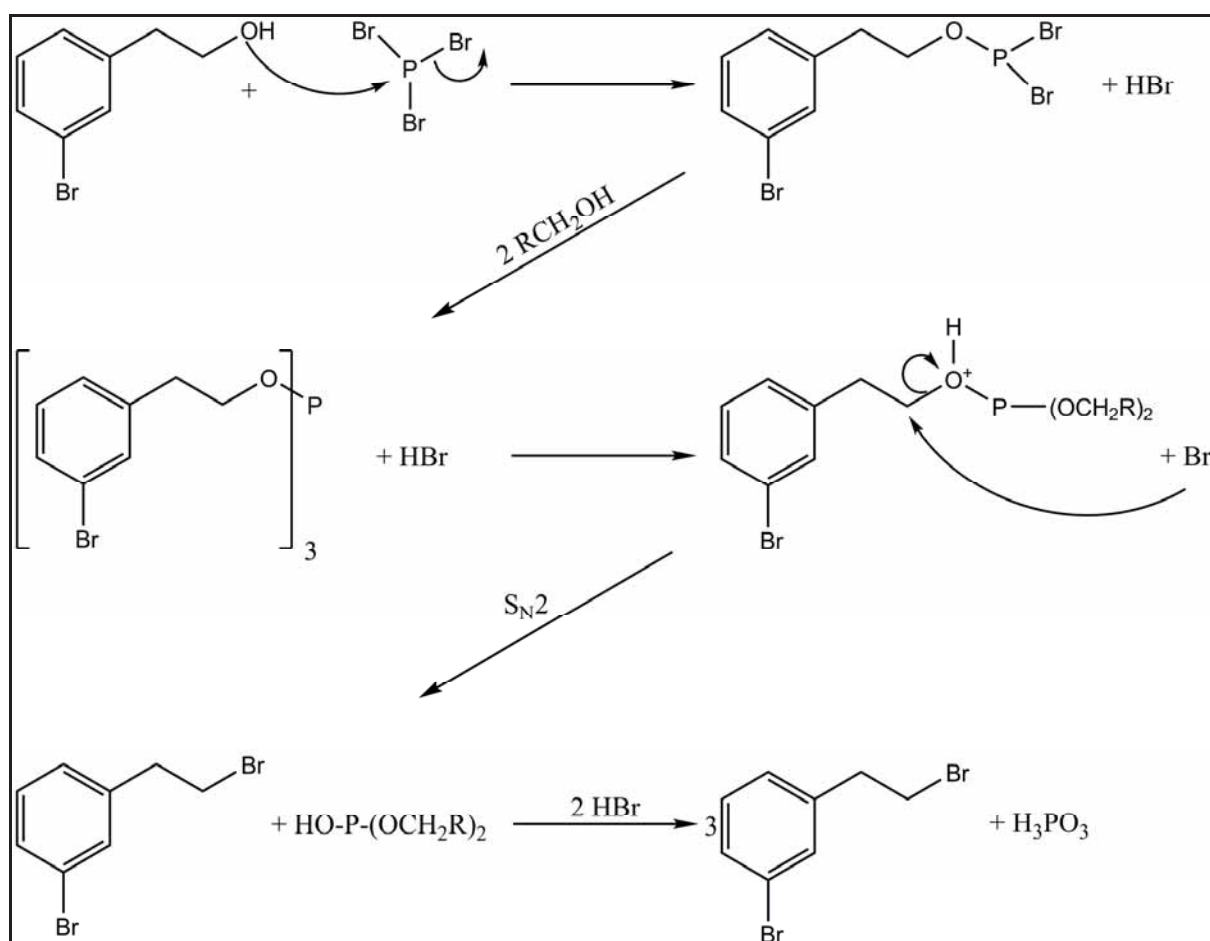
Figure 4.9: Bromination of 2-(3-Bromophenyl)ethanol (**2**)

2-(3-Bromophenyl)ethanol (**2**) (4g, 20 mmol) was cooled to 0°C under nitrogen atmosphere, and phosphorus tribromide (6.8g, 25 mmol, 2.4 ml) was added dropwise. The reaction was stirred under nitrogen atmosphere for 16h. The mixture was poured onto crushed ice (100g). Saturated $NaHCO_3$ solution (100 ml) was added and the mixture was stirred for 30 min. The product was extracted with dichloromethane (3 x 100 ml).

The combined extracts were washed with saturated NaCl solution (100 ml). The organic phase was dried over anhydrous sodium sulphate, filtered and evaporated under reduced pressure. The residue was dissolved in dichloromethane (200 ml) and filtered through silica gel. After removal of the solvent under reduced pressure, a slightly orange oil was obtained (4.7g, 90%).

^{1}H-NMR (d$_6$-DMSO, δ): 7.30-7.20 (m, 2H, 2-Ar-H and 4-Ar-H), 7.10-7.0 (m, 2H, 5-Ar-H and 6-Ar-H), 3.63 (t, 2H, R-CH$_2$-Br), 3.05 (t, 2H, Ar-CH$_2$-R).

4.2.3. Synthesis of (1-(3-bromophenethyl)piperidin-4-yl)(4-fluorophenyl) methanone (5)

(1-(3-Bromophenethyl)piperidin-4-yl)(4-fluorophenyl)methanone (**5**) was synthesized by a nucleophilic substitution reaction, following an S_N2 reaction mechanism (figure 4.10).
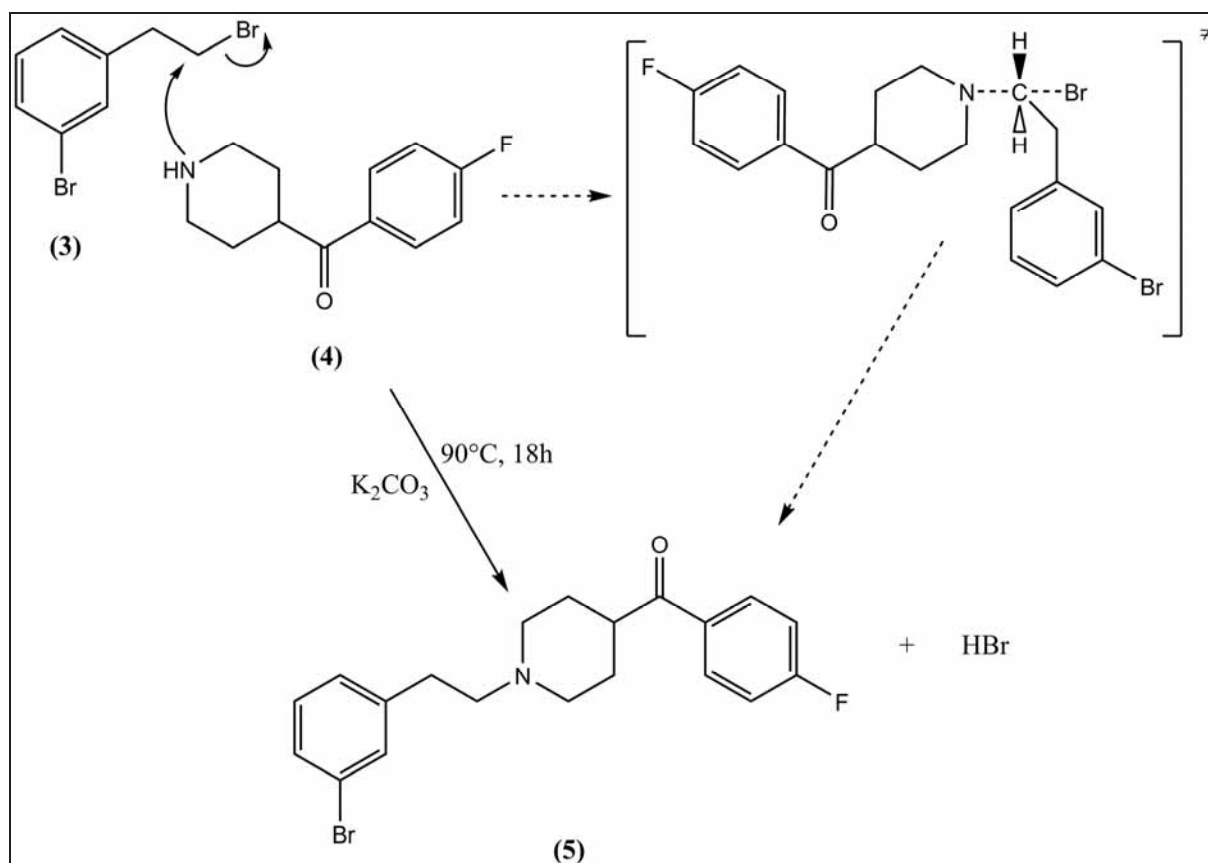
Figure 4.10: Synthesis of (1-(3-bromophenethyl)piperidin-4-yl)(4-fluorophenyl)methanone

To a solution of 4-(4-fluorobenzoyl)piperidine (**4**) (2.5g, 12 mmol) in dry dimethylformamide (DMF, 40 ml) was added 1-bromo-3-(2-bromoethyl)benzene (**3**) (4g, 15 mmol) under nitrogen atmosphere, followed by K_2CO_3 (4.2g, 30 mmol). The resulting mixture was heated to 90°C in an oil bath and stirred for 18h. After cooling to room temperature, the reaction mixture was filtered over celite and the filter cake was washed with DMF (2 x 10 ml). The combined filtrate was dried over anhydrous sodium sulphate, filtered, and stripped of solvent under reduced pressure. The residue was purified with flash column chromatography using dichloromethane/methanol/triethylamine (90/10/5) as eluent. An orange solid was obtained (60%).

^{1}H-NMR (d$_6$-DMSO, δ): 8.10 (m, 2H, 2-Ar-F and 6-Ar-F), 7.37 (m, 2H, 3-Ar-F and 5-Ar-F), 7.30-7.25 (m, 2H, 2-Ar-Br and 4-Ar-Br), 7.10-7.0 (m, 2H, 5-Ar-Br and 6-Ar-Br), 3.0 (q, 1H, F-Ar-CO-CH-R$_2$), 2.70-2.65 (m, 4H, Br-Ar-CH$_2$-CH$_2$-R), 2.24 (m, 4H, N-(CH$_2$)$_2$), 1.65 (m, 4H, F-Ar-CO-CH-(CH$_2$)$_2$-R).

ESI-MS: 390/392 (MH$^+$).

4.2.4. Synthesis of (4-fluorophenyl)(1-(3-tributylstannylphenethyl)piperidin-4-yl) methanone (6)

(1-(3-bromophenethyl)piperidin-4-yl)(4-fluorophenyl)methanone (**5**) was treated in toluene with hexabutylditin and tetrakistriphenylphosphinepalladium as a catalyst at 120°C for 18h, to yield (4-fluorophenyl)(1-(3-tributylstannyl-phenethyl)piperidin-4-yl)methanone (**6**) (figure 4.11).
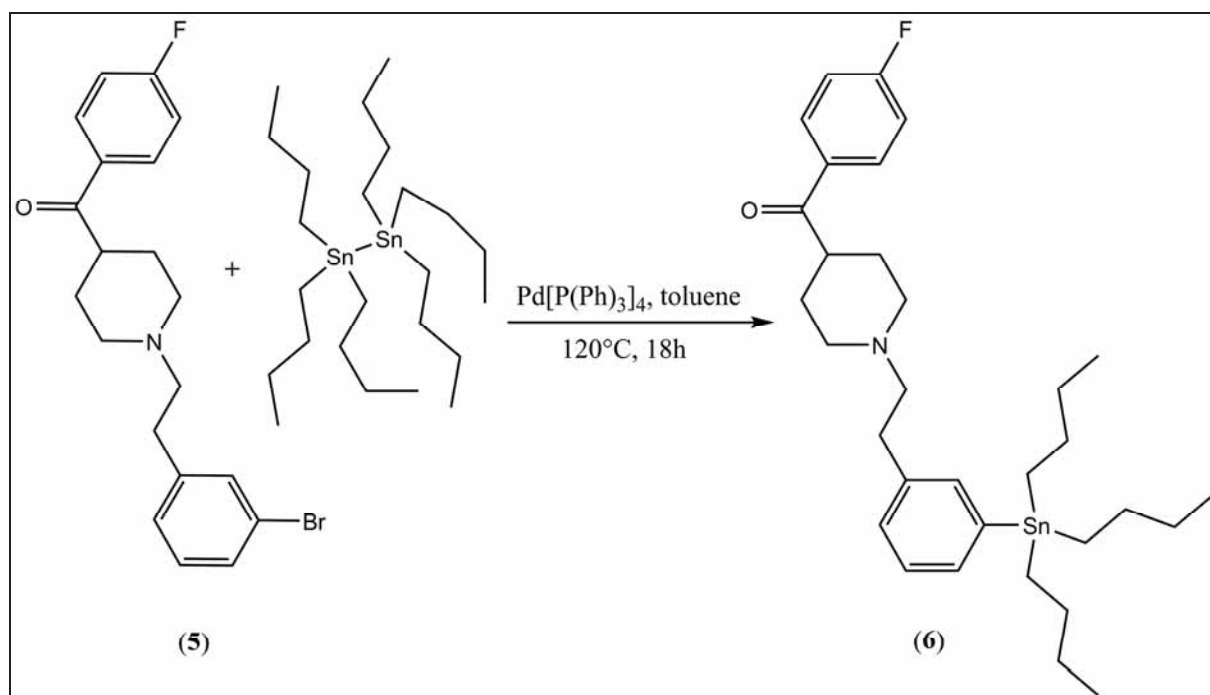
Figure 4.11: Synthesis of (4-fluorophenyl)(1-(3-tributylstannyl-phenethyl)piperidin-4-yl)methanone (**6**)

The reaction mechanism is a Stille type coupling, in different steps (figure 4.12): the first step in the cycle is an oxidative addition of Pd^0 to the carbon-bromine bond of (1-(3-bromophenethyl)piperidin-4-yl)(4-fluorophenyl)methanone (**5**) ($Pd^0 \rightarrow Pd^{II}$). The second step is a transmetallation with hexabutylditin, replacing the bromine for a tributylstannyl group. This is followed by isomerisation and a reductive elimination step, in which the carbon-tin bond is formed. Simultaneously, Pd^{II} is reduced back to Pd^0.
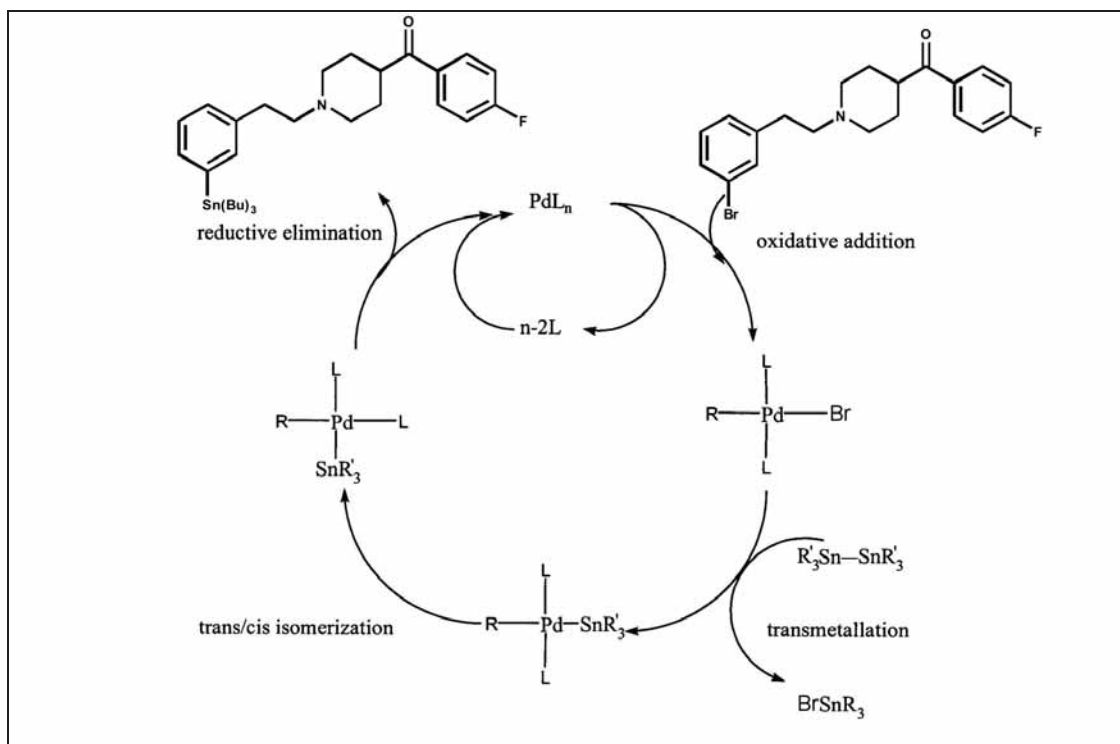
Figure 4.12: Reaction mechanism of Stille coupling

(1-(3-bromophenethyl)piperidin-4-yl)(4-fluorophenyl)methanone (**5**) (100mg, 0.25 mmol) was dissolved in anhydrous toluene (10 ml). Under nitrogen atmosphere a catalytic amount of tetrakistriphenylphosphinepalladium (10 mg) was added, followed by hexabutylditin (0.4 ml, 0.75 mmol). The reaction mixture was heated in the dark to 120°C for 18h under nitrogen atmosphere. After cooling to room temperature, the mixture was filtered over celite. The filter cake was washed with anhydrous toluene (2 x 5 ml) and the combined filtrates were evaporated under reduced pressure. The residue was purified using preparative thin layer chromatography with dichloromethane/methanol/triethylamine (90/10/5) as the eluent. The zone containing the product was marked, the silica gel scraped off and extracted with methanol (50 ml). Silica gel was removed by filtration and the solvent was evaporated under reduced pressure to yield (4-fluorophenyl)(1-(3-tributylstannyl-phenethyl)piperidin-4-yl)methanone (**6**) (45 mg, 30%).

^{1}H-NMR (d_6-DMSO, δ): 8.10 (m, 2H, 2-Ar-F and 6-Ar-F), 7.37 (m, 2H, 3-Ar-F and 5-Ar-F), 7.2-7.1 (m, 4H, Sn(Bu)$_3$-Ar-H), 3.0 (q, 1H, F-Ar-CO-CH-R$_2$), 2.70-2.65 (m, 4H, Br-Ar-CH$_2$-CH$_2$-R), 2.24 (m, 4H, N-(CH$_2$)$_2$), 1.65 (m, 4H, F-Ar-CO-CH-(CH$_2$)$_2$-R), 1.2-0.8 (m, 27H, tributylstannyl).

ESI-MS: 602 (MH$^+$).

4.2.5. Synthesis of (4-fluorophenyl)(1-(3-iodophenethyl)piperidin-4-yl) methanone (7)

The reference compound (4-fluorophenyl)(1-(3-iodophenethyl)piperidin-4-yl) methanone (**7**) was synthesized by treatment of (4-fluorophenyl)(1-(3-tributylstannylphenethyl)piperidin-4-yl)methanone (**6**) with iodine in chloroform. The reaction mechanism, an electrophilic aromatic substitution reaction, is shown in figure 4.13. In this case iodine acts as an electrophile (I^+---I^-), and the tributylstannyl group is a good leaving group. Reaction is quenched by the addition of sodium metabisulphite.
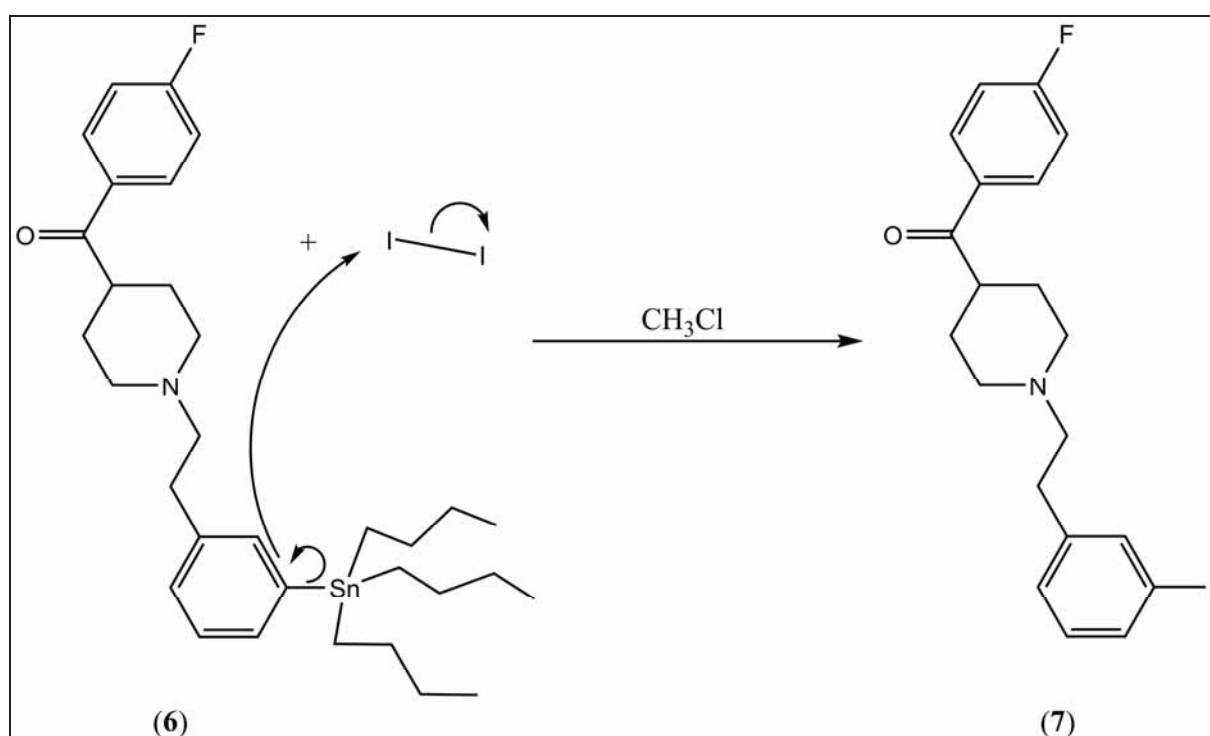
Figure 4.13: Cold iodination of (4-fluorophenyl)(1-(3-tributylstannyl-phenethyl)piperidin-4-yl) methanone

(4-fluorophenyl)(1-(3-tributylstannylphenethyl)piperidin-4-yl)methanone (**6**) (50mg, 0.08 mmol) was dissolved in anhydrous chloroform (10 ml) under nitrogen atmosphere. Iodine in chloroform (0.2 ml, 1M solution, 0.2 mmol) was added dropwise. The mixture was stirred for 1h at room temperature. The reaction was quenched by addition of sodium metabisulphite (1.5 ml, 5% solution in water). The resulting mixture was stirred for 30 min and the phases were separated. The aqueous phase was extracted with chloroform (3 x 10 ml).

The combined organic phases were washed with brine (10 ml), dried over anhydrous sodium sulphate and filtered. The solvent was removed under reduced pressure and the residue was purified with preparative TLC using dichloromethane/methanol/triethylamine (90/10/5) as eluent. The band corresponding to the product was scraped off and extracted with methanol (50 ml). After solvent removal under reduced pressure, an orange solid was obtained (11 mg, 0.025 mmol, 30%).

^{1}H-NMR (d$_6$-DMSO, δ): 8.10 (m, 2H, 2-Ar-F and 6-Ar-F), 7.60-7.50 (m, 2H, 2-Ar-I and 4-Ar-I), 7.37 (m, 2H, 3-Ar-F and 5-Ar-F), 7.11-7.0 (m, 2H, 5-Ar-I and 6-Ar-I), 3.0 (q, 1H, F-Ar-CO-CH-R$_2$), 2.70-2.65 (m, 4H, Br-Ar-CH$_2$-CH$_2$-R), 2.24 (m, 4H, N-(CH$_2$)$_2$), 1.65 (m, 4H, F-Ar-CO-CH-(CH$_2$)$_2$-R).
ESI-MS: 438 (MH$^+$).

4.2.6. Synthesis of 4-(4-fluorobenzoyl)piperidine (4)

The total synthesis of 4-(4-fluorobenzoyl)piperidine is shown above in figure 4.7.

4.2.6.1. Synthesis of 1-benzoylpiperidine-4-carboxylic acid (4b)

1-Benzoylpiperidine-4-carboxylic acid (**4b**) was synthesized by protection of piperidine-4-carboxylic acid (**4a**) with a benzoyl function. The reaction mechanism (shown in figure 4.14) is a nucleophilic acyl substitution reaction, where the chloride anion acts as a good leaving group. The generated HCl is neutralised by K_2CO_3 as soon as it forms.
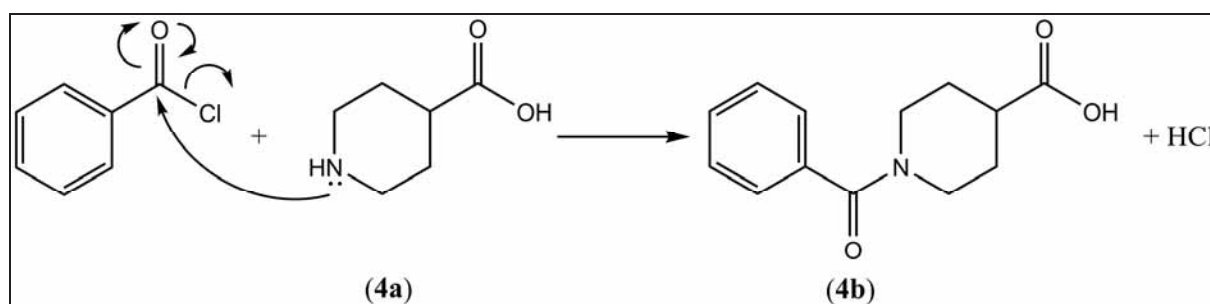
Figure 4.14: Synthesis of 1-benzoylpiperidine-4-carboxylic acid (**4b**)

Piperidine-4-carboxylic acid (**4a**, 25 g, 0.2 mol) was dissolved in distilled H_2O (500 ml) and potassium carbonate (K_2CO_3, 64g, 0.45 mol) was added. The mixture was cooled to 0 °C. Benzoyl chloride (24,3 ml, 0.2 mol) was added dropwise under nitrogen atmosphere and the mixture was stirred for 30 min at 0 °C. The mixture was slowly warmed to room temperature and stirred for 2 h. At the end of the reaction, concentrated HCl (65 ml, 37% v/v in water) was added slowly. The mixture was placed in the fridge overnight. The precipitate was filtered off and dried, yielding 1-benzoylpiperidine-4-carboxylic acid (**4b**, 42 g, 90% yield).

4.2.6.2. Synthesis of 1-benzoylpiperidine-4-carbonyl chloride (**4c**)

1-Benzoylpiperidine-4-carboxylic acid (**4b**) was chlorinated by treatment with thionyl chloride to obtain 1-benzoylpiperidine-4-carbonyl chloride (**4c**). The reaction mechanism is shown in figure 4.15 and takes place with formation of an intermediate reactive chlorosulphite-ester (*****).
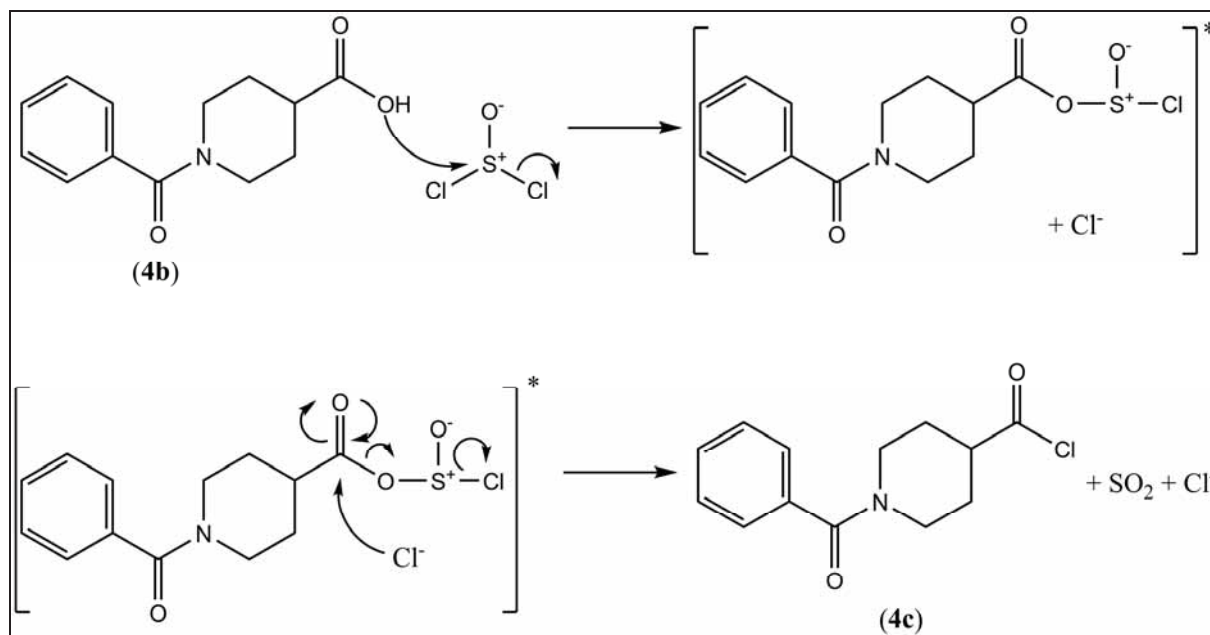
Figure 4.15: Synthesis of 1-benzoylpiperidine-4-carbonyl chloride (**4c**)

1-Benzoylpiperidine-4-carboxylic acid (**4b**, 42 g, 0.175 mol) was dissolved in dichloromethane (125 ml). Thionyl chloride (SOCl$_2$, 20 ml, 0.275 mol) was added dropwise to the solution. When SOCl$_2$ addition was complete, the mixture was slowly heated and refluxed under nitrogen for 2 h. After cooling to room temperature the solvent and excess reagent were evaporated under reduced pressure. The crude residue obtained, 1-benzoylpiperidine-4-carbonyl chloride (**4c**), was used without further purification.

4.2.6.3. Synthesis of (1-benzoylpiperidin-4-yl)(4-fluorophenyl)methanone (4e)

1-Benzoylpiperidine-4-carbonyl chloride (**4c**) was used in an aluminum chloride catalyzed Friedel-Craft's acylation reaction with fluorobenzene to obtain (1-benzoylpiperidin-4-yl)(4-fluorophenyl)methanone (**4e**). The reaction mechanism of this acylation reaction is shown in figure 4.16. Only the para-fluoro compound is formed because of the ortho/para directing effect of the fluorine atom.
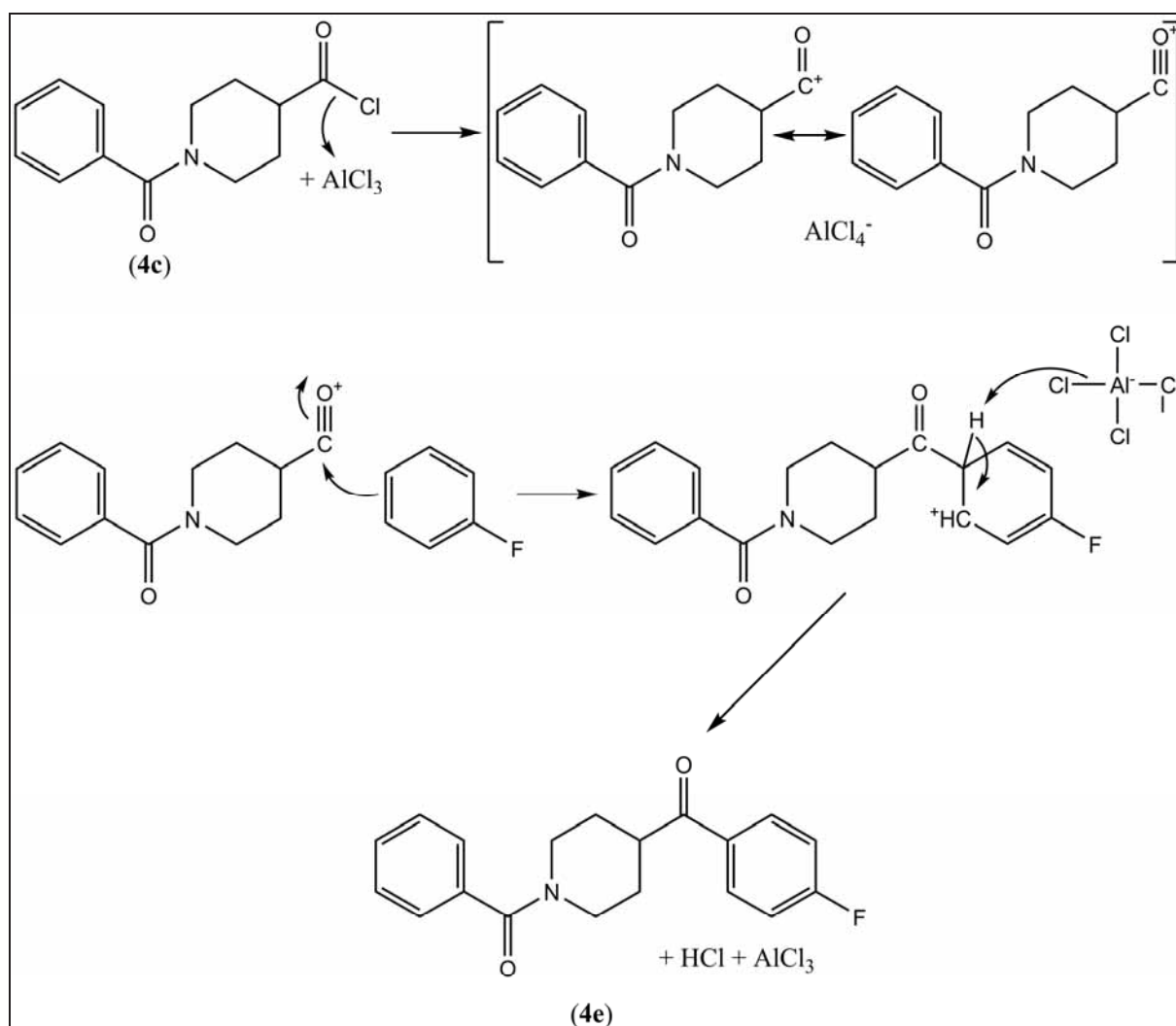
Figure 4.16: Friedel-Craft's acylation of fluorobenzene and 1-benzoylpiperidine-4-carbonyl chloride (**4c**)

The crude acid chloride 1-benzoylpiperidine-4-carbonyl chloride (**4c**, 42g, 0.175 mol) was dissolved in dichloromethane (80 ml). Aluminum chloride (AlCl$_3$, 61 g, 0.45 mol) was suspended in dichloromethane (80 ml) under nitrogen. Fluorobenzene (25 ml, 0.45 mol) was quickly added to the reaction mixture at room temperature. The mixture was cooled to 0 °C, stirred and the crude acid chloride 1-benzoylpiperidine-4-carbonyl chloride (**4c**, 42g, 0.175 mol dissolved in 80 ml of dichloromethane) was added dropwise under nitrogen. The mixture was slowly warmed to room temperature and stirred for 2 h. The reaction mixture was poured on ice (500 g) and extracted with dichloromethane (3 x 250 ml). The organic phase was washed with HCl (1N in water, 200 ml), saturated NaHCO$_3$-solution (200 ml) and water (100 ml). The organic layer was dried with anhydrous sodium sulphate, filtered and evaporated under reduced pressure. The residue was recrystallized from *tert*-butyl methyl ether and (1-benzoylpiperidin-4-yl)(4-fluorophenyl)methanone (**4e**, 50g, 90 % yield) was obtained.

4.2.6.4. Synthesis of 4-(4-fluorobenzoyl)-piperidine (**4**)

This reaction is a deprotection reaction, in which the protecting benzoyl function is hydrolysed from the piperidine nitrogen under acidic conditions to obtain the title compound, 4-(4-fluorobenzoyl)-piperidine (**4**). The hydrolysis reaction mechanism is shown in figure 4.17.
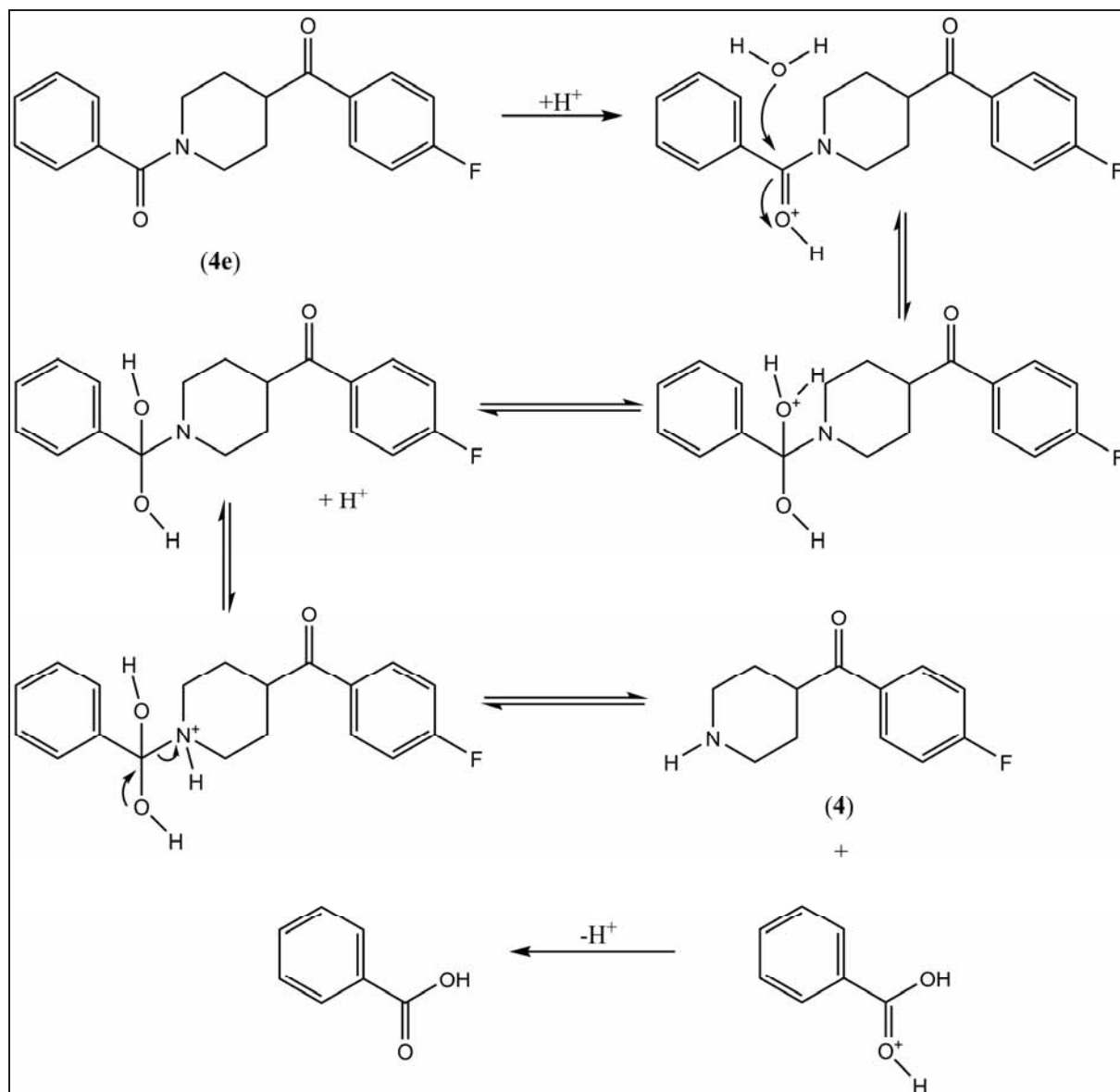
Figure 4.17: Acid hydrolysis of (1-Benzoylpiperidin-4-yl)(4-fluorophenyl)methanone (**4e**)

(1-Benzoylpiperidin-4-yl)(4-fluorophenyl)methanone (**4e**, 50g, 0.16 mol) was dissolved in HCl (200 ml, 37% in water) and water (100 ml). The resulting solution was refluxed under nitrogen for 6 h. After cooling to room temperature, the mixture was extracted with *tert*-butyl methyl ether (150 ml). The aqueous phase was cooled to 0 °C, basified with 5M sodium hydroxide solution and extracted with dichloromethane (3 x 100 ml). The organic phase was washed once with water (100 ml) and once with brine (100 ml). The organic layer was dried over anhydrous sodium sulphate, filtered and evaporated under reduced pressure. The residue was dissolved in ethanol (100 ml) and HCl (1M solution in diethylether, 100 ml) was added at 15 °C. The mixture was allowed to precipitate at 15 °C for 12 h. The mixture was filtered and 4-(4-fluorobenzoyl)-piperidine (**4**) was obtained (16.5 g, 50 %).

^{1}H-NMR (d$_6$-DMSO, δ): 8.11 (m, 2H, 2-Ar-F and 6-Ar-F), 7.35 (2H, m, 3-Ar-F and 5-Ar-F), 3.74 (m, 1H, F-Ar-CO-C**H**), 3.31-3.24 (m, 4H, H-N-(C**H$_2$**)$_2$-R), 2.48 (s, 1H, R$_2$-N-H), 1.76-1.92 (m, 4H, F-Ar-CO-CH-C**H$_2$**)$_2$-R).
ESI-MS: 208 (MH$^+$).

4.3. Radiolabelling

4.3.1. Methods

$[^{123}I]$-(4-Fluorophenyl)(1-(3-iodophenethyl)piperidin-4-yl)methanone ($[^{123}I]$-3-I-CO) was labelled with ^{123}I using an electrophilic iododestannylation on the tributylstannylprecursor (**6**). Chloramine-T was used as an oxidant for the *in situ* oxidation of the radioiodide. Sodium metabisulphite was used to terminate the reaction. The reaction scheme is shown in figure 4.18.
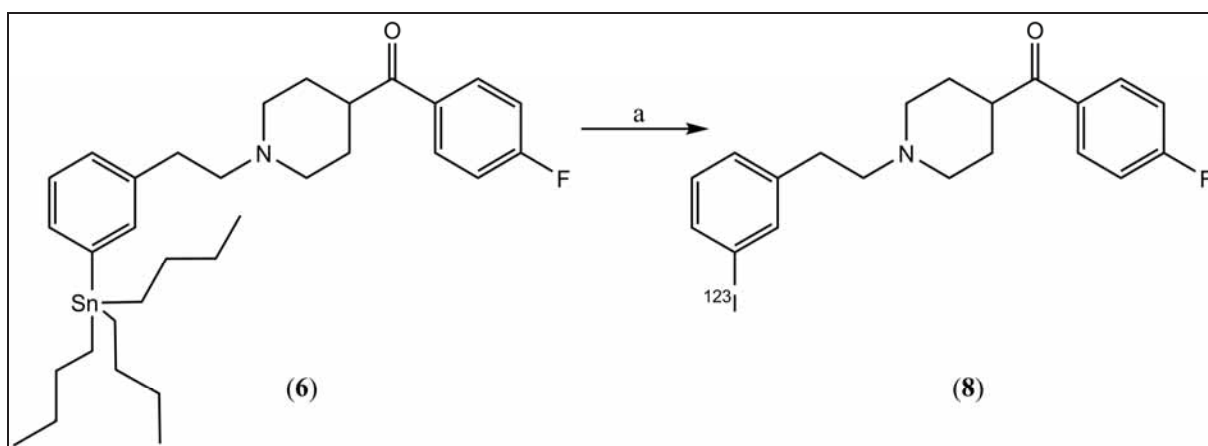
Figure 4.18: Radiosynthesis of $[^{123}I]$-3-I-CO (**8**). (a) (i) Na^{123}I, 0.01N NaOH, ethanol, (ii) acetic acid, chloramine T, 10 min, (iii) NaHS0$_3$, 85%, radiochemical purity > 95%.

The mechanism of the radioiodination reaction is an electrophilic aromatic substitution reaction of the tributylstannyl-compound (**6**) and is shown in figure 4.19. The electrophilic species is the iodonium ion H_2OI^+, which is formed *in situ* and reacts with the precursor (**6**) in an electrophilic substitution reaction, to yield the iodinated tracer $[^{123}I]$-3-I-CO (**8**). Chloramine-T is used as the oxidant in this reaction, to oxidise $[^{123}I]$-I$^-$ to $[^{123}I]$-I$^+$. In reality, the oxidative species is hypochlorous acid (HOCl), formed by the hydrolysis of N-chloro-p-toluenesulphonamide (= chloramine-T) in acidic medium. The reaction is quenched by the addition of sodium metabisulphite (NaHSO$_3$), used to remove the excess of chloramine-T.
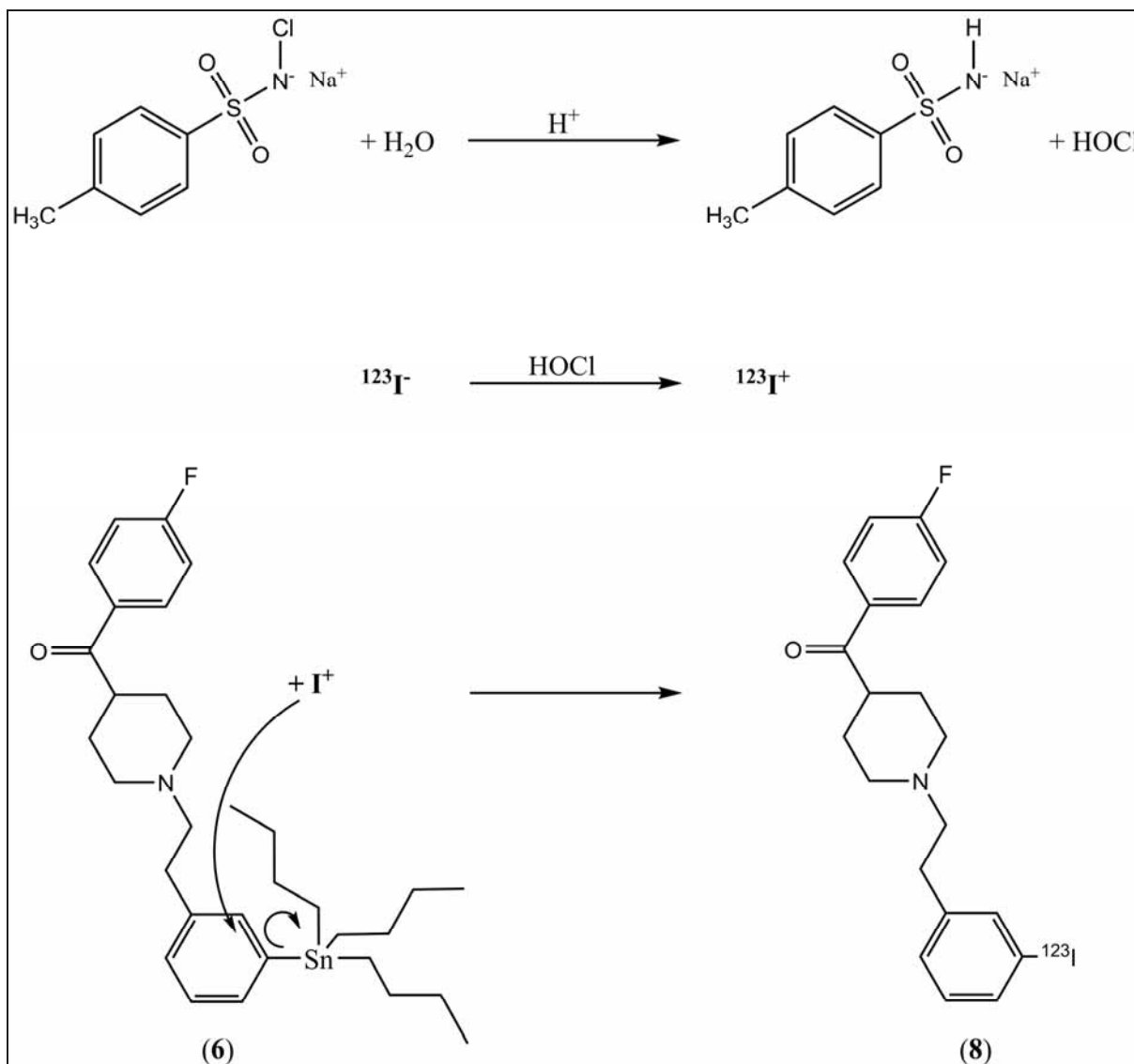
Figure 4.19: Radioiodination of the tributylstannyl precursor (**6**)

The precursor (**6**) (100 μg, 0.16 μmol) was dissolved in absolute ethanol (50 μl). No carrier added (nca) [^{123}I]-NaI (in 0.05 M sodium hydroxide, 5 - 30 μl, 37 - 1000 MBq), chloramine-T (15 μl, 18.8 mg/ml solution in water) and glacial acetic acid (20 μl) were added. The radiolabelling proceeded for 10 min at room temperature. The reaction was quenched by the addition of sodium metabisulphite (15 μl, 19 mg/ml solution in water). HPLC mobile phase (100 μl, 50/50 acetonitrile/phosphate buffer pH7) was added. The mixture was injected onto a reversed-phase C$_{18}$ HPLC column (Alltech Apollo C$_{18}$ 7 x 250 mm) for purification and eluted with 50/50 acetonitrile/0.02M phosphate buffer pH7 as eluent at a flow rate of 4 ml/min. The fraction corresponding to [^{123}I]-3-I-CO (T$_R$ = 70 min) was collected and diluted with water for injection to decrease the concentration of acetonitrile to maximum 10%.

The diluted mixture was passed over a C_{18}-cartridge (Alltech Maxi-Clean SPE Prevail C_{18} Sep-PAK previously activated with 1 ml methanol and rinsed with 1 ml of water). The cartridge was rinsed with water (5 ml) and the tracer was eluted with absolute ethanol (1 ml). Ethanol was evaporated under a nitrogen flow, and the tracer was redissolved in sterile 5% ethanol in water. The solution was sterilized by sterile filtration over a 0.22 μm filter (Schleicher & Schuell, FP 013/AS 0.22 μm filter) for use in biodistribution and brain studies. A typical chromatogram of a [^{123}I]-3-I-CO synthesis run is shown in figure 4.20.
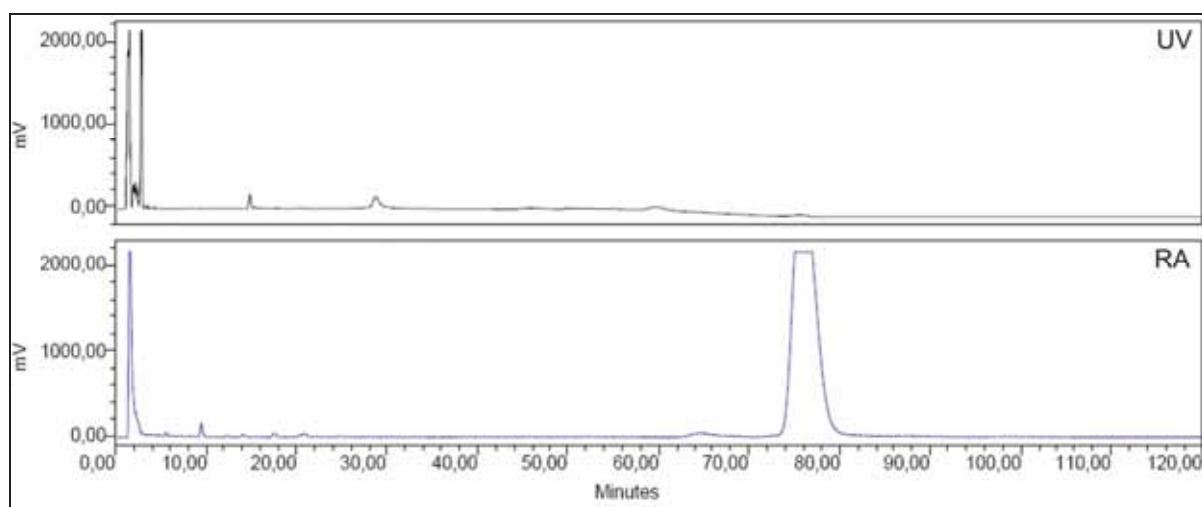
Figure 4.20: HPLC Chromatogram of [^{123}I]-3-I-CO synthesis. The UV-chromatogram is shown in the upper part of the figure, the radiochromatogram can be found in the lower part.

4.3.2. Results

Radiochemical purity of the tracer was determined by re-injecting a tracer aliquot on the same HPLC-system as described above (but with a 55/45 acetonitrile/buffer mixture as eluent). Radiochemical yield of the radioiodination was 85% ± 5%. Radiochemical purity was always >95% as determined on HPLC. A typical quality control chromatogram is shown in figure 4.21.
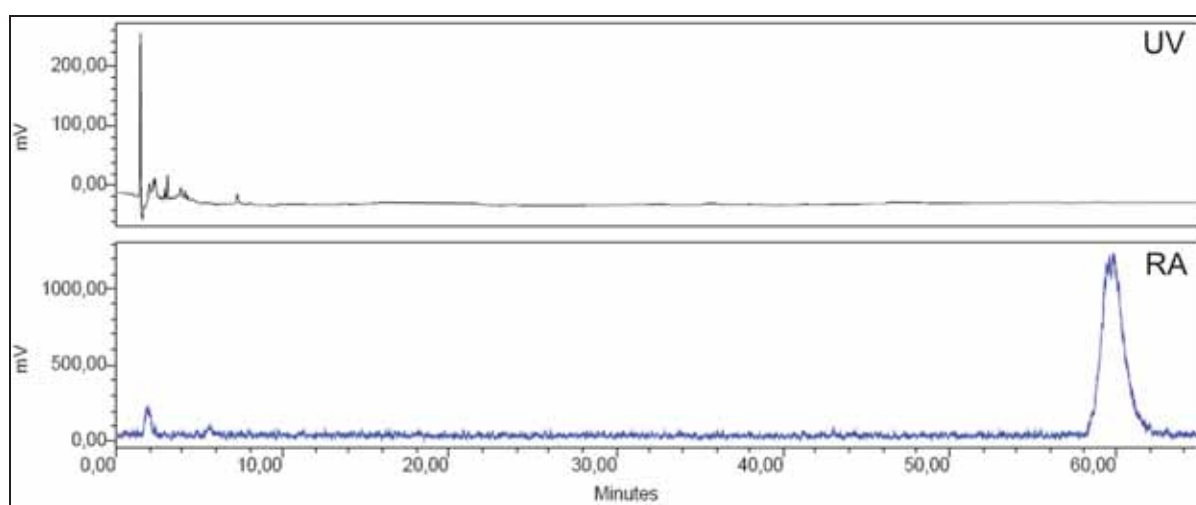
Figure 4.21: HPLC chromatogram of [^{123}I]-3-I-CO quality control. The upper part of the figure shows the UV-chromatogram; the radiochromatogram is shown in the lower part.

Stability of the tracer was tested by incubating the tracer (± 100 KBq) at room temperature in phosphate buffered saline solution (PBS buffer, pH 7.4). Aliquots of the tracer solution were taken at different time points and injected onto the same HPLC system as described above. Radiochemical purity of the tracer solution remained >95% until 48 hours after synthesis.

Varying amounts of radioactivity were used in this synthesis. We produced up to 20 mCi of [^{123}I]-3-I-CO in one synthesis and purification run, which is more then enough for possible clinical SPECT imaging studies with the tracer in humans.

4.4. Measurement of partition coefficient (LogP) and specific activity of [^{123}I]-3-I-CO

4.4.1. Determination of LogP

4.4.1.1. Methods

The partition coefficient of the tracer [^{123}I]-3-I-CO was meassured according to the 'shake flask' method[32]. [^{123}I]-3-I-CO (30 µl, 0.1 mCi) was added to a tube containing n-octanol (5 ml) and phosphate buffered saline (PBS buffer, pH = 7.4, 5 ml). The tube was shaken in a vortex mixer for 5 min followed by centrifugation for 5 min. After separation of the layers, the aqueous layer was discarded to remove possible free iodide, and fresh PBS-buffer (5 ml) was added to the tube. The tube was vortexed and centrifuged; 0.5 ml aliquots of both phases were taken and counted for radioactivity with an automated gamma counter (Cobra Autogamma, five 1 in X 1 in NaI(Tl) crystals, Packard Canberra). All radioactivity measurements were corrected for decay. The aqueous phase in the tube was discarded, and fresh PBS buffer (4.5 ml) was added. The tube was vortexed and centrifuged, aliquots were taken and counted, and the aqueous layer was again discarded. This process was repeated once more after addition of fresh PBS buffer (4 ml). All experimental measurements were performed in triplicate, and mean ± standard deviation values are indicated.

4.4.1.2. Results

The partition coefficient P was calculated as: P = (counts/g in n-octanol)/(counts/g in PBS).
A log P value of 3.10 ± 0.10 was obtained. An ideal log P value should be between 2 and 3 for optimal brain penetration of a given molecule. Higher log P values implicate a risk of increased aspecific binding, due to lipophilicity issues. Nevertheless, a log P value of 3.10 should provide adequate blood-brain barrier penetration for our animal biodistribution studies, without compromising lipophilicity too much.

4.4.2. Specific activity determination

The specific activity of a tracer can be defined as the amount of radioactivity present per mole of product. Specific activity is usually expressed as Ci/µmol.

Tracer specific activity is usually determined using HPLC: the peak area of the tracer in the UV-chromatogram (after injection of a known amount of tracer radioactivity) is compared to the peak area values of a standard curve, obtained by injection of varying amounts of cold unlabelled product.

In this case no detectable carrier UV-signal could be obtained after HPLC injection of the $[^{123}I]$-3-I-CO synthesis mixture. A standard curve was obtained by injecting known amounts of cold 3-I-CO and recording the UV peak area. Decreasing amounts of cold 3-I-CO were used, until there was no more UV signal present. This lowest concentration was used to calculate a minimum specific activity. It was not possible to determine the real specific activity of our $[^{123}I]$-3-I-CO tracer. Only an minimum specific activity could be obtained by determining the detection limit of the used UV-detector (Waters 2487 UV detector).

Nevertheless, the use of no carrier added $[^{123}I]$-NaI with very high specific activity (approaching the theoretical specific activity value of 22000 Ci/µmol for $[^{123}I]$-iodide) ensures that the labelled end product will be of high specific activity, probably approaching the theoretical value because no carrier should be present in any of the reagents/recipients used during radiosynthesis.

4.5. References

1. Fu X, Tan PZ, Kula NS, Baldessarini R, Tamagnan G, Innis RB et al. Synthesis, receptor potency, and selectivity of halogenated diphenylpiperidines as serotonin 5-HT2A ligands for PET or SPECT brain imaging. J Med Chem 2002; 45:2319-2324.

2. Dezi C, Brea J, Alvarado M, Ravina E, Masaguer CF, Loza MI et al. Multistructure 3D-QSAR Studies on a Series of Conformationally Constrained Butyrophenones Docked into a New Homology Model of the 5-HT2A Receptor. J Med Chem 2007;

3. Ballesteros JA, Jensen AD, Liapakis G, Rasmussen SGF, Shi L, Gether U et al. Activation of the beta(2)-adrenergic receptor involves disruption of an ionic lock between the cytoplasmic ends of transmembrane segments 3 and 6. Journal of Biological Chemistry 2001; 276:29171-29177.

4. Bissantz C, Bernard P, Hibert M, Rognan D. Protein-based virtual screening of chemical databases. II. Are homology models of G-protein coupled receptors suitable targets? Proteins-Structure Function and Genetics 2003; 50:5-25.

5. Shapiro DA, Kristiansen K, Weiner DM, Kroeze WK, Roth BL. Evidence for a model of agonist-induced activation of 5-hydroxytryptamine 2A serotonin receptors that involves the disruption of a strong ionic interaction between helices 3 and 6 (vol 277, pg 11441, 2002). Journal of Biological Chemistry 2002; 277:18244-18244.

6. Sylte I, Bronowska A, Dahl SG. Ligand induced conformational states of the 5-HT1A receptor. European Journal of Pharmacology 2001; 416:33-41.

7. Almaula N, Ebersole BJ, Ballesteros JA, Weinstein H, Sealfon SC. Contribution of a helix 5 locus to selectivity of hallucinogenic and nonhallucinogenic ligands for the human 5-hydroxytryptamine(2A) and 5-hydroxytryptamine(2C) receptors: Direct and indirect effects on ligand affinity mediated by the same locus. Molecular Pharmacology 1996; 50:34-42.

8. Shapiro DA, Kristiansen K, Kroeze WK, Roth BL. Differential modes of agonist binding to 5-Hydroxytryptamine(2A) serotonin receptors revealed by mutation and molecular modeling of conserved residues in transmembrane region 5. Molecular Pharmacology 2000; 58:877-886.

9. Ismaiel AM, Arruda K, Teitler M, Glennon RA. Ketanserin Analogs - the Effect of Structural Modification on 5-Ht2 Serotonin Receptor-Binding. J Med Chem 1995; 38:1196-1202.

10. Janssen PAJ. Pharmacology of Potent and Selective S2-Serotonergic Antagonists. Journal of Cardiovascular Pharmacology 1985; 7:S2-S11.

11. Lundkvist C, Halldin C, Ginovart N, Nyberg S, Swahn CG, Carr AA et al. [C-11]MDL 100907, a radioligand for selective imaging of 5-HT2A receptors with positron emission tomography. Life Sciences 1996; 58:L187-L192.

12. Lemaire C, Cantineau R, Guillaume M, Plenevaux A, Christiaens L. Fluorine-18-Altanserin - A Radioligand for the Study of Serotonin Receptors with Pet - Radiolabeling and Invivo Biologic Behavior in Rats. Journal of Nuclear Medicine 1991; 32:2266-2272.

13. Mathis CA, Mahmood K, Huang Y, Simpson NR, Gerdes JM, Price JC. Synthesis and preliminary in vivo evaluation of [C-11]MDL 100907: A potent and selective radioligand for the 5-HT2A receptor system. Medicinal Chemistry Research 1996; 6:1-10.

14. Price JC, Lopresti BJ, Mason NS, Holt DP, Huang Y, Mathis CA. Analyses of [F-18]altanserin bolus injection PET data. I: Consideration of radiolabeled metabolites in baboons. Synapse 2001; 41:1-10.

15. Staley JK, van Dyck CH, Tan PZ, Al Tikriti M, Ramsby Q, Klump H et al. Comparison of [F-18]altanserin and [F-18]deuteroaltanserin for PET imaging of serotonin(2A) receptors in baboon brain: pharmacological studies. Nuclear Medicine and Biology 2001; 28:271-279.

16. Tan PZ, Baldwin RM, van Dyck CH, Al-Tikriti M, Roth B, Khan N et al. Characterization of radioactive metabolites of 5-HT2A receptor PET ligand [F-18]altanserin in human and rodent. Nuclear Medicine and Biology 1999; 26:601-608.

17. Watabe H, Channing MA, Der MG, Adams HR, Jagoda E, Herscovitch P et al. Kinetic analysis of the 5-HT2A ligand [C-11]MDL 100,907. Journal of Cerebral Blood Flow and Metabolism 2000; 20:899-909.

18. Prabhakaran J, Parsey RV, Majo VJ, Van Heertum RL, Mann JJ, Kumar JSD. Synthesis and in vivo evaluation of [O-methyl-C-11] 2-(4-methoxyphenyl)-N-(4-methylbenzyl)-N-(1-methyl-piperidin-4-yl)acetamide as as imaging probe for 5-HT2A receptors. Journal of Labelled Compounds & Radiopharmaceuticals 2006; 49:1069-1077.

19. Meyer JH, Kapur S, Houle S, DaSilva J, Owczarek B, Brown GM et al. Prefrontal cortex 5-HT2 receptors in depression: An [F-18]setoperone PET imaging study. American Journal of Psychiatry 1999; 156:1029-1034.

20. Crouzel C, Venet M, Sanz G, Denis A. Labeling of A New Serotoninergic Ligand - [F-18] Ritanserin. Journal of Labelled Compounds & Radiopharmaceuticals 1988; 25:827-832.

21. Kumar JSD, Prabhakaran J, Erlandsson K, Majo VJ, Simpson NR, Pratap M et al. Synthesis and in vivo evaluation of [O-methyl-C-11] (2R,4R)-4-hydroxy-2-[2-[2-[2-(3-methoxy)phenyl]ethyl]phenoxy]ethyl-1-methylpyrrolidine as a 5-HT2A receptor PET ligand. Nuclear Medicine and Biology 2006; 33:565-574.

22. Catafau AM, Danus M, Bullich S, Llop J, Perich J, Cunningham VJ et al. Characterization of the SPECT 5-HT2A receptor ligand I-123-R91150 in healthy volunteers: Part 1 - Pseudoequilibrium interval and quantification methods. Journal of Nuclear Medicine 2006; 47:919-928.

23. Catafau AM, Danus M, Bullich S, Nucci G, Llop J, Abanades S et al. Characterization of the SPECT 5-HT2A receptor ligand I-123-R91150 in healthy volunteers: Part 2 - Ketanserin displacement. Journal of Nuclear Medicine 2006; 47:929-937.

24. Still WC, Kahn M, Mitra A. Rapid Chromatographic Technique for Preparative Separations with Moderate Resolution. Journal of Organic Chemistry 1978; 43:2923-2925.

25. Elsinga PH, Hendrikse NH, Bart J, van Waarde A, Vaalburg W. Positron emission tomography studies on binding of central nervous system drugs and P-glycoprotein function in the rodent brain. Molecular Imaging and Biology 2005; 7:37-44.

26. Hendrikse NH, Schinkel AH, De Vries EGE, Fluks E, Van der Graaf WTA, Willemsen ATM et al. Complete in vivo reversal of P-glycoprotein pump function in the blood-brain barrier visualized with positron emission tomography. British Journal of Pharmacology 1998; 124:1413-1418.

27. Hendrikse NH, Franssen EJ, Van der Graaf WTA, Vaalburg W, De Vries EGE. Visualization of multidrug resistance in vivo. European Journal of Nuclear Medicine 1999; 26:283-293.

28. Ishiwata K, Kawamura K, Yanai K, Hendrikse NH. In vivo evaluation of P-glycoprotein modulation of 8 PET radioligands used clinically. Journal of Nuclear Medicine 2007; 48:81-87.

29. Joseph B, Bhargava KK, Malhi H, Schilsky ML, Jain D, Palestro CJ et al. Sestamibi is a substrate for MDR1 and MDR2 P-glycoprotein genes. European Journal of Nuclear Medicine and Molecular Imaging 2003; 30:1024-1031.

30. Kiyono Y, Yamashita T, Doi H, Kuge Y, Katsura T, Inui KI et al. Is MIBG a substrate of P-glycoprotein? European Journal of Nuclear Medicine and Molecular Imaging 2007; 34:448-452.

31. Liow JS, Lu SY, McCarron JA, Hong JS, Musachio JL, Pike VW et al. Effect of a P-glycoprotein inhibitor, cyclosporin A, on the disposition in rodent brain and blood of the 5-HT1A receptor radioligand, [C-11](R)-(-)-RWAY. Synapse 2007; 61:96-105.

32. Wilson AA, Jin L, Garcia A, DaSilva JN, Houle S. An admonition when measuring the lipophilicity of radiotracers using counting techniques. Applied Radiation and Isotopes 2001; 54:203-208.

Chapter 5

IN VIVO EVALUATION IN RODENTS OF

[^{123}I]-3-I-CO

♋♋♋

5. *In vivo evaluation in rodents of [^{123}I]-3-I-CO*

5.1. Evaluation of [^{123}I]-3-I-CO in NMRI mice

5.1.1. Introduction

Several conditions have to be met before [^{123}I]-3-I-CO can be considered as a potential 5-HT$_{2A}$ receptor tracer. The molecule must be able to pass through the blood-brain barrier and bind to the 5-HT$_{2A}$ receptor dense regions with good specificity and selectivity. Aspecific binding should be minimal and tracer selectivity is important. Besides good *in vitro* characteristics, the *in vivo* characteristics should be optimal.

To verify the ability of [^{123}I]-3-I-CO to pass through the blood-brain barrier, a mouse biodistribution study was performed. This study will also provide information about the *in vivo* pharmacokinetic behaviour of the compound. A blocking study with a known specific 5-HT$_{2A}$ antagonist (ketanserin) will be performed to demonstrate specific binding to the 5-HT$_{2A}$ receptor *in vivo*.

It is also important to verify possible metabolism of the tracer into labelled lipophilic metabolites, because these can also cross the blood-brain barrier and interfere with brain imaging. Possible metabolism of [^{123}I]-3-I-CO will be verified by analyzing mouse blood and brain samples on HPLC.

Male NMRI (Naval Medical Research Institute) mice were purchased from Charles River Laboratories. All test animals were allowed to acclimatise in the lab prior to their use in biodistribution studies. All animal experiments were conducted following the principles of laboratory animal care and the Belgian law regulations laboratory test animal well-being. Our research protocols were pre-approved by the Gent University ethical committee (approval number 05/14).

5.1.2. Biodistribution study in NMRI mice

5.1.2.1. Methods

A biodistribution study with [^{123}I]-3-I-CO was performed in male NMRI mice. The radioligand was dissolved in ethanol/water (10/90 v/v), and the radioactivity concentration was adjusted to 200 µCi/ml of injectable tracer solution. Adult male NMRI mice (weight 20 – 25 g) were injected in the tail vein with [^{123}I]-3-I-CO (20 µCi dissolved in 100 µl). At various time points post injection (30 sec, 1 min, 2 min, 5 min, 10 min, 30 min, 1 hour, 2 h and 6 h, n = 3 per time point) the animals were sacrificed by decapitation. Blood was collected and the animals were rapidly dissected. Blood samples and organs of interest were weighed and counted for radioactivity in an automated gamma counter. Aliquots of the injected tracer solution (n = 3) were weighed and counted for radioactivity to determine the injected radioactivity dose received by the animals. Results were corrected for decay and tissue radioactivity concentrations were expressed as a percentage of the injected dose per gram of tissue (% ID/g tissue, mean ± standard deviation).

5.1.2.2. Results and discussion

A summary of the radioactivity concentrations for all organs at all time points studied is shown in table 5.1. Radioactivity concentrations were decay corrected and are expressed as a percentage of the injected dose per gram of tissue (% ID/g tissue). Mean ± standard deviation values are indicated (n = 3 animals per time point).

Tissue	30 s	60 s	2 min	5 min	10 min	30 min	1 h	2 h	6 h
Blood	5,60 ± 1,03	3,48 ± 0,25	2,58 ± 0,19	2,01 ± 0,34	2,37 ± 0,20	1,80 ± 0,29	1,51 ± 0,40	0,80 ± 0,50	0,40 ± 0,21
Brain	4,37 ± 0,48	4,31 ± 0,32	4,79 ± 0,13	5,94 ± 1,56	6,26 ± 1,36	3,37 ± 0,61	1,94 ± 0,37	0,98 ± 0,30	0,74 ± 0,17
Heart	15,9 ± 1,82	10,9 ± 0,77	7,04 ± 0,91	4,83 ± 1,41	3,96 ± 0,73	2,11 ± 0,38	1,56 ± 0,07	1,22 ± 0,12	0,45 ± 0,14
Lungs	29,6 ± 4,77	28,6 ± 1,95	21,1 ± 2,11	18,0 ± 2,72	13,2 ± 4,21	5,40 ± 0,46	3,68 ± 0,19	3,31 ± 0,83	2,84 ± 0,74
Stomach	1,45 ± 0,33	2,01 ± 0,54	3,46 ± 0,45	5,49 ± 3,21	7,90 ± 3,63	5,90 ± 0,50	11,4 ± 3,96	18,1 ± 3,11	12,4 ± 3,23
Spleen	3,24 ± 2,24	3,99 ± 0,49	5,52 ± 1,07	9,85 ± 0,16	10,1 ± 0,97	5,42 ± 1,15	5,64 ± 1,61	4,70 ± 2,79	3,34 ± 1,74
Liver	5,40 ± 3,07	8,96 ± 1,55	12,8 ± 1,39	19,9 ± 5,79	21,7 ± 3,29	13,5 ± 1,36	9,64 ± 0,10	6,93 ± 0,63	4,47 ± 0,96
Kidney	15,7 ± 4,26	17,7 ± 5,23	19,2 ± 1,01	16,5 ± 4,33	11,2 ± 2,84	8,15 ± 0,30	8,96 ± 3,59	5,24 ± 0,48	3,01 ± 0,84
Small Int.	1,92 ± 0,58	2,94 ± 0,14	3,29 ± 0,39	4,43 ± 0,67	6,34 ± 1,73	5,67 ± 0,97	11,5 ± 6,99	19,0 ± 4,49	15,3 ± 3,21
Large Int.	0,82 ± 0,25	1,32 ± 0,28	1,45 ± 0,40	2,20 ± 0,82	2,26 ± 0,85	1,77 ± 0,36	1,84 ± 0,53	4,21 ± 3,16	6,30 ± 1,41
Blatter	1,86 ± 0,72	2,06 ± 0,62	2,89 ± 0,75	4,48 ± 1,91	5,53 ± 2,03	10,7 ± 8,95	16,4 ± 7,31	16,2 ± 7,11	10,1 ± 3,24
Fat	1,20 ± 0,85	1,30 ± 0,20	1,66 ± 1,22	1,17 ± 0,26	1,29 ± 0,36	2,54 ± 0,48	3,54 ± 0,24	4,95 ± 1,83	3,22 ± 0,74

Animals were injected intravenously with 20 μCi of [^{123}I]-3-I-CO and sacrificed at designated time points after injection. Radioactivity concentrations are expressed as percentage of the injected dose per gram of tissue (% ID/g tissue). Results are decay corrected and are expressed as mean ± standard deviation (n = 3 animals per time point).

Table 5.1: Tissue radioactivity concentrations at different time points after injection of [^{123}I]-3-I-CO in male NMRI mice

Radioactivity concentrations for $[^{123}I]$-3-I-CO in blood and brain of NMRI mice are shown in figure 5.1.
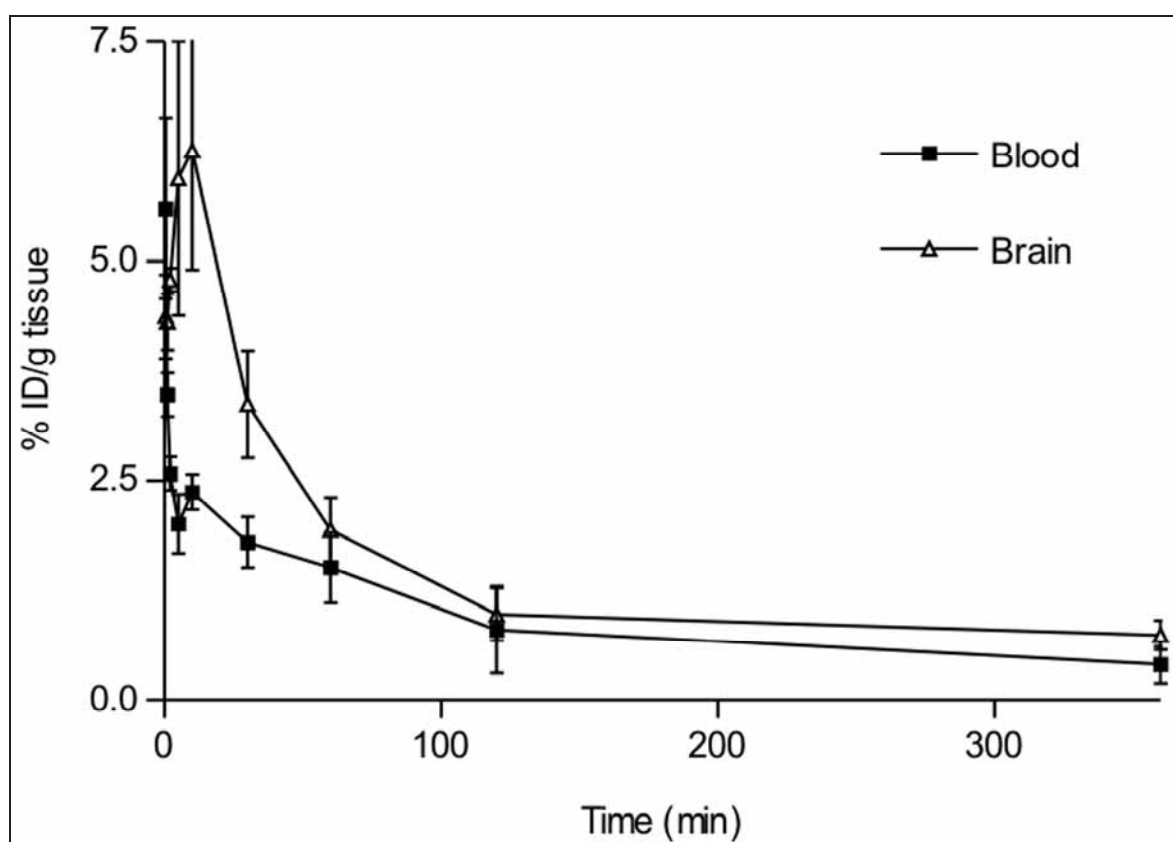
Figure 5.1: Biodistribution of $[^{123}I]$-3-I-CO in brain and blood of male NMRI mice. Mean ± standard deviation (n = 3 per time point).

It is clear from figure 5.1 that the radioactivity concentration of $[^{123}I]$-3-I-CO in brain is higher than the concentration in blood, at all time points studied. This indicates that $[^{123}I]$-3-I-CO readily crosses the blood-brain barrier. A maximum concentration of 6.26 % ± 1.36 % ID/g tissue was obtained 10 min post injection.. At 1 h post injection, the radioactivity concentration of $[^{123}I]$-3-I-CO in mouse brain was 1.94 % ± 0.37% ID/g tissue. The ratio brain-to-blood was always higher than 1 (a ratio of 3 was observed 5 min post injection, decreasing to 1.3 at 2 h post injection).

The brain uptake of [123I]-3-I-CO was compared with the total brain uptake in mice of a clinically used 5-HT$_{2A}$ tracer, [123I]-R91150. For [123I]-R91150, total brain uptake in mice was 0.73 ± 0.01 % ID/g tissue at 1 h after injection[1]. Compared to these values, the total brain uptake of [123I]-3-I-CO is high. When comparing the brain-to-blood ratios, the situation is different. Brain-to-blood ratios of 1.5 were obtained at the earliest time points for [123I]-R91150, increasing to 2 at 2 hours after injection. Brain-to-blood ratios varied between 1.8 and 3 for the earliest time points in the [123I]-3-I-CO biodistribution study. A ratio of 1.25 was obtained for the study at 1 and 2 hours after injection of [123I]-3-I-CO.

Although the absolute brain uptake of [123I]-3-I-CO in NMRI mice was increased compared to the [123I]-R91150 mouse biodistribution study, the blood radioactivity concentration was also higher, resulting in a decreased brain-to-blood ratio for the [123I]-3-I-CO study. Also, [123I]-3-I-CO brain radioactivity uptake decreased quite rapidly over time compared to the results obtained with [123I]-R91150, where a slower decrease in brain radioactivity concentration could be observed.

The biodistribution pattern of [123I]-3-I-CO in blood, heart and lungs of male NMRI mice is shown in figure 5.2.
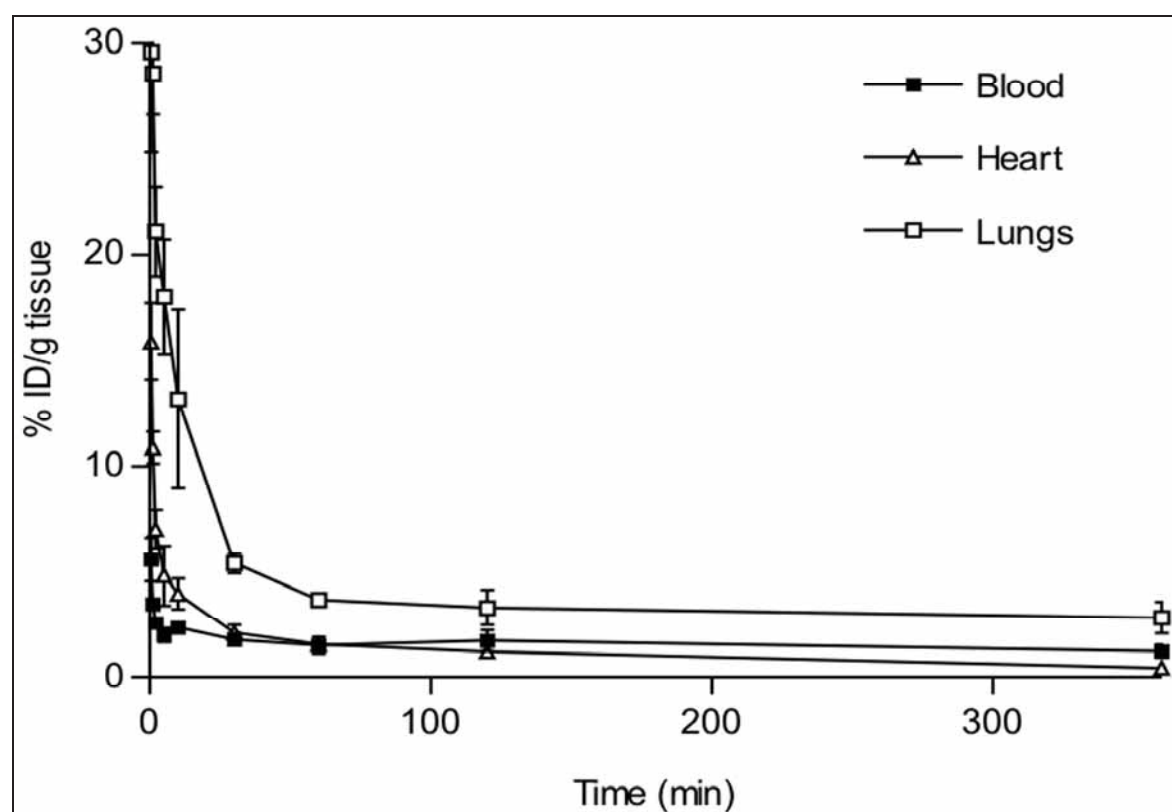
Figure 5.2: Biodistribution of [123I]-3-I-CO in NMRI mice. Mean $\pm$ s.d. (n = 3 per time point).

Uptake of the tracer [^{123}I]-3-I-CO in heart and lungs of male NMRI mice was high initially (lungs: 28.6% ± 1.95% ID/g tissue at 1 min post injection and 18% ± 2.72% % ID/g tissue at 5 min post injection; heart: 10.9% ± 0.77% % ID/g tissue at 1 min post injection and 4.83% ± 1.41% % ID/g tissue at 5 min post injection), but there was a rapid wash-out of radioactivity from these organs (lungs: 5.40% ± 0.46% % ID/g tissue at 30 min post injection; heart: 2.11% ± 0.38% ID/g tissue at 30 min post injection), as shown in figure 5.2. The radioactivity concentration curves in these organs are probably a reflection of the blood radioactivity concentration curve.

A high initial uptake of [^{123}I]-3-I-CO was seen in the liver: a maximum uptake of 21.7% ± 3.29% ID/g tissue was found at 10 min post injection. The radioactivity gradually decreased to 4.47% ± 0.96% ID/g tissue at 6 h post injection. Approximately the same washout pattern could be found in the kidneys: a maximum uptake of radioactivity was seen at 2 min post injection (19.2% ± 1.01% ID/g tissue), and this decreased to 3.01% ± 0.84% ID/g tissue.

Uptake in the intestines was initially low, but gradually increased over time: 3.29% ± 0.39% ID/g tissue at 2 min for the small intestines, 1.45% ± 0.40% ID/g tissue at 2 min for the large intestines. This activity increased to 19.0% ± 4.49% ID/g tissue at 2 h post injection for small intestines and 4.21% ± 3.16% ID/g tissue at 2 h post injection for the large intestines. The relatively high uptake in the intestines suggests that [^{123}I]-3-I-CO is at least partly biliary excreted.

5.1.3. Metabolite analysis in NMRI mice

<u>5.1.3.1. Methods</u>

Male NMRI mice (weighing 20 - 25g, n = 3) were injected in the tail vein with [^{123}I]-3-I-CO (100 μCi dissolved in ethanol/water 10/90 v/v). At 30 min post injection, the animals were sacrificed by decapitation. Blood was collected and the animals were rapidly dissected. Blood samples were centrifuged for 3 min at 3000g and the pellet was discarded. Mouse plasma (200 μl) was mixed with acetonitrile (800 μl) and the mixture was vortexed for 30 s, followed by centrifugation for 3 min at 3000g. The supernatant (500 μl) was analysed on HPLC.

The brain was transferred to a tube and acetonitrile (2 ml) was added. The mixture was cooled on ice, homogenized for 30 sec using a mixer (Ultra Turrax T18 basic, IKA Works Inc, USA, setting 5) and finally centrifuged at 3000g for 3 min. The supernatant (500 μl) was analysed on HPLC. An Alltech Econosil C$_{18}$ column (250 mm x 10 mm; 10 μm particle size) was used. The mobile phase was a mixture of ethanol and buffer (60/40 v/v, 0.02 M phosphate buffer pH 7.4) at a flow rate of 5 ml/min. A fraction collector was placed at the end of the HPLC column, and the eluate was collected in fractions of 5 ml (= 1 min). The fractions were then counted for radioactivity with an automated gamma counter (Packard Canberra, five 1"x1" NaI(Tl) crystals). The retention time (t_R) of the tracer was 25 min.

The above extraction method was validated by repeating the procedure with animals not treated with the tracer [^{123}I]-3-I-CO. Blood and brain from non-treated mice were collected in heparinised tubes. The blood was centrifuged at 3000g for 3 min, and [^{123}I]-3-I-CO (1 μCi) was added to 200 μl of plasma (= 'spiking' of the plasma). Acetonitrile (800 μl) was added, and the mixture was vortexed for 30 sec and centrifuged for 3 min at 3000g. Pellet and supernatant were separated and counted for radioactivity. To the brain samples acetonitrile (2 ml) and [^{123}I]-3-I-CO (1 μCi) were added, the mixture was mixed for 30 sec and centrifuged for 3 min at 3000g. Pellet and supernatant were separated and counted for radioactivity in an automated gamma counter.

The extraction efficiency (extraction yield) was expressed as percentage of total activity found in the supernatant compared to the total amount of radioactivity present in the tissue or blood sample.

To exclude the formation of possible $[^{123}I]$-3-I-CO metabolites by the extraction method, aliquots of the above supernatants of brain and blood were also injected on the same HPLC system. An aliquot of authentic $[^{123}I]$-3-I-CO tracer solution was first injected to determine the retention time of unmetabolised $[^{123}I]$-3-I-CO.

5.1.3.2. Results

Extraction yield results were always > 90%, indicating that the followed extraction methodology was adequate for determination of $[^{123}I]$-3-I-CO and possible metabolites.

An aliquot of authentic $[^{123}I]$-3-I-CO tracer solution was first injected onto the same HPLC system to determine the retention time of unmetabolised $[^{123}I]$-3-I-CO ($T_R = 25$ min).
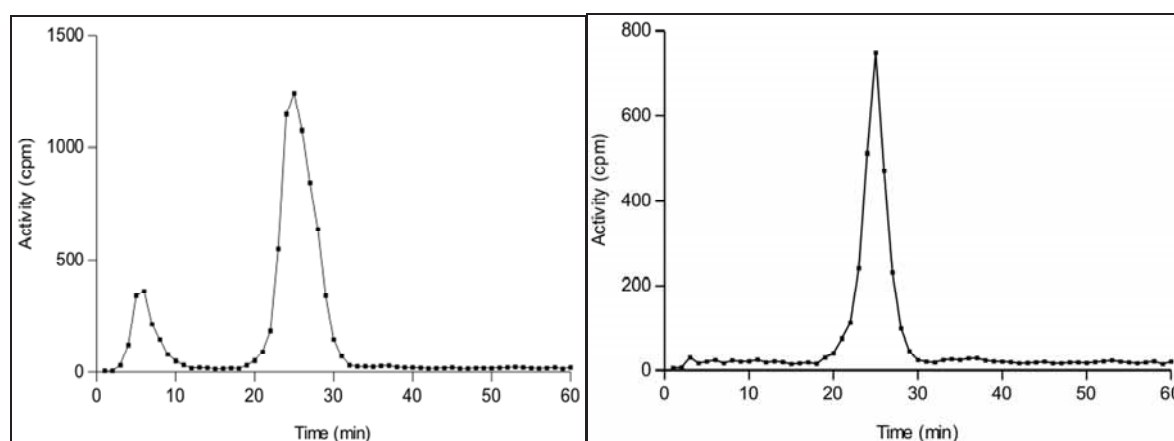
Figure 5.3: $[^{123}I]$-3-I-CO metabolism pattern in NRMI mouse blood (left) and brain (right) at 30 min post injection

It is clear from figure 5.3 that two major radioactivity peaks are present in the NRMI mouse blood sample at 30 min post injection of $[^{123}I]$-3-I-CO: a small part is under the form of a polar metabolite, which was identified as being free radioiodide $^{123}I^-$ by comparing retention times of authentic $[^{123}I]$-NaI (in 0.05M NaOH solution) on the HPLC system used for metabolite determination. The remainder of the radioactivity in the blood was identified as $[^{123}I]$-3-I-CO by comparison of the retention times on the HPLC system. This partial dehalogenation of $[^{123}I]$-3-I-CO should present no problems with later brain imaging, since $[^{123}I^-]$ radioiodide does not penetrate the blood-brain barrier.

Figure 5.3 also shows the presence of only one radioactive compound in the NMRI mouse brain samples at 30 min post injection of $[^{123}I]$-3-I-CO. Comparison of its retention time with the retention time of authentic $[^{123}I]$-3-I-CO revealed that only unmetabolised $[^{123}I]$-3-I-CO was present in the brain samples. All the radioactivity in the different parts of the brain is due to the presence of $[^{123}I]$-3-I-CO, and no radioactive metabolites are present in the brain.

We can conclude that no radiolabelled metabolites could be detected in blood or brain of NRMI mice that could interfere with later imaging and receptor binding studies.

5.1.4. Blocking study with ketanserin in NMRI mice

5.1.4.1. Methods

For the blocking study, male NMRI mice (n = 3 per time point) were treated with ketanserin tartrate (dissolved in ethanol/water for injection 10/90 v/v). A dosage of 1 mg/kg was administered intravenously half an hour before injection of [^{123}I]-3-I-CO. The tracer was dissolved in ethanol/water for injection (10/90 v/v) in a concentration of 200 µCi/ml. [^{123}I]-3-I-CO (20 µCi) was administered 30 minutes after ketanserin injection. At various time points post injection (2 min, 10 min, 30 min, 60 min, 120 min and 240 min) the animals were sacrificed by decapitation. Blood was collected and the animals were rapidly dissected. Blood samples and organs of interest were weighed and counted for radioactivity in an automated gamma counter (Cobra, Packard Canberra). Aliquots of the injected tracer solution (n = 3) were weighed and counted for radioactivity to determine the injected radioactivity dose received by the animals. Results were corrected for decay and tissue radioactivity concentrations were expressed as a percentage of the injected dose per gram of tissue (% ID/g tissue, mean ± standard deviation, n = 3). Data were analysed and the different groups were compared using non-parametric statistical analysis (Mann-Whitney U-test). Results were considered statistically significant when $p < 0.05$.

5.1.4.2. Results and discussion

The results of the biodistribution study with [^{123}I]-3-I-CO in male NMRI mice after ketanserin blocking are shown in table 5.2 for all organs. Radioactivity concentrations were corrected for decay and are expressed as a percentage of the injected dose per gram of tissue (n = 3, mean ± standard deviation).

Tissue	2 min		10 min		30 min		1 h		2 h		4 h	
Blood	1,61	± 0,76	1,35	± 0,25	1,22	± 0,13	0,66	± 0,02	0,88	± 0,56	0,93	± 0,03
Brain	3,74	± 0,14	3,29	± 0,18	2,66	± 0,08	1,41	± 0,02	0,84	± 0,03	0,65	± 0,10
Heart	4,55	± 1,28	2,78	± 0,38	1,32	± 0,17	0,69	± 0,04	0,64	± 0,17	0,72	± 0,00
Lungs	20,60	± 1,20	19,49	± 1,18	6,20	± 3,05	2,16	± 0,29	2,39	± 0,95	2,51	± 0,64
Stomach	3,91	± 2,15	9,65	± 2,15	7,12	± 4,96	7,41	± 2,01	11,01	± 2,97	14,82	± 2,65
Spleen	7,11	± 1,61	7,20	± 0,93	4,95	± 1,40	3,70	± 1,49	1,57	± 0,35	3,16	± 1,92
Liver	9,64	± 1,91	10,76	± 0,70	11,02	± 0,97	5,79	± 1,31	4,82	± 1,98	7,95	± 2,31
Kidney	10,10	± 0,52	11,57	± 1,39	7,96	± 2,56	3,37	± 0,45	5,62	± 4,37	5,40	± 0,27
Small Int.	2,54	± 0,56	1,61	± 0,14	18,72	± 1,50	10,99	± 2,95	11,47	± 2,97	10,00	± 1,84
Large Int.	1,26	± 0,13	2,14	± 0,02	1,62	± 0,58	2,46	± 1,72	16,24	± 2,90	20,98	± 2,06
Blatter	1,38	± 0,28	1,69	± 0,47	7,72	± 1,15	3,16	± 1,06	2,85	± 0,23	6,05	± 1,46
Fat	1,45	± 0,80	5,08	± 2,76	4,46	± 0,58	5,81	± 1,64	3,93	± 1,63	3,01	± 0,58

Animals were injected intravenously with 1mg/kg ketanserin solution. ± 20 μCi of $[^{123}I]$-3-I-CO was injected 30 min later and the animals were sacrificed at designated time points after injection. Radioactivity concentrations are expressed as a percentage of the injected dose per gram of tissue (% ID/g tissue). Results are decay corrected and are expressed as mean ± standard deviation (n = 3 animals per time point).

Table 5.2: Tissue radioactivity concentrations of $[^{123}I]$-3-I-CO after ketanserin blocking in male NMRI mice

In vivo evaluation of $[^{123}I]$-3-I-CO

Radioactivity concentration values for blood and brain after blocking with ketanserin are shown in figure 5.4. For reasons of clarity, the results of the normal biodistribution for blood and brain are also indicated.
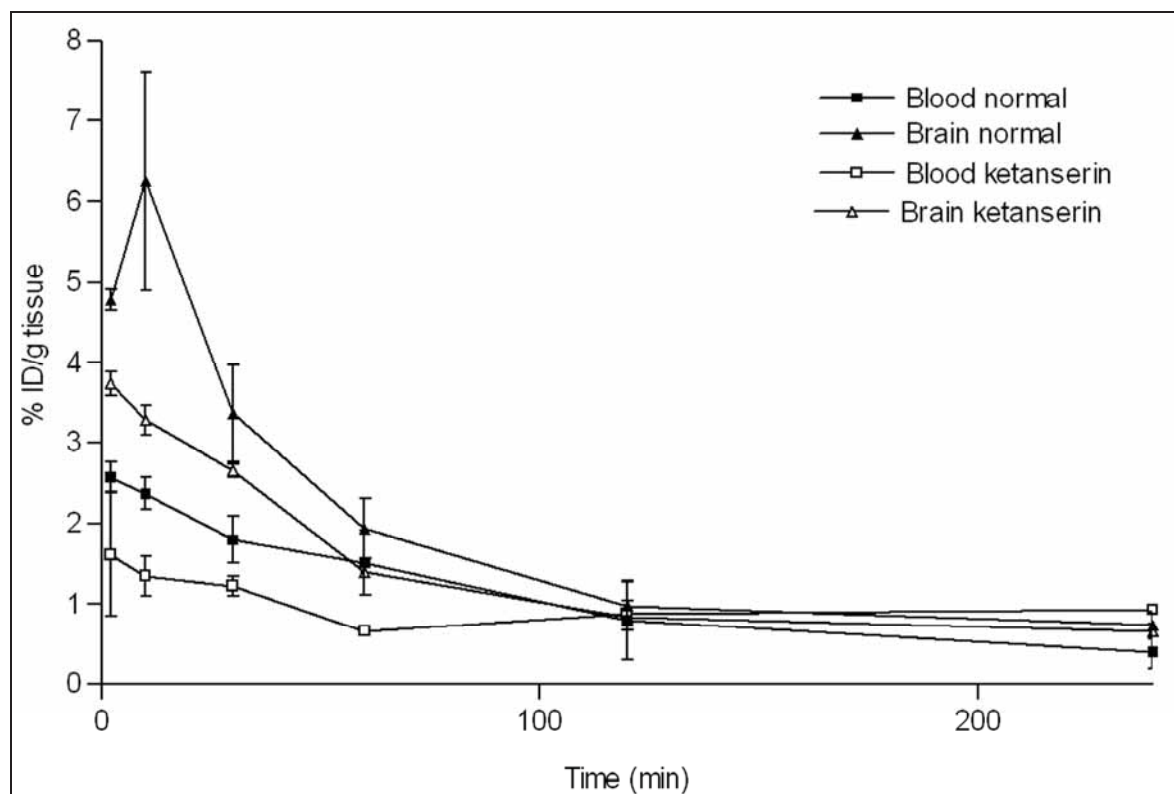
Figure 5.4: Blocking study results of $[^{123}I]$-3-I-CO in male NMRI mice. Mean ± standard deviation values (n = 3 per time point).

A maximum uptake of $[^{123}I]$-3-I-CO in mouse brain of 3.74 ± 0.14 % ID/g was obtained 2 min post injection after displacement with ketanserin. Radioactivity concentration in brain rapidly declined to reach a value of 1.40 ± 0.019 % ID/g at 60 min post tracer injection.

When comparing the results of the ketanserin blocking study with the normal $[^{123}I]$-3-I-CO mouse biodistribution study (figure 5.4), it is clear that part of the radioactivity in the brain was blocked by ketanserin, resulting in reduced $[^{123}I]$-3-I-CO brain concentrations. The remaining activity after ketanserin blocking is probably due to aspecific binding of the tracer to brain tissue.

Blood radioactivity concentration after ketanserin blocking is also lower compared to the normal group. This could be a direct pharmacological effect of ketanserin administration, since ketanserin is known to interact with the α-adrenergic receptor and is also used for its hypotensive effect[2, 3, 4].

The obtained radioactivity concentration data for the other organs were comparable to the data obtained in the normal biodistribution study with [^{123}I]-3-I-CO in NMRI mice.

The uptake of the radioligand in NMRI mouse brain was compared to the brain radioactivity concentration of [^{123}I]-R91150 in mice. For [^{123}I]-R91150, a maximum brain radioactivity concentration of 0.95 ± 0.02 % ID/g tissue was observed at 10 min post injection, at 1 h post injection a radioactivity concentration of 0.73 ± 0.01 % ID/g tissue was observed. Brain radioactivity concentration values for [^{123}I]-3-I-CO were 3.29 ± 0.18 % ID/g tissue at 10 min post injection and 1.41 ± 0.02 % ID/g tissue at 1 h post injection. Compared to [^{123}I]-R91150, our newly developed radioligand [^{123}I]-3-I-CO shows a markedly increased uptake in mouse brain. Starting 120 min after radioligand injection, no significant difference could be observed between the displacement and the control group, indicating that all specifically bound tracer was displaced by ketanserin.

The ketanserin blocking study demonstrated specific binding of [^{123}I]-3-I-CO to the 5-HT$_{2A}$ receptor in male NMRI mouse brain. A regional brain biodistribution study in larger animals (for example Sprague-Dawley rats) could indicate whether the distribution of [^{123}I]-3-I-CO overlaps with the currently known distribution of 5-HT$_{2A}$ receptors in the brain. These results warrant further evaluation of [^{123}I]-3-I-CO as a potential 5-HT$_{2A}$ brain tracer in rats.

5.2. Evaluation of [^{123}I]-3-I-CO in Sprague-Dawley rats

5.2.1. Introduction

The aim of this research is to evaluate the possible use of [^{123}I]-3-I-CO as a tracer for visualizing the 5-HT$_{2A}$ receptor in the brain. The tracer must be able to cross the blood-brain barrier and reach the target in the brain. Secondly, it needs to bind to the 5-HT$_{2A}$ receptor with good affinity, specificity and selectivity.

The potential of [^{123}I]-3-I-CO for crossing the blood-brain barrier has been studied in the biodistribution study in male NMRI mice, from which we can conclude that [^{123}I]-3-I-CO does indeed cross the blood-brain barrier. Specific binding to the 5-HT$_{2A}$ receptor was also demonstrated by the ketanserin blocking experiment.

Pharmacokinetics of the tracer (distribution over time in the different organs) have also been studied in the [^{123}I]-3-I-CO mouse biodistribution experiment. However, mouse brains are too small to dissect further in their different brain parts. A regional brain biodistribution study will be performed in male Sprague-Dawley rats to determine if the brain distribution of [^{123}I]-3-I-CO radioactivity is in accordance with the distribution of 5-HT$_{2A}$ receptors in the brain, obtained from the literature. The expression pattern of the serotonin 5-HT$_{2A}$ receptor depends on the localisation in the brain. High concentrations of 5-HT$_{2A}$ receptors have been found in many forebrain regions, such as the cortical areas, caudate nucleus, nucleus accumbens, olfactory tubercle and hippocampus[5]. Practically no 5-HT$_{2A}$ receptors have been found in the cerebellum[6].

To demonstrate specific binding of [^{123}I]-3-I-CO to the 5-HT$_{2A}$ receptor, a displacement experiment will be performed with a ligand with known affinity for the 5-HT$_{2A}$ receptor. If [^{123}I]-3-I-CO can be displaced from the receptor by a selective 5-HT$_{2A}$ antagonist, we can conclude that [^{123}I]-3-I-CO does indeed bind to the 5-HT$_{2A}$ receptor *in vivo*. In all displacement studies, ketanserin will be used as the 5-HT$_{2A}$ antagonist.

Because it is possible that rats show a different tracer metabolism pattern than mice, a metabolism study in Sprague-Dawley rat blood and brain will be performed to exclude the presence of radiolabelled metabolites of [^{123}I]-3-I-CO in the brain.

5.2.2. Regional brain biodistribution of [^{123}I]-3-I-CO in male Sprague-Dawley rats

5.2.2.1. Methods

Male Sprague-Dawley rats (n = 3) were anesthetized with isoflurane and injected in the penile vein with [^{123}I]-3-I-CO (100 - 150 µCi dissolved in ethanol/water 10/90 v/v). At different time points after injection of [^{123}I]-3-I-CO (20 min, 40 min, 60 min, 2 hours and 4 hours) the animals were sacrificed by decapitation under isoflurane anaesthesia. Blood was collected and the brain was rapidly removed and dissected into different regions: the cortex (which was further dissected into the frontal cortex, parietal cortex, occipital cortex and temporal cortex), cerebellum and a subcortical region. The brain and blood samples were weighed and counted for radioactivity in an automated gamma counter (Cobra, Packard Canberra). Aliquots of the injected tracer solution (n = 3) were weighed and counted for radioactivity to determine the injected radioactivity dose received by the animals. Results were corrected for decay and tissue radioactivity concentrations were expressed as a percentage of the injected dose per gram of tissue (% ID/g tissue, mean ± standard deviation values, n = 3).

5.2.2.2. Results and discussion

The results of the regional brain biodistribution study with [^{123}I]-3-I-CO in male Sprague-Dawley rats are shown in figure 5.5. Brain radioactivity concentration values are shown in table 5.3. Initial brain uptake of [^{123}I]-3-I-CO was the highest in the occipital cortex (0.942 ± 0.034 % ID/g tissue at 20 min post injection) and frontal cortex (0.674 ± 0.074 % ID/g tissue at 20 min post injection).
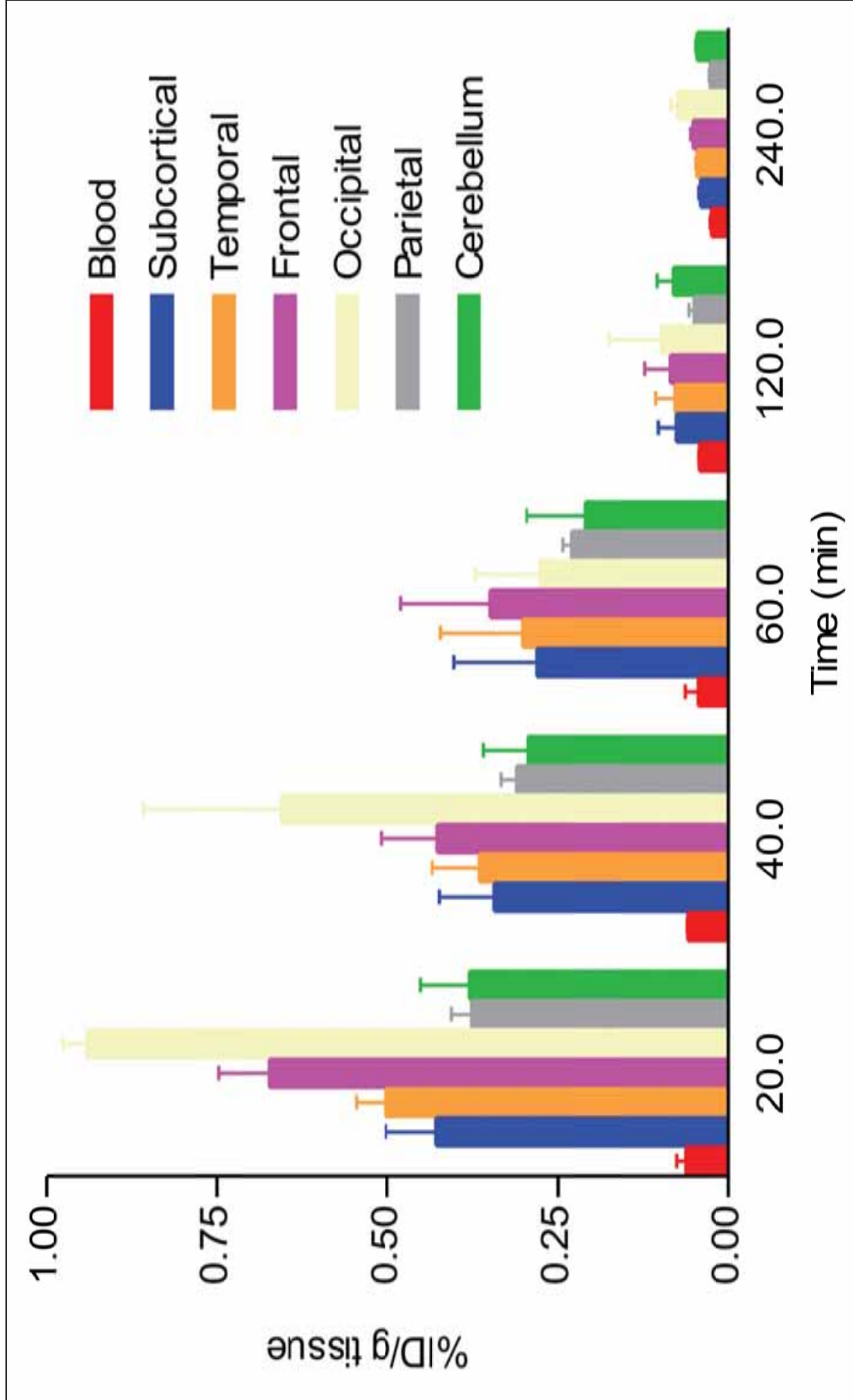
Figure 5.5: Results of the regional brain biodistribution study with [^{123}I]-3-I-CO in male Sprague-Dawley rats. Mean ± standard deviation values (n = 3 per time point) are shown.

In vivo evaluation of [^{123}I]-3-I-CO

179

	Time				
	20 min	40 min	1 hour	2 hours	4 hours
Blood	0,062 ± 0,014	0,059 ± 0,001	0,045 ± 0,018	0,043 ± 0,001	0,026 ± 0,001
Subcortical area	0,429 ± 0,074	0,343 ± 0,08	0,281 ± 0,122	0,076 ± 0,026	0,042 ± 0,002
Temporal Cortex	0,504 ± 0,043	0,366 ± 0,069	0,303 ± 0,119	0,078 ± 0,029	0,046 ± 0,002
Frontal Cortex	0,674 ± 0,074	0,427 ± 0,083	0,349 ± 0,131	0,085 ± 0,038	0,052 ± 0,004
Occipital Cortex	0,942 ± 0,034	0,657 ± 0,203	0,276 ± 0,096	0,098 ± 0,079	0,075 ± 0,009
Parietal Cortex	0,377 ± 0,029	0,312 ± 0,022	0,231 ± 0,013	0,051 ± 0,007	0,027 ± 0,001
Cerebellum	0,38 ± 0,072	0,294 ± 0,065	0,211 ± 0,086	0,081 ± 0,024	0,046 ± 0,002

Animals were injected intravenously with 100-150 μCi of [^{123}I]-3-I-CO solution. The animals were sacrificed by decapitation under isoflurane anesthaesia at designated time points after injection. Organs and blood were rapidly removed, weighed and counted for radioactivity. Radioactivity concentrations were expressed as a percentage of the injected dose per gram of tissue (% ID/g). Values represent mean ± standard deviation (n = 3 per time point).

Table 5.3: Brain tissue radioactivity concentrations at different time points after injection of [^{123}I]-3-I-CO in male Sprague-Dawley rats

Uptake of [123I]-3-I-CO activity in the blood was consistently low (maximum value was 0.062 ± 0.014 % ID/g tissue at 20 min post injection). At one hour after tracer injection, brain uptake of [123I]-3-I-CO was the highest in the frontal cortex (0.349 ± 0.131 % ID/g tissue at 1 hour post injection).

Radioactivity concentration values for the frontal cortex lay above the radioactivity concentrations in cerebellum until 2 hours after tracer injection. Starting from 2 hours after injection, radioactivity concentrations in all cortical regions and cerebellum are more or less the same (figure 5.5). Radioactivity concentrations for the other parts of the cortical tissue were also high at the earliest time points, and slowly decreased in function of time. Highest relative uptake in cortical tissue was observed in the occipital cortex (except for the 1 h time point, where highest relative tracer uptake was observed in the frontal cortex). Lowest relative brain uptake was observed in the cerebellum throughout the study.

The binding index was calculated as (% ID/g)$_{cortex}$/(% ID/g)$_{cerebellum}$, and is shown in table 5.4.

	Time (min)				
	20	**40**	**60**	**120**	**240**
Temp/CER	1,32	1,25	1,43	0,97	1,01
Frontal/CER	1,77	1,45	1,66	1,05	1,13
Occipital/CER	2,48	2,23	1,31	1,21	1,63
Parietal/CER	0,99	1,06	1,1	0,63	0,59

Table 5.4: Binding index values for the [123I]-3-I-CO brain biodistribution study in male Sprague-Dawley rats.

The highest cortex-to-cerebellum ratio was achieved in the occipital cortex: a maximum ratio of 2.48 was obtained at 20 min post injection. Starting at 1 h after radioligand injection, the ratio occipital cortex-to-cerebellum is stabilised, varying between 1.3 and 1.2. For the frontal cortex, a maximal frontal cortex-to-cerebellum ratio of 1.77 was reached at 20 min post injection, decreasing to 1.66 at 1 h after radioligand injection. The ratio stabilised around 1.1 at the later time points. This indicates that specific binding was minimal at 120 and 240 min after radioligand injection.

Cortical tissue-to-cerebellum ratios for temporal and parietal cortex were significantly lower than the ratios observed in frontal and occipital cortical tissues: at the later time points, ratios were even lower than 1, indicating that the concentration of radioligand was higher in cerebellum compared to these cortical regions.

When comparing these results with the data obtained with $[^{123}I]$-R91150, it is obvious that the cortex-to-cerebellum ratios were much lower in the $[^{123}I]$-3-I-CO study, although the absolute radioactivity concentration values in brain were higher. Also, blood radioactivity concentration values approached the radioactivity levels of the cerebellum in the $[^{123}I]$-R91150 study; in the $[^{123}I]$-3-I-CO study, cerebellar radioactivity concentration levels were much higher than the blood levels. This could possibly indicate an increased aspecific binding of $[^{123}I]$-3-I-CO to brain tissue, which would also explain the lower cortex-to-cerebellum ratios obtained with $[^{123}I]$-3-I-CO. Also, cortical radioactivity concentration data for the $[^{123}I]$-3-I-CO study showed a more rapid washout of radioligand out of the brain compared to the $[^{123}I]$-R91150 data in rats.

When comparing our results with the results obtained by other authors with $[^{18}F]$-altanserin [7], $[^{123}I]$-3-I-CO showed a higher absolute radioactivity concentration in the brain (0.5 % ID/g tissue for $[^{18}F]$-altanserin), but a much lower cortex-to-cerebellum ratio was observed for $[^{123}I]$-3-I-CO (cortex-to-cerebellum ratios of 11 were obtained in the $[^{18}F]$-altanserin study). Also, $[^{18}F]$-altanserin radioactivity concentration values in cerebellum averaged around 0.1 % ID/g tissue, comparable with the results obtained with $[^{123}I]$-R91150. The increased radioactivity concentration values in cerebellum for the $[^{123}I]$-3-I-CO study could indicate that the radioligand shows considerable aspecific binding to brain tissue.

It can be concluded from these results that $[^{123}I]$-3-I-CO readily enters the brain, with a maximum uptake in frontal cortex of 0.674 ± 0.074 % ID/g tissue at 20 min post injection. Highest absolute uptake of the radioligand was seen in the occipital cortex (0.942 ± 0.034 % ID/g tissue at 20 minutes after injection).

Specificity of $[^{123}I]$-3-I-CO binding to the 5-HT$_{2A}$ receptor in the brain of male Sprague-Dawley rats remains to be demonstrated with a displacement study, using a well known specific 5-HT$_{2A}$ antagonist. A metabolite study will also be performed to exclude the unwanted effect of possible radiolabelled metabolites of $[^{123}I]$-3-I-CO.

5.2.3. Metabolite determination in male Sprague-Dawley rats

5.2.3.1. Methods

Male Sprague-Dawley rats (n = 3) were injected in the penile vein with [^{123}I]-3-I-CO (200 μCi dissolved in ethanol/water 10/90 v/v). At 30 min post injection, the animals were sacrificed by decapitation under isoflurane anaesthesia. Blood was collected in heparinised tubes and the animals were rapidly dissected. Blood samples were centrifuged for 3 min at 3000g and the tracer extraction yield was calculated. The plasma (200 μl) was mixed with acetonitrile (800 μl) and the mixture was vortexed for 30 s, followed by centrifugation for 3 min at 3000g. The supernatant (500 μl) was analysed on HPLC after filtration through a 0.22 μm filter.

The brain was cut into pieces and transferred to a tube and acetonitrile (2 ml) was added. The mixture was cooled on ice, homogenized for 30 sec and finally centrifuged at 3000g for 3 min. The supernatant (500 μl) was analysed on HPLC, using an Alltech Econosil C_{18} column (250 mm x 10 mm; 10 μm particle size) at a flow rate of 5 ml/min (60/40 ethanol/0.02 M phosphate buffer pH 7.4). The HPLC eluate was collected with an automated fraction collector in fractions of 5 ml (= 1 min). The fractions were then counted for radioactivity with an automated gamma counter (Cobra, Packard Canberra).

The extraction efficiency (extraction yield) was expressed as percentage of total activity found in the supernatant compared to the total amount of radioactivity present in the tissue or blood sample. Retention times of the possible radiometabolites were compared with the retention times of authentic [^{123}I]-3-I-CO and free radioiodide.

5.2.3.2. Results

Values for extraction yields were always > 90 %. The metabolism pattern of [^{123}I]-3-I-CO in Sprague-Dawley rats was roughly the same as the metabolism pattern obtained in NMRI mice at 30 min after radioligand injection. In blood, only two radiolabelled components were present: one component (± 90 %) had the same retention time as authentic [^{123}I]-3-I-CO, and the other component (5-10 %) was identified as free radioiodide (figure 5.6 - left). In the brain, only unchanged [^{123}I]-3-I-CO was present (figure 5.6 – right).

It is safe to conclude that no lipophilic radiolabelled metabolites were found that could possibly interfere with later brain imaging with [^{123}I]-3-I-CO. A small amount of radioiodide in the blood should also have no effect in imaging studies.
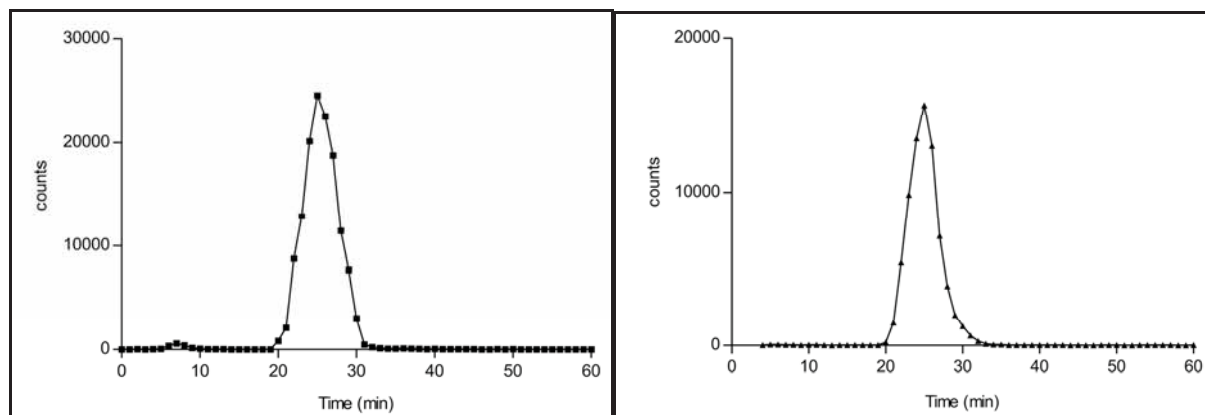

Figure 5.6: Metabolisation pattern of [^{123}I]-3-I-CO in Sprague-Dawley rats 30 min after injection of [^{123}I]-3-I-CO. Patterns in blood (left) and brain (right) are shown.

5.2.4. Displacement study with [^{123}I]-3-I-CO in male Sprague-Dawley rats

5.2.4.1. Methods

Ketanserin tartrate was used to displace [^{123}I]-3-I-CO in rats. The ketanserin tartrate salt was obtained from Tocris (Tocris Bioscience, Bristol, UK) and dissolved in a mixture of ethanol/water (5/95 v/v) in a concentration of 1 mg/ml. The dosage used to displace [^{123}I]-3-I-CO in rats was 1 mg ketanserin tartrate per kg of bodyweight. This resulted in an average displacement dose of 0.25 mg per animal.

Male Sprague-Dawley rats (n = 3) were anesthetized with isoflurane and injected in the penile vein with [^{123}I]-3-I-CO (100 - 150 μCi). Thirty minutes after administration of the tracer, the animals were injected in the penile vein with ketanserin solution under isoflurane anaesthesia. The animals were sacrificed by decapitation under isoflurane anaesthesia one hour after tracer injection (30 min after ketanserin injection). Blood was collected and the brain was rapidly removed and dissected into different regions: the cortex (which was further dissected into the frontal cortex, parietal cortex, occipital cortex and temporal cortex), cerebellum and a subcortical region. The different brain and blood samples were weighed and counted for radioactivity with an automated gamma counter (Cobra, Packard Canberra). Aliquots of the injected tracer solution (n = 3) were weighed and counted for radioactivity to determine the injected radioactivity dose received by the animals. Results were corrected for decay and tissue radioactivity concentrations were expressed as a percentage of the injected dose per gram of tissue (% ID/g tissue, mean ± standard deviation values). The results were compared with the normal brain biodistribution results. Differences between groups were calculated using non-parametrical statistical analysis (Mann-Whitney). Results were considered statistically significant when $p < 0.05$.

5.2.4.2. Results and discussion

The effect of displacement with ketanserin on the biodistribution of $[^{123}I]$-3-I-CO in male Sprague-Dawley rat brain can be clearly seen in figure 5.7. For reasons of clarity, the normal biodistribution data of $[^{123}I]$-3-I-CO at the 1h time point are also shown in figure 5.7.
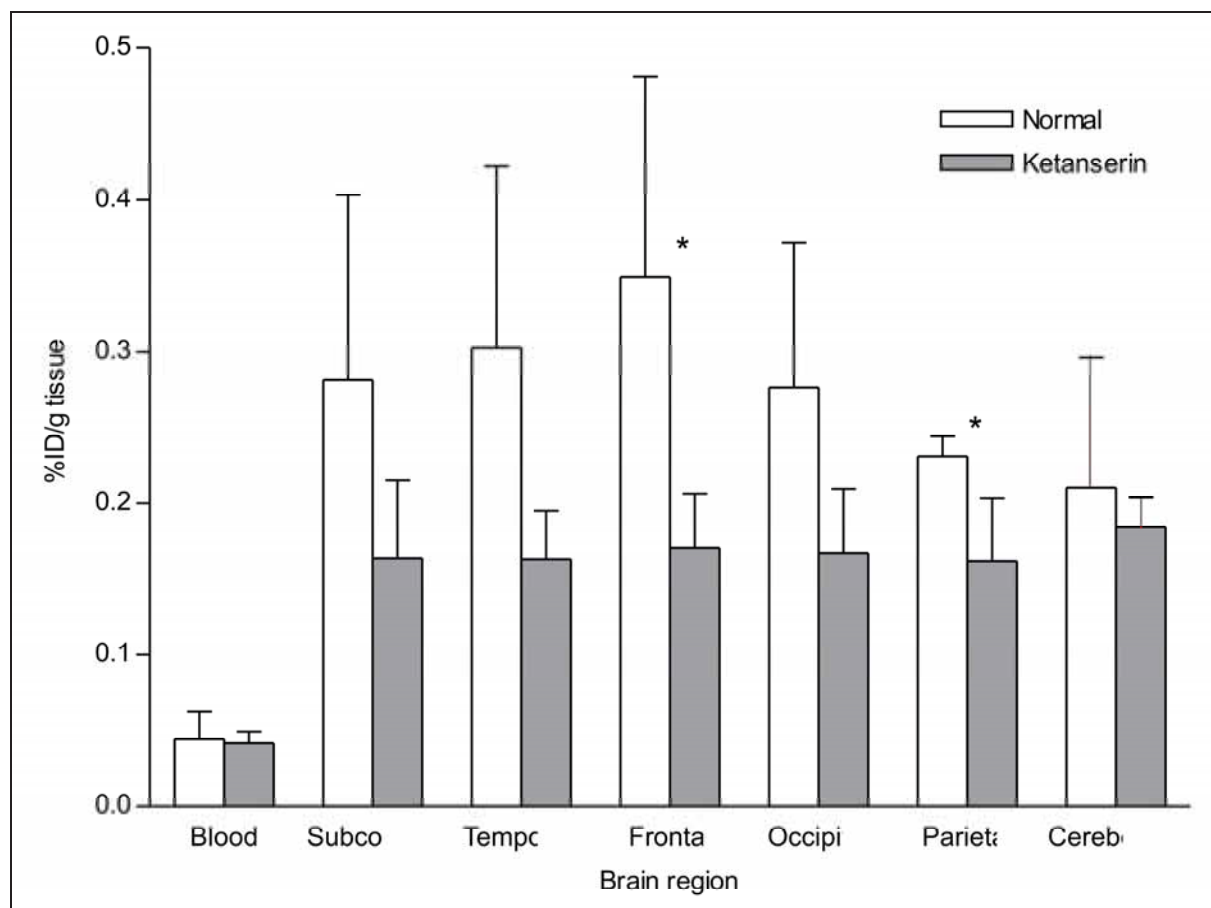
Figure 5.7: Results of the ketanserin blocking study with $[^{123}I]$-3-I-CO in male Sprague-Dawley rats. Results were expressed as % ID/g tissue, mean ± standard deviation values are shown (n = 3 animals per group, * indicates a p-value < 0.05).

It can be seen in figure 5.7 that $[^{123}I]$-3-I-CO radioactivity was displaced by ketanserin in the cortical areas of the brain. No significant difference in $[^{123}I]$-3-I-CO radioactivity concentration could be observed in blood or cerebellum. In the frontal cortex, radioactivity concentration decreased from 0.349 ± 0.131 % ID/g tissue at 1h post injection to 0.17 ± 0.036 % ID/g tissue after displacement with ketanserin.

[^{123}I]-3-I-CO activity also decreased in other parts of the cortex (temporal, occipital and parietal cortex), although the relative decrease in radioactivity concentration was the highest in frontal cortex (50% decrease in radioactivity concentration after displacement with ketanserin).

Radioactivity concentration in blood and cerebellum did not change significantly after ketanserin displacement (0.211 ± 0.086 % ID/g tissue at 1h post injection in cerebellum and 0.184 ± 0.02 % ID/g tissue after ketanserin displacement. Values for blood were 0.045 ± 0.018 % ID/g tissue and 0.042 ± 0.008 % ID/g tissue respectively). This is in accordance with the use of the cerebellum as a reference region when performing PET or SPECT brain scans with 5-HT$_{2A}$ tracers.

Radioactivity concentration values for the other brain regions are shown in table 5.5.

	Normal	BI	Ketanserin	BI
Blood	0,045 ± 0,018		0,042 ± 0,008	
Subcortical	0,281 ± 0,122		0,163 ± 0,052	
Temporal	0,303 ± 0,119	1,43	0,165 ± 0,032	0,89
Frontal	0,349 ± 0,131	1,65	0,17 ± 0,036	0,92
Occipital	0,276 ± 0,096	1,31	0,167 ± 0,043	0,91
Parietal	0,231 ± 0,013	1,09	0,161 ± 0,042	0,88
Cerebellum	0,211 ± 0,085		0,184 ± 0,02	

Table 5.5: Influence of ketanserin displacement on regional brain biodistribution with [^{123}I]-3-I-CO in Sprague-Dawley rats. Results are expressed as % ID/g tissue (mean ± standard deviation, n = 3). The cortex/cerebellum ratios (BI) are displayed in the table.

As can be seen in table 5.5, highest absolute uptake of [^{123}I]-3-I-CO could be seen in the frontal cortex. After displacement with ketanserin, the highest radioactivity concentration was found in the cerebellum. Radioactivity concentration values were comparable for the different brain regions after displacement with ketanserin. This could indicate that the amount of [^{123}I]-3-I-CO aspecific binding is comparable throughout the brain.

The binding index (BI) was defined as the ratio of cortical region to cerebellum. It was calculated as (% ID/g)$_{cortex}$/(% ID/g)$_{cerebellum}$ for all areas in the cortex. Results are also indicated in table 5.5. The highest ratio was observed in frontal cortex for the normal group.

In contrast with the results obtained in the [^{123}I]-R91150 displacement study, radioactivity levels in the cortex in the [^{123}I]-3-I-CO study did decrease to the levels observed in cerebellum.

Nevertheless, the residual radioactivity levels in cerebellum after ketanserin displacement remained significantly higher in the [^{123}I]-3-I-CO study, and could be caused by aspecific binding of the radioligand to brain tissue.

5.3. Influence of P-glycoprotein modulation on the biodistribution of [^{123}I]-3-I-CO in rodents

5.3.1. Introduction

Considering the importance of cyclosporin A modulation on the biodistribution in rodents of [^{123}I]-R91150, we decided to also investigate the influence of cyclosporin A administration on the biodistribution and brain uptake in rodents of [^{123}I]-3-I-CO, our in-house developed potential SPECT tracer for the serotonin 5-HT$_{2A}$ receptor.

A regional brain biodistribution will be performed in male Sprague-Dawley rats after treatment of the animals with cyclosporin A. Also, a displacement study with ketanserin will investigate possible effects of P-glycoprotein modulation on specific binding of [^{123}I]-3-I-CO to the 5-HT$_{2A}$ receptor.

To exclude possible altered metabolism of [^{123}I]-3-I-CO after administration of cyclosporin A, a metabolite assay will be performed in Sprague-Dawley rats after treatment of the animals with cyclosporin A.

5.3.2. Influence of cyclosporin A administration on brain uptake of [^{123}I]-3-I-CO in Sprague-Dawley rats

5.3.2.1. Methods

Male Sprague-Dawley rats (n = 3 per group) were anesthetized with isoflurane and injected in the penile vein with cyclosporin A (a dosage of 50 mg/kg was used). Thirty minutes after cyclosporin A administration, the rats were anesthetized with isoflurane and injected in the penile vein with [^{123}I]-3-I-CO (100 - 150 µCi in ethanol/water 10/90 v/v). The animals were sacrificed by decapitation under isoflurane anaesthesia at selected time points after tracer injection (2 min, 5 min, 30 min, 60 min, 2 hours and 4 hours). Blood was collected and the brain was rapidly removed and dissected into different regions: the cortex (which was further dissected into the frontal cortex, parietal cortex, occipital cortex and temporal cortex), cerebellum and a subcortical region. The different brain and blood samples were weighed and counted for radioactivity with an automated gamma counter (Cobra, Packard Canberra). Aliquots of the injected tracer solution (n = 3) were weighed and counted for radioactivity to determine the injected radioactivity dose received by the animals. Results were corrected for decay and tissue radioactivity concentrations were expressed as a percentage of the injected dose per gram of tissue (% ID/g tissue, mean ± standard deviation values, n = 3). The results were compared with the normal brain biodistribution results, without pre-treatment of the animals with cyclosporin A using non-parametric statistical analysis (Mann-Whitney). Differences were considered statistically significant when p-values < 0.05 were obtained.

5.3.2.2. Results and discussion

The influence of cyclosporin A pre-treatment (50 mg/kg intravenously, administered one hour before injection of [^{123}I]-3-I-CO) on the regional brain biodistribution results with [^{123}I]-3-I-CO in Sprague-Dawley rats can be seen in table 5.6. Brain radioactivity concentration values are expressed as % ID/g tissue (mean ± standard deviation, n = 3 per time point).

	Time (min)				
	20	**40**	**60**	**120**	**240**
Blood	0,07 ± 0,01	0,041 ± 0,006	0,056 ± 0,014	0,037 ± 0,01	0,034 ± 0,003
Subcortical	0,65 ± 0,12	0,67 ± 0,06	0,35 ± 0,085	0,18 ± 0,12	0,075 ± 0,01
Temporal	0,56 ± 0,25	0,81 ± 0,23	0,32 ± 0,065	0,14 ± 0,09	0,063 ± 0,003
Frontal	0,61 ± 0,17	0,91 ± 0,11	0,58 ± 0,084	0,22 ± 0,08	0,07 ± 0,005
Occipital	0,91 ± 0,26	0,85 ± 0,18	0,58 ± 0,065	0,18 ± 0,07	0,071 ± 0,01
Parietal	0,60 ± 0,15	0,72 ± 0,12	0,357 ± 0,07	0,17 ± 0,07	0,055 ± 0,009
Cerebellum	0,63 ± 0,1	0,65 ± 0,093	0,34 ± 0,09	0,15 ± 0,06	0,072 ± 0,008

Table 5.6: Influence of cyclosporin A (50 mg/kg 1 h before radioligand injection) on the regional brain biodistribution with [^{123}I]-3-I-CO in Sprague-Dawley rats. Results are expressed as % ID/g tissue (mean ± standard deviation, n = 3 animals per time point).

A maximum uptake value of 0.905 ± 0.114 % ID/g tissue was obtained in the frontal cortex at 40 min post injection after treatment with cyclosporin A. At 1 hour after injection, radioactivity concentration in frontal cortex was 0.582 ± 0.084 % ID/g tissue. The occipital cortex followed about the same radioactivity uptake and clearance pattern as the frontal cortex. The radioactivity concentration in the reference region, the cerebellum, was 0.355 ± 0.094 % ID/g tissue at 1 h after injection of [^{123}I]-3-I-CO for the cyclosporin group. The highest concentration of [^{123}I]-3-I-CO in blood (0.070 ± 0.012 % ID/g tissue) was found at 20 min post injection. Activity concentration in blood remained low and was fairly constant over time (0.037 ± 0.010 % ID/g tissue at 2h after injection, 0.034 ± 0.003% ID/g tissue at 4h after injection). Radioactivity concentration values in temporal and parietal cortex were comparable throughout the study, but were significantly lower than the values obtained in frontal and occipital cortex.

The results obtained after the regional brain biodistribution with cyclosporin A treatment were compared with the results obtained from the normal regional brain biodistribution study with $[^{123}I]$-3-I-CO. Radioactivity concentration values for frontal cortex and cerebellum are shown for both groups in figure 5.8.
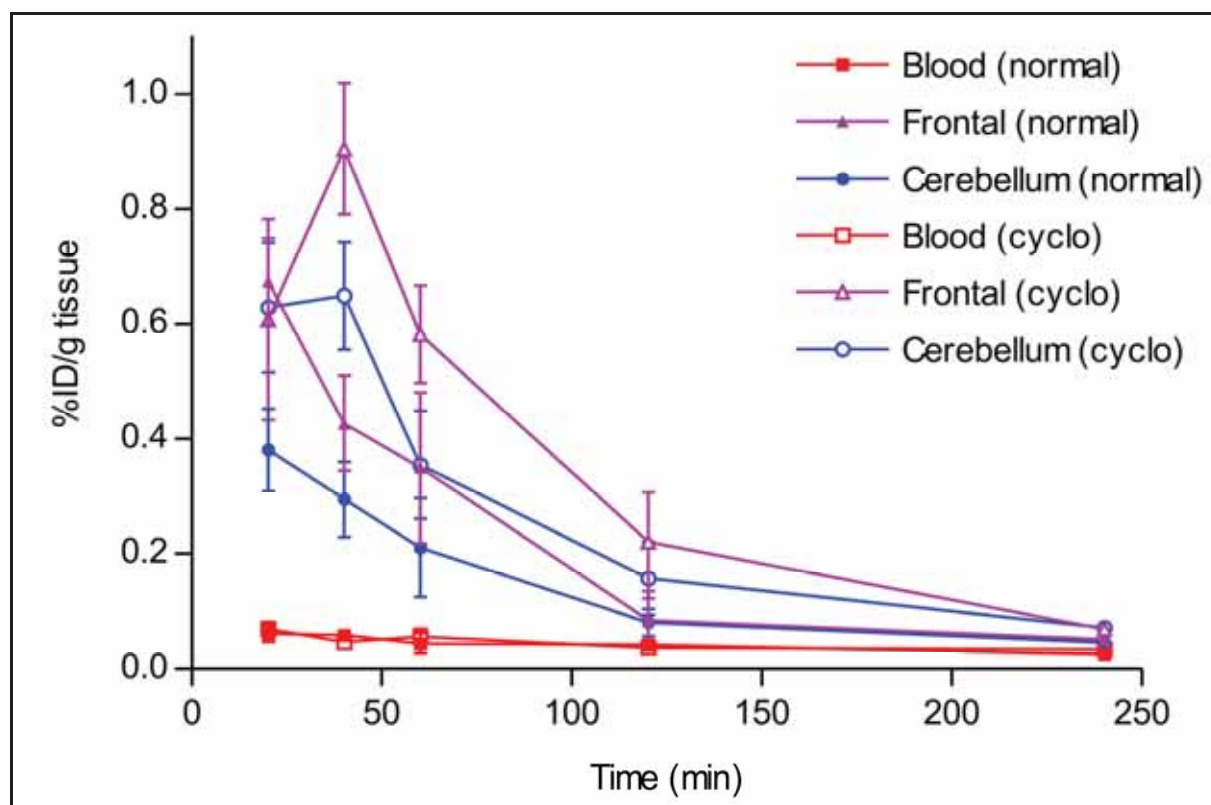
Figure 5.8: $[^{123}I]$-3-I-CO biodistribution results for frontal cortex and cerebellum (with and without cyclosporin A pre-treatment). Results are expressed as % ID/g tissue (mean ± standard deviation, n = 3 animals per time point).

It is evident from figure 5.8 that both the target region (frontal cortex) and the reference region (cerebellum) of Sprague-Dawley rats show an increased uptake of $[^{123}I]$-3-I-CO radioactivity after pre-treatment of the animals with cyclosporin A.

For example, at 1 hour after injection of $[^{123}I]$-3-I-CO, radioactivity concentration in frontal cortex increased from 0.349 ± 0.131 % ID/g tissue for the normal group to 0.582 ± 0.084 % ID/g tissue after treatment of the animals with cyclosporin A (or an increase in radioactivity concentration of 67 % after cyclosporin A administration).

A similar pattern was observed in the cerebellum: radioactivity concentration increased from 0.211 ± 0.086 % ID/g tissue at 1 hour after injection for the normal group to 0.355 ± 0.094 % ID/g tissue at 1 hour after injection for the cyclosporin A group (figure 5.8).

The relative increase in $[^{123}I]$-3-I-CO radioactivity concentration was the same for the cerebellum as for the frontal cortex (or an increase in radioactivity concentration of 67 % after cyclosporin A administration). All other brain regions followed more or less the same pattern: radioactivity concentration values increased markedly after pre-treatment of the rats with cyclosporin A.

On the contrary, no significant difference in radioactivity concentration in blood could be found between the two treatment groups. For example, the radioactivity concentration in blood was 0.045 ± 0.018 % ID/g tissue at 1 hour after injection of $[^{123}I]$-3-I-CO for the normal group. In the cyclosporin A treated group, radioactivity concentration in blood at 1 hour after injection was 0.056 ± 0.014 % ID/g tissue. The other time points showed the same behaviour: no significant difference could be observed between the two groups, at all time points.

This could indicate that the increase in brain $[^{123}I]$-3-I-CO radioactivity concentration after treatment with cyclosporin A is not the result of an increased influx of tracer to the brain, but rather the consequence of a decreased tracer efflux out of the brain as a result of the P-glycoprotein blocking effect of cyclosporin A.

It should be noted however that the increase in brain radioactivity concentration after treatment of the animals with cyclosporin A was not as marked as in the cyclosporin A study with $[^{123}I]$-R91150: in the $[^{123}I]$-3-I-CO study, brain radioactivity concentrations doubled after cyclosporin A treatment, whereas in the $[^{123}I]$-R91150 study, brain tracer concentrations increased up to seven-fold after animal treatment with cyclosporin A. This could indicate that $[^{123}I]$-R91150 is a stronger substrate for P-glycoprotein efflux than $[^{123}I]$-3-I-CO.

The binding index was calculated as the ratio of cortical tissue-to-cerebellum (% ID/g tissue)$_{cortex}$/(% ID/g tissue)$_{cerebellum}$. The results are shown in table 5.7.

	Time (min)				
	20	40	60	120	240
Temp/CER	0,89	1,25	0,94	0,94	0,86
Frontal/CER	0,97	1,4	1,71	1,47	0,97
Occipital/CER	1,45	1,31	1,71	1,2	0,99
Parietal/CER	0,95	1,11	1,05	1,14	0,77

Table 5.7: $[^{123}I]$-3-I-CO binding index calculations in Sprague-Dawley rats after treatment of the animals with cyclosporin A (50 mg/kg).

Binding index data from the cyclosporin A regional brain biodistribution with [123I]-3-I-CO (table 5.7) were compared with the data obtained from the normal regional brain biodistribution study (table 5.4) with [123I]-3-I-CO.

In frontal cortex, no significant difference in binding index could be observed between the control group and the cyclosporin-treated group at 40 min, 1 hour and 4 hours after injection of [123I]-3-I-CO.

Frontal cortex binding indices were significantly different for the control group and the cyclosporin-treated group at 20 min post tracer injection ($BI_{control}$ = 1.77; BI_{cyclo} = 0.97) and at 2 hours after injection of the tracer ($BI_{control}$ = 1.05; BI_{cyclo} = 1.47). In the other cortical tissues, binding index values for the cyclosporin A group versus the control group were comparable.

When comparing the binding index data with the results obtained from the regional brain biodistribution study with [123I]-R91150 in Sprague-Dawley rats with and without cyclosporin A pre-treatment, it is obvious that the values obtained for [123I]-3-I-CO are well below the values obtained with [123I]-R91150. Binding index values for [123I]-3-I-CO averaged around 1.2 both with and without cyclosporin A pre-treatment, whereas the values for [123I]-R91150 were around 7 for the control and around 4 for the cyclosporin A pre-treated group. These results could indicate that [123I]-3-I-CO demonstrates an increased aspecific binding to brain tissues (cerebellum) compared to [123I]-R91150.

Contrary to the results obtained in the [123I]-R91150 cyclosporin A study, binding index values did not decrease after animal pre-treatment with cyclosporin A in the biodistribution study with [123I]-3-I-CO, but remained at the same level. Also, no influence of cyclosporin A was observed on the pharmacokinetics of [123I]-3-I-CO in blood, since blood radioactivity levels were comparable before and after cyclosporin A pre-treatment.

We can conclude from this study that modulation of P-glycoprotein by pre-treatment of the animals with cyclosporin A resulted in an increased concentration of [123I]-3-I-CO in the brain. However, the increase in brain radioactivity concentration was not as large as the increase observed in research with other brain tracers, for example [123I]-R91150 (chapter 3) and [11C]-(R)-(-)-RWAY [8].

5.3.3. [^{123}I]-3-I-CO displacement study after cyclosporin A treatment in Sprague-Dawley rats

5.3.3.1. Methods

Ketanserin tartrate was used to displace [^{123}I]-3-I-CO in rats. The ketanserin tartrate salt was obtained from Tocris (Tocris Bioscience, Bristol, UK) and dissolved in a mixture of ethanol/water (5/95 v/v) in a concentration of 1 mg/ml. The dosage used to displace [^{123}I]-3-I-CO in rats was 1mg/kg bodyweight.

Male Sprague-Dawley rats were pre-treated with cyclosporin A (50 mg/kg) via the penile vein 30 min before injection of the radioligand. The animals (n = 3) were anesthetized with isoflurane and injected in the penile vein with [^{123}I]-3-I-CO (100 - 150 µCi dissolved in ethanol/water 10/90 v/v). Thirty minutes after administration of the tracer, the animals were injected in the penile vein with ketanserin solution under isoflurane anaesthesia. The animals were sacrificed by decapitation under isoflurane anaesthesia one hour after tracer injection (30 min after ketanserin injection). Blood was collected and the brain was rapidly removed and dissected into different regions: the cortex (which was further dissected into the frontal cortex, parietal cortex, occipital cortex and temporal cortex), cerebellum and a subcortical region. The different brain and blood samples were weighed and counted for radioactivity with an automated gamma counter (Cobra, Packard Canberra). Aliquots of the injected tracer solution (n = 3) were weighed and counted for radioactivity to determine the injected radioactivity dose received by the animals. Results were corrected for decay and tissue radioactivity concentrations were expressed as a percentage of the injected dose per gram of tissue (% ID/g tissue, mean ± standard deviation values, n = 3). The results were compared with the normal brain biodistribution results. Results were compared with a non-parametric method (Mann-Whitney). P-values < 0.05 were considered as significant.

5.3.3.2. Results and discussion

The results of the ketanserin displacement study with [123I]-3-I-CO in male Sprague-Dawley rats after treatment of the animals with cyclosporin A can be seen in figure 5.9. Radioactivity concentration values are indicated in table 5.8 as % ID/g tissue (mean ± standard deviation, n = 3 animals per treatment group). For reasons of clarity, the results for the normal regional brain biodistribution study are also shown in figure 5.9.
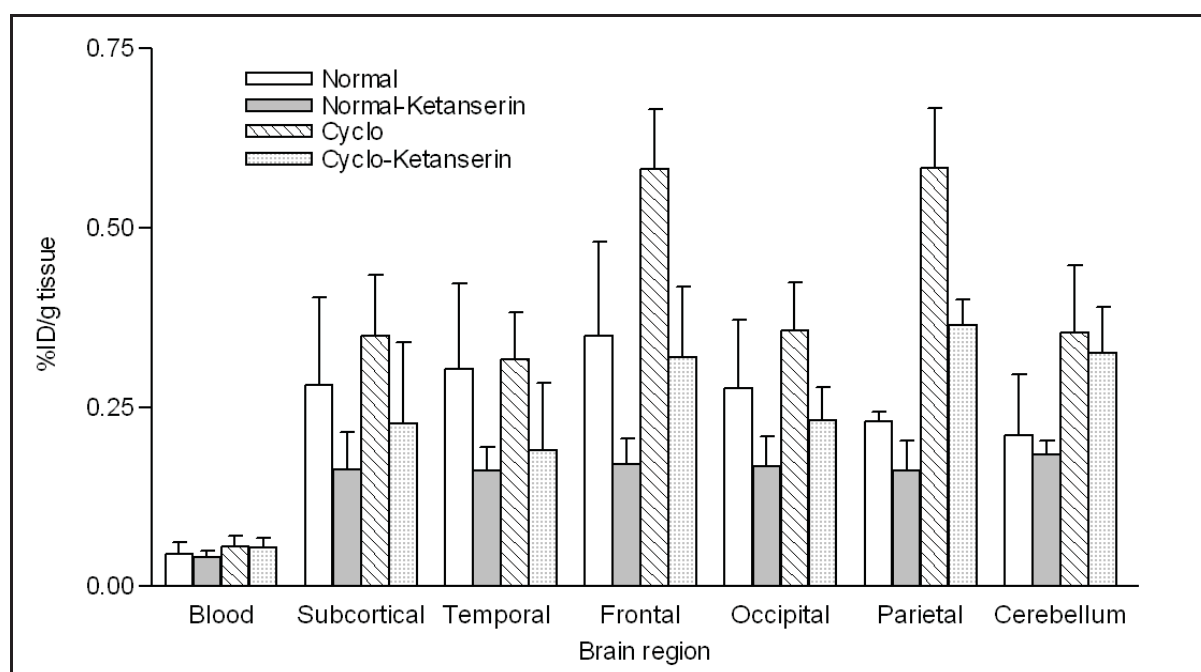
Figure 5.9: Brain biodistribution displacement results with [123I]-3-I-CO after treatment with cyclosporin A. Values are expressed as % ID/g (mean ± standard deviation, n = 3).

[123I]-3-I-CO radioactivity concentration was significantly reduced in the brain after displacement with ketanserin. An average decrease in radioactivity concentration of 55 to 60 % was observed throughout the cortex after displacement of [123I]-3-I-CO with ketanserin.

The relative reduction in [123I]-3-I-CO radioactivity concentration obtained after displacement in the cyclosporin pre-treated animals was about the same as the reduction obtained after ketanserin displacement in the normal groups (= animals not treated with cyclosporin).

Nevertheless, absolute radioactivity concentration after displacement was higher in the cyclosporin group than in the normal control group.

This might indicate an increase in aspecific binding in the brain, since the increased radioactivity concentration after cyclosporin A administration could not be fully displaced by ketanserin. No significant differences were observed between the cyclosporin-only and the displacement group in the blood and in cerebellum.

	Cyclosporin	ratio	Cyclo-ketanserin	ratio
Blood	0,05 ± 0,01		0,05 ± 0,01	
Subcortical	0,35 ± 0,08		0,22 ± 0,11	
Temporal	0,31 ± 0,06	0,89	0,19 ± 0,09	0,6
Frontal	0,58 ± 0,08	1,66	0,32 ± 0,09	1
Occipital	0,36 ± 0,07	1,03	0,23 ± 0,04	0,72
Parietal	0,58 ± 0,08	1,66	0,36 ± 0,03	1,1
Cerebellum	0,35 ± 0,09		0,32 ± 0,06	

Table 5.8: Ketanserin displacement results with [^{123}I]-3-I-CO after animal treatment with cyclosporin A. Results are expressed as % ID/g tissue (mean ± standard deviation, n = 3).

Cortex-to-cerebellum ratios after treatment of the animals with cyclosporin were comparable to the ratios obtained in the normal group. After displacement of the radioligand with ketanserin, binding index ratios decreased with about 30 %. This value is comparable with the decrease in binding index obtained after displacement of [^{123}I]-R91150 with ketanserin in rats.

We can conclude from these results that modulation of P-glycoprotein by animal pre-treatment with cyclosporin A results in an increased radioactivity concentration of [^{123}I]-3-I-CO throughout the brain, resulting in an increase of both specific and aspecific radioligand binding. Also, since no change was observed in binding index after cyclosporin A pre-treatment, it is safe to conclude that the increased radioligand radioactivity concentration did not result in saturation of the 5-HT$_{2A}$ receptors.

5.3.4. Influence of cyclosporin A on pinhole μSPECT imaging with [^{123}I]-3-I-CO in Sprague-Dawley rats

5.3.4.1. Materials and methods

Male Sprague-Dawley rats (250 – 266 g) were anesthetized with isoflurane and injected with cyclosporin A (50 mg/kg). 30 minutes later [^{123}I]-3-I-CO (800 μCi) was injected into the tail vein. A U-SPECT-II scan was performed 10 minutes after radioligand injection using the rat collimator (75 pinholes of 1.0 mm) for a continuous 90 minutes (18 frames of 5 minutes) with list mode output enabled.

As a reference, animals were also scanned in a similar protocol with [^{123}I]-3-I-CO but without administration of cyclosporin A. For all datasets a 20 % photopeak was selected around 159 keV while background correction was performed using two additional 10 % windows around 133 and 188 keV. The selected time frames ranged from 20 to 50 min post-injection. Each time the data were reconstructed on 0.75 mm voxels by 3 iterations of 16 OSEM subsets. The images were 3D postfiltered by a 15 pixel Gaussian kernel with a width of 1.5 mm. Two ROI's were drawn around the frontal cortex and the cerebellum using Amide (OpenSource) with 3D Freehand on the coronal slices. The mean value and standard deviation over all voxels in the respective ROI's were calculated for post-analysis.

All experiments were conducted following the principles of laboratory animal care and the Belgian law on the protection of animals. Our research protocol was approved by the Ghent University Hospital ethical committee (ECP 05-14).

5.3.4.2. Results and discussion

A pinhole μSPECT imaging study was performed with [123I]-3-I-CO in Sprague-Dawley rats. Both the normal group and the animals pre-treated with cyclosporin A were scanned.

The results of the scans are presented in figure 5.10. Increased levels of [123I]-3-I-CO radioactivity were present in the cortical tissues, but compared to the imaging results with [123I]-R91150, an increased aspecific binding of radioligand throughout the cerebellum and the rest of the brain was observed.
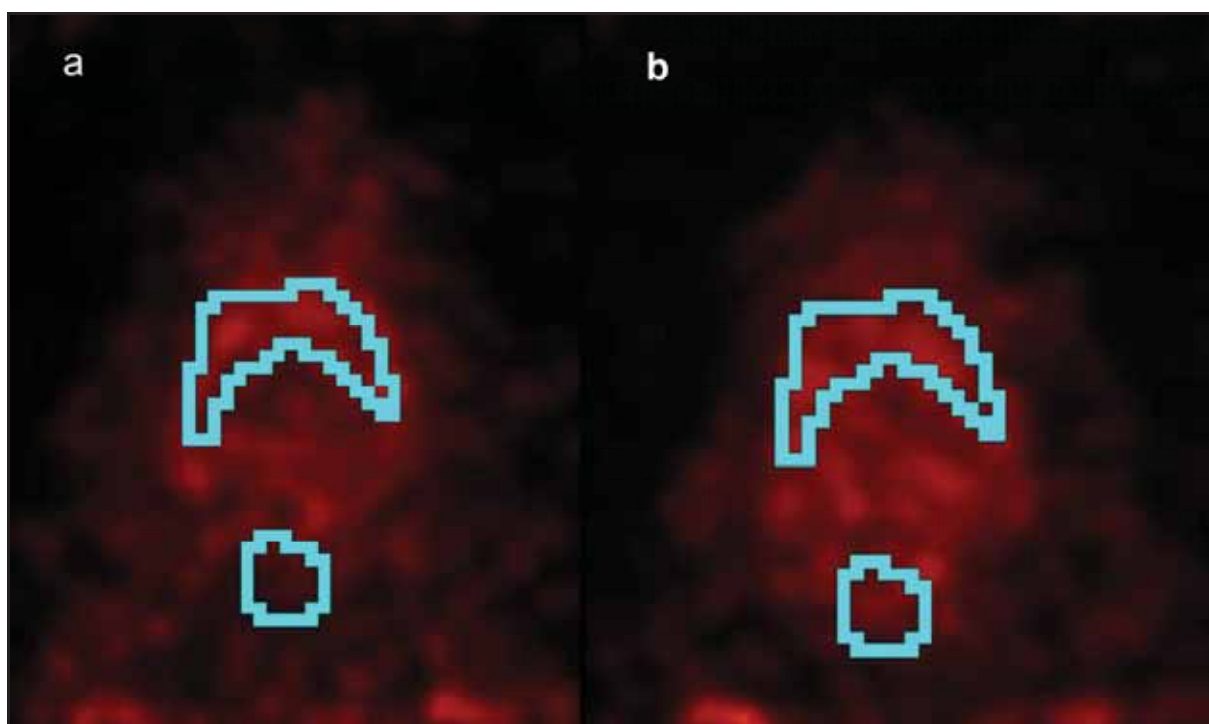
Figure 5.10: Pinhole μSPECT imaging with [123I]-3-I-CO (800 μCi) in Sprague-Dawley rats. Panel a: control group; panel b: pre-treatment with cyclosporin A (50 mg/kg). Regions-of-interest were drawn around cortical tissues and cerebellum.

Regions-of-interest (ROI) were drawn around the frontal region of the cortical tissue and the cerebellum. Radioligand uptake in cerebellum was used as a reference for non-specific binding.

For semi-quantification, the cortex-to-cerebellum ratio (mean counts in cortex)/(mean counts in cerebellum/ was determined using the ROI's.

In the control group (figure 5.10 part a), a cortex-to-cerebellum ratio of 1.57 was found. As comparison, in the regional brain biodistribution study with [^{123}I]-3-I-CO in Sprague-Dawley rats, a frontal cortex-to-cerebellum ratio between 1.45 and 1.66 was observed 40 and 60 minutes after injection of the radioligand.

In the cyclosporin A treated group (figure 5.10 part b), a cortex-to-cerebellum ratio of 1.2 was obtained. The regional brain biodistribution study with [^{123}I]-3-I-CO after cyclosporin A treatment in rodents revealed a cortex-to-cerebellum ratio of 1.4.

When comparing cortex-to-cerebellum binding index values obtained from the biodistribution study with the values obtained from the μSPECT scans, a good correlation was observed. Administration of cyclosporin A did not result in drastically changed [^{123}I]-3-I-CO cortex-to-cerebellum ratios. Also, P-glycoprotein blocking with cyclosporin A did not have the same effect on [^{123}I]-3-I-CO imaging, compared to [^{123}I]-R91150. This is also in accordance with the biodistribution studies with [^{123}I]-3-I-CO in rodents, where only a small increase in radioligand brain uptake was found after cyclosporin A treatment.

5.3.5. Metabolite analysis in Sprague-Dawley rats of [^{123}I]-3-I-CO after cyclosporin A treatment

5.3.5.1. Methods

Cyclosporin A (50 mg/kg) was injected into the penile vein of Sprague-Dawley rats 30 minutes before injection of the radioligand. The animals (n = 3) were injected in the penile vein with [^{123}I]-3-I-CO (100 – 150 µCi dissolved in ethanol/water 10/90 v/v) 30 minutes after cyclosporin A administration. At 30 min post radioligand injection, the animals were sacrificed by decapitation under isoflurane anaesthesia. Blood was collected in heparinised tubes and the animals were rapidly dissected. Blood samples were centrifuged for 3 min at 3000g and the pellet was discarded after calculation of tracer extraction yield. The plasma (200 µl) was mixed with acetonitrile (800 µl) and the mixture was vortexed for 30 s, followed by centrifugation for 3 min at 3000g. The supernatant (500 µl) was analysed on HPLC after filtration through a 0.22 µm filter.

The brain was cut into pieces and transferred to a tube and acetonitrile (2 ml) was added. The mixture was cooled on ice, homogenized for 30 sec and finally centrifuged at 3000g for 3 min. The supernatant (500 µl) was analysed on HPLC, using an Alltech Econosil C_{18} column (250 mm x 10 mm; 10 µm particle size) at a flow rate of 5 ml/min (60/40 ethanol/0.02 M phosphate buffer pH 7.4). The HPLC eluate was collected with an automated fraction collector in fractions of 5 ml (= 1 min). The fractions were then counted for radioactivity with an automated gamma counter (Cobra, Packard Canberra).

The extraction efficiency (extraction yield) was expressed as percentage of total activity found in the supernatant compared to the total amount of radioactivity present in the tissue or blood sample. Retention times of the possible radiometabolites were compared with the retention times of authentic [^{123}I]-3-I-CO and free radioiodide.

5.3.5.2. Results

The only radiolabelled compounds present in the blood and brain samples of Sprague-Dawley rats after cyclosporin A treatment were free radioiodide and the unchanged tracer [^{123}I]-3-I-CO. No difference in metabolism pattern could be observed between the normal and the cyclosporin A pre-treated group.

5.4. Conclusion

[^{123}I]-3-I-CO was evaluated *in vivo* in biodistribution studies in NMRI mice and Sprague-Dawley rats. The mouse biodistribution study revealed high initial uptake of the radioligand in the brain (a maximum concentration of 6.26 ± 1.36 % ID/g tissue was obtained at 10 min post injection) but also a rapid washout of the radioligand from the brain (radioactivity concentration decreased to 0.98 ± 0.30 % ID/g tissue at 2 h post injection). Specific binding to the 5-HT$_{2A}$ receptor in the brain of NMRI mice was demonstrated by a displacement study with ketanserin. A metabolite assay revealed that no radiolabelled metabolites were present in the blood or brain of NMRI mice.

The regional brain biodistribution study with [^{123}I]-3-I-CO in Sprague-Dawley rats also revealed high initial uptake of the radioligand in cortical tissues (maximum concentrations of 0.94 ± 0.03 % ID/g tissue and 0.67 ± 0.07 % ID/g tissue in occipital and frontal cortex respectively at 20 min post injection). A rapid washout of radioactivity from the brain was observed: radioactivity concentrations decreased to 0.085 ± 0.03 % ID/g tissue at 2 h post injection. Also, radioactivity uptake in cerebellum was quite high (0.211 ± 0.086 % ID/g tissue at 1 h post injection) compared to other 5-HT$_{2A}$ tracers. Radioactivity concentration levels in cortical tissues decreased to the level observed in cerebellum after displacement of [^{123}I]-3-I-CO with ketanserin. Also, no radiolabelled metabolites could be detected in the blood or brain of Sprague-Dawley rats. For the regional brain biodistribution study, cortex-to-cerebellum ratios of 1.5 were obtained throughout the study. When comparing these results with other 5-HT$_{2A}$ tracers, it becomes evident that the specific 'signal' of [^{123}I]-3-I-CO in the brain was limited. Other clinically used tracers have cortex-to-cerebellum binding index ratios that are much higher (for [^{123}I]-R91150 a BI of 7 was obtained 1 h post injection, for [^{18}F]-altanserin a BI of 11 was obtained [9]). This could limit the clinical usefulness of [^{123}I]-3-I-CO as a radioligand for the 5-HT$_{2A}$ receptor. Aspecific binding of [^{123}I]-3-I-CO to brain tissues could probably be responsible for the low binding index ratios observed.

The influence of P-glycoprotein modulation (by pre-treatment of the animals with cyclosporin A) on the regional brain biodistribution and metabolism of [123I]-3-I-CO in Sprague-Dawley rats was investigated. Pre-treatment of the animals with cyclosporin A (50 mg/kg) resulted in a marked increase of radioactivity concentration throughout the brain: a maximal radioactivity concentration of 0.91 ± 0.11 % ID/g tissue was obtained in frontal cortex at 40 min post injection. Radioactivity concentration in cerebellum was also markedly increased after cyclosporin A treatment, but no influence was observed on radioactivity concentrations in blood. Nevertheless, it should be pointed out that the increase in brain radioactivity concentration after treatment of the animals with cyclosporin A was not as marked as in the cyclosporin A study with [123I]-R91150: in the [123I]-3-I-CO study, brain radioactivity concentrations doubled after cyclosporin A treatment, whereas in the [123I]-R91150 study, brain tracer concentrations increased up to seven-fold after animal treatment with cyclosporin A. From these results we can conclude that [123I]-3-I-CO is a substrate for P-glycoprotein efflux *in vivo* in rodents. However, our data indicate that [123I]-R91150 is a stronger substrate for P-glycoprotein efflux in rodents than [123I]-3-I-CO.

When comparing the *in vivo* evaluation of [123I]-3-I-CO with the data obtained from the [123I]-R91150 studies in rodents, several conclusions can be drawn. Although the absolute uptake of radioligand in the brain was much higher for [123I]-3-I-CO, resulting cortex-to-cerebellum binding index ratios were never higher than 1.5. Compared to the mean value of 7 for the [123I]-R91150 studies, this indicates that the specific 'signal' in cortical tissue is a lot higher for [123I]-R91150 compared to [123I]-3-I-CO. This could severely limit the clinical usefulness of [123I]-3-I-CO as a 5-HT$_{2A}$ receptor tracer *in vivo*, and is probably caused by aspecific binding of the radioligand to brain tissues. Also, compared to [123I]-R91150, [123I]-3-I-CO showed a more rapid washout out of the brain.

A possible solution to the aspecific binding problems observed with [123I]-3-I-CO could be the development of the corresponding [18F]-fluorinated derivative. Lipophilicity should be reduced, resulting in lower aspecific binding to brain tissues. Of course, affinities of this [18F]-compound for the 5-HT$_{2A}$ receptor and other receptor systems should be evaluated first. It should also be taken into account that a lowered lipophilicity might result in a lower total brain uptake of the radioligand.

5.5. References

1. Terriere D, Janssen PMP, Gommeren W, Gysemans M, Mertens JJR, Leysen JE.
    Evaluation of Radioiodo-4-Amino-N-[1-[3-(4-Fluorophenoxy)-Propyl]-4-
    Methyl-4-Piperidinyl]-5-Iodo-2-Methoxybenzamide As A Potential 5Ht2
    Receptor Tracer for Spe(C)T. Nuclear Medicine and Biology 1995; 22:1005-
    1010.

2. Orallo F, Tristan H, Garcia-Ferreiro T, De Francisco S, Masaguer C, Ravina E et al.
    Study of the in vivo and in vitro cardiovascular effect of four new analogues of
    ketanserin: Implication of 5-HT2A and alpha(1) adrenergic antagonism in their
    hypotensive effect. Biological & Pharmaceutical Bulletin 2000; 23:558-565.

3. Bunag RD and Davidow LW. Does chronic ketanserin treatment enhance bradycardia in
    old rats by serotonergic blockade? Aging-Clinical and Experimental Research
    1998; 10:102-111.

4. Lin HC, Yang MCM, Huang YT, Yu PC, Hou MC, Hong CY et al. The hemodynamic
    effects of AT-112, an analog of ketanserin, in portal hypertensive rats.
    Pharmacology 1997; 54:16-23.

5. Pazos A, Probst A, Palacios JM. Serotonin Receptors in the Human-Brain .4.
    Autoradiographic Mapping of Serotonin-2 Receptors. Neuroscience 1987;
    21:123-139.

6. Barnes NM and Sharp T. A review of central 5-HT receptors and their function.
    Neuropharmacology 1999; 38:1083-1152.

7. Lemaire C, Cantineau R, Guillaume M, Plenevaux A, Christiaens L. Fluorine-18-
    Altanserin - A Radioligand for the Study of Serotonin Receptors with Pet -
    Radiolabeling and Invivo Biologic Behavior in Rats. Journal of Nuclear
    Medicine 1991; 32:2266-2272.

8. Liow JS, Lu SY, McCarron JA, Hong JS, Musachio JL, Pike VW et al. Effect of a P-glycoprotein inhibitor, cyclosporin A, on the disposition in rodent brain and blood of the 5-HT1A receptor radioligand, [C-11](R)-(-)-RWAY. Synapse 2007; 61:96-105.

9. Lemaire C, Cantineau R, Guillaume M, Plenevaux A, Christiaens L. Fluorine-18-Altanserin - A Radioligand for the Study of Serotonin Receptors with Pet - Radiolabeling and Invivo Biologic Behavior in Rats. Journal of Nuclear Medicine 1991; 32:2266-2272.

Chapter 6

SUMMARY

SAMENVATTING

♋ ♋ ♋

SUMMARY

The aim of this doctoral dissertation was the precursor synthesis, radiosynthesis and *in vivo* evaluation of [^{123}I]-3-I-CO as a possible new tracer for imaging of the central serotonin 5-HT$_{2A}$ receptor with SPECT. [^{123}I]-(4-fluorophenyl)[1-(3-iodophenethyl)piperidin-4-yl] methanone ([^{123}I]-3-I-CO) demonstrates good affinity for the 5-HT$_{2A}$ receptor (K$_i$ = 0.51 nM) and good selectivity ratios over other receptor types and was therefore selected as the ligand.

First, the *in vivo* behaviour of a currently used 5-HT$_{2A}$ SPECT tracer, [^{123}I]-R91150, was evaluated (chapter 3), and brain uptake of the tracer was assessed in rodents, as a standard for comparison. The influence of P-glycoprotein blocking (with cyclosporin A) on the biodistribution and brain uptake of [^{123}I]-R91150 was also evaluated in rodents, and these results were compared with the data obtained from the normal biodistribution studies with [^{123}I]-R91150. Also, the influence of P-glycoprotein blocking on pinhole μSPECT imaging with [^{123}I]-R91150 in rodents was investigated.

In NMRI mice, a dose-dependent influence of cyclosporin A on the brain uptake of [^{123}I]-R91150 was observed, indicating that the increased brain uptake is the result of a decreased efflux of tracer out of the brain after blocking of the P-glycoprotein efflux transporter with cyclosporin A. Pre-treatment of Sprague-Dawley rats with cyclosporin A resulted in a drastically increased brain uptake of [^{123}I]-R91150 (brain uptake increased seven-fold after P-glycoprotein blocking) and a vastly improved pinhole μSPECT imaging quality. From these results it can be concluded that [^{123}I]-R91150 is a substrate for P-glycoprotein efflux *in vivo*, and that it's brain efflux can be blocked by administration of cyclosporin A.

Organic synthesis of the tributylstannyl precursor for the radiosynthesis of [^{123}I]-3-I-CO was performed in adequate yield. An average yield of about 85 % was obtained in the radiosynthesis reaction. The radioligand was purified with semi-preparative HPLC, and radiochemical purities of > 95 % were obtained consistently. The radioligand was stable at room temperature until 48 h after synthesis. A logP value of 3.10 ± 0.10 was obtained for [^{123}I]-3-I-CO (chapter 4).

In vivo evaluation of $[^{123}I]$-3-I-CO in NMRI mice revealed high initial brain uptake (6.26 ± 1.36 % ID/g tissue at 10 min post injection), but radioactivity concentrations in brain decreased rapidly over time. No radiolabelled metabolites were observed in blood or brain of NMRI mice. Brain uptake of $[^{123}I]$-3-I-CO was also investigated in Sprague-Dawley rats (chapter 5): highest brain radioactivity concentrations were obtained in the occipital (0.942 ± 0.034 % ID/g tissue at 20 min post injection) and frontal cortex (0.674 ± 0.074 % ID/g tissue at 20 min post injection). Blood radioactivity concentrations were consistently low (a maximum value of 0.062 ± 0.014 % ID/g tissue was obtained at 20 min post injection).

An average frontal cortex-to-cerebellum ratio of about 1.7 was obtained. In the Sprague-Dawley rat biodistribution studies, a rapid washout of radioactivity from the brain was observed. $[^{123}I]$-3-I-CO was displaced from the 5-HT$_{2A}$ receptor by ketanserin: radioactivity concentration in the 5-HT$_{2A}$ rich areas of the brain decreased by 50 % after ketanserin displacement. Nevertheless, the residual radioactivity levels in cerebellum after ketanserin displacement remained high, especially compared to the results obtained with $[^{123}I]$-R91150, and are probably caused by aspecific binding of the radioligand to brain tissues. No radiolabelled metabolites could be detected in the blood or brain of Sprague-Dawley rats.

The influence of P-glycoprotein modulation with cyclosporin A on the brain uptake of $[^{123}I]$-3-I-CO was also investigated. On average, a 67 % increase in $[^{123}I]$-3-I-CO radioactivity concentration was observed throughout the brain after treatment of the animals with cyclosporin A. We can conclude from these results that $[^{123}I]$-3-I-CO is at least a partial substrate for P-glycoprotein efflux, but the increase in brain radioactivity concentration after cyclosporin A treatment was not as large as the increase observed with $[^{123}I]$-R91150 (chapter 3).

Although cortical tissues could be visualized using pinhole μSPECT imaging with $[^{123}I]$-3-I-CO, aspecific binding of the radioligand was observed in the cerebellum, probably limiting its application as a serotonin 5-HT$_{2A}$ receptor tracer in humans. μSPECT imaging quality also did not improve after cyclosporin A pre-treatment of the animals.

Summary - Samenvatting

Although the initial rodent studies demonstrated promising brain uptake of the radioligand, it can be concluded that $[^{123}I]$-3-I-CO probably has very limited potential as a 5-HT$_{2A}$ tracer for SPECT, due to high aspecific binding and rapid washout of the radioligand out of the brain. Also, compared to other clinically used brain tracers (for example $[^{123}I]$-R91150), the specific 'signal' of $[^{123}I]$-3-I-CO in brain is too limited for application as a tracer in brain receptor imaging studies.

Summary - Samenvatting

SAMENVATTING

Deze doctoraatsthesis had tot doel de precursorsynthese, radiosynthese en de *in vivo* evaluatie van [^{123}I]-3-I-CO als een mogelijke nieuwe SPECT tracer voor het in beeld brengen van de serotonine 5-HT$_{2A}$ receptoren in de hersenen. [^{123}I]-(4-fluorophenyl)[1-(3-iodophenethyl) piperidin-4-yl]methanone ([^{123}I]-3-I-CO), een molecule met hoge affiniteit voor de serotonine 5-HT$_{2A}$ receptor (Ki = 0.51 nM) en een goede selectiviteit ten opzichte van andere receptor types, werd gekozen als ligand.

Ook werd het *in vivo* gedrag bestudeerd van [^{123}I]-R91150 (hoofdstuk 3), een serotonine 5-HT$_{2A}$ tracer die momenteel in kliniek bij patiënten gebruikt wordt. De hersenopname van deze tracer werd onderzocht in knaagdieren en zal later als referentie gebruikt worden. De invloed van blokkering van de P-glycoproteine efflux pompen in de bloed-hersenbarrière met cyclosporine A op de biodistributie en de hersenopname van [^{123}I]-R91150 werd onderzocht, en vergeleken met de normale hersenopname. De invloed van cyclosporine A toediening op de beeldvorming met een pinhole μSPECT camera werd ook nagegaan.

Toediening van cyclosporine A had een dosisafhankelijke invloed op de hersenopname van [^{123}I]-R91150 in NMRI muizen. Dit toont aan dat de verhoogde hersenopname het gevolg is van een verlaagde efflux van tracer uit de hersenen (wegens blokkering van P-glycoproteine). Behandeling van de Sprague-Dawley ratten met cyclosporine A resulteerde in een drastisch verhoogde hersenopname van [^{123}I]-R91150 (de hersenopname verhoogde met een factor 7 na toediening van cyclosporine A). De kwaliteit van de beeldvorming met de pinhole μSPECT camera verbeterde ook merkelijk na toediening van cyclosporine A. Uit deze resultaten kunnen we besluiten dat [^{123}I]-R91150 een substraat is voor de P-glycoproteine efflux transporter, en dat de efflux van tracer uit de hersenen geblokkeerd kan worden door toediening van cyclosporine A.

De precursor voor radiosynthese (het tributyltinderivaat) werd gesynthetiseerd in voldoende rendement. Een radiochemisch rendement van 85 % werd bekomen tijdens de radiosynthese-reactie. De tracer werd opgezuiverd met behulp van semi-preparatieve HPLC chromatografie. De radiochemische zuiverheid bedroeg meer dan 95 %. Het radioligand was stabiel gedurende minstens 48 uur op kamertemperatuur. De logP waarde van $[^{123}I]$-3-I-CO bedroeg 3.10 ± 0.10 (hoofdstuk 4).

Een hoge initiële hersenopname van $[^{123}I]$-3-I-CO werd gezien in NMRI muizen (6.26 ± 1.36 % ID/g 10 min na injectie), maar de concentratie aan radioactiviteit in de hersenen daalde snel in functie van de tijd. Er werden geen radioactieve metabolieten gevonden in bloed of hersenen. De hersenopname van $[^{123}I]$-3-I-CO werd ook onderzocht in Sprague-Dawley ratten (hoofdstuk 5): de hoogste concentratie werd gezien in de occipitale (0.942 ± 0.034 % ID/g 20 min na injectie) en frontale cortex (0.674 ± 0.074 % ID/g 20 min na injectie). De concentratie in het bloed was laag (maximum waarde: 0.062 ± 0.014 % ID/g 20 min na injectie).

De ratio frontale cortex/cerebellum was maximaal 1.7. In de biodistributiestudies met ratten werd een snel wegwassen van de tracer uit de hersenen vastgesteld. $[^{123}I]$-3-I-CO werd verdrongen van de 5-HT$_{2A}$ receptor door ketanserine: de tracer concentraties in de 5-HT$_{2A}$ rijke zones in de hersenen daalden met gemiddeld 50 % na verdringing. Toch bleef de concentratie aan $[^{123}I]$-3-I-CO in het cerebellum hoog na verdringing, vooral vergeleken met de resultaten met $[^{123}I]$-R91150. Deze hoge activiteitsniveaus werden waarschijnlijk veroorzaakt door aspecifieke binding van de tracer aan hersenweefsel. Er werden geen radioactieve metabolieten gevonden in de proeven met ratten.

De invloed van cyclosporine A toediening op de hersenopname van $[^{123}I]$-3-I-CO werd eveneens onderzocht. Gemiddeld werd een 67 % hogere opname van $[^{123}I]$-3-I-CO gezien in de hersenen na toediening van cyclosporine A. Hieruit kunnen we besluiten dat $[^{123}I]$-3-I-CO minstens een partieel substraat is voor de P-glycoproteine efflux transporter. Het verschil tussen beide groepen was echter niet zo groot als in de studies met $[^{123}I]$-R91150 en cyclosporine A (hoofdstuk 3).

Summary - Samenvatting

Hoewel de corticale weefsels gevisualiseerd konden worden met behulp van [^{123}I]-3-I-CO en pinhole µSPECT, werd toch binding van het radioligand gezien in het cerebellum. Hierdoor is het toepassingsgebied van [^{123}I]-3-I-CO bij mensen waarschijnlijk vrij klein. In tegenstelling tot de studies met [^{123}I]-R91150, verbeterde de beeldvorming met [^{123}I]-3-I-CO ook niet na toediening van cyclosporine A.

Hoewel in de initiële muizenstudies een veelbelovende hersenopname aangetoond werd van [^{123}I]-3-I-CO, kunnen we besluiten dat [^{123}I]-3-I-CO waarschijnlijk geen geschikte kandidaat is als tracer voor de serotonine 5-HT$_{2A}$ receptor. Hoofdredenen hiervoor zijn een hoge aspecifieke binding in de hersenen en een snel wegwassen van het radioligand uit de hersenen. Vergeleken met andere bij mensen gebruikte tracers (bijvoorbeeld [^{123}I]-R91150) is het specifieke 'signaal' van [^{123}I]-3-I-CO té gelimiteerd om bruikbaar te zijn in hersenbeeldvorming bij patiënten.